VLE Measurements of Ether Alcohol Blends for Investigation on Reformulated Gasoline

Submitted in fulfilment of the requirements of the
degree of Master of Engineering in
the Department of Chemical Engineering, Faculty of Engineering and the Built Environment at the Durban
University of Technology

Travis Pio Benecke

AUGUST 2016

ABSTRACT

Separation processes in the chemical process industries is dependent on the science of chemical thermodynamics. In the field of chemical separation process engineering, phase equilibrium is a primary area of interest. This is due to separation processes such as distillation and extraction which involves the contacting of different phases for effective separation. The focal point of this research project is the measurement and modeling of binary vapour-liquid equilibrium (VLE) phase data of systems containing ether-alcohol organic compounds.

The VLE data were measured with the use of the modified apparatus of Raal and Mühlbauer, (1998). The systems of interest for this research arose from an industrial demand for VLE data for systems containing ether-alcohol organic compounds. This gave rise to the experimental VLE data isotherms being measured for the following binary systems:

a) Methyl tert-butyl ether (1) + 1-pentanol (2) at 317.15 and 327.15 K
b) Methyl tert-butyl ether (1) + 2, 2, 4-trimethylpentane (2) at 307.15, 317.15 and 327.15K
c) 2, 2, 4-Trimethylpentane (1) + 1-pentanol (2) at 350.15, 360.15 and 370.15K
d) Diisopropyl ether (1) + 2,2,4-trimethylpentane (2) at 320.15, 330.15 and 340.15K
e) Diisopropyl ether (1) + 1-propanol (2) at 320.15, 330.15 and 340.15K
f) Diisopropyl ether (1) + 2-butanol (2) at 320.15, 330.15 and 340.15K

The data for all the measured binary systems investigated at these temperatures are currently not available in the open source literature found on the internet and in library text resources. The systems were not measured at the same temperatures because certain system isotherm temperatures correlate to a pressures above 1 bar. This pressure of 1 bar is the maximum operating pressure specification of the VLE apparatus used in this project.

The experimental VLE data were correlated for model parameters for both the $(\gamma-\phi)$ and $(\phi-\phi)$ methods. For the $(\gamma-\phi)$ method, the fugacity coefficients (vapour-phase non-idealities) were tabulated using the virial equation of state and the Hayden-O'Connell correlation (1975); chemical theory and the Nothnagel et al. (1973) correlation method. The activity coefficients (liquid phase non-idealities) were calculated using three local-composition based activity coefficients models: the Wilson (1964) model, the NRTL model (Renon and Prausnitz, 1968); and the UNIQUAC model (Abrams and Prausnitz, 1975). Regarding the direct method, the Soave-Redlich-Kwong (Redlich and Kwong, 1949) and Peng-Robinson (1976) equations of state

were used with the temperature dependent alpha-function (α) of Mathias and Copeman (1983) with the Wong-Sandler (1992) mixing rule.

Thermodynamic consistency testing, which presents an indication of the quality and reliability of the data, was also performed for all the experimental VLE data. All the systems measured showed good thermodynamic consistency for the point test of Van Ness et al. (1973) - the consistency test of choice for this research. This however, was based on the model chosen for the data regression of a particular system. Therefore, the combined method of VLE reduction produced the most favourable results for the NRTL and Wilson models.

Declaration

I, Travis Pio Benecke, hereby declare that:

i. The research reported in this research project, except where otherwise indicated, is my original work.
ii. This research project has not been submitted for any degree or examination at any other university.
iii. This research project does not contain other persons' data, pictures, graphs or other information, unless specifically acknowledged as being sourced from other persons.
iv. This research project does not contain other persons' writing, unless specifically acknowledged as being sourced from other researchers. Where other written sources have been quoted, then:
    a. Their words have been re-written but the general information attributed to them has been referenced;
    b. Where their exact words have been used, their writing has been placed inside quotation marks, and referenced.
v. This thesis does not contain text, graphics or tables copied and pasted from the internet, unless specifically acknowledged, and the source being detailed in the thesis and in the References sections.

Signed:

_____ _____

Travis Benecke Date

As the candidate's supervisor, I agree/do not agree to the submission of this thesis.

_____ _____

Professor D. Ramjugernath Mr.Suresh Ramsuroop

DEDICATION

For my mother, June Theresa

Ephesians 1:20-21 (AMP) "… He raised Him from the dead and seated Him at His [own] right hand in the heavenly [places], [21]Far above all rule and authority and power and dominion and every name that is named [above every title that can be conferred], not only in this age *and* in this world, but also in the age and the world which are to come."

1 John 4:16-17 (NASB) "We have come to know and have believed the love which God has for us. God is love, and the one who abides in love abides in God, and God abides in him. [17]By this, love is perfected with us, so that we may have confidence in the day of judgement; because as He is, so also are we in this world."

ACKNOWLEDGEMENTS

I would like to take this opportunity to acknowledge and thank the people and organizations who have made a tremendous contribution to this project and my career in postgraduate studies:

- To the King of Kings, Jesus the Christ through whom all things have been made possible for me, thank you for being my personal Lord and Saviour.
- My supervisors, Professor D. Ramjugernath, and Mr. Suresh Ramsuroop for their expert knowledge, guidance and support.
- The National Research Foundation (NRF) for their financial assistance.
- The workshop and laboratory staff at UKZN.
- My family for their amazing love and support.

All my personal friendships gained within the Thermodynamics Research Unit from 2009 until the present day whom all have been a blessing in some way or the other.

Table of Contents

LIST OF TABLES

Chapter 6

Chapter 7

Chapter 8

Appendix A

Appendix B

Appendix C

LIST OF FIGURES

Chapter 1

Chapter 2

Chapter 3

Chapter 4

Chapter 5

Chapter 6

Chapter 7

NOMENCLATURE

English Letters

a_i	Parameter for intermolecular attraction force in the Peng-Robinson (1976) and Soave - Redlich-Kwong (1972) equation of state
a_{ij}	Constants for temperature dependency of model parameters
a_m	Mixture parameter for intermolecular attraction force in the Peng-Robinson (1976) and Soave-Redlich-Kwong (1972) equation of state
a_{vdw}	Van der Waals (1873) equation of state intermolecular attraction force parameter
A_i^*	Constant in the Antoine equation
A	Antoine vapour pressure constant
A^*	Peak area from gas chromatograph
A_{ij}	Parameter in the Van Laar (1910) model
A_{ji}	Parameter in the Van Laar (1910) model
b	Molecular size parameter in Peng-Robinson (1976) equation of state
b_{ij}	Constants for temperature dependency of model parameters
b_{vdw}	Van der Waals (1873) equation of state intermolecular attraction force parameter
b_m	Mixture molecular size parameter in Peng-Robinson (1976) equation of state
B_i	Constant in the Antoine equation
B_{ii}	Second virial coefficient of pure component *i* [cm^3/mol]
B_{ij}	Second virial coefficient for species *i* – species *j* interaction [cm^3/mol]
B^*	Parameter for Peng-Robinson equation of state
C_i	Constant in the Antoine equation
c_{ij}	Constants for temperature dependency of model parameters
D	Wong and Sandler (1992) mixing rule summation term
F	Response factor
f	Fugacity [kPa]
$\hat{f}_i$	Fugacity in solution [kPa]
f_i	Fugacity of the pure component *i* [kPa]

G_i	Molar or specific Gibbs energy [J/mol]
$\overline{G}_i$	Partial molar Gibbs free energy
G_{ij}	NRTL model parameter of Renon and Prausnitz (1968)
$g_{ij} - g_{ii}$	Parameter in NRTL (1968) model representing interactions between species
H	Enthalpy [J/mol]
$\overline{H}$	Partial molar enthalpy [J/mol]
$\Delta H_{VAP,i}$	Enthalpy of vapourisation [J/mol]
k_{ij}	Binary interaction parameter in the Wong-Sandler (1992) mixing rule
l_i	Parameter in the UNIQUAC (1975) model
l_{ij}	Binary interaction parameter for the Twu-Coon (1992) mixing rule
$L^{'}$	Parameter in the Twu et al. (1991) alpha correlation
$M^{'}$	Parameter in the Twu et al. (1991) alpha correlation
M	General thermodynamic property
n_i	Number of moles of component *i*
N	Number of chemical species or components present in a system
P	System pressure [kPa]
P_i^{sat}	Pure component vapour pressure [kPa]
$P^{'}$	Parachor factor
q_i	Pure component are in UNIQUAC model of Abrams and Prausnitz (1975)
q_i^m	Pure component are in modified UNIQUAC model of Anderson and Prausnitz (1978)
r_i	UNIQUAC model (Abrams and Prausnitz, 1975) pure component volume parameter
R	Universal gas constant [J/mol/K]
R_d	Mean radius of gyration $\left[\overset{\circ}{A}\right]$
S	Molar/Specific entropy [cm^3/mol]
T	System temperature [°C or K]
$u_{ij} - u_{ii}$	Parameter for the energy interactions between species in the UNIQUAC model of Abrams and Prausnitz (1975)
$\overline{V}$	Partial molar volume [cm^3/mol]

V	Molar/Specific volume [cm^3/mol]
x	Liquid phase mole fraction or composition
y	Vapour phase mole fraction
z	Co-ordination number in UNIQUAC model of Abrams and Prausnitz (1975)
Z	Compressibility factor

Greek Letters

α	Scaling factor in Peng-Robinson (1976) equation of state
α_{ij}	NRTL model parameter for non-randomness of solution
δ	Denotes a residual property, e.g. δP
δ_{ij}	An expression constituting the second virial coefficients
ε_P^*	Constant temperature term in direct test of Van Ness (1995)
ε_T^*	Constant pressure term in direct test of Van Ness (1995)
Φ	Ratio of Poynting correction factor and fugacity coefficients
Φ_i^*	Segment fraction in the UNIQUAC model of Abrams and Prausnitz (1975)
ϕ	Fugacity coefficient
$\hat{\phi}$	Fugacity coefficient in solution
Γ_i	Temperature dependant constant of integration
γ	Activity coefficient
γ_i^∞	Activity coefficient at infinite dilution
η	Parameter representing solvation and association
κ	Constant for peng-Robinson (1976) equation of state
Λ_{ij}	Wilson (1964) model parameter
$\lambda_{ij} - \lambda_{ii}$	Wilson (1964) model parameter representing molar interactions between species
μ_d	Dipole moment
μ_i	Chemical potential of species *i*
θ_i	Area fraction in the UNIQUAC model of Abrams and Prausnitz (1975)
σ	Standard deviation
τ_{ij}	NRTL model parameter of Renon and Prausnitz (1968)
ω	Accentric factor

Subscript

AAD	Absolute average deviation in a property
c	Critical property
calc	Calculated value
exp	Experimental value
i	Component 1
j	Component 2
m	Mixture property
r	Reduced property
1	Component 1
2	Component 2

Superscript

β	Thermodynamic phase
α	Thermodynamic phase
π	Thermodynamic phase
^{o}	Standard state
C	Combinatorial property for UNIQUAC model (Abrams and Prausnitz, 1975)
E	Excess property
ig	Ideal gas
l	Liquid phase
R	Residual property
sat	Property at saturation
v	Vapour phase

1

Chapter One

INTRODUCTION

Phase equilibrium data of chemical compounds and their mixtures are significant in chemical process industries as they are required for efficient design and operation of separation processes. The scientific methods utilized to acquire thermodynamic data are experimental methods; predictive models and molecular simulations. Concentration in the development of predictive thermodynamic models has become an increased *trend* in the area of phase equilibrium thermodynamics (Gmehling, 2003, Jaubert and Mutelet, 2004, Vetere, 2004). In addition, molecular simulation has acquired notability as an area of interest (Deiters and De Reuck, 1999, Sandler, 2003). Together, computer simulations and predictive models allow the determination of quantitative estimates of the phase equilibrium properties (namely, vapour-liquid equilibria, LLE, SLE etc.) of a particular chemical system.

This emphasis on predictive methods compared to experimental measurements can be attributed to, long time periods during conduction of experiments, high costs, unwanted phenomena and countless experimental difficulties (Van'T Hof et al., 2004). The thermodynamic characterization of a large magnitude of chemical compounds and combinations thereof further creates an aversion toward experimental measurements. However, systems of industrial importance are commonly non-ideal as they normally involve chemicals consisting of chemical nature being dissimilar as opposed to members of the same homologous series (Pillay, 2010). These dissimilarities all contribute to deviations from a predictive modeling point of view (Seker and Somer, 1992). The phase equilibrium compositions of such mixtures are best determined experimentally as predictive thermodynamic data acquisition methods can result in severe inaccuracy in process simulations. (Turton et al., 1998). Based on this, it becomes evidently clear that experimental methods remain an accurate means of data acquisition, validation and modification of predictive thermodynamics. The latter is so because models used for phase behaviour predictions require a set of experimental data points to adjust model parameters in order to proper correlate the system of interest (Ashour and Aly, 1996).

Phase equilibrium data remains an integral asset in the successful design of separation processes such as: distillation, extractive distillation, azeotropic distillation and flash operations. Among

these processes distillation is the most widely used separation process (representing also a large percentage of separation processes) in the chemical and petrochemical industry. Industrial companies use distillation for separation of various reaction mixtures for the ultimate purpose of transformation into useful end products. Distillation is based on phase equilibrium, that is, accurate vapour-liquid equilibrium (VLE) data and vapour-liquid-liquid equilibrium (VLLE) data in certain cases. They also account for more than 50% of total capital costs and 90% of total energy usage (Streicher et al., 1995). This is due to the multitude of advantages that distillation possesses over alternate methods used in the chemical industry (Gmehling, 1999).

Hence the industrial demand arises for accurate and thermodynamically consistent experimental phase equilibrium data (VLE, LLE, solubility). This is due to the optimal design of equipment and separation sequences i.e., the sizing of distillation columns for an industrial separation process, weighs heftily upon the economics of the entire chemical plant. The costly effects of unreliable design become visible when seemingly minute errors between experimental and predicted data are neglected in the final design and consequently result in significant errors during the actual operational run of the distillation column.

1.1. Background of Research Project

Biological fuels (or *biofuels*) are key ingredient in revolutionizing the petroleum industry among the multitude of renewable energy forms recognized in industry today. The reduction of greenhouse gas (CO_2) is one of the main factors promoting renewable energies, thus creating a demand due to economic challenges for biofuels to be re-invented. Therefore this research study had to be undertaken.

Phase equilibrium studies on oxygenate blends (such as alcohols and ethers to be studied in this project) are important for the automotive fuels industry due to the efficacy of these types of additive combinations in enhancing the octane rating of reformulated gasoline (RFG – a biofuel) and reducing harmful emissions from the combustion of fuel mixtures (Rezanova et al., 1999). Thermal decomposition of biomass, cellulose lignin etc. can produce alcohol compounds.

Methyl tert-butyl ether (MTBE), ethyl tert-butyl ether (ETBE) and tert-amyl methyl ether (TAME) have been the primary focus for studies on alkyl ether oxygenate additives in gasoline blends (Da Silva et al., 2005). However, concerns over environmental persistence and toxicity of some of these ethers have sparked numerous debates about their usage (Martienssen et al., 2006, Nadim et al., 2001). In this project however, MTBE which is one some of these ethers, will be studied as there is still relevance for accurate thermodynamic data in industry for such tertiary ether-alcohol blends (Vorenberg et al., 2005). MTBE is still utilised in the petrochemical industry

for its ability to reduce aromatic compound and hydrocarbon emissions as well as increase the octane number in reformulated gasoline (Da Silva et al., 2005). Therefore there is an important need for accurate VLE data of systems (tertiary ether alcohol oxygenate blends) containing MTBE. Thermodynamic data describing this chemical's behavior in mixtures is still relevant also when being utilized as a benchmarking tool (Vorenberg et al., 2005). 2, 2, 4-trimethylpentane (iso-octane) is another important constituent of gasoline that will be investigated. One of several isomers of octane, it can be used itself as a higher quality gasoline enhancer, as it defines the 100 point on the octane rating (with the zero point being *n*-heptane).

MTBE will be studied in conjunction with significantly more environmentally favourable ether, namely, diisopropyl ether (DIPE). DIPE is a branched or tertiary ether which is regarded as a less polluting and non-toxic alkyl-ether and has been the subject of recent studies as a possible additive in oxygenate blends (Hwang et al., 2008, Oh et al., 2009). In particular, the low water solubility of DIPE (Hwang et al., 2008) eases concerns over groundwater contamination (associated with ethers like MTBE and ETBE). Ethanol has the status of a commonly used biomass-based renewable fuel that is used as an oxygenate additive for enhancing the octane rating in RFGs, however, the water solubility of ethanol compromises the homogeneity of the RFG blend, due to the incompatibility of "wet ethanol" with gasoline (Reddy et al., 2013). The blending of a poorly water-soluble oxygenate such as DIPE with ethanol can assist in this regard, by increasing the miscibility gap in the ethanol + water system, as observed in the liquid-liquid equilibrium studies by Arce et al. (2002).

Other alcohols that have been studied with a tertiary ether like DIPE, includes 1-butanol, which has been investigated by Villamañán (Villamañán et al., 2006b). We have measured this system (DIPE + 1-butanol) at conditions (temperatures and pressures) that have not been investigated before, along with DIPE in conjunction with the alcohols ethanol and methanol found in the publication Reddy *et al*. (2013).

In addition to the function of oxygenate blends in enhancing the combustion characteristics of RFGs, it is also desirable to have a reduction in the emission levels from the combustion of gasoline. The study of phase equilibrium properties such as VLE, are important to determine the volatility characteristics of the system (Reddy et al., 2013).

The VLE datasets obtained will also contribute towards being available as an open literature source for both academic and industrial use (due to possibly being published; some of the work has already been published). The data will be used in industry (in this case SASOL) for optimisation purposes such as the correct process control operating conditions for reaching optimal and efficient separation of the binary mixtures. In reality, in industry, the gasoline blends that are made available are not binary mixtures, instead consisting of multicomponent mixtures.

Therefore the binary VLE data is reduced to fit multicomponent model parameters, thus allowing the binary data to predict multicomponent VLE data between the different temperature isotherms required, by using iterative procedures or simulation software. All data that is measured must be reduced in order to fit mathematical model parameters. This technique is described as data regression. There is a vast array of techniques available for the reduction of phase equilibrium data. For each technique which has been rigorously developed, there are advantages and disadvantages to utilizing a specific one.

The objective of data regression is specifically to condense the large quantities of experimental thermodynamic data into a simple and useable form for future reference. This is achieved by using predictive thermodynamic models such as equation of state models (EOS) and liquid phase activity coefficient models to produce thermodynamic interaction parameters specific to each system being analyzed. Another beneficial aspect of regression of data is that interpolation and extrapolation of experimental data is achievable. This enables the prediction of thermodynamic data in areas which are complex to measure.

1.2. Objectives of Research

The research focussed on the measurement of new phase equilibrium data for MTBE and DIPE with alcohols and an octane that included: 1-pentanol, 1-propanol, 2-butanol and 2, 2, 4-trimethylpentane. All measurements were undertaken at the research laboratories of the Thermodynamics Research Unit (TRU) based with the discipline of chemical engineering of the University of KwaZulu-Natal.

The VLE data were measured using the modified apparatus of Raal (Raal, 1998). This apparatus was however further modified by Ndlovu (2005) to facilitate measurements for potential VLLE systems. The study entailed:

- Re-locating the VLE/VLLE apparatus from one laboratory to a new laboratory facility, setting up, further modifying the equipment for VLE purposes only (described in detail in chapter 4) and testing the apparatus.
- A thorough literature survey was performed utilizing the university database and its international affiliate databases to determine the VLE data that have been measured for binary systems in the same area of research before any experimental work could commence.
- Once it was evident that the systems had not been measured before, the suitability of the apparatus available and operating conditions (isotherm temperatures correlating to a

pressure below 1 bar – the maximum pressure of the VLE apparatus) were scrutinized, then the systems were able to be measured.

- Thereafter the vapour pressures of all the components studied were measured.

- The binary vapour-liquid equilibria (VLE) data for the components were measured. Most of the systems were measured at three isotherm temperatures to achieve thermodynamic parameters having temperature dependence. The systems and conditions at which experiments were measured were:

    a) MTBE (1) + 1-pentanol (2) at 317.15 and 327.15 K
    b) MTBE (1) + 2, 2, 4-trimethylpentane (2) at 307.15, 317.15 and 327.15K
    c) 2, 2, 4-Trimethylpentane (1) + 1-pentanol (2) at 350.15, 360.15 and 370.15K
    d) DIPE (1) + 2,2,4-trimethylpentane (2) at 320.15, 330.15 and 340.15K
    e) DIPE (1) + 1-propanol (2) at 320.15, 330.15 and 340.15K
    f) DIPE (1) + 2-butanol (2) at 320.15, 330.15 and 340.15K

- Lastly the correlation with the various thermodynamic models in order to determine the models' parameters and the data being subjected to thermodynamic consistency testing.

1.3. Overview of Alcohols, Ethers and Constituents of Biofuel

1.3.1. Classification of Alcohols

Compounds of alcohol develop through processes like normal oxidation of hydrocarbons, the fermentation of molasses and oil pyrolysis. Alcohol compounds are described as having one or more hydrogen atoms in alkanes replaced by an -OH group. The -OH group produces high polarity of the alcohols. This, results in their boiling point being higher than that of hydrocarbons with a congruent number of carbon atoms.

Alcohols are classified as primary, secondary and tertiary because they are generally grouped depending on the position of the -OH group on the chain of carbon atoms. For a primary alcohol, the hydroxyl group is bonded to one R group, e.g. $CH_3CH_2^-$. With a secondary alcohol, the hydroxyl group is bonded to a carbon atom with two R groups attached to the carbon atom, and a tertiary-alcohol has the hydroxyl group bonded to a carbon atom with three R groups attached (Petrucci et al., 2006).

When alcohols are subjected to oxygen/air, each class displays a different reaction. Primary

alcohols become oxidized to aldehydes and to carboxylic acids with excess oxygen. Secondary alcohols however can undergo only one stage of oxidization to ketones. The structure of a tertiary alcohol does not undergo any oxidation to another compound.

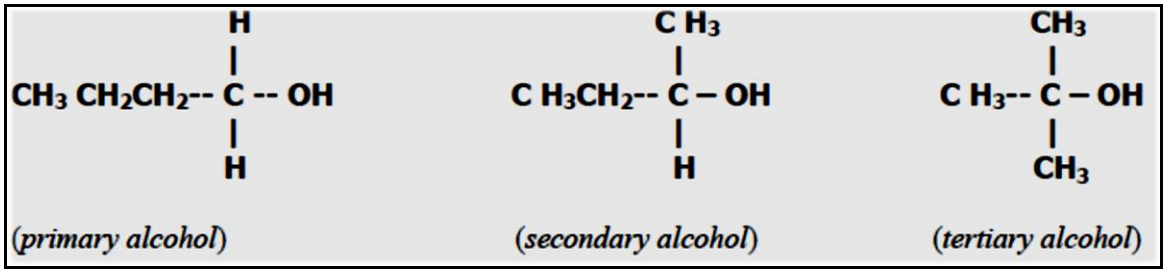

Figure 1-1: Different examples of classes of alcohols (Petrucci et al., 2006).

1.3.1.1. Hydrogen Bonding in Alcohols

In the case of alcohols, highly electronegative lone pair electrons on oxygen atoms attract free electrons of a hydrogen atom (H^+) in close proximity to form a *hydrogen bond*. The electronegative atom (which is covalently bonded to the hydrogen atom) attracts and pulls away electron density from the H nucleus. This leaves a proton which is attracted to a lone pair of electrons on an electronegative atom of a neighbouring molecule (Petrucci et al., 2006). This constitutes a higher boiling point than the corresponding alkanes with van der Waals dispersion forces being the only intermolecular force.

Hydrogen bonding can affect the physical properties of *associating* compounds (Fu and Sandler, 1995). Association in compounds occur when hydrogen bonding takes place between molecules that have both electron donors and acceptors such as alcohols and acids and occur between associating molecules of a similar (self-association) or different (cross-association) type (Soo, 2011). Alcohols have dipole-dipole interactions which are the same for all the alcohols, with hydrogen bonding having the same condition. This does not affect the dispersion forces increasing as the size of the alcohol molecule increases. As the dispersion forces increase in strength, the molecule length and the lone pair electrons consequently increase. The boiling points of alcohols therefore increase with an increase in the number of carbon atoms in the chains as more energy is required to avoid dispersion forces (Iwarere, 2009).

During boiling, more heat is needed for the breaking down of double bonds formed due to effect of hydrogen bonding on the physical properties of alcohols. Alcohol molecules that

possess two or more -OH groups are more likely to form hydrogen bonds. Therefore it is of significance to note that simple alcohols have lower boiling point temperatures than these types.

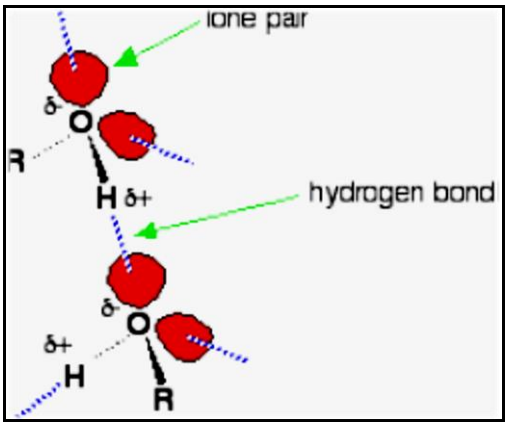

Figure 1-2: Formation of hydrogen bond in alcohols (Iwarere, 2011).

1.3.1.2. Solubility of Alcohols

Alcohols are completely soluble in water, although poor solubility of alcohols becomes visible from the forth carbon chain length onwards. Consequently, this results in two phases of liquid. It can therefore be concluded that solubility can decrease with an increase in the length of the carbon chain. It is also understood that alcohols display two types of solubility trends. This occurs because the carbon chain (non-polar R group) has the ability to halt solubility and the hydroxyl group (OH^-) enables solubility.

1.3.2. Classification of Ethers

From the elimination of water from two molecules of alcohol by incorporation of a dehydrating agent such as concentrated sulphuric acid, ether compounds can be acquired (Petrucci et al., 2006). The general formula for compounds of ether is R–O–R. The stability of the linkage to most reducing and oxidizing agents illustrates how the structure of ethers makes them non-reactive (comparatively speaking) with most organic compounds. They can however form highly explosive peroxides and are extremely flammable. Care must be taken not to store ethers in direct sunlight and storage temperatures must be regularly monitored to avoid health risks. Two structural forms of ethers exist namely, acyclic or straight chained and cyclic.

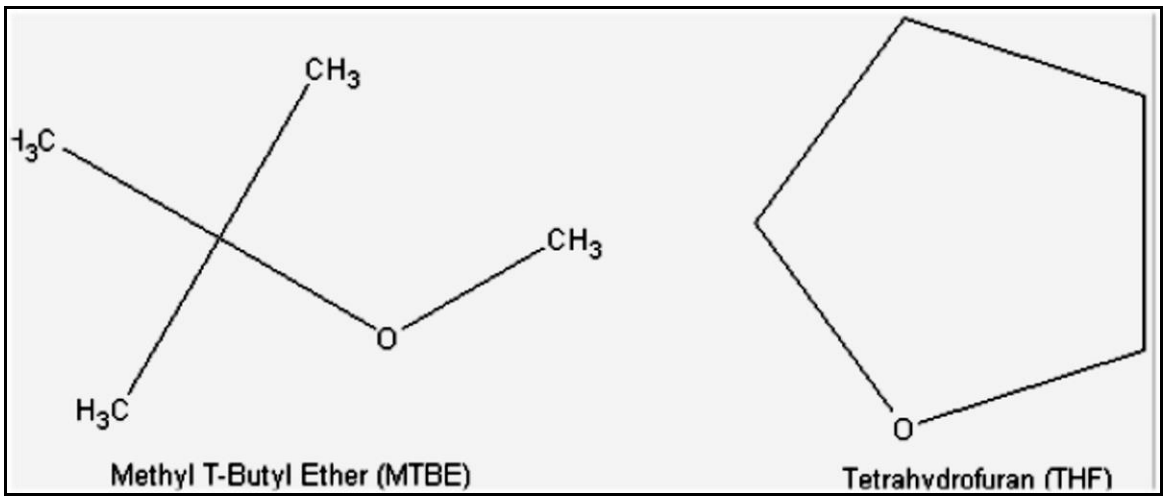

Figure 1-3: The two examples of structural types of Ethers (Mqondisi, 2012)

1.3.2.1. Solubility of Ethers

Ethers are slightly soluble in water because of the oxygen atom that they possess. This becomes evident by the observance of dimethyl ether which is an ether of small molecular weight. Ethers with large molecular weights are not water soluble. Ethers are also considered to be immiscible in water.

1.3.3. Classification of Iso-octane as a significant constituent of biofuel

1.3.3.1. Iso-octane as an Anti-knocking Agent

A thud or knock sound from the engine usually indicates engine knocking. Not only does knocking work against the motive power of the engine, it is also detrimental to the engine's motive power. Hence, it became a key discovery during the early stages of engine development, that several gasoline component types exhibited different behaviour. The main characteristic was the compression ratio, which is the ratio of volume at the bottom of the stroke is to the volume at the top of the stroke (See Figure 1-4). Therefore, when gasoline is used in high compression internal combustion engines, it may have a tendency to ignite early (i.e., *pre-ignition* or *detonation*) causing a damaging "engine knocking" sound. Iso-octane however behaves as an anti-knocking agent in gasoline. Anti-knocking agents not only reduce engine knocking but also boost the octane rating of fuel.

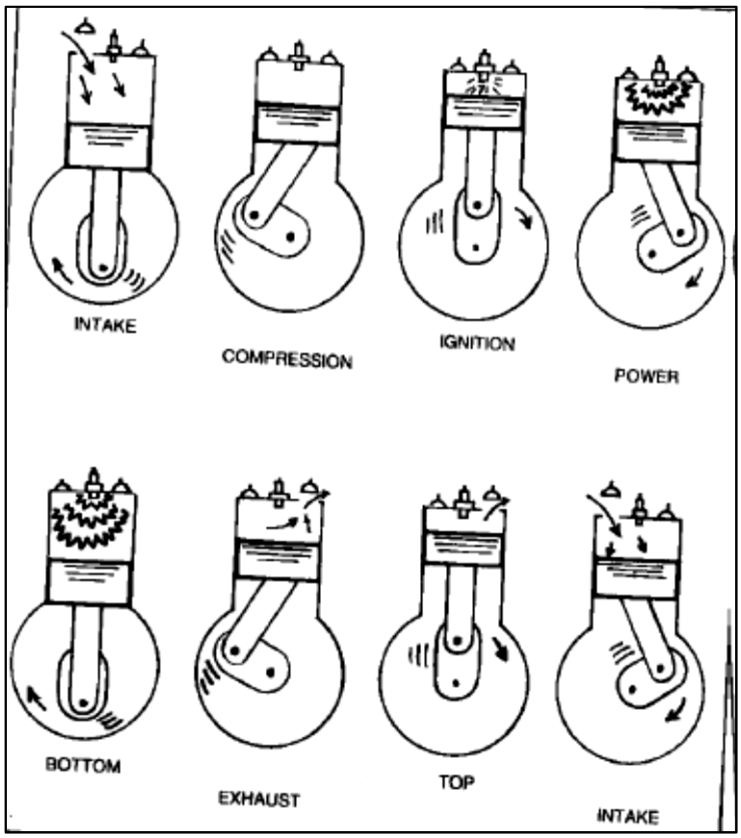

Figure 1-4: The Four-Stroke Cycle Internal Combustion Engine (Leffler, 1985)

1.3.3.2. Iso-octane and Octane number

Octane numbers or ratings are measures of whether a gasoline will knock in an engine. When the octane number of a gasoline or its component is measured, an exact compression ratio is of significance which is the one with which self-ignition occurs at the very top of the stroke. In order to measure the compression ratio where any gasoline component knocks, a series of guide numbers were devised. Iso-octane was defined as 100 octane rated gasoline with heptane (which knocks at a substantially lower compression ratio) as zero octane gasoline. The octane number is equalled to the percentage of iso-octane within the blend that knocks at the same compression ratio (Leffler, 1985).

2

Chapter Two

THERMODYNAMIC PRINCIPLES OF VAPOUR-LIQUID EQUILIBRIUM

In order to obtain understanding in chemical thermodynamics regarding the molecular interactions between different species and phases, thermodynamic principles of phase equilibrium are applicable. Phase equilibrium is of interest particularly in separation processes such as distillation, extraction, leaching, adsorption and absorption, as these involve phase contacting.

Reason being, where the equilibrium compositions of two phases are usually significantly different from one another, this difference enables one to separate mixtures by phase contacting operations (Prausnitz et al., 1999). Distillation is deemed more effective a separation technique for mixtures with compounds of different boiling temperatures. Thermodynamic properties and equations play an important role for the design of separation processes like distillation columns. Therefore it is important to have accurate and thermodynamically consistent experimental and correlation data for their design.

This chapter presents are view of the fundamental theory affiliated with the treatment (correlation and analysis) of experimental binary low pressure VLE data. A detailed review along with discussions on thermodynamic principles of VLE can be found in the following texts by the following authors: Walas (1985), Prausnitz et al. (1999), Raal and Mühlbauer (1998) and Smith et al. (2001).

2.1. Overview of Solution Thermodynamics

An overview of solution thermodynamics that can be applied to phase equilibrium data, is demonstrated by Figure 3-1. This demonstrates the interrelationships of the thermodynamic principles and associated equations that can typically be used to determine phase equilibria of real systems. Smith (Smith and VanNess, 1996) provides a more rigorous expansion on the theoretical treatment of phase equilibrium thermodynamics.

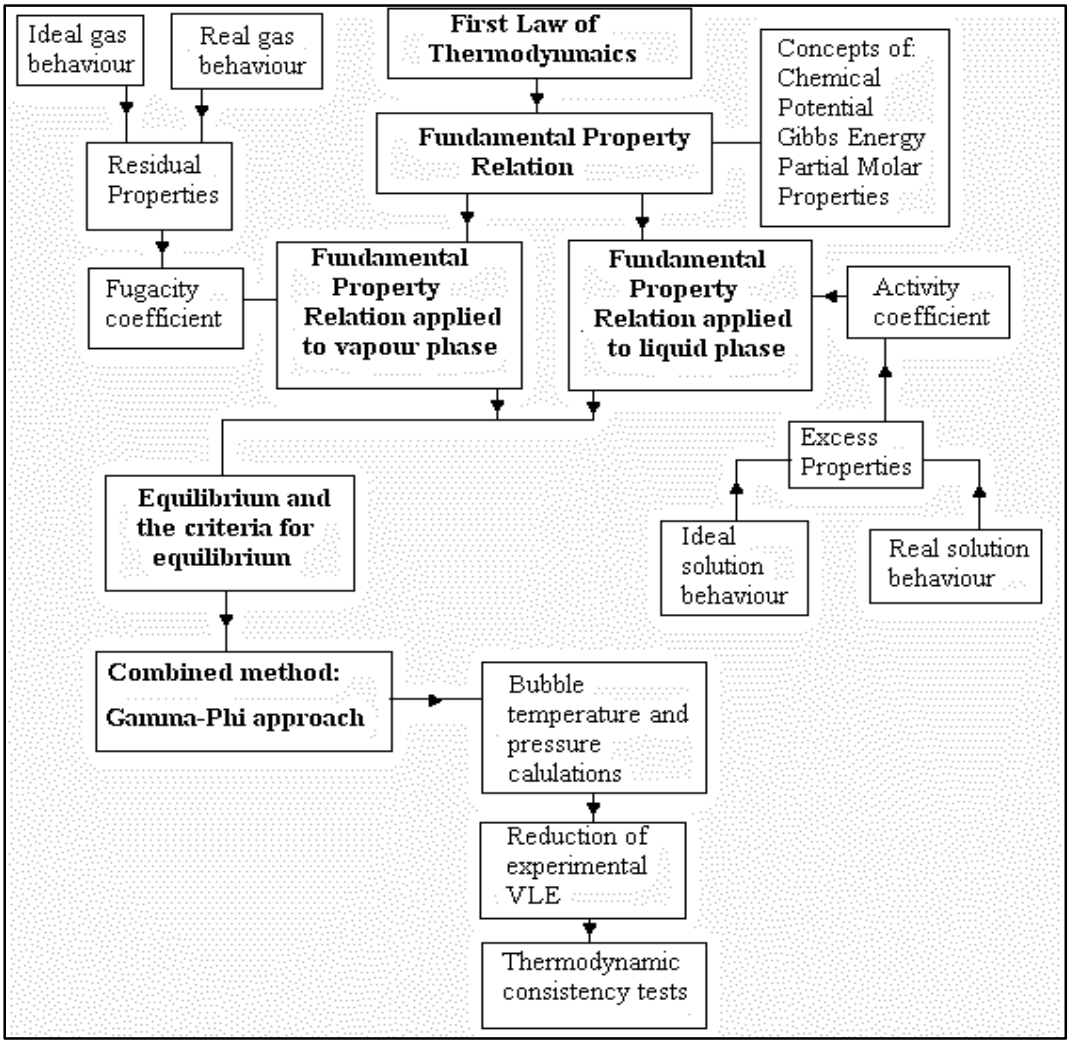

Figure 2-1: An Overview of Thermodynamics for Phase Equilibria (Bownath, 2008)

2.2. Phase Equilibrium Behaviour Exhibited in Plots

A fundamental operative of experimental measurements and data reduction in solution chemical thermodynamics is to represent phase equilibrium behaviour of systems in the form of phase diagrams. Differentiating equilibrium behaviours can be observed from phase equilibrium plots for the different chemical systems measured.

These phase equilibrium diagrams assist engineers in the design and configuration of separation units such as decanters, distillation columns and azeotropic distillation columns. Sizing of a distillation column to separate two binary components of a mixture, using the McCabe-Thiele graphical method, is a major application of VLE diagrams that is used in industry for design purposes (Mqondisi, 2012).

Solution thermodynamics literature contains the myriad of phase equilibrium type diagrams illustrating the various system behaviours.

2.2.1. Vapour Liquid Equilibrium Phase Diagrams

The five types of phase diagram presented by Raal and Mühlbauer (1998) to categorize VLE behaviour of binary systems will be briefly expanded on in this section; with the first three types commonly experienced during experimentation shown in Figure 2-2.

Type I classifies intermediate-boiling systems or systems that exhibit boiling points which are in between those of pure components for all mixture compositions. For systems exhibiting homogenous azeotropes, types II and III are used for classification. Types II and III are known as minimum and maximum boiling homogenous azeotropes respectively. The region where both the liquid and vapour compositions are exactly the same is known as the azeotrope. This concept is realised by inspection of Figure 2-2(a) and (b) and noticing the difference in shape. Conventional distillation system cannot separate the binary system past azeotropic point, therefore other means can be utilised to eliminate or move the azeotrope. The addition of an entrainer or extractive solvent as a third component may be able to effectively eliminate the azeotrope. Gmehling and Onken have provided a phase data compilation for such systems (Gmehling and Onken, 1977-1982). The first three types are most commonly encountered and are displayed in Figure 2-2.

Types IV and V are classified as mixtures of (Mqondisi, 2012):

i. partial miscible liquid phase split, with a single heterogeneous azeotrope and
ii. partial liquid miscibility with both a homogenous and heterogeneous azeotrope respectively.

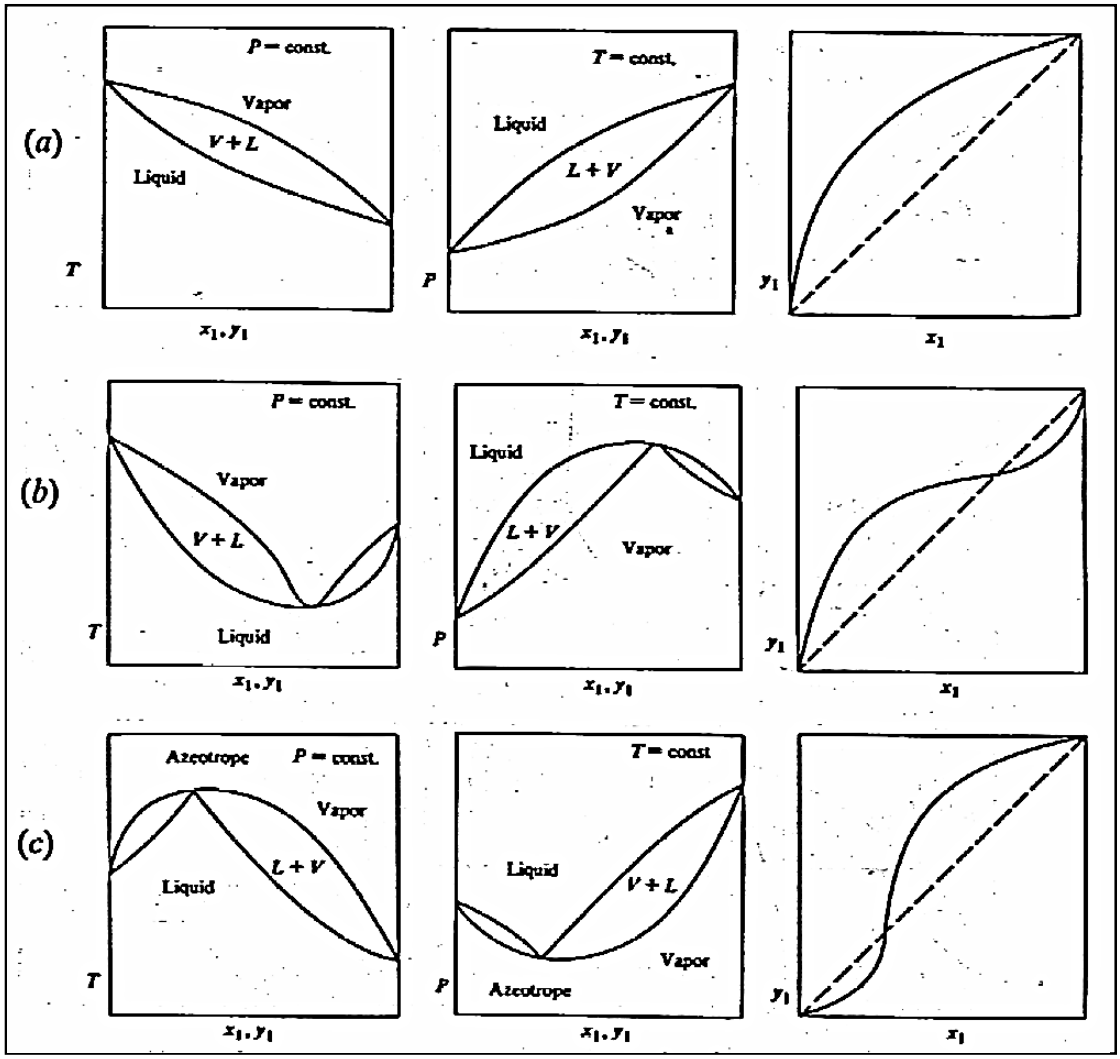

Figure 2-2: Common types of binary T-*x*-*y*, P-*x*-*y* and *x*-*y* phase equilibrium diagrams: (a) intermediate-boiling systems; (b) systems displaying a minimum boiling azeotrope; (c) systems displaying a maximum boiling azeotrope (Raal, 1998).

2.3. The Criterion for Phase Equilibrium

Model representation of phase diagrams is one of the main objectives in phase equilibria studies. However, understanding phase equilibrium principles through the fundamental definition of thermodynamic equilibrium leads to data treatment methods developed for the regression of VLE.

On a microscopic level, thermodynamic equilibrium can be defined as a stateof a system when it is static, in which no change occurs. When equilibrium is established, the chemical potentials of the system are balanced. The chemical potentials of a system bring about change. In isolated systems such as the VLE stills employed in this study, there is intimate contact between the liquid and vapour phases. The system reaches equilibrium when the temperature, pressure and chemical potential are the same in all phases, even when more heat is applied to the system after each run. The system, however, remains dynamic on a microscopic level though equilibrium is established.

Molecules of the liquid and vapour phase are constantly changing and can pass into the other phase with a high enough velocity by overcoming surface forces present. The rate at which these molecules cross the interface in both the directions is approximately equivalent. It is therefore assumed that the net mass transfer of molecules across the phase boundary is negligible (Sewpersad, 2012).

The molecules move in and out of the system with ease for the single-phase open system case. *nG* will therefore become dependent upon the number of moles (*n*) of chemical components (*i*) in the system. The Gibbs energy remains a function of temperature and pressure rendering the relationship:

$$nG = g(P, T, n_i) \tag{2-1}$$

$$d(nG) = \left[\frac{\partial(nG)}{\partial P}\right]_{T,n} dP + \left[\frac{\partial(nG)}{\partial T}\right]_{P,n} dT + \sum_i \left[\frac{\partial(nG)}{\partial n_i}\right]_{P,T,n_j} dn_i \tag{2-2}$$

The definition of the chemical potential of a species *i* in the mixture is:

$$\mu_i = \left[\frac{\partial(nG)}{\partial n_i}\right]_{P,T,n_j} \tag{2-3}$$

$$d(nG) = (nV)dP - (nS)dT + \sum_i \mu_i dn_i \tag{2-4}$$

Smith *et al*. (2001) describes equilibrium for multiple phases at the same temperature and pressure as the condition occurring when the chemical potential of each constituent species is the same in all phases. Using this concept, it can be shown that at equilibrium:

$$\mu_i^{\alpha} = \mu_i^{\beta} = ... = \mu_N^{\pi} \; (i = 1, 2, 3, \ldots\ldots, N) \tag{2-5}$$

2.4. Fugacity and Fugacity Coefficient

Gess *et al*. (1991), report that the thermodynamic relationship for a system becomes useful, if it is expressed in terms of quantities that can be measured experimentally (Gess et al., 1991). Fugacity is a property related to both chemical potential and experimental properties. Chemical potential is defined in terms of internal energy and entropy. These thermodynamic quantities are

immeasurable. Fugacity is a property related to chemical potential (at constant temperature) by the following equation:

$$\overline{G}_i = \Gamma_i(T) + RT \ln f_i \tag{2-6}$$

$$\overline{G_i} = \left[\frac{\partial(nG)}{\partial(n_i)} \right]_{T,P,n_j} \tag{2-7}$$

Taking into consideration the concept of fugacity for a closed system at equilibrium, all phases in equilibrium within the still are at constant temperature, hence giving:

$$f_i^{\alpha} = f_i^{\beta} = ... = f_i^{\pi} \ (i = 1, 2, 3, ..., N) \tag{2-8}$$

Also for species in solutions the fugacity of a species *i* is:

$$\hat{f}_i^{\alpha} = \hat{f}_i^{\beta} = ... = \hat{f}_i^{\pi} \tag{2-9}$$

Liquid and vapour phases can be taken into account in order to re-write equation (2-9) in the case of equilibrium where multi-component systems are involved:

$$\hat{f}_i^{L} = \hat{f}_i^{V} \quad (i=1, 2, ..., N) \tag{2-10}$$

2.4.1. Fugacity Coefficient

The dimensionless quantity called thefugacity coefficient can be defined as:

$$\phi_i = \frac{f_i}{P} \tag{2-11}$$

Characterization of the fugacity coefficient for a pure species ϕ_i can be extended to include the fugacity coefficient for species *i* in a solution, $\hat{\phi}_i$ (Van Ness et al., 2001). Fugacity of components in solution (or a mixture) can also be expressed for the liquid and vapor phase:

$$\hat{f}_i^{\,L} = x_i \gamma_i f_i \tag{2-12}$$

$$\hat{f}_i^{\,V} = \hat{\phi}_i y_i P \tag{2-13}$$

where γ_i = activity coefficient of species *i* in solution.

With a change of state occurring from saturated liquid to saturated vapour, giving the vapour phase and liquid phase at temperature *T*, along with the vapour pressure, $P^{saturated}$, the following expression is achieved:

$$f_i^{\,V} = f_i^{\,L} = f_i^{\,sat} \tag{2-14}$$

The corresponding fugacity coefficient therefore becomes:

$$\phi_i^{\,sat} = \frac{f_i^{\,sat}}{P_i^{sat}} \tag{2-15}$$

Subsequently: $\phi_i^{\,V} = \phi_i^{\,L}{}_i = \phi_i^{\,sat}$ (2-16)

For a species *i* in solution, at constant temperature and composition, the property relation for excess Gibbs energy, $dG = VdP - SdT$ becomes:

$$dG_i = V_i dP \tag{2-17}$$

Differentiation of Equation (2-6) leads to:

$$dG_i = RTd \ln f_i \tag{2-18}$$

By the equating equations (2-17) and (2-18) for the cancellation of dG_i, the following is achieved:

$$d \ln f_i = \frac{V_i}{RT} dP \tag{2-19}$$

By integrating (2.19) under isothermal conditions from an initial state of saturated liquid, to a

final state of compressed liquid at a pressure *P*, the following is obtained:

$$\ln \frac{f_i}{f_i^{sat}} = \frac{1}{RT} \int_{P_i^{sat}}^{P} V_i dP \tag{2-20}$$

Liquid-phase molar volume V_i^L, is minutely dependent on pressure *P* at temperatures much less than the critical temperature T_c. An accurate approximation in calculations is obtained when V_i^L is assumed constant at the particular value for saturated liquid (Sewpersad, 2012). Therefore, taking the effects of pressure to be negligible, equation (2-20) becomes:

$$\ln \frac{f_i}{f_i^{sat}} = \frac{V_i^l \left(P - P_i^{sat}\right)}{RT} \tag{2-21}$$

By substitution of equation (2-15) into (2-21) and solving for f_i :

$$f_i = \phi_i^{sat} P_i^{sat} \exp\left[\frac{V_i^l \left(P - P_i^{sat}\right)}{RT}\right] \tag{2-22}$$

The exponential term is known as the *Poynting factor*. This allows for the correction of liquid phase fugacity from vapour pressure to system pressure (Narasigadu, 2006). The Poynting factor is small at low pressures but increases at higher pressures. Smith et al. (2001) report the assumption that the Poynting factor differs from unity by only a few parts per thousand at low to moderate pressures, therefore its omission introduces negligible error. According to Prausnitz et al. (1980), this is acceptable for non-polar molecules at low pressure, but becomes irrational regarding mixtures having polar or associating molecules (Prausnitz et al., 1980).

By combining (2-12) and (2-13) and solving for f_i we obtain*:*

$$y_i \Phi_i P = x_i \gamma_i P_i^{sat} \tag{2-23}$$

with: $$\Phi_i = \frac{\hat{\phi}_i}{\phi_i^{sat}} \tag{2-24}$$

Substituting (2-23) in (2-22) will yield:

$$\Phi_i = \frac{\hat{\phi}_i}{\phi_i^{sat}} \exp\left[\frac{-V_i^l\left(P - P_i^{sat}\right)}{RT}\right] \tag{2-25}$$

The saturated liquid molar volume, V_i^l may be evaluated using the Rackett (1970) equation:

$$V_i = (V_c)_i (Z_c)_i^{[1-(T_r)_i]^{0.285}} \tag{2-26}$$

where:

V_c= critical molar volume

Z_c= compressibility factor

$(T_r)_i$= reduced temperature defined as $(T_r)_i = \frac{T}{(T_c)_i}$

T_c= critical temperature of component *i*

Liquid and vapour phases during equilibrium become related by the general equation (2-23). In an ideal system, an ideal gas represents the vapour phase. An ideal solution represents the liquid phase. In a system such as this, the VLE relation in its simplest form is shown. This is known as Raoult's Law (Van Ness et al., 2001). Raoult's Law is obtained from (2-25) by setting both Φ and γ to the value of one (Narasigadu, 2006).

2.4.2. Calculation of Fugacity Coefficient from the Virial Equation of State

From the various methods for determining the fugacity coefficients of species in gas mixtures, the virial Equation of State (EOS) uses sound theoretical basis in statistical mechanics. It is represented by the Taylor series expansion, consequently rendering it impractical to realistic cases. Therefore, at low pressures, the coefficients may be evaluated by presuming that the vapour phase is described by the truncated (at the second term), generalized, pressure explicit form of the virial EOS (Clifford, 2004). The virial equation adequately describes the vapour phase for a system at low pressure and is also sufficient to consider the two term viral EOS (Perry et al., 1998). The equation is defined as:

$$Z = 1 + \frac{BP}{RT} \tag{2-27}$$

where:

Z = Compressibility factor which equals $\frac{PV}{RT}$

B = Second virial coefficient

In a mixture, the second Virial coefficient, *B*, is a function of composition and temperature and is evaluated by the application of statistical mechanics:

$$B_{mixture} = \sum_i \sum_j y_i y_j B_{ij} \tag{2-28}$$

where*:*

i, j=component species

y= mole fractions of species in the gas mixture

B_{ij}= cross virial coefficient

B_{ij}= bimolecular interaction between molecules *i* and *j*; hence $B_{ij}= B_{ji}$

Equation (2-28) expands to the following for a binary mixture:

$$B_{mixture} = y_1^2 B_{11} + 2y_1 y_2 B_{12} + y_2^2 B_{22} \tag{2-29}$$

where B_{11} and B_{22} are the mixture and pure species virial coefficients respectively, with B_{12} as the mixture cross coefficient. These terms are temperature dependent only. The mixture coefficients to pure species and cross coefficients are congruent via equations (2-28) and (2-29). As a result these then become known as **mixing rules** (Sewpersad, 2012). When the truncated virial EOS is used to describe non-ideality in the vapour phase, the fugacity coefficient Φ_i of Equation (2-25) becomes modified to:

$$\Phi_i = \exp\left[\frac{\left(B_{ii} - V_i^l\right)\left(P - P_i^{sat}\right) + P y_j^2 \delta_{ij}}{RT}\right] \tag{2-30}$$

$$\text{with} \qquad \delta_{ji} = 2B_{ji} - B_{jj} - B_{ii} \tag{2-31}$$

Second virial coefficients for pure components, B_{ii}, and mixtures, B_{ij} can be determined experimentally utilising compilations available in literature. The second virial coefficients are available in compilations such as Dymond and Smith (Dymond and Smith, 1980) and Cholinski *et al*. (Choliński et al., 1986).

It is often impossible to obtain experimental values for the species of interest, with B_{ij} generally presenting the greatest difficulty at the necessary temperature. Hence, it is essential to use an appropriate correlation to determine the second virial coefficients. The correlations that are available for the determination of second virial coefficients are:

- (Black, 1958),
- O'Connell and Prausnitz (1967),
- Nothnagel *et al.* (1973),
- Tsonopoulos (1974) and
- Hayden and O'Connell (1975).

Some of the correlations that have found widespread popularity due to their versatility, and those used in this study, are discussed below.

2.4.2.1. The Nothnagel (NTH) formulation

The method proposed by Nothnagel et al. (Nothnagel et al., 1973) for determining fugacity coefficients, is based on a chemical theory of imperfections. The ideal gas law is the bases for the Nothnagel EOS. It incorporates a volume exclusion term due to the finite size of the molecules in compound mixtures. The ideal gas law is expressed as follows:

$$P = \frac{RT}{V_m - b} \tag{2-32}$$

The term V_m is the molar volume of the mixture (calculated by the total volume divided by true total number of moles). Term b is the molar excluded volume due to the finite size of molecules:

$$b = \sum y_i b_i + \sum_i \sum_j y_{ij} b_{ij} \tag{2-33}$$

where:

$$b_{ij} = \frac{\left(b_i^{0.33} + b_j^{0.33}\right)^3}{8} \tag{2-34}$$

Chemical theory assumes that reversible dimerization reactions occur in the vapour phase (for low to moderate pressures):

$$2A_1 \xleftrightarrow{K_A} A_2 \tag{2-35}$$

$$2B_1 \xleftrightarrow{K_B} B_2 \tag{2-36}$$

A_1 and B_1 represent the species in the mixture including the monomers that are present. The dimers are A_2 and B_2. The chemical equilibrium constants, K_A and K_B, represent the formation of the dimers from the monomers. They are expressed on a pressure basis as follows:

$$K_A = \frac{Z_{A_2}\varphi_{A_2}}{Z^2{}_{A_1} P \varphi_{A_1^2}} \tag{2-37}$$

$$K_B = \frac{Z_{B_2}\varphi_{B_2}}{Z^2{}_{B_1} P \varphi_{B_1^2}} \tag{2-38}$$

Here:

P = total system pressure;

z_i (where i $\rightarrow A_1, A_2, B_1, B_2$) = the "true species" mole fractions in the vapour phase

φ_i = the "true species" fugacity coefficient of component *i*.

The total number of moles is dependent on the equilibrium constant and the pressure. Nothnagel et al. (1973) suggest that ϕ_i can be calculated from the equation below (Pillay, 2010):

$$\phi_i = \frac{z_i \varphi_i}{y_i} \tag{2-39}$$

Here y_i is the apparent vapour phase mole fraction of species i and the true species fugacity coefficients can be obtained from the following (Nothnagel et al., 1973):

$$\varphi_i = \exp\frac{b_i P}{RT} \tag{2-40}$$

The equilibrium constant is calculated from the pure component dimerization constants for association between two different components (cross association or hetero-dimerization) from the equation below (Prausnitz, 1969):

$$K_{ij} = 2\sqrt{K_i K_j} \tag{2-41}$$

where:

$$K_i = A_i + \frac{B_i}{T} \tag{2-42}$$

The K_i values here are assumed to be temperature dependent. Equation (2-32) can now be re-written as the following:

$$Z = \frac{PV_m}{RT} = 1 + \frac{Pb}{RT} \tag{2-43}$$

Equation (2-43) is similar to the virial EOS stated above. Several authors, including Nothnagel et al., 1973, have illustrated that the chemical theory of gas imperfections can lead to an EOS of the virial form. This occurs within the limit where the fraction of molecules dimerized reaches zero (Pillay, 2010).

2.4.2.2. The Hayden-O'Connell Correlation (HOC)

Hayden and O'Connell (Hayden and O'Connell, 1975) developed a method that is well-accepted for evaluation of second virial coefficients. The method covers a large range of compounds including associating, nonpolar and polar compounds.

The correlation was developed based on intermolecular interactions existing between molecule pairs. The HOC formulation incorporates the chemical theory of dimerization and accounts for

strong association and solvation effects that include those found in systems with organic acids (Pillay, 2010). This is accomplished by using a parameter which is dependent on the group interaction only (Hayden and O'Connell, 1975).

The calculation procedure is given in detail in Appendix A of Prausnitz *et al*. (Prausnitz et al., 1980) and the publication of Hayden and O'Connell (1975). The total second virial coefficient can be considered the sum of several individual contributions:

$$B_{ij}(T) = (B_{free})_{ij} + (B_{metastable})_{ij} + (B_{bound})_{ij} + (B_{chem})_{ij} \quad (2\text{-}44)$$

where:

$(B_{free})_{ij}$ = contributions by free pairs of non-association molecules and non-polar

$(B_{metastable})_{ij}$ = facilitates for metastable bound molecular pairs

$(B_{bound})_{ij}$ = types of interactions between pairs of molecules as a result of potential energy and the distance between the centre of molecules; also physically strongly bound pairs of molecules

$(B_{chem})_{ij}$ = chemical bonds of molecules

The parameters involved in calculations are Thompson's mean radius of gyration R_d or the parachor, critical pressure P_c, critical temperature T_c, solvation and association parameters η, and dipole moment, μ, (Hayden and O'Connell, 1975). These are found in literature resources such as Fredenslund (Fredenslund, 1977) *et al.,* (1977), Prausnitz *et al.* (1980), Reid *et al.* (1988), and the Dortmund Data Bank (DDB, 2011).

The dipole moments may be obtained from the method by Smyth (Smyth, 1955) or the extensive compilation of McClellan (McClellan, 1963-1974). The mean radius of gyration is evaluated using the parameter parachor, P'. This is computed from a group contribution method by Reid (Reid et al., 1988). Harlacher and Braun state that the radius of gyration and parachor factor, are related by the following equation (Harlacher and Braun, 1970):

$$P' = 50 + 7.6R_d + 13.75R_d^2 \quad (2\text{-}45)$$

Once the parachor factor for each species is computed, the mean radius of gyration, R_d, is obtained by the following equation (Hayden and O'Connell, 1975):

$$R_d = -0.2764 + 0.2697\sqrt{P' - 48.95} \quad (2\text{-}46)$$

The positive real root is the mean radius of gyration (Mqondisi, 2012). Salvation and association parameters are obtained from tables within the publication of Prausnitz *et al.* (1980). Should the system under investigation not be available in the tables, Prausnitz *et al.* (1980) suggests that the values of a similar chemical system be used. If certain parameters are not available in the Prausnitz *et al*., (1980) publication, Fredenslund *et al.* (Fredenslund et al., 1977) suggest that the association and solvation parameters for pure halogenated alkanes, sulphides, ethers and hydrocarbons be set to a value of zero.

2.4.3. Fugacity Coefficients from Cubic Equations of State

Cubic equations of state (EOS) can also be used to evaluate fugacity coefficients and are capable of accurately describing both liquid and vapor phase behavior. The first development of an actual application based EOS was made by J.D. van der Waals (Van der Waals and van der Waals, 1873). This EOS was a simple and generalized semi-empirical EOS, facilitating for the behaviour of fluids both above and below the critical point (Narasigadu, 2006).

The parameters in the van der Waals (1873) equation were not temperature dependent. This therefore, made its application more favourable to describe highly non-ideal systems (Anderko, 1990). Fortunately, successfully recognised modifications (to this day) were developed for the aforementioned limitation of van der Waals (1873), by Redlich and Kwong (Redlich and Kwong, 1949) and Soave (Soave, 1972). Peng and Robinson (Peng and Robinson, 1976) had also proposed a modification that was found widely acceptable. These equations of state have been the most popular and successfully applied models for the representation of thermodynamic, and phase equilibrium properties of both pure components and mixtures (Twu et al., 1998, Ghosh, 1999, Valderrama, 2003).

Anderko (Anderko, 1990), suggest that if a suitable mixing rule is employed in conjunction with these equations of state, then systems that exhibit high levels of non-ideality can be accurately described. Two such mixing rules will be discussed later on this this chapter.

2.4.3.1. The Soave-Redlich-Kwong (SRK) Cubic Equation of State

There are still some shortcomings which the modifications of Redlich and Kwong (1949) according to Peng and Robinson (1976). The most evident, is the failure to supply an efficient representation for liquid phase non-ideality. Soave (1972), therefore, modified this equation by proposing:

$$P = \frac{RT}{V-b} - \frac{a(T,\omega)}{V(V+b)} \tag{2-47}$$

Constant *a*, relates to the intermolecular force of attraction between molecules and is temperature dependent. The constant *b* is for the molecular size of the molecule, and is independent of temperature. Both constants are determined from the following equations:

$$a\ (T,\omega) = a_c \alpha\ (T,\omega) \tag{2-48}$$

where:

$$a_c = 0.42747\left(\frac{R^2 T_c^2}{P_c}\right) \tag{2-49}$$

$$b = 0.08664\left(\frac{RT_c}{P_c}\right) \tag{2-50}$$

$$\alpha(T,\omega) = \left[1+\kappa\left(1-T_r^{0.5}\right)\right]^2 \tag{2-51}$$

The parameter κ is a constant characteristic of each component. A correlation proposed by Soave (1972) of this constant with respect to the acentric factor is as follows:

$$\kappa = 0.480 + 1.574\omega - 0.176\omega^2 \tag{2-52}$$

For reasons pertaining to the assisting in computational calculations, equation (2-47) may be expressed in terms of the compressibility factor (*Z*) for a mixture as:

$$Z^3 - Z^2 + Z(A - B - B^2) - AB = 0 \tag{2-53}$$

where:

$$A = \frac{aP}{R^2T^2} \tag{2-54}$$

$$B = \frac{bP}{RT} \tag{2-55}$$

For a binary system, the largest real root of equation (2-53) corresponds to the vapour phase compressibility factor. The smallest real root corresponds to that of the liquid phase compressibility factor. The fugacity coefficient for a pure component is as follows:

$$\ln\phi = Z - 1 - \ln(Z - B) - \frac{A}{B}\ln\left[\frac{Z + B}{Z}\right] \tag{2-56}$$

The SRK EOS provides a more feasible calculation method of vapour pressures. It is applicable for several hydrocarbons and correlation of VLE behaviour for systems consisting of non-polar and slightly polar fluids compared to the Redlich-Kwong EOS (Narasigadu, 2011).

Soave (Soave, 1993) had modified the temperature dependence for the attraction term in the SRK EOS for the incorporation of polar and non-polar fluids for improving vapour pressure calculations. However, Peng and Robinson (1976) report, that the calculation of liquid phase specific volume with the SRK EOS, is significantly higher than the literature values (by approximately 27 %).

2.4.3.2. The Peng Robinson (PR) Cubic Equation of State

Peng and Robinson (1976), state that there are still some shortcomings which the modifications of Redlich and Kwong (1949) and Soave (1972) have in common. The most evident, is the failure to supply efficient representative values for liquid density. The improvement of the accuracy of the equation situated near the critical point was also of interest (Peng and Robinson, 1976); therefore the following equation is proposed:

$$P = \frac{RT}{V-b} - \frac{a(T,\omega)}{V(V+b)+b(V-b)} \tag{2-57}$$

The constants *a* and *b* are similarly described for the SRK EOS. Both constants however, are determined differently for the PR EOS by the following equations:

$$a_i(T,\omega) = a_{c\,i}\alpha_{\ i}(T,\omega) \tag{2-58}$$

$$b_i(T) = b_i(T_c)_i \tag{2-59}$$

where:

$$a_{c\,i} = 0.45724\left(\frac{R^2 T_{c_i}^{\ 2}}{P_{c_i}}\right) \tag{2-60}$$

$$b_i = 0.07780\left(\frac{RT_{c_i}}{P_{c_i}}\right) \tag{2-61}$$

$$a_i\{(T_c)_i;\omega_i\} = \left[1+\kappa_i\left(1-(T_r)_i^{0.5}\right)\right]^2 \tag{2-62}$$

$$\kappa_i = 0.37464 + 1.54226\omega_i - 0.26992\omega_i^{\ 2} \tag{2-63}$$

The relation in terms of the compressibility factor (*Z*) for equation (2-57) is:

$$Z^3 - (1-B)Z^2 + (A-3B^2-2B)Z - (AB-B^2-B^3) = 0 \tag{2-64}$$

where:

$$A = \frac{a_m(T)P}{R^2T^2} \tag{2-65}$$

$$B = \frac{b_m P}{RT} \tag{2-66}$$

Expressions a_m and b_m from are obtained from mixing rules (discussed in section 2.4.4. of this chapter). The PR EOS uses following mixing rules, which were implemented by Soave (1972), and also used for the SRK EOS in the same manner:

$$a_m = \sum_i \sum_j x_i x_j a_{ij} \tag{2-67}$$

$$a_{ij} = (1-\delta_{ij})(a_i a_j)^{0.5} \tag{2-68}$$

$$b_m = \sum_i x_i b_i \tag{2-69}$$

where δ_{ij} is the binary interaction parameter (with $\delta_{ij}= \delta_{ji}$). It is unique to every binary system and can be obtained from the regression of experimental VLE data.

In a similar manner (to that of the SRK EOS), the largest and smallest real roots of equation (2-64) correspond to the vapour and liquid compressibility factor respectively. The expression for the fugacity coefficient of a pure component becomes:

$$\ln\phi = (Z-1) - \ln(Z-B) - \frac{A}{2\sqrt{2}B}\ln\left[\frac{Z+(1+\sqrt{2})B}{Z+(1-\sqrt{2})B}\right] \tag{2-70}$$

The SRK and PR Cubic EOS are still widely used in the petroleum industry as the models of choice as they require only critical properties and acentric parameters as input information for the generalised parameters. Short iteration computation times during result in reasonable VLE

predictions for hydrocarbon systems. Its simplified fluid theory however, may not be able to address new molecular interactions brought upon by oxygenated biofuel components (Soo, 2011). A detailed review outlining the shortcomings of the traditional forms of cubic EOS can be found in the literature sources Abbott (1979) and Martin (1979) (Abbott, 1979, Martin, 1979).

2.4.3.3. The Alpha Correlation of Mathias and Copeman

The vapour pressure of the pure components including the properties of the mixture must be accurately predicted in order for a cubic EOS to accurately correlate the phase equilibrium data of mixtures (Twu et al., 1991). The alpha (α) function (the temperature dependent *attraction* term), greatly contributes to the prediction of accurate vapour pressure. In turn, the mixing rule employed significantly influences the mixture properties.

An α-function possessing adjustable parameters that are expressed in the form of a series was proposed by Mathias and Copeman (Mathias and Copeman, 1983). It can be used in any cubic EOS and various researchers (Kang et al., 2002, Valtz et al., 2002, Horstmann et al., 2005), have discovered that truncating the series to only three adjustable parameters was sufficient for obtaining accurate results. Using the three adjustable parameters subjects the α-function to becoming more flexible, with respect to these parameters being found from the reduction of experimental vapour pressure data (Narasigadu, 2011). The Mathias and Copeman (1983) α-function is expressed as:

$$a_i\left\{\left(T_c\right)_i;\omega_i\right\}=\left\{\left[1+\kappa_1\left(1-T_{ri}^{\frac{1}{2}}\right)+\kappa_2\left(1-T_{ri}^{\frac{1}{2}}\right)^2+\kappa_3\left(1-T_{ri}^{\frac{1}{2}}\right)^3\right]\right\}^2 \qquad (2\text{-}71)$$

The adjustable parameters differ from one EOS to the next because the α-function can be applied to any EOS. κ_1, κ_2 and κ_3 are the adjustable parameters. They are unique to each component and are determined from regressing measured vapour pressure data.

2.4.4. Mixing Rules for Cubic Equations of State

Mixing rules are used for the characterization of interactions occurring between molecules in a mixture when using an EOS to correlate VLE data. Mixing rules are essential in the implementation of EOS for acquiring the accurate representation of phase equilibrium data of a mixture, by determining the a_m and b_m parameters (described above) used in the cubic EOS.

There are numerous types of mixing rules with different classifications available for use. Raal and Mühlbauer (1998) provide a detailed review of these mixing rules, many of which exhibit an empirical nature. The mixing rules used by Soave (1972) and Peng and Robinson (1976), Stryjek and Vera (Stryjek and Vera, 1986), known as the van der Waals one-fluid-theory classical mixing rules, are the simplest known and shown above from equations (2-67) to (2-69) . Extrapolation of many mixing rules to multi-component mixtures becomes incoherent due to the invariance problem and the dilution effect (Hernández-Garduza et al., 2001). Michelsen and Kistenmacher report these inefficiencies in their trials as Michelsen Kistenmacher-Syndrome (Michelsen and Kistenmacher, 1990).

The Wong-Sandler (Wong and Sandler, 1992) and Twu-Coon (Twu and Coon, 1996) mixing rules do not succumb to the Michelsen-Kistenmacher-Syndrome shortcomings, and have consequently been used in this study and will be further discussed in this chapter.

2.4.4.1. The Wong-Sandler Mixing Rule

According to Wong and Sandler (1992), this mixing rule is applicable to both simple and complex systems that are comprised of polar and associating species (Wong and Sandler, 1992). Use of this mixing rule is therefore invaluable due to the type of systems investigated in this study. The Wong and Sandler (1992) mixing rule is density independent (developed for cubic equations of state).

It requires an *activity coefficient model* (described in 2.5) which is used to calculate the excess Helmholtz free energy (A^E), a useful thermodynamic property like that of the excess Gibbs free energy (Narasigadu, 2006). The Wong and Sandler (1992) mixing rule is widely successful and applied to equations of state because the quadratic composition dependence of the second virial coefficient, which maintains consistency with statistical mechanics (Raal and Muhlbauer, 1998), is combined with the excess Gibbs free energy (G^E) models.

At infinite pressure, Helmholtz free energy, allows the calculation of the correct low and high densities without becoming dependent upon density (Sewpersad, 2012). The Wong and Sandler (1992) mixing rule states the mixture parameters a_m and b_m as:

$$\frac{a_m}{RT} = \frac{QD}{(1-D)} \tag{2-72}$$

$$b_m = \frac{Q}{(1-D)} \tag{2-73}$$

where:

m = mixture properties

and:

$$Q = \sum_i \sum_j x_i x_j \left(b - \frac{a}{RT} \right)_{ij} \tag{2-74}$$

$$D = \sum_i x \frac{a_i}{b_i RT} + \frac{A_\infty{}^E}{cRT} \tag{2-75}$$

The fugacity coefficient for both the liquid and vapour phases is determined as follows:

Soave-Redlich-Kwong EOS (Naidoo, 2004):

$$\ln \hat{\phi}_i = -\ln\left[\frac{P(V-b_m)}{RT}\right] + \frac{1}{b_m}\left(\frac{\partial n b_m}{\partial n_i}\right)\left(\frac{PV}{RT}-1\right) + \left(\frac{a_m}{b_m RT}\right)\left[\frac{1}{a_m}\left(\frac{1}{n}\frac{\partial n^2 a_m}{\partial n_i}\right) - \frac{1}{b_m}\frac{\partial n b_m}{\partial n_i}\right]\ln\left[\frac{V}{V+b_m}\right] \tag{2-76}$$

$$c = -\ln(2) \tag{2-77}$$

Peng-Robinson EOS (Naidoo, 2004):

$$\ln \hat{\phi}_i = -\ln\left[\frac{P(V-b_m)}{RT}\right] + \frac{1}{b_m}\left(\frac{\partial n b_m}{\partial n_i}\right)\left(\frac{PV}{RT}-1\right) + \frac{1}{2\sqrt{2}}\left(\frac{a_m}{b_m RT}\right)\left[\frac{1}{a_m}\left(\frac{1}{n}\frac{\partial n^2 a_m}{\partial n_i}\right) - \frac{1}{b_m}\frac{\partial n b_m}{\partial n_i}\right]\ln\left[\frac{V+(1-\sqrt{2})b_m}{V+(1+\sqrt{2})b_m}\right] \tag{2-78}$$

$$c = \frac{1}{\sqrt{2}}\ln\left(\sqrt{2}-1\right) \tag{2-79}$$

Further information pertaining to the partial differentials required for evaluation of the fugacity coefficient can be found in Appendix E.

At infinite dilution the activity coefficient is:

$$\ln \gamma_i^{\infty} = \frac{1}{RT} \frac{\partial n A_{\infty}^{E}}{dn_i} \tag{2-80}$$

Wong and Sandler (1992), state that the excess Helmholtz free energy is significantly less pressure dependent than the excess Gibbs free energy. Greater accuracy in results, is therefore, obtained at very low and infinite pressures.

At very low pressures, A^E is weakly dependent upon pressure and its value at infinite pressure is equivalent to that of G^E (Satyro and Trebble, 1998). Taking this into account, low pressure vapour-liquid equilibrium data can be utilized to predict VLE data at higher pressures. Raal and Mühlbauer (1998) further postulate that excess Helmholtz free energy and excess Gibbs free energy are interchangeable at constant temperature.

The NRTL activity coefficient model was used in this research project to describe A^E at infinite pressure, as well as the activity coefficient at infinite dilution:

$$\frac{A_{\infty}^{e}}{RT} = \sum_i x_i \left(\frac{\sum_j x_j \tau_{ji} g_{ji}}{\sum_k x_k g_{ki}} \right) \tag{2-81}$$

$$\ln \gamma_i^{\infty} = \frac{\sum_j x_j \tau_{ji} g_{ji}}{\sum_k x_k g_{ki}} + \sum_j \frac{x_j g_{ij}}{\sum_k x_k g_{kj}} \left(\tau_{ij} - \frac{\sum_l x_l \tau_{lj} g_{lj}}{\sum_k x_k g_{ki}} \right) \tag{2-82}$$

2.4.4.2. The Twu-Coon Mixing Rule

Twu and Coon (1996) developed new mixing rules dependant on temperature and composition only and were developed for cubic equations of state. They were applied successfully to complex mixtures, both polar and non-polar, containing hydrocarbons and inorganic gases, including industrial gases.

The Twu and Coon (1996) mixing rule is suited for highly non-ideal systems and is based on the

Wong-Sandler (1992) mixing rule, though more flexible in application. It incorporates all the advantageous features of the Wong-Sandler mixing rule without being hindered by the shortcomings associated with it. When the non-random excess Helmholtz free energy approaches zero, the Twu-Coon (1996) mixing rule will simplify to the van der Waals one-fluid mixing rule. However, a singularity problem was encountered at supercritical conditions with the conventional Wong-Sandler mixing rule.

The parameter b^* in the Twu-Coon (1996) mixing rule is described as:

$$b^* = \frac{b_{vdw} - a_{vdw}}{\left(\frac{a_{vdw}}{b_{vdw}} + \frac{1}{c} \frac{A_\infty^E}{RT} \right)} \tag{2-83}$$

with parameter a^* defined as:

$$a^* = b^* \left(\frac{a_{vdw}}{b_{vdw}} + \frac{1}{c} \frac{A_\infty^E}{RT} \right) \tag{2-84}$$

The a_{vdw} and b_{vdw} parameters according to the van der Waals mixing rule are:

$$a_{vdw} = \sum_i \sum_j x_i x_j \sqrt{a_i a_j} \left(1 - k_{ij}\right) \tag{2-85}$$

$$b_{vdw} = \sum_i \sum_j x_i x_j \left[\frac{1}{2} \left(b_i + b_j\right) \right] \left(1 - l_{ij}\right) \tag{2-86}$$

Parameters $\boldsymbol{a}^*$ and $\boldsymbol{b}^*$ are evaluated as follows (Sewpersad, 2012):

$$a^* = \frac{aP}{R^2 T^2} \tag{2-87}$$

$$b^* = \frac{bP}{RT} \tag{2-88}$$

The fugacity coefficient expressions for both liquid and vapour phases are represented below as:

Peng-Robinson Equation of State (Naidoo, 2004):

$$\ln\hat{\phi}_i = -\ln\left[\frac{PV}{RT} - b^*\right] + \frac{1}{b}\left(\frac{\partial nb}{\partial n_i}\right)\left(\frac{PV}{RT} - 1\right) - \frac{1}{2\sqrt{2}}\left(\frac{a^*}{b^*}\right)\left[\frac{1}{b}\frac{\partial nb}{\partial n_i} - \left(\frac{1}{na}\frac{\partial n^2 a}{\partial n_i}\right)\right]\ln\left[\frac{V + (1-\sqrt{2})b^*}{V + (1+\sqrt{2})b^*}\right] \quad (2\text{-}89)$$

Soave-Redlich-Kwong Equation of state (Naidoo, 2004):

$$\ln\hat{\phi}_i = -\ln\left[\frac{PV}{RT} - b^*\right] + \frac{1}{b}\left(\frac{\partial nb}{\partial n_i}\right)\left(\frac{PV}{RT} - 1\right) + \left(\frac{a^*}{b^*}\right)\left[\frac{1}{b}\frac{\partial nb}{\partial n_i} - \left(\frac{1}{na}\frac{\partial n^2 a}{\partial n_i}\right)\right]\ln\left[\frac{V + b^*}{V}\right] \quad (2\text{-}90)$$

The parameters *Q* and *D* are defined as follows:

$$Q = b_{vdw} - \frac{a_{vdw}}{RT} \quad (2\text{-}91)$$

$$D = \frac{a_{vdw}}{b_{vdw}} + \frac{1}{c}\frac{A_{\infty}^{E}}{RT} \quad (2\text{-}92)$$

The Twu and Coon (1996) mixing rule could have been used as a good alternative in this project should the Wong-Sandler (1992) mixing rule have rendered poor correlation results.

2.5. Activity Coefficient

The activity coefficient concept was introduced to account for deviation from ideality (i.e. an ideal solution) with respect to the liquid phase during phase equilibrium calculations. Deviations from ideality are quantified using excess functions. Detailing the standard state fugacity formulates the basis for defining the activity coefficient model. The activity coefficient in solution for a component *i* is:

$$\gamma_i = \frac{\hat{f}_i}{x_i f_i^o} \tag{2-93}$$

The Gibbs/Duhem equation in terms of activity as follows:

$$d\left(\frac{nG^E}{RT}\right) = \frac{nV^E}{RT}dP - \frac{nH^E}{RT^2}dT + \sum_i \ln\gamma_i dn_i \tag{2-94}$$

For full details on the following derivation, refer to Appendix F; by substituting equation (F-02) in (F-03), the summability relationship may then be simplified to be expressed in terms of the excess properties as follows:

$$\sum_i x_i \, d\ln\gamma_i = \frac{\overline{V}^E}{RT}dP - \frac{\overline{H}^E}{RT^2}dT \tag{2-95}$$

At the physical conditions of constant temperature and pressure, equation (2.84) reduces to:

$$\sum_i x_i \, d\ln\gamma_i = 0 \tag{2-96}$$

2.5.1. Excess Gibbs energy models and the Activity Coefficient

An excess Gibbs energy expression must be determined in order to evaluate the activity coefficient. Amidst multitude of models available for the description of liquid phase non- ideality, the application of more complex modeling is warranted by varying systems behavior, the components chemical nature and molecular size. The most common liquid activity coefficient models used for description of liquid phase imperfections include; Van Laar, Wilson and TK Wilson, NRTL and UNIQUAC. Of the models proposed, those implemented in this investigation are:

- Wilson
- Non-Random Two Liquid (NRTL)
- Universal Quasi-Chemical Theory (UNIQUAC)

A brief discussion of each of the above will be discussed for the case of binary mixtures only. Binary parameters are required to evaluate multi-component VLE in many cases. For isothermal measurements (performed primarily in this study), the models represent the excess Gibbs energy as a function of pressure and composition. The effect of pressure may be ignored (at no expense of accuracy) for low pressure measurement VLE (Prausnitz et al., 1986). The models have adjustable parameters (determined from experimental isothermal VLE data) which may be temperature dependant and/or temperature independent (Soni, 2003).

2.5.1.1. The Wilson Equation

Wilson (1964) developed an activity coefficient model by considering local composition (as opposed to overall liquid composition) occurring in liquid solution (Wilson, 1964). Local composition is presumed to account for the short-range order and non-random molecular orientations that result from differences in molecular size and intermolecular forces according to (Van Ness and Abbott, 1997).

The Wilson equation can provide a good representation for a variety of miscible mixtures. It is specifically most suitably inclined toward solutions containing polar or associating components in non-polar solvents (Prausnitz et al., 1999). The model contains two adjustable parameters, (λ_{12}-λ_{11}) and (λ_{21}-λ_{22}), with the temperature dependence of these adjustable parameters taken into consideration for accurate phase equilibrium computations (Moodley, 2009). Furthermore, the Wilson model can be readily extended to multi-component systems with parameters evaluated from the constituent binary systems. It cannot however, be applied for predicting liquid immiscibility or extrema in the activity coefficients (Prausnitz et al., 1986).

The detailed derivation of the Wilson equation is given by Prausnitz *et al*. (1986). The excess Gibbs energy for the Wilson model for a binary system is expressed as:

$$\frac{G^E}{RT} = -x_1 \ln\left(x_1 + \Lambda_{12} x_2\right) - x_2 \left(x_1 \Lambda_{21} + x_2\right) \tag{2-97}$$

The corresponding equations that allow calculation of the activity coefficients are:

$$\ln \gamma_1 = -\ln\left(x_1 + \Lambda_{12} x_2\right) + x_2 \left[\frac{\Lambda_{12}}{x_1 + \Lambda_{12} x_2} - \frac{\Lambda_{21}}{\Lambda_{21} x_1 + x_2} \right] \tag{2-98}$$

$$\ln \gamma_2 = -\ln\left(x_2 + \Lambda_{21} x_1\right) - x_1 \left[\frac{\Lambda_{12}}{x_1 + \Lambda_{12} x_2} - \frac{\Lambda_{21}}{\Lambda_{21} x_1 + x_2} \right] \tag{2-99}$$

where:

Λ_{21} and Λ_{12} = Wilson adjustable parameters

The Wilson adjustable parameters are related to pure component liquid volumes by:

$$\Lambda_{ij} = \frac{V_i}{V_j} \exp\left[\frac{\lambda_{ij} - \lambda_{ii}}{RT} \right] \tag{2-100}$$

$$\Lambda_{ij} = \frac{V_i}{V_j} \exp\left[\frac{\lambda_{ij} - \lambda_{ii}}{RT} \right] \tag{2-101}$$

where:

V_j and V_i are molar volumes of pure liquids at temperature T

And λ_{ij} and λ_{ii} are temperature and composition independent

The Wilson model version implemented in Aspen Plus® (used for the data regression in this he Λ_{ij} term instead becomes a function of temperature only in the following equation expressed in Aspen Plus® :

$$\Lambda_{ij} = \exp\left(a_{ij} + \frac{b_{ij}}{T} + c_{ij} \ln T + d_{ij} T \right) \tag{2-102}$$

The Wilson equation is notable to predict liquid immiscibility or extrema in the activity coefficients (Prausnitz et al., 1986). The T-K Wilson (Tsuboka and Katayama, 1975) equation is a modification to the equation, discussed by Walas (1985), is able to predict limited miscibility.

Of equal significance is that Barniki (2002), mention that adjustable parameters Λ_{12} and Λ_{21} are not unique, and a range of values will fit the data equally well. The parameter pair obtained from the data reduction evaluation depends on the objective function algorithm and initial guesses.

Taking this into consideration, it becomes unfortunate that Λ_{ij} values have no real physical significance, so they are hard to guess *apriority* (Pillay, 2010). With values ranging from approximately 3500 to -500, little observable patterns become apparent based on deviations from ideality or system type (Barnicki, June 2002).

2.5.1.2. The NRTL Equation

Renon and Prausnitz (Renon and Prausnitz, 1968) developed an improved local composition model to overcome the Wilson equation's inability to model systems with liquid immiscibility known as the Non- Random Two Liquid (NRTL) model. Both partially miscible and completely miscible systems can be represented satisfactorily with the NRTL model.

The NRTL equation is a two cell theory (Walas, 1985) that is based on the two-liquid model of Scott (Scott, 1956). It operates under the guise of the same assumption used by Wilson (1964), namely, that of non-randomness. The NRTL model comprises of three adjustable parameters: $(g_{12}-g_{11}),(g_{21}-g_{22})$ and the non-randomness parameter, α_{12}. The parameter α_{12} represents the non-randomness of the fluid, i.e. for a completely random mixture, it equals zero (Moodley, 2009). It is also estimated to have a value from 0.1 - 0.47. This depends on the nature of the chemicals present in the system under investigation (Renon and Prausnitz, 1968). Walas (1985), states that the activity coefficients appear insensitive to values of α_{12} ranging between 0.1 and 0.5. Values of 0.3 (based on regressed values of data sets from Dechema) for non-aqueous mixtures and 0.4 for aqueous organic mixtures are recommended by Walas (1985). Raal and Mühlbauer (1998) and Joseph (Joseph et al., 2001) however, suggest that results are more conclusive by finding a value from experimental data regression and not setting a fixed value.

The NRTL model can also be extended to model multi-component mixtures using binary parameters like the Wilson equation, (Walas, 1985). It has the advantage over the Wilson equation in that it can be applied to liquid-liquid equilibria, but is inferior to the Wilson model in treating strongly asymmetric systems in the range of very low molar concentrations (Vetere, 2000). Moreover, it can be applied to highly non-ideal systems to yield a good representation of phase equilibrium (Raal and Muhlbauer, 1998). The expression for G^E and the activity coefficients are exhibited below as follows:

$$\frac{G^E}{RT}=\frac{\tau_{21}G_{21}}{x_1+G_{21}x_2}+\frac{\tau_{12}G_{12}}{x_2+G_{12}x_1} \tag{2-103}$$

$$\ln\gamma_1 = x_2^2\left[\tau_{21}\left(\frac{G_{21}}{x_1 + x_2 G_{21}}\right)^2 + \frac{\tau_{12}G_{12}}{\left(x_2 + x_1 G_{12}\right)^2}\right] \tag{2-104}$$

$$\ln\gamma_2 = x_1^2\left[\tau_{12}\left(\frac{G_{12}}{x_2 + x_1 G_{12}}\right)^2 + \frac{\tau_{12}G_{21}}{\left(x_1 + x_2 G_{21}\right)^2}\right] \tag{2-105}$$

where:
$$G_{ij} = \exp\left(-\alpha_{ij}\tau_{ji}\right) \tag{2-106}$$

$$\tau_{ij} = \frac{g_{ij} - g_{ii}}{RT} \tag{2-107}$$

In Aspen Plus®, the τ_{ji} parameter is defined:

$$\tau_{ij} = \left(a_{ij} + \frac{b_{ij}}{T} + e_{ij}\ln T + f_{ij}T\right) \tag{2-108}$$

2.5.1.3. The UNIQUAC Equation

The semi-theoretically developed UNIQUAC equation by Abrams and Prausnitz (Abrams and Prausnitz, 1975) is also based on the concept of local concentration like the Wilson and NRTL models. This model was developed to represent Gibbs excess energy which extends the quasi-chemical lattice theory of Guggenheim. The assumption that a liquid is represented by a three dimensional lattice, where a segment of a molecule occupies each lattice site, is the basis of the model and has a total of r_i segments for each molecule of type *i* (Hirawan, 2007).

The UNIQUAC model stipulates that the excess Gibbs energy is composed of two parts (Walas, 1985), namely, a combinatorial part (accounting for molecular size and shape differences) and a residual part (accounting for molecular interactions). Additionally, the combinatorial part is attributed to and attempts to describe dominance in entropic contribution (Prausnitz et al., 1986). It requires pure component data only for regression. Subsequently, the residual section is a function of the energy and temperature parameters $u_{ji} - u_{ii}$. A third parameter known as the

coordination number, *z*, which is always fixed at a value of 10 (for most liquids under normal conditions) is also included in the model. Two adjustable parameters per binary system are used in the UNIQUAC equation only. It can be extended to polar and non-polar multi-component systems requiring no higher parameters. The following is the form for the excess Gibbs energy:

$$G^E = G^E(combinatorial) + G^E(residual) \tag{2-109}$$

where for a binary system, the two parts of G^E are:

$$\frac{G^E(combinatorial)}{RT} = \sum_i x_i \ln\frac{\Phi_i}{x_i} + \frac{z}{2}\sum_i q_i x_i \ln\frac{\phi_i}{\Phi_i} \tag{2-110}$$

$$\frac{G^E(residual)}{RT} = -\sum_i q_i' x_i \ln\left[\sum_j \phi_j' \lambda_{ji}\right] \tag{2-111}$$

From Equations 2-110 and 2-111, the segment fractions (Φ_i) and area fractions (ϕ_i and ϕ_i'') are as follows:

$$\Phi = \frac{x_i r_r}{x_1 r_1 + x_2 r_2} \tag{2-112}$$

$$\phi_i = \frac{x_i q_i}{x_1 q_1 + x_2 q_2} \tag{2-113}$$

$$\phi_i' = \frac{x_i q_i'}{x_1 q_1' + x_2 q_2'} \tag{2-114}$$

where the adjustable model parameters are given by:

$$\lambda_{ji} = \exp\left[\frac{-\left(u_{ji} - u_{ii}\right)}{RT}\right] \tag{2-115}$$

Parameters r_i and q_i are the size and surface parameters respectively, which are pure component molecular structure parameters. They are calculated using molecular structure contributions for various groups and subgroups i.e., *r* and *q* (Roger, 2004). Fredenslund (Fredenslund et al., 1977) and Raal & Mühlbauer (1998) outline this group contribution method of determining r_i and q_i as well as the values for *r*and *q*. The parameters $q_i = q_i^{'}$ in the original formulation of Abrams and Prausnitz (1975). Anderson and Prausnitz (Anderson and Prausnitz, 1978) however, introduced empirically adjusted values for q_i (denoted $q_i^{'}$) to improve the results of the UNIQUAC equation for systems containing water and lower alcohols. The characteristic energy, $u_{ji} - u_{ii}$, in Equation (2-115) is often weakly dependent on temperature (Prausnitz et al., 1986).

The version of the UNIQUAC model implemented in Aspen Plus® differs as with the Wilson and NRTL model. In the Aspen Plus® definition, the adjustable model parameters, λ_{ji} are defined as:

$$\lambda_{ji} = \exp\left(a_{ij} + \frac{b_{ij}}{T} + c_{ij}\ln T + d_{ij}T + \frac{e_{ij}}{T^2}\right) \tag{2-116}$$

The G^E expression consists of two terms; therefore, the analogous activity coefficient expression equation must contain a combinatorial and residual part:

$$\ln\gamma_i = \ln\gamma_i^{\,c}\left(combinatorial\right) + \ln\gamma_i^{\,r}\left(residual\right) \tag{2-117}$$

where:

$$\ln\gamma_i^c = \ln\frac{\Phi_1}{x_1} + \frac{z}{2}q_1 n\frac{\phi_1}{\Phi_1} + \Phi_2\left(l_1 - \frac{r_1}{r_2}l_2\right) - q_1^{'}\ln\phi_1^{'} + \phi_2^{'}\lambda_{21} + \phi_2^{'}q_1^{'}\left(\frac{\lambda_{21}}{\phi_1^{'} + \phi_2^{'}\lambda_{21}} - \frac{\lambda_{12}}{\phi_2^{'} + \phi_1^{'}\lambda_{12}}\right) \tag{2-118}$$

$$\ln\gamma_i^r = \ln\frac{\Phi_2}{x_2} + \frac{z}{2}q_2 n\frac{\phi_2}{\Phi_2} + \Phi_1\left(l_2 - \frac{r_2}{r_1}l_1\right) - q_2^{'}\ln\phi_2^{'} + \phi_1^{'}\lambda_{21} + \phi_2^{'}q_2^{'}\left(\frac{\lambda_{12}}{\phi_2^{'} + \phi_1^{'}\lambda_{12}} - \frac{\lambda_{21}}{\phi_1^{'} + \phi_2^{'}\lambda_{21}}\right) \tag{2-119}$$

Considered one of the major advantages of the UNIQUAC equation is its extension to predicting system parameters from pure component data utilising the group-contribution UNIFAC method (Clifford, 2004). The method is described in detail in Smith et al. (Smith and VanNess, 1996). It also uses surface fractions for concentration variable as opposed to using mole fractions (Reid et al., 1988). The UNIQUAC model has the added advantage of the previous models (predicting immiscibility and activity coefficient extrema) and is also superior in representing mixtures of widely different molecular sizes (Walas, 1985).

The main drawbacks to the UNIQUAC model is the complexity of the model equation compared to the NRTL and Wilson equations and that there presentation of the VLE is poorer than for some simpler equations (Walas, 1985). Also high quality data with high accuracy due to only two adjustable binary parameters cannot always be represented (Prausnitz et al., 1986).

2.6. VLE Data Reduction

Quantitative estimates of fluid phase equilibria are required for design methodologies pertaining to separation processes. Unfortunately, measured phase equilibrium data that is required for these estimates to be determined are not always available. In such cases were it becomes irrational to make rough estimates, predictive models have been developed to assist with chemical process design. These models include the utilisation of liquid phase activity coefficient models and cubic equations of state with mixing rules for phase separation processes. Measured phase equilibrium data is usually correlated to these models using regression techniques available.

The role of data regression is to condense the large volume of experimental VLE data into a simple and useable form for future reference (Sewpersad, 2012). Therefore, a set of parameters are yielded that are uniquely inclined to each system studied and the model employed, with the emphasis of these model parameters being placed in their ability to predict equilibrium data at experimentally difficult conditions (Narasigadu, 2006). The two most feasible methods available for the reduction of isothermal and isobaric VLE data are the combined method (gamma-phi/ $\gamma-\phi$ approach) and the direct method (phi-phi/ $\phi-\phi$approach). The $\gamma-\phi$ approach (the gamma-phi formulation of VLE) is commonly used in the reduction of low to medium pressure VLE data. The combined method makes use of an activity coefficient model to calculate the activity coefficients that describe the liquid phase non-ideality. An equation of state (like the virial equation of state used in this research regression) is used in conjunction with this in the combined method to calculate the fugacity coefficients that describe the vapour phase non-idealities. For the direct method on the other hand, the fugacity coefficients from an EOS (such as a cubic EOS used in this project,) are used to describe the non-ideality in both the vapour and

liquid phase. A mixing rule (Wong-Sandler and Tw-Coon) is employed to describe the mixture properties.

Different calculation procedures exist for each method; hence for isothermal VLE data, the bubble point pressure computation calculation procedure is used to calculate the pressure and vapour composition for each experimental point. Regarding isobaric VLE data, the temperature and vapour composition are calculated using the bubble point temperature computational technique. Smith et al. suggests that the vapour composition measurements are the most susceptible to error (Smith et al., 2001). This renders the bubble point computation for isothermal VLE data generally more superior to the dew point computation for a fully determined regressed data set. Furthermore, the reduction of isothermal VLE data is considered less tedious (Narasigadu, 2011). This is because the model parameters can be treated as constants since the temperature is constant and have strong temperature (Raal and Muhlbauer, 1998).

2.6.1. The Combined ($\gamma - \Phi$) Method

In this investigation the virial EOS with the Hayden and O'Connell (1975) correlation for second virial coefficient was used to describe the vapour phase non-ideality. Gibbs excess energy models were used to describe the non-ideality in the liquid phase. Hence the combined method uses two different equations to regress VLE data. The Wilson, NRTL and UNIQUAC liquid phase activity coefficient models (described in Section 2.5.1) were all used to compute imperfections in the liquid phase. This is common as a comparison can be made in order to check which model fits the experimental data most accurately.

For the attainment of model parameters, a suitable applicable mathematical algorithm must be selected for the regression iterations. Many techniques are used for data regression such as the method of least squares (used primarily in this project); by Marquardt and Gess *et al*. (Marquardt, 1963, Gess et al., 1991). This technique of reduction is based on minimizing the deviation between the experimental and predicted values, with the difference being the residual (δ). The residual for VLE is defined as the following:

$$\delta y_i = y_i^{\exp} - y_i^{calc} \tag{2-120}$$

$$\delta P_i = P_i^{\exp} - P_i^{calc} \tag{2-121}$$

δP and δy are the primary residualsselected for minimization (objective function). All other residual quantities (i.e., temperature, liquid composition, excess Gibbs energy and activity

coefficients) can be written in terms of these quantities and the iterative process of regression of experimental data is deployed until the minimum value, a certain tolerance, ε of the objective function is obtained (Abbott and Van Ness, 1982). Barker (1953) minimized the objective function (*OF*) a simple form expressed as follows:

$$OF = \sum \left(\delta P_i\right)^2 \tag{2-122}$$

The objective function used in this study combining both the P and y_i residuals, are minimized simultaneously using normalizing factors:

$$OF = \sum \left(\frac{\delta P}{w_p} \right)^2 + \left(\frac{\delta y_i}{w_y} \right)^2 \tag{2-123}$$

The normalizing factors w_p and w_y used are usually the root mean squared values taken from the minimization of $\sum \left(\delta P\right)^2$ and $\sum \left(\delta y_i\right)^2$ respectively (Pillay, 2010).

Values for pressure and vapour composition are determined by bubble point pressure iterations where isothermal VLE data is available (for each experimental data point). Similarly, for isobaric VLE measured data, temperature and vapour composition values are evaluated by bubble point temperature iterations. The regression of isobaric and isothermal data is represented below in the corresponding figures.

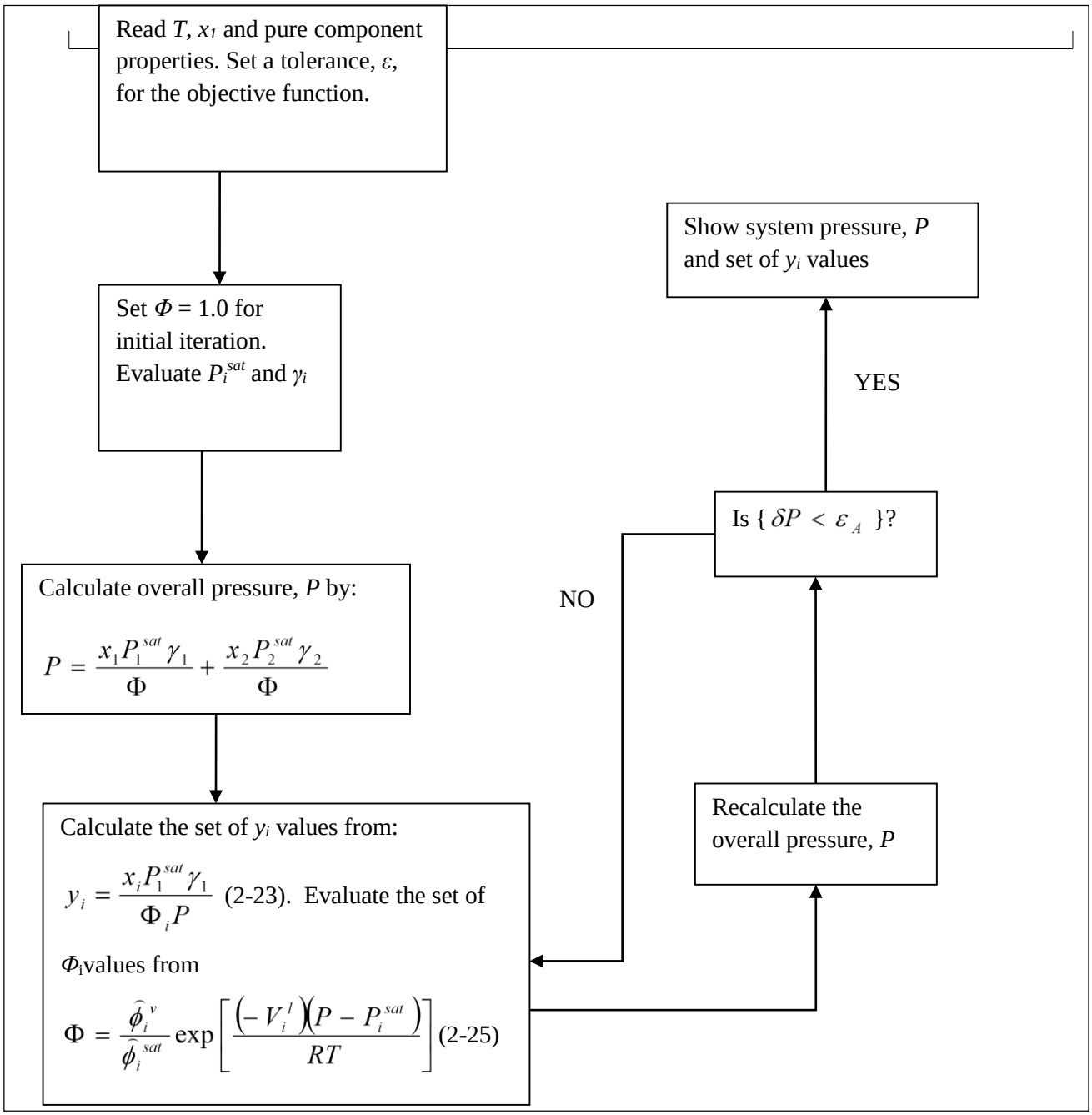

Figure 2-1: Bubble-point pressure iteration flow diagram using the Combined method (Smith et al., 2005).

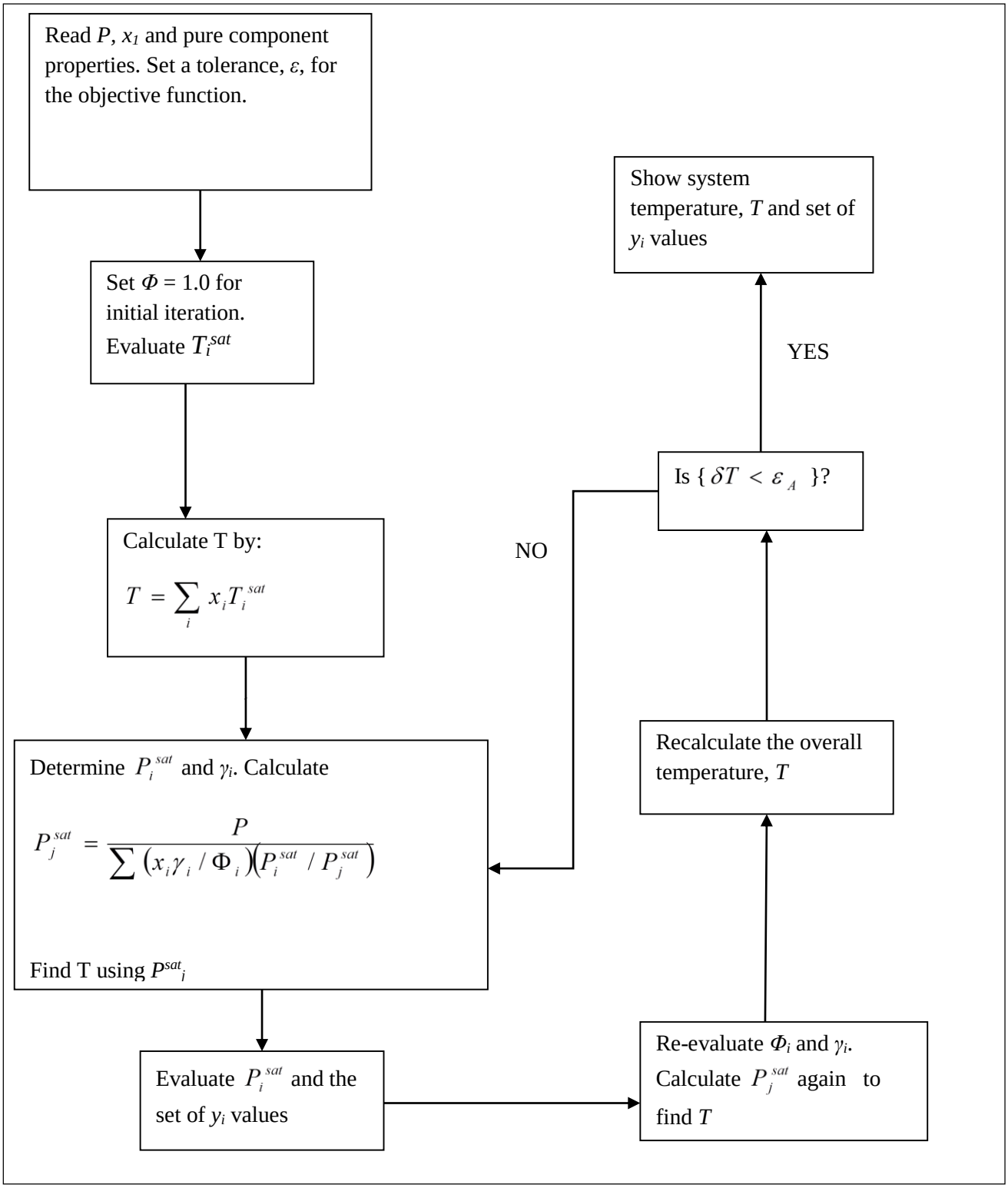

Figure 2-2: Bubble-point temperature iteration flow diagram for the Combined Method (Smith et al., 2005).

2.6.2. The Direct ($\Phi - \Phi$) Method

A cubic EOS for computing the fugacity coefficients represents both the vapour and liquid phase non-idealities with this method. The equilibrium criterion requirement of equation 2-17 can be expanded from the definition for the fugacity coefficient equations 2-16 for both the liquid and vapour phases as:

$$x_i \hat{\phi}_i^l = y \hat{\phi}_i^v \tag{2-124}$$

A suitable EOS needs to be chosen to determine $\hat{\phi}_i^l$ and $\hat{\phi}_i^V$. Similar to the combined method, the best model must thereafter be selected that correlates the experimental data most adequately. The figures illustrating the bubble pressure and the bubble temperature iteration for the direct case are presented below.

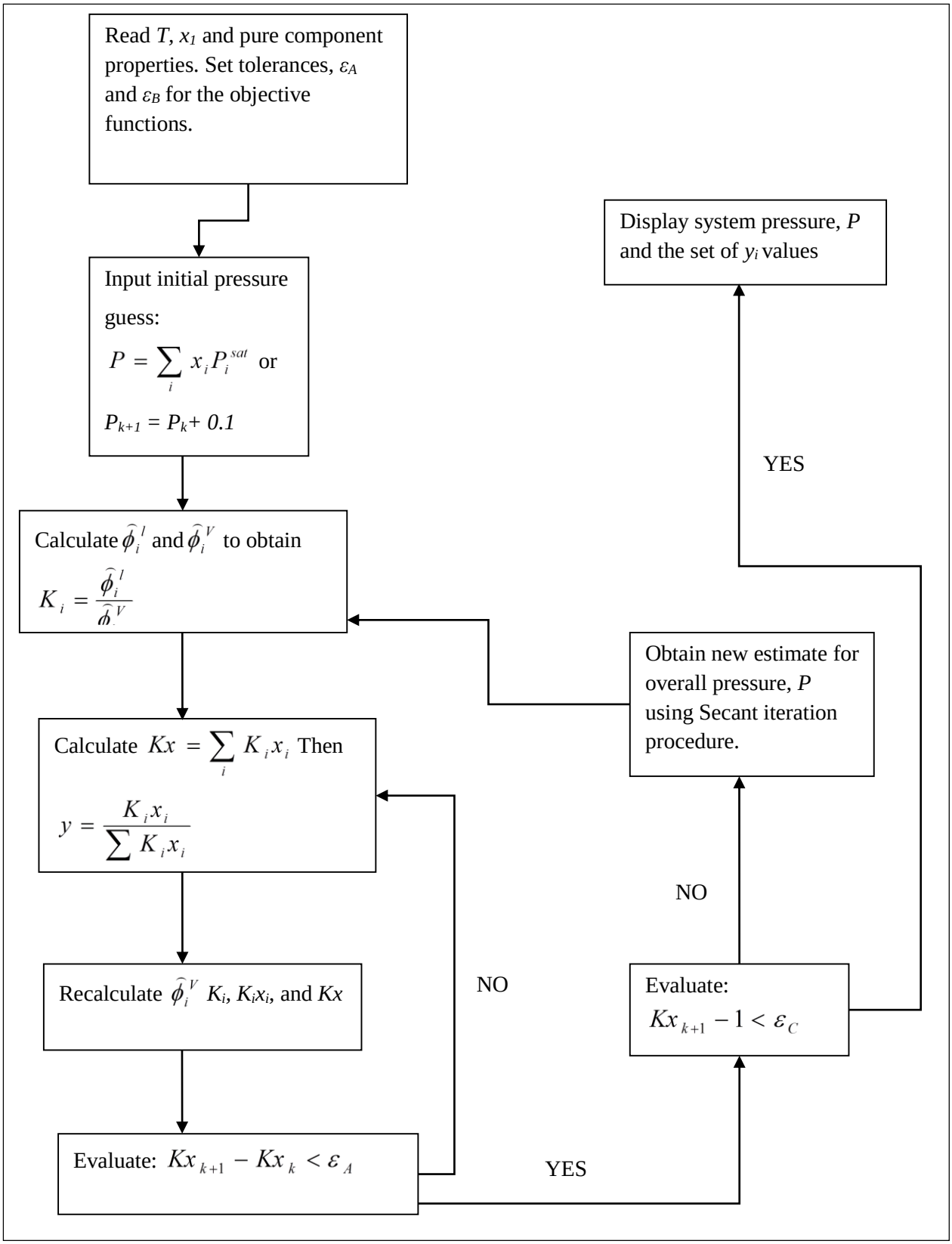

Figure 2-3: Bubble-point pressure iteration flow diagram for using the Direct method (Smith et al., 2005).

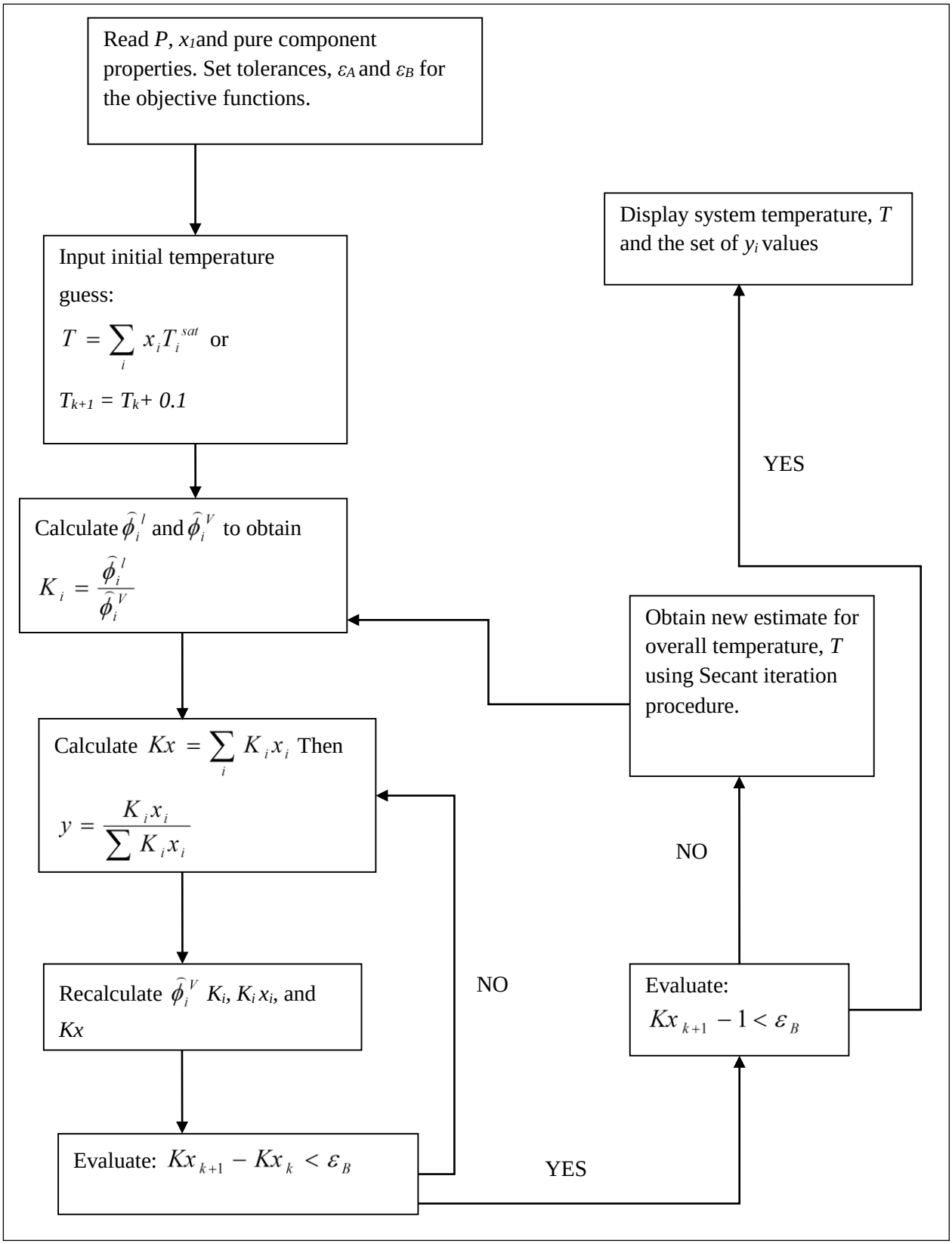

Figure 2-4: Bubble-point temperature iteration flow diagram for the Direct method (Smith et al., 2005).

2.7. Models Chosen for Data Correlation

Vapour and liquid phase non-ideality is normally expressed in terms of the ideal associated solution models (Apelblat, 2007). Therefore, the objective of data correlation is to acquire the more suitable model to accurately express the description of phase behaviour of systems under investigation mainly for reliable design and simulation of separation units.

Before selecting a model, it is essential to choose a less sophisticated one in order to avoid tedious model calculations during design implementation. This especially holds true for process design engineers based in industry where wasted time and unwarranted expenditure coincide. Successful applications of suitable models to systems of similar nature under similar operating conditions that are located in literature are also an asset to design engineers. Hence, the growing demand for the measurement and computation of reliable phase equilibrium data that has not been investigated before becomes clearer. Another significant asset is the availability of a vast range of models in widely recognised process design simulation software packages such as Aspen Plus®. For this project, less sophisticated yet well-defined methods of Hayden and O'Connell (1974) and Nothnagel *et al*. (1973) for description of vapour phase non-idealities (fugacity coefficient) were selected. These models yielded most satisfactory results for the systems measured which exhibited high polarity, induced polarity and solvation. The Peng and Robinson (1976) EOS was selected and used as a comparison to the aforementioned models. It too yielded favourable results, as this model has gained much notoriety for its successful application in the process industries sector. The highly recognized Wilson, NRTL and UNIQUAC activity coefficient models were chosen to describe liquid phase non-idealities. The limitations and capabilities of the models that were selected for use in data regression were thoroughly understood before being implemented. All models used are available in Aspen Plus® process simulator which was used for the correlation of all measured data to model parameters.

The Wilson and NRTL models were clearly the most favourable models for consideration for VLE data reduction for most of the systems in this study as outlined in Chapter 8 Table 8.1. Walas, (1985) illustrates in the figure the frequency of best fit results using various activity coefficient models for mixtures with alcohols, hence suiting the model selection criteria for this project as it deals primarily with ether-alcohol blends. The UNIQUAC model has favourable capabilities even though it has the lowest best fit frequency out of the three activity coefficient models, thus influencing its use for regression.

2.8. Thermodynamic Consistency Tests

Palmer (Palmer, 1987) commented that VLE data can be deceptively easy to measure yet extraordinarily difficult to do so accurately. Phase equilibrium data measured accurately are the key ingredient for the successful design of industrial separation processes. For the majority of chemical and petrochemical plants this accurate data will contribute heavily to the most significant and costly aspects of plant operation. It is therefore important to test the quality and reliability of experimental data. This is achieved by employing a universally accepted method for the quantification of the integrity of data achieved experimentally thus ensuring the adherence or consistency of the experimental data with regards to the thermodynamics framework (Reddy, 2006).

When measuring binary VLE data it is acceptable to measure only three out of the four variables viz., *P*, *T*, *x* and *y*. Since the fourth property can be obtained from the other three, the measurement of the fourth variable is said to inevitably "over-specify" the system. This nonetheless, can allow one of the four measured variables to be used for the thermodynamic consistency testing of the data. According to Smith et al. (Smith et al., 2001), the vapour compositions normally show the highest error. Hence, the thermodynamic consistency tests usually focus on the vapour compositions (i.e., y_i variables) for checking the consistency of the VLE data. For this reason the statement by (Van Ness and Abbott, 1978), that the main purpose for measuring the vapour composition is to test the thermodynamic consistency, holds much credence. Smith et al. (2001) proclaim that the Gibbs-Duhem equation plays an integral role in developing the thermodynamic consistency tests and are given by:

$$\sum_i x_i d\ln\gamma_i = \frac{\overline{V}_i^E}{RT}dP - \frac{\overline{H}_i^E}{RT^2}dT \tag{2-125}$$

The VLE data is said to be thermodynamically consistent if it conforms to the Gibbs-Duhem equation. On the contrary however, there have been cases whereby the data may be taken as consistent, passing the consistency test, yet in actual fact is inconsistent (Jackson and Wilsak, 1995). The consistency tests (whereby the Gibbs-Duhem equation forms the basis) that will be briefly discussed in this section are the:

- Point test - Van Ness and Abbott (1982) - and
- Direct test - Van Ness (1995).

2.8.1. The Point Test

The more rigorous thermodynamic consistency test proposed by Van Ness et al. (Van Ness et al., 1973) – the *point test* - was introduced as an improvement to the *area test.* The premise of the point test becomes the "over-specification" of the measurable VLE data (P, T, x_i, y_i) variables. Any three variables (computed via data reduction) are utilized for testing, with the fourth variable being calculated from an appropriate correlation and is then compared to the measured data value, hence testing the accuracy.

In the majority of cases, the vapour phase compositions are considered to introduce the most error (Smith et al., 2001). Thus, measured vapour molar compositions ($y_{i,exp}$) and calculated/predicted values ($y_{i,calc}$) vapour molar composition data are compared to one another, generating residuals Δy, and used for data consistency testing using the combined or the direct method. Danner and Gess (Danner and Gess, 1990) supply a quantitative criterion regarding the consistency of VLE data by proposing that the "absolute average deviation, Δy_{ad}," should be a maximum value of 0.01 for the thermodynamic consistency of the data. The quantitative criterion equation is:

$$\Delta y_{AAD} = \frac{1}{n}\sum_{i=1}^{n}\left|\Delta y - \Delta\bar{y}\right| \tag{2-126}$$

where n corresponds to the experimental data point number, Δy refers to the difference between the experimental and the calculated value and $\Delta\bar{y}$ is the average difference between the experimental and calculated values. Another stipulation of the *point test* requires that Δy vs. y_1 is plotted and should scatter about zero to represent the thermodynamic consistency.

The following criteria are necessary to perform the consistency test:

- The excess Gibbs energy model should sufficiently be flexible for the pressure residual to scatter about zero and
- pure component vapour pressures must be measured accurately as erroneous values give rise to systematic errors in Δy_i.

3

Chapter Three

REVIEW OF EXPERIMENTAL TECHNIQUES FOR LOW PRESSURE VLE

Design engineers and researchers face significant challenges in the chemical and separations technology industry due to the increased use and synthesis of numerous organic compounds. Researchers have begun investigating predictive mathematical modelling techniques, as the number of potential chemical systems to be investigated for phase equilibrium behaviour, are now near infinite.

Predictive modelling results however, do not adequately account for certain deviations in phase behaviour. In this regard, poor separations technology designs are imminent. Therefore, for the foreseeable future, reliable and accurate phase equilibrium data measurement remains a significant priority (Weir and de Loos, 2005). This can only become a reality through the development of proper equipment and experimental methods (Mqondisi, 2012). Numerous techniques for measuring phase equilibrium data are used. These involve the measurement of temperature, pressure, vapour and liquid compositions. For the most accurate measurement in pressure and temperature, the region/s measured that are assumed to be at equilibrium, must actually be at equilibrium. If the region is not actually at equilibrium, it results in the data point analysed being inaccurate (Walas, 1985). Additionally, vapour and liquid samples withdrawn from their respective sampling points, must be done so with minimal disturbance to equilibrium (Walas, 1985).

Direct methods for the measurement of vapour-liquid equilibrium data include distillation methods, dynamic methods, static methods, flow methods as well as Dew point and Bubble Point methods (Hala et al., 1967). Of the techniques available for measuring VLE data, the most common techniques are the static and dynamic method (Seker and Somer, 1992). This chapter will therefore focus on these two techniques, as the classification of the equipment used in this study is based on principals of circulation of the vapour phase only, the liquid phase only, or both concurrently. Circulation refers to dynamic equipment, whereas no circulation is classified as static equipment.

3.1. The Static method

During the Static method a liquid mixture is charged into an evacuated equilibrium cell, which is placed in a thermostat. Mechanical agitation of the mixture within the cell occurs, until equilibrium is established between the liquid and its vapour. Samples are thereafter taken from one or both of the phases in order to be analysed. The principles of the static method are illustrated in Figure 3.1.

At low pressures, the amount of vapour required for analysis is of the same order as the total amount of the vapour phase in the equilibrium cell (Hala et al., 1958). This creates the problem of upsetting equilibrium upon removal of the vapour sample. This issue was solved by Inoue et al. (Inoue et al., 1975). However, their solutions where not favourable with most researchers who had measured the liquid phase compositions only (Abbott, 1986). As a result of this, the vapour phase is not sampled in most static equilibrium cells according to (Raal and Muhlbauer, 1998). The vapour composition then has to be computed from the measured pressure and liquid phase compositions. In doing so however, the possibility of thermodynamic consistency testing is not possible (Raal and Muhlbauer, 1998).

Complete degassing the system, which is a time-consuming process, is another drawback associated with this method. In order to acquire accurate VLE data, this must be done.

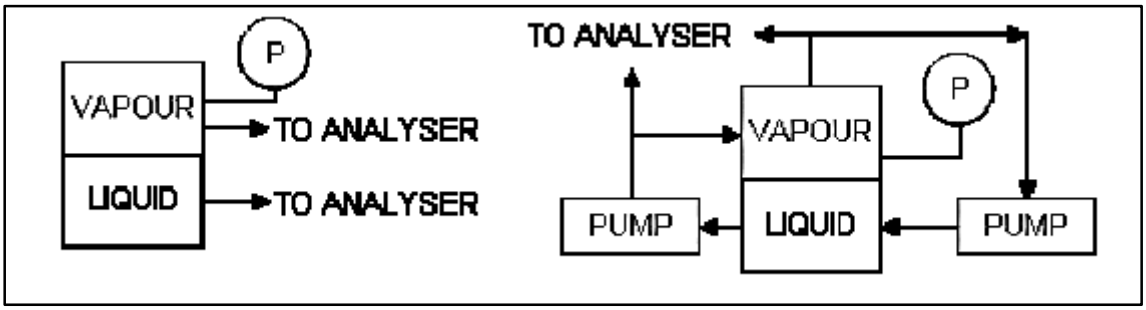

Figure 3-1: The principles of static VLE measurement apparatuses (Uusi-Kyyny et al., 2002).

3.1.1. The Apparatus of Gibbs and Van Ness

A proposed static cell by (Gibbs and Van Ness, 1972), is shown in Figure 2-1. The degassed liquids are transferred into a magnetically stirred cell, placed in a thermostatic bath by utilising piston injectors, and degasses via refluxing, cooling, and evacuating into a specialised flask. Operation commences by introducing one of the pure liquids into the equilibrium cell that has a capacity of approximately 100 cm^3. The vapour pressure is measured when equilibrium is reached after which a small amount of the second component is added to the cell from a separate but similar injector (Ndlovo, 2005).

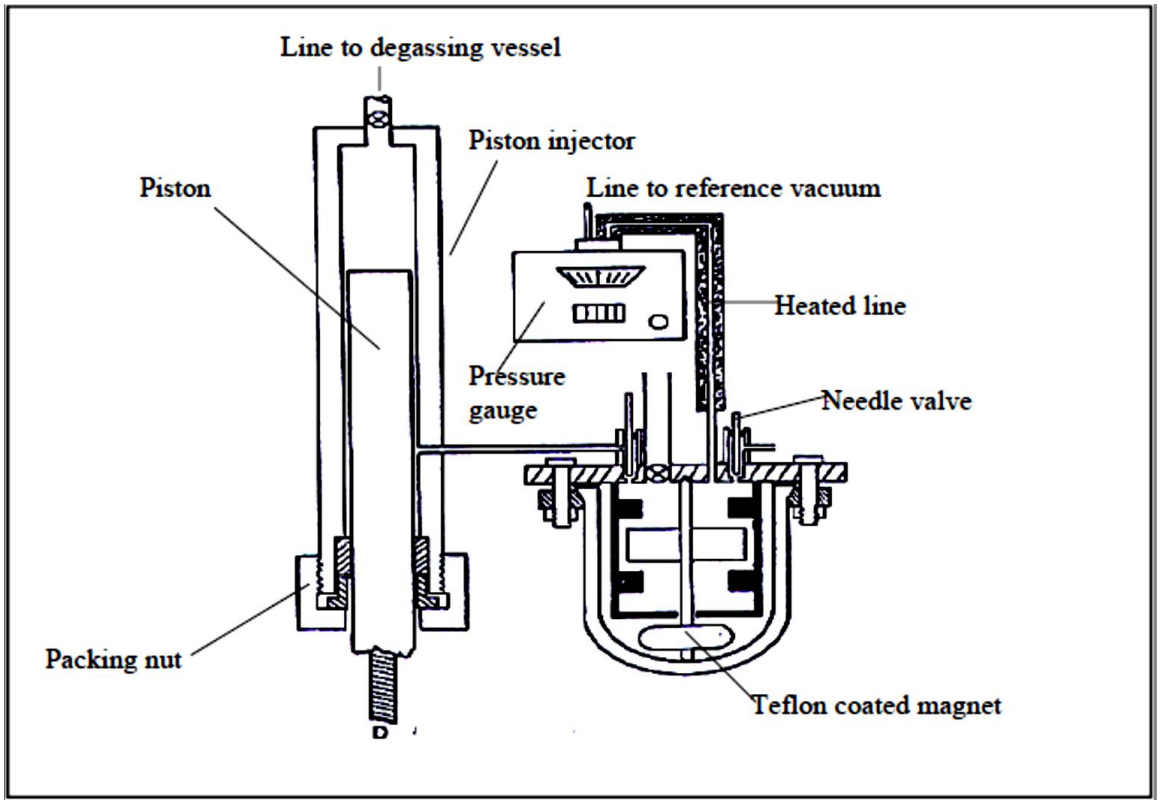

Figure 3-2: The Apparatus of Gibbs and Van Ness (Gibbs and Van Ness, 1972)

3.1.2. The Apparatus of Raal and Mühlbauer

The static cell by Raal and Mühlbauer (1998) is a glass cell (Figure 2-2) having two time-saving innovations that avert the insufficiencies associated with the degassing process (Soni, 2003). These developments are:

- The static cell cluster

  Maher and Smith (Maher and Smith, 1979) developed an apparatus which consisted of 15 static cells. The cells are connected to a common manifold and multiple data

points can be measured simultaneously (Soni, 2003).

- The degassing condenser

  Maher and Smith (1979) used freeze-thawing cycles which are time-consuming. Degassing can now be achieved by boiling the mixture in a cell fitted with a condenser. The cell includes a liquid sample point (Figure 2-2) to account for the loss of any volatiles (Soni, 2003).

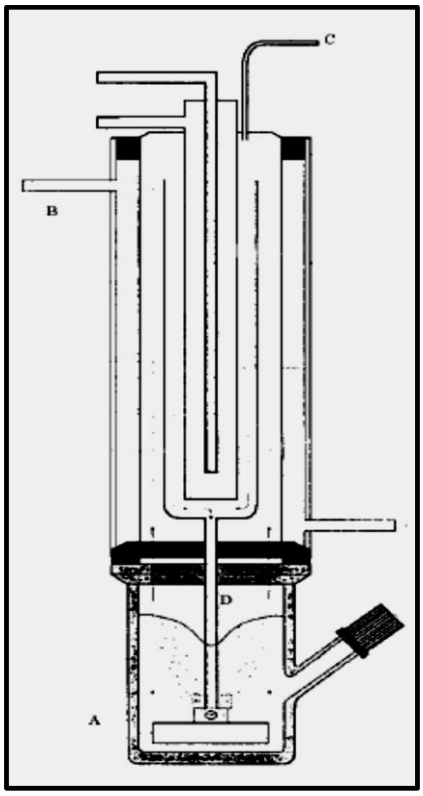

Figure 3-3: Static cell cluster (Raal and Mühlbauer, 1998): A, Stirred cell, B, Degassing condenser; C, Vapour line to manifold; D, Draft tube

3.1.3. The Apparatus of Kolbe and Gmehling

Due to the difficulties of degassing components in a static cell associated with erroneous equilibrium compositions being measured if the air is not removed, a more efficient cell developed by Kolbe and Gmehling (Kolbe and Gmehling, 1985).

One of the cells used by Fisher and Gmehling (Fischer and Gmehling, 1994) and De Haan (de Haan et al., 1995) is represented in figure 2-2 below. Suitable for high pressure measurements, the static cell of Kolbe and Gmehling (1985) was built with a glass equilibrium cell that facilitates measurements of up to 1 MPa. Kolbe and Gmehling (1985) and Fischer and Gmehling (1994)

reveal in detail the description of the equipment and its operating procedure.

Kolbe and Gmehling (1985) reported uncertainties in measurement from experimental trials with their apparatus as ± 0.0001, ± 0.1 kPa and ± 0.02 K for molar composition, pressure and temperature respectively.

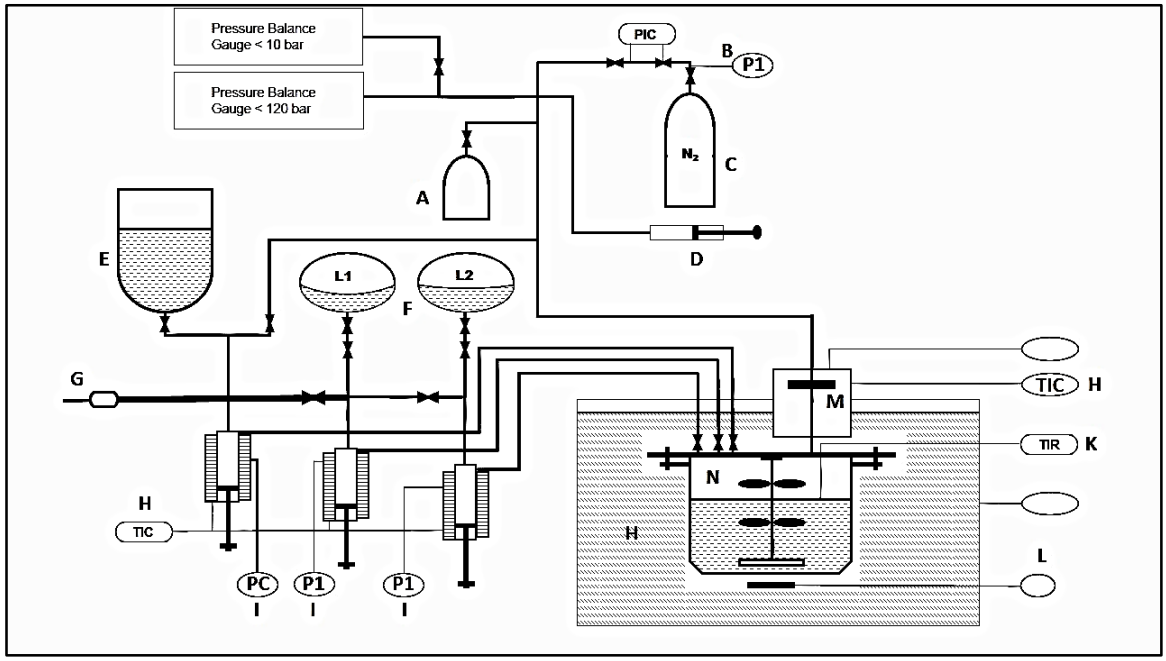

Figure 3-4: The static apparatus used for the P-*x* measurements (Kolbe and Gmehling, 1985).

A – Buffer Volume; **B** – Pressure Regulator; **C** – Nitrogen Flask; **D** – Variable Volume; **E** – Container for Liquefied Gas; **F** – Container for Degassed Liquids; **G** – Vacuum Pump; **H** – Constant Temperature Bath; **I** – Bourdon Pressure Gauge; **K** – Quarts Thermometer; **L** – Rotating Magnetic Field; **M** – Differential Pressure Null Indicator; **N** – Equilibrium Cell.

3.2. The Dynamic Method

This method is also known as the circulation method. According to Marsh, the dynamic still type apparatus is considered to have reached a mature stage of progress (Marsh, 1989). It is more advantageous than other methods as it allows highly accurate VLE data measurement in a simple manner, and the amount of test chemicals required for each run is minimal.

A liquid mixture is charged into a distilling flask and then brought to boil where a continuous separation of the vapour phase from the liquid phase occurs. Except for methods using direct circulation of the vapour phase, the vapour phase is then condensed into a receiver, and returns as

condensate to the distilling flask to mix with the liquid that is boiling (Narasigadu, 2006). The thermodynamic properties (temperature, pressure, liquid and vapour compositions) are recorded once steady state conditions have been reached (Joseph et al., 2001).

The dynamic method can be operated under isobaric or isothermal and steady-state conditions. The design of a dynamic is classified based on two types of circulating categories (Hala et al., 1967):

- circulation of the vapour phase only
- circulation of both vapour and liquid phases

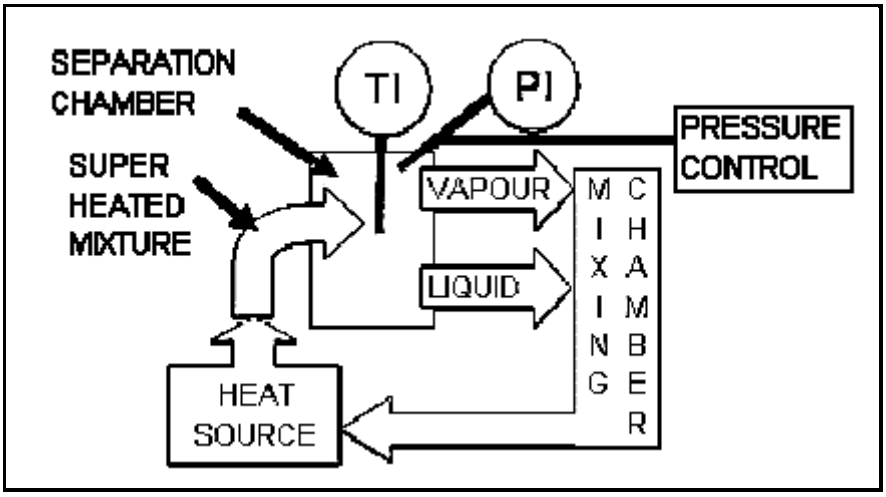

Figure 3-5: The principle of a dynamic equilibrium still (Uusi-Kyyny et al., 2002)

3.2.1. Vapour phase recirculation

The recirculating glass VLE still of Othmer (Othmer, 1928) was based on previous work by Sameshima (Sameshima, 1918). The vapour generated from the boiling liquid was sent to a condenser and the condensate was then returned to the boiling flask (refer to Figure 3-1). Malanowski (Malanowski, 1982) reported that more than 150 modifications were made to the original Othmer design. One of the significant features of the Othmer (1928) still is that it is equipped with sampling points for both vapour and liquid.

One of the latest versions of the Othmer still (Othmer, 1948) is shown in Figure 3-1. The operation is as follows:

- The mixture is brought to a boil in the boiling chamber (A).
- The vapour is directed to the condenser (C) after passing over the thermowell (D).
- The condensate is then returned to the boiling chamber (Soni, 2003).

The design of Othmer (1928) was a vast improvement to that of Sameshima (1918); however it contains numerous drawbacks according to Raal and Mühlbauer (1998):

i. The condensate was not well stirred as a result of the condensate receiver being large.
ii. The accuracy of measured data has a high probability of being affected by the possibility of saturated vapour on the wall of the reboiler. Partial condensation of equilibrium vapour would change its composition making this a faux paus of note.
iii. The temperature measurement was off the mark as the temperature sensor was not in contact with both equilibrium phases.
iv. Another problem was the flashing of the vapour that is richer in the volatile component.
v. In addition there was no thorough agitation of the contents within the reboiler.

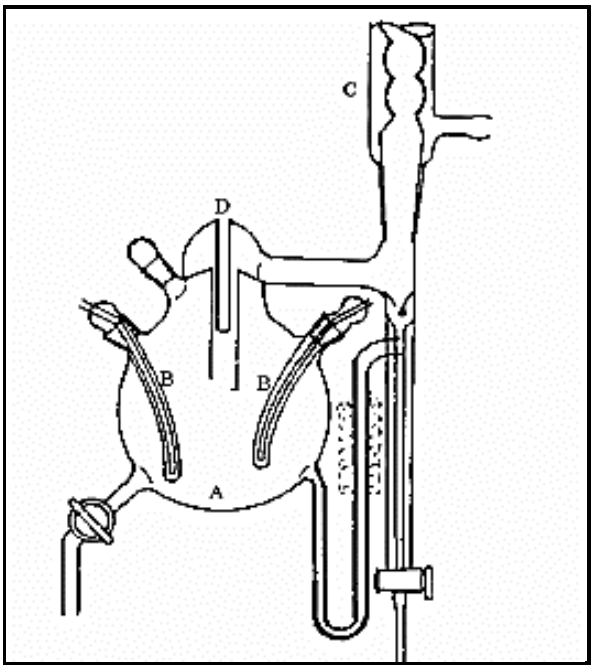

Figure 3-6: A schematic diagram of the Othmer still (Malanowski, 1982). A – boiling chamber; B – immersion heaters; C – condenser; D – thermowell.

Raal and Mühlbauer (1998) advise that the use of the Othmer-type still is not suitable for accurate measurements due to its numerous shortcomings. Vapour condensate recirculation stills that utilise a Cottrell pump such as that of Scatchard et al. (Scatchard et al., 1938) produce more satisfactory results (Malanowski, 1982). Vapour recirculating stills employing a Cottrell pump do however require longer equilibration times according to Malanowski, (1982).

3.2.2. Recirculation of Vapour and Liquid Phases

3.2.2.1. The apparatus of Gillespie

Circulation of both the liquid and vapour phases with the aid of a Cottrell pump (Cottrell, 1919) was pioneered by (Lee, 1931). Gillespie (Gillespie, 1946) had published a still which was based on an earlier version of Lee (1931). Coulson (Coulson et al., 1948), reported that the still of Gillespie (1946), was far superior to earlier designs of Othmer (Othmer and Morley, 1943), having vapour condensate circulation, and those modified with the additional Cottrell pump by Scatchard et al. (1938).

His still, had a separator for the liquid and vapour streams, and provision for the removal of both the liquid and vapour samples without interrupting the operation of the still (Ndlovo, 2005). The still of Gillespie (Gillespie, 1946) however, also had certain drawbacks (mentioned by Narasigadu, 2006 and Sewpersad, 2012); therefore better designs have been proposed over time to produce more efficient VLE measurements. Some of these drawbacks include:

- The liquid sample drawn from the boiling chamber is not actually at equilibrium with the recirculated vapour sampled as condensate.
- The disengagement chamber of the apparatus is not insulated and this prevents partial condensation of the equilibrium vapour.
- The still operation is interrupted by the sampling procedure, hence disrupting the equilibrium compositions.
- Mass transfer is limited because of small contact times and interfacial areas and this renders the Cottrell tube insufficient for rapid attainment of equilibrium.

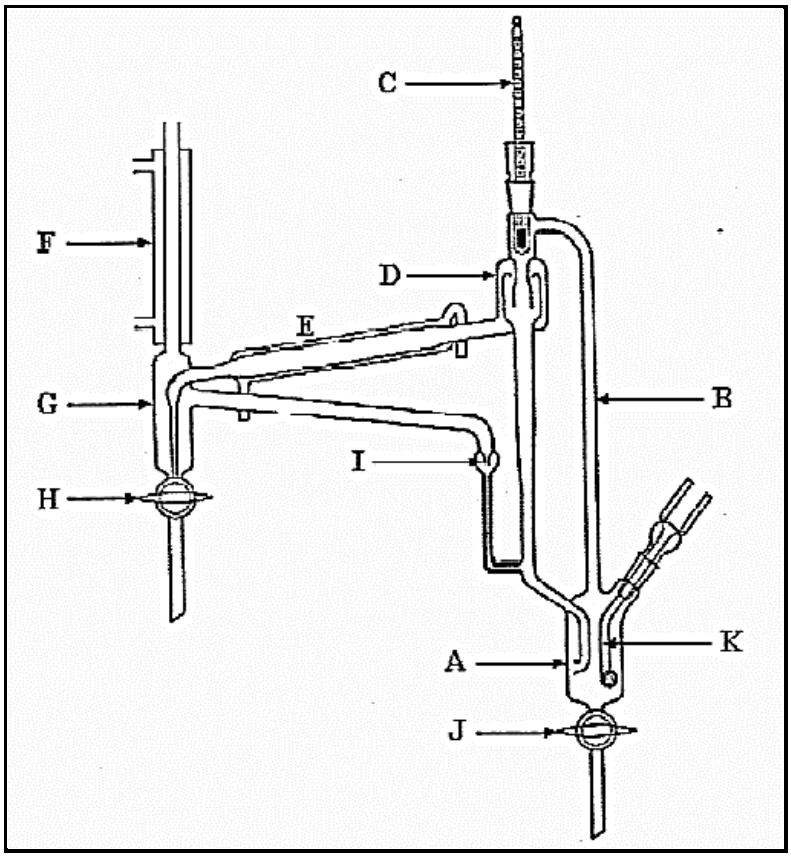

Figure 3-7: The original apparatus of Gillespie (Gillespie, 1946).

A – boiling chamber; **B** – Cottrell tube; **C** – thermometer; **D** – vapour-liquid separating chamber; **E**,**F** – condensers; **G** – condensate receiver; **H** – condensate sample cock; **I** – droplet counter; **J** – liquid sample cock; **K** – internal heater.

Yerazunis et al. (Yerazunis et al., 1964) designed a still in order to overcome most of these drawbacks by modifying the separation chamber. This modification was based on the work by Heertjies (Heertjies, 1960) together with that of Rose and Williams (Rose and Williams, 1955). Yerazunis et al. (1964) exhibited high thermodynamic consistency with their data, proving the modification to be successful.

3.2.2.2. The still of Raal and Mühlbauer

One of the modern VLE stills used for low pressure measurements is that of Raal and Mühlbauer (1998), based on the work of Heertjies (1960) and Yerazunis et al. (1964) to eliminate the sources of error in previous designs (Narasigadu, 2006). Key features are discussed by Clifford, (2004).

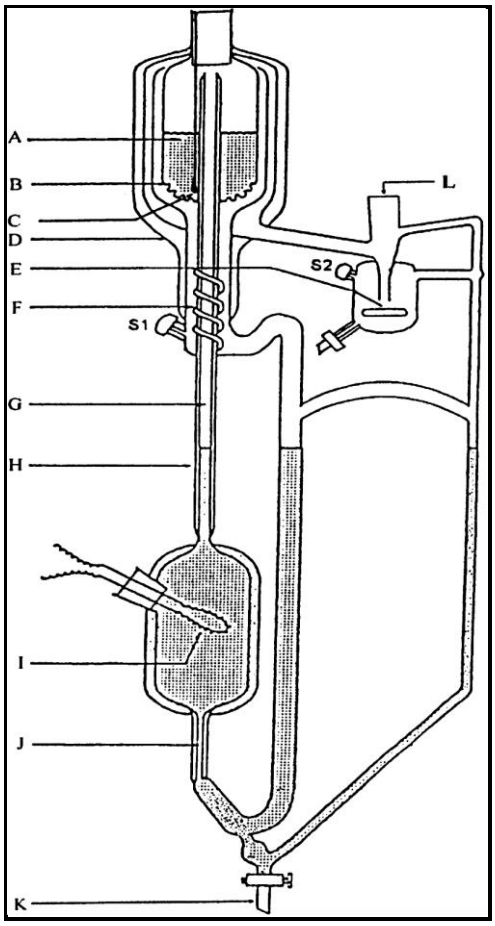

Figure 3-8: Schematic diagram of VLE equilibrium still (Raal and Muhlbauer, 1998):

A - stainless steel wire mesh packing; **B** - drain holes; **C** - Pt-100 sensor; **D** - vacuum jacket; **E** - magnetic stirrer; **F** - stainless steel mixing spiral; **G** - insulated Cottrell pump; **H** - vacuum jacket; **I** - internal heater; **J** - capillary tube; **K** - drain valve; **L** - condenser attachment position; **S1** – liquid sampling point; **S2** - vapour sampling point.

3.2.2.3. The still of Ndlovu

A design modification to the still of Joseph et al. (2001) was implemented by Ndlovu (2005) to attain binary VLE data for partially miscible systems (refer to Figure 4-1). Partial vapour condensation from contact with the outside walls in the downward pass of vapour in the equilibrium chamber was formed in the still of Joseph et al. (2001). Partial condensation of the vapour must be avoided before sampling regarding systems of partial immiscibility, as this affects vapour composition uncertainty. Figure 4-1 reveals how vapour sampling was improved by transporting the sample directly to the gas chromatograph Minute condensation was circumvented by slightly superheating the vapour exiting the equilibrium chamber and withdrawing the vapour sample via the six-port gas chromatography valve (Bownath, 2008).

4

Chapter Four

EQUIPMENT DESCRIPTION

The experimental equipment utilised for research this project has already been introduced in chapter 3. Other recirculating glass stills for the measurement of vapour-liquid equilibrium (VLE) have also been described previously. This chapter is dedicated to a thorough description of the experimental apparatus used to measure the phase equilibrium data for this project. The VLE measurements were undertaken in a modified Raal and Mühlbauer (1998) re-circulating adapted for systems of partial liquid miscibility by Ndlovu (2005). Control and measurement of temperature, pressure, along with the analysis of the liquid and vapour equilibrium phases and sampling techniques will be discussed in this chapter. The peripheral equipment used to aid in measurement with the modified VLE still will also be described.

4.1.1. The Vapour-Liquid Equilibrium Still.

The entirely glass dynamic re-circulating VLE apparatus used in this study, was based on the one used by Ndlovu (2005). The still was originally designed for Vapour-Liquid Equilibrium measurements for systems of partial miscibility and was constructed by Mr. Peter Siegling, a professional glass blower. It was slightly modified for simple VLE measurements for this study. The still depicted in figure 4.1 is a modification of the Raal and Mühlbauer (1998) dynamic apparatus by Ndlovu (2005) and is based on the designs of Heertjies (Heertjies, 1960) and Yerazunis (Yerazunis et al., 1964). They used a packed equilibrium chamber successfully where the liquid and vapour phases are forced downward co currently to achieve dynamic and rapid equilibrium (Ndlovo, 2005).

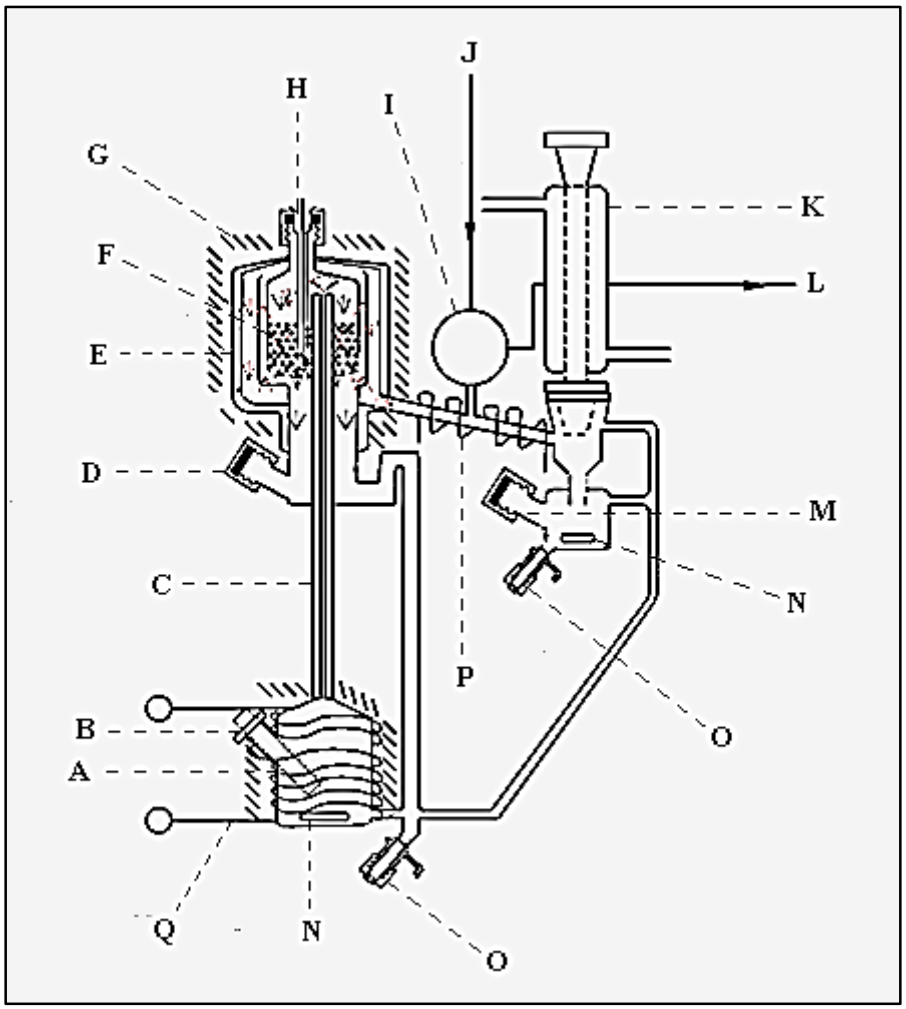

Figure 4-1(a): Schematic diagram of the VLE still (Ndlovu, 2005).

A - boiling chamber; **B** - glass tube insert housing the internal heater; **C** - insulated Cottrell tube; **D** - liquid sampling point; **E** - vacuum jacket; **F** - equilibrium chamber with stainless steel wire mesh packing; **G** - insulation; **H** - glass insert housing the Pt-100 temperature sensor; **I** - six- port GC valve; **J** - helium gas from cylinder; **K** - condenser; **L** - superheated sample to GC; **M** - vapour sampling point; **N** - magnetic stirrers; **O** - drain valves; **P** - nichrome resistance wire for superheated vapour; **Q** - nichrome resistance wire for external heating (Narasigadu, 2006).

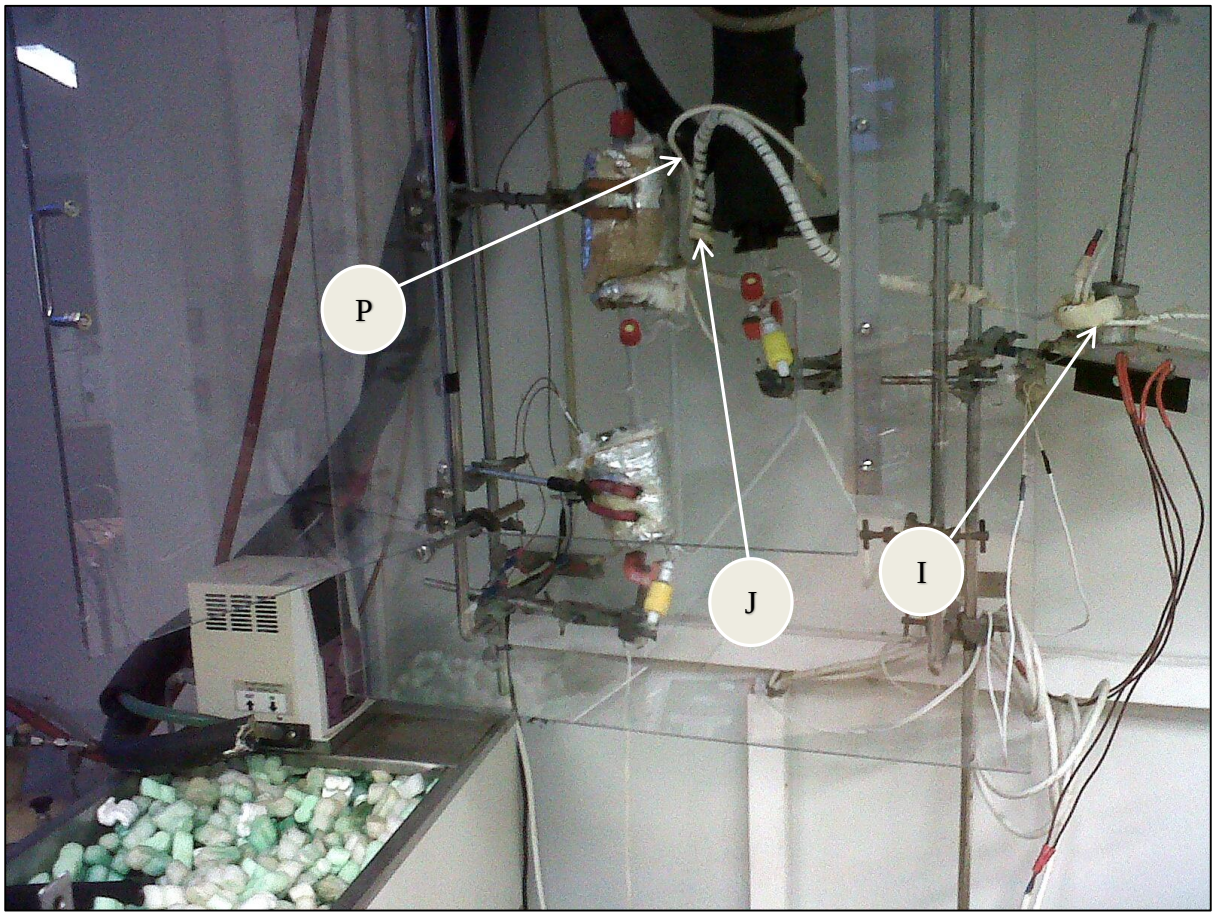

Figure 4-1(b): Photographic representation of the VLE apparatus used in this project modified by Ndlovu (2005).

The equilibrium still used in this study does not include the six- port GC valve (I) and the helium gas line from the cylinder (J), both illustrated in Figures 4.1 (a) and 4.1 (b) above. These were removed/de-activated in order to create more efficient operation of the still in terms of creating more space and also economising by reducing energy usage and avoiding depletion of helium gas. Additionally, since VLE measurements were being undertaken, 'on-line' sampling (superheated take-off of the vapour samples directly to the gas chromatograph) of the vapour phase as when performing VLLE measurements, was not necessary here. This feature was implemented for systems of partial liquid miscibility, for which the vapour forms a two-liquid phase upon condensation (Ndlovo, 2005). Both liquid and vapour phase compositions were sampled manually via direct injection into a gas chromatograph. Lastly the nichrome resistance wire (P) - also shown in figure 4.1 - was not required as it is not necessary to superheat the vapour as the systems that were studied in this project were not found to be partially miscible through analysis of literature and their chemical make-up.

Ultimately these were removed as the on-line GC (Hewlett Packard 5890 Series II Gas Chromatograph) had ceased to function. It was subsequently removed and replaced with another GC and the vapour take off line intersection where the glass still joins with the stainless steel take off line was sealed with a Swagelok connecting-nut fitting.

The simplified still of the modified VLE still of Ndlovu (2005) and its peripheral equipment used to aid in operation is represented in a schematic shown in Figure 4.2 with ancillary items (I), (J) and (P) removed.

The pivotal feature of this still is the packed equilibrium chamber that is concentrically shaped in its design. The chamber is surrounded by a vacuum jacket (E) in order to facilitate adiabatic operation within it.

Upon commencement of experimental trials, a binary mixture is charged into the boiling chamber (A). Here the external and internal heaters bring the sample to a boil. The external heater is composed of resistance nichrome wire wrapped around the boiling chamber (L) and accounts for environmental losses. The glass tube insert encases the internal heater cartridge (B) which initiates the boil-up process. Furthermore the internal heater induces rapid boiling, and nucleation sites are produced by the roughened glass tube for smoother boiling and control of the circulation rate (Clifford, 2004). The mixture of vapour and liquid then moves up through the vacuum insulated Cottrell tube (C) into the equilibrium chamber equilibrium chamber with stainless steel wire mesh packing (F) 3mm in diameter. The hollow, wire mesh cylinders reduce pressure drop through the packing. The Cottrell tube (pump) is insulated to prevent the heat transfer from the superheated mixture from entering the equilibrium chamber. The mixture then flows downward through the mesh packing in the equilibrium chamber. As mentioned by Yerazunis (Yerazunis et al., 1964), the packing creates a larger interfacial surface area, increasing residence (hold up) time of the mixture thus increasing the contact time between the liquid and vapour phase. In turn, this produces efficient and rapid equilibrium within the chamber even for systems with components possessing high relative volatilities. A glass insert housing the Pt-100 temperature sensor (H) is situated within the packing of the equilibrium chamber. The equilibrium mixture exits the equilibrium chamber through tiny holes at the bottom of the chamber near the base. This is where the liquid and vapour phases disengage. The vapour will then flow upwards and around the equilibrium chamber (M) in order to create thermal lagging which is essential to create adiabatic conditions around the equilibrium chamber with stainless steel wire mesh packing (M). The vapour then flows down toward the condenser (K) and is sampled in the vapour sample point (M) where it is magnetically stirred in order to homogenise the two phases in the mixture. The liquid flows out from beneath the base of the equilibrium chamber and downward into the liquid sampling point (D) (Bownath, 2008).

Further significant features included in the design of the still entailed:

- The still was designed such that the packing can be accessed easily through the top of the still just above the equilibrium chamber. This enables the packing height within the chamber to be adjusted by addition or subtraction of packing material. This is advantageous when measuring highly volatile systems that could have difficulty in attaining equilibrium.
- The equilibrium chamber has angular symmetry due to the central design location of the Cottrell pump. This ensures no preferential radial flow of the vapour-liquid mixture hence preventing the formation of either temperature or concentration gradients.
- Magnetic stirrers are situated within the boiling chamber and the condensate receiver at their base. In addition to the internal heater serving as a nucleation site, so are the boiling chamber stirrers. The condensate returning through dynamic re-circulation from the condensate sampling point overflow, is lower in temperature and rich with the more volatile component. It is thoroughly mixed in the boiler before evaporation hence preventing flashing. The stirring in the condensate receiver eliminates possible temperature and concentration gradients that might have existed in the vapour condensate, therefore ensuring good reproducibility for gas chromatography sample analysis.
- The PT-100 temperature sensor positioned within the packing in the equilibrium chamber. In previous designs the vapour-liquid mixture exiting the Cottrell tube came in direct contact with the temperature sensor bulb. In this case the superheated vapour was unable to dissipate (as when the sensor is submerged in packing) rendering the measurement less accurate. In the current design the returning liquid flows around the sensor through the packing making this a more precise measure of the system temperature.
- The packing within the equilibrium chamber increases the mass transfer between the vapour and liquid phases, thus facilitating for the rapid attainment of equilibrium. This eliminates the dependence on the Cottrell tube as the primary means of establishing phase equilibrium.

4.1.2. The Vapour-Liquid Equilibrium Apparatus

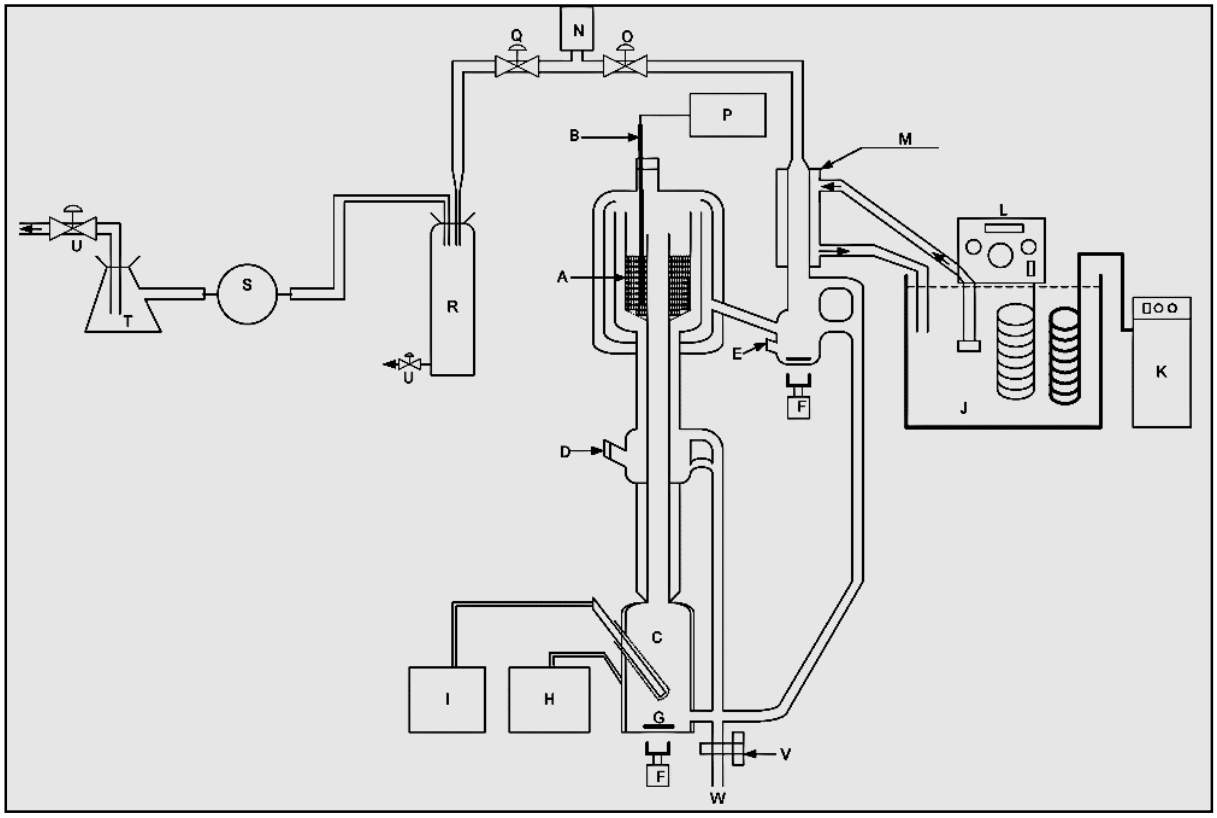

The experimental VLE apparatus operated in this study was described previously in detail and utilized for research by Joseph (Joseph et al., 2001), Sewnarain (Sewnarain et al., 2002) and (Clifford, 2004).

The followingperipheral equipment was employed in the design of this still to handle measurements over a range of pressures and temperatures:

- A, packing chamber;
- B, Pt-100;
- C, reboiler;
- D, liquid sampling point;
- E, vapour sampling point;
- F, stirring motor;
- G, magnetic stirrer;
- H, external heater;
- I, internal heat;
- J, water bath with chilling fluid;

- K, cold finger;
- L, temperature programmable circulator;
- M, condenser;
- N, pressure transducer;
- O, control valve;
- P, digital multimeter;
- Q, fine tune valve;
- R, ballast;
- S, vacuum pump;
- T, vacuum flask;
- U, vent valve to atmosphere;
- V, drain valve and
- W, drain.

4.1.3. Temperature Measurement and Control

Temperatures within the equilibrium chamber were measured using a class A Pt-100 temperature sensor probe. The probe was calibrated using the WIKA CTB 9100 calibration unit (refer to Chapter 5 for the calibration procedure). The uncertainty in the temperature measurement is ± 0.1 K with a confidence factor of k=2 (Reddy et al., 2013).

The temperature control for the isothermal runs (±0.03 K) was achieved through a variation of pressure (with an algorithm for dT/dP) with a pressure controller (Shinko model ACS-13A, USA) and pulse-width modulation of the Clippard solenoid valves (Reddy, 2012). The temperature for each isothermal VLE system was manually controlled by adjusting the pressure set-point in the pressure controller, where increasing the pressure results in an increase of the system temperature and decreasing the pressure lowers the system temperature.

4.1.4. Pressure Measurement and Control

A WIKA model P-10 pressure transducer was used for the measurement of the pressure. The pressure transducer was calibrated with a WIKA CPH 600 pressure transducer standard. Pressure calibrations are detailed in Chapter 5. The uncertainty in the reported pressure is ± 0.1 kPa with a confidence factor of k=2. Pressure control was facilitated below atmospheric by solenoid valves connected to an Edwards vacuum pump (model RV3).The vacuum pump was connected to a 25 litre ballast tank that reduced fluctuations in pressure.

4.1.5. Sampling

Liquid and vapour samples were withdrawn from the sample points using a gas-tight syringe through a chemically resistant septum. The purpose of utilising gas tight syringes was to ensure that no sample was lost during the process of sample withdrawal. The gas-tight liquid syringe used for sampling had a volume of 1 µl and a needle diameter of 0.1 mm. This significantly small diameter insured that when injecting through the chemical resistant septum, this action does not affect the measured equilibrium pressure and temperature within the VLE still.

4.1.6. Composition Analysis

Compositional measurements were obtained using a gas chromatograph (Shimadzu model 2014, Japan) equipped with a TCD and a SupelcoOV-17 packed column (10% silicone, 3m x 1/8 inch SS). Vapour samples followed by liquid samples were then withdrawn for compositional analysis. The TCD was calibrated with the area ratio method suggested by Raal and Mühlbauer (Raal and Muhlbauer, 1998). The operation, calibration and sampling procedures of the GC are discussed in greater detail in Chapter 5.

5

Chapter Five

EXPERIMENTAL PROCEDURE

This chapter will outline the experimental procedure and methods pertaining to operation of the VLE apparatus described in Chapter 4. Successive trial runs were carried out with the aim of achieving accurate and reproducible experimental results hence resulting in the descriptive procedure presented in this chapter. With the two operational modes of the VLE apparatus being isobaric and isothermal operation, different operating procedures pertaining to each specific mode were necessary. Ancillary equipment of the VLE apparatus such as the pressure transmitter, pt-100 temperature sensing probe and gas chromatograph for phase composition had to be calibrated before operation could commence. It is imperative that calibration at this stage of experimentation be carried out as accurately as possible with minimum amount of error possible as the accuracy of the final measured experimental data depends directly on the accuracy and precision of the calibration of variables obtained.

The following focal points will be covered in this chapter:

a. Preparation of the experimental equipment

b. Operation of the VLE apparatus

c. Calibration of equipment used in the apparatus

5.1. The VLE apparatus

5.1.1. Preparation

5.1.1.1. Cleaning of the equilibrium still

The VLE still initially has to be cleaned prior to any calibrations or measurements being undertaken. Any contaminants present within the still could significantly affect the validity of the VLE data

produced. The still was cleaned thoroughly by circulating pure acetone using the same operating procedure outlined in section 5.1.3. This was achieved by allowing the acetone to circulate for approximately an hour under isobaric conditions. The process was repeated by draining the acetone (using the drain valves in figure 4.1) from the apparatus and inserting clean acetone by following the loading procedure in section 5.1.3.1. The VLE still was cleansed for a third time for chemicals that were difficult to remove (such as methyl-tert butyl ether) by using the aforementioned procedure with acetone. Once the cleaning process was completed, the acetone was drained and any acetone remaining within the still that could not be removed by merely draining due to the position (trapped at bends or in areas not visible) was flashed off. This was achieved by bringing the still to a very low pressure (i.e. approximately 0.1 kPa) using the vacuum pump of the apparatus, thus allowing excess acetone to be vapourised.

5.1.1.2. Leak detection

The occurrence of leaks is a major concern to be addressed before using the VLE apparatus. Leaks can result in loss of material which adversely affects liquid and vapour phase composition measurements and pressure control which in turn results in erroneous temperature measurement.

The typical method of testing for leaks would have been to pressurise the apparatus and apply a commercial soapy solution (Snoop®) to the joints on the apparatus where leaks are suspected to occur. Bubbles become visible where leaks are present due to the air being released combined with soapy solution. The VLE still however was constructed of glass suitable to withstand pressures below atmospheric only. Additionally all measurements performed in this study were performed at pressures below atmospheric pressure.

An alternative method was therefore selected for testing. This method involved the evacuation of the still completely (until the pressure display read 0.0 kPa) using a vacuum pump followed by total isolation of the vacuum pump via the control valves on the connecting lines between the vacuum pump and the still. Upon stabilisation of the pressure, the apparatus was left in isolation for approximately two hours. The presence of any leaks resulted in a significant rise in system pressure becoming visible on the pressure display.

5.2. Chemical Purity

It was imperative that the chemicals that were utilized in experimental trials were tested for impurities by gas chromatography. The purity of the chemicals specified by the suppliers has to be confirmed therefore analysis of purity via chromatography is required. Experimental results obtained can be severely affected should the quantity of impurities present in the supplied chemical be substantial.

5.2.1. Calibration

5.2.1.1. Pressure transmitter calibration

Pressure calibration was undertaken first because the equilibrium temperature sensor calibration required an accurate pressure indication (equilibrium temperature is dependent on the system pressure). A standard pressure transmitter was connected to the VLE apparatus in order to calibrate the actual (WIKA) pressure transmitter. The calibration of the standard pressure transmitter was performed by WIKA such that it displayed an accurate pressure reading.

The Shinko ACS-13A pressure controller was used to set a specific pressure reading on the graphical user interface (in this case the data logger from Agilent® technologies) for the VLE apparatus. The pressure controller was operated to control pressure at set-points within the range of 1kPa to 100kPa (absolute). The WIKA P10 pressure transmitter was calibrated with a low pressure calibration unit (WIKA model CPH 6000, Germany). The calibration units were supplied by WIKA Instruments (South Africa). When system pressure had stabilised, the WIKA P10 pressure transmitter reading and that of the standard pressure transmitter were recorded. The pressure of the standard was read from a handheld pressure display device (part of the WIKA pressure calibration unit).

This procedure was repeated within the aforementioned pressure range for various pressure readings in increments of 5 to 10 kPa. The pressure from the standard pressure transmitter (actual pressure) was plotted against the pressure from the WIKA P10 pressure transmitter (display pressure). A linear response was obtained. This is represented in Figure 5-1. The uncertainty arising from the calibrated pressure sensor was 0.03 kPa.

5.2.1.2. Temperature sensor calibration

Equilibrium temperature measurement using a class A Pt-100 temperature sensor was previously discussed in detail (Chapter 4 Section 4.1.3). This temperature sensor required calibration.

This was achieved using a standard Pt-100 reference probe connected to a WIKA CTH 6500 display and submerging both Pt-100 probes into the WIKA 9100 oil bath which contained silicon oil. The silicon oil provides a good heat transfer medium creating uniform temperature throughout the bath for a greater precision in measurement. Monotonical increase and decrease of the temperature of the oil bath was done in order to detect presence of hysteresis until a large temperature range was covered.

5.2.1.3. Gas chromatograph detector calibration

For the analysis of the equilibrium vapour and liquid compositions, the Shimadzu model 2014 gas chromatograph was utilised.

Well separated, visibly sharp and uniformly shaped GC peaks are generally preferred for accurate analysis of equilibrium compositions. The GC therefore, had to bet set using the GC solutions™ computer program (designed to interface with Shimadzu model GC's) to operate at conditions that would generate acceptably formed peaks.

The operating conditions for this GC are presented in Tables 6-4 and Table 6-5. The area ratio method GC detector calibration technique by Raal was used. This technique was most suitable as it is independent of the amount of sample injected into the GC.Mixture samples for calibration analysis were prepared by injection in 2 ml vials placed on a mass balance. Calibration GC curves were produced by gravimetrically preparing standard solutions by using pure chemicals. Analysis was carried out over a ratio of mole fraction(x_1/x_2) range of 0 to 1 in increments of 0.2.

For binary systems the equation representing the area ratio is:

$$\frac{n_1}{n_2} = \left(\frac{A_1}{A_2}\right)\left(\frac{F_1}{F_2}\right) = \frac{x_1}{x_2} \tag{4-1}$$

where

n_1 and n_2 - number of moles of component 1 and 2 in the mixture;

A_1 and A_2 - peak areas from GC analysis;

F_1/ F_2 - response factor ratio;

x_1 and x_2 - mole fraction of component 1 and 2 in mixture.

The calculation of uncertainty in the phase composition from calibration is crucial in determining the overall uncertainty in phase composition measurement (Soo, 2011, (NIST), 1994). The estimated uncertainties in the mole fractions are listed in Table 6-2 for the binary systems of 2, 2, 4-trimethylpentane + 1-pentanol, MTBE + 1-pentanol, MTBE + 2, 2, 4-trimethylpentane, DIPE + 2, 2, 4-trimethylpentane, DIPE + 1-pentanol and DIPE + 2-butanol.

The response factors (F_1/F_2) were calculated by injecting micro-litre samples into the GC. Area ratios were plotted against composition ratios, A_1/A_2 vs. x_1/x_2 and A_2/A_1 vs. x_2/x_1 in order to generate the

response factors. The test for the calibration procedure as stated by Raal and Mühlbauer (Raal and Muhlbauer, 1998) says that the inverse of the gradient of the first response factor must equal the gradient of the second response factor. This should hold true if the plot is linear, which it always should be if the calibration analysis procedure is performed accurately.

5.3. Operating procedures

5.3.1. Loading/Filling of the VLE still

The still was initially charged with approximately 90 ml of one of the components of the binary mixture using a 10 ml standard syringe. The vapour and/ or liquid sampling traps of the VLE still can be used to inject the sample into the still.

5.3.2. Plateau Region

There is a steady relationship between heat supply to the reboiler and temperature input when performing VLE measurements (Kneisl et al., 1989). As a consequence of hydrostatic head, the vapour-liquid mixture moving up the Cottrell tube becomes slightly superheated according to Kniesl et al. (1989). The superheated portion of the mixture becomes relieved as the mixture exits the Cottrell tube then moves onto the packing within the equilibrium chamber. The vapour-liquid mixture then cools down to its equilibrium temperature. This is a result of the expansion of the mixture and the evaporation of a minute amount of the liquid phase upon entry to the equilibrium chamber.

The figure 5.1 below illustrates how the equilibrium temperature of the vapour-liquid mixture responds and varies with an increase of energy input. Figure 5-1 exhibits that when low heating rates are implemented, increasing the internal heater energy input results in a sharp rise in the measured equilibrium temperature. This temperature profile will flatten hence leading to a broad “plateau region” (Kneisl et al., 1989). Within this region small increases in the energy input will not change/affect the measured temperature. As a consequence of expansion of the vapour-liquid mixture, the heating rate becomes insufficient to superheat the liquid and offset the cooling effect (Kneisl et al., 1989). When further heating is induced (resulting in going beyond the plateau region), the superheating effect becomes greater than the cooling effect.

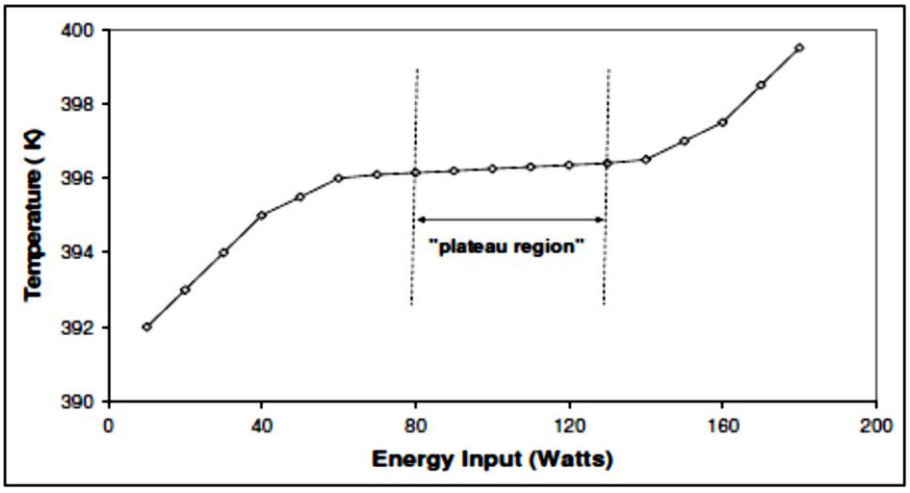

Figure 5-1: Temperature response curve showing an ideal plateau region (Pillay, 2010).

The plateau region is not necessarily a flat region visually when generated. The chemistry of the compounds is significant with regards to the position over which the plateau region will reside. Large and distinct plateau regions are evident for low boiling non-polar alkanes (Kneisl et al., 1989). The opposite effect hold true for high boiling polar compounds like alcohols and amides as their plateaus are not easy to distinguish. In such cases the plateau region is determined as the area that has the smallest slope. It is however of great significance that the true plateau region is measured; incorrect determination of the region will result in erroneous phase equilibrium data being measured.

5.3.3. Plateau Region Measurement

The plateau region initially had to be found before each phase equilibrium data point was measured. The external heater was set and maintained at 25V for all the systems measured to account for environmental heat losses. A low heat setting was then implemented via the internal heater. Heat input was incremented higher by approximately 5V, whenever the system would stabilise after a higher energy input. The measured temperature was logged after each system stabilisation. The power input initially selected, used the lowest voltage, where even boil-up of the vapour-liquid mixture was visible (through the Cottrell tube). This initial voltage was therefore selected and the system was allowed to equilibrate for approximately 20 minutes. Thereafter the voltage to the internal heater was increased in increments of 5 V and about 10 minutes was required to reach equilibration at each subsequent increase in the power input (Pillay, 2010).

5.3.4. Reaching Equilibrium

Attaining a state of thermodynamic equilibrium was the next step required once the plateau region had been established. An equilibrium time of 45-50 minutes was allowed. These times may vary with each system, due to the molecular interactions between chemicals within each system. The equilibrium time depends on the relative volatility of the binary systems measured and the circulation rate in the still.

The three criteria utilised to ascertain equilibrium are as follows:

- The drop rate of vapour-liquid mixture from the condenser into the sample trap will be fast;
- The vapourisation rate of the vapour-liquid mixture flowing up the Cottrell tube, has a continuous and stable flow without any type of pulsing flow;
- The simultaneous constancy of temperature and pressure in measurement; reproducible phase compositions from direct method GC analysis (for binary mixtures).

5.3.5. Isobaric procedure

Start-up procedure

Measurements commenced by switching on the power supplies to the temperature and pressure displays, pressure controller, Agilent® data logging device and the two magnetic stirrer motors. The PolyScience® cold finger was switched on to bring the cooling medium (ethylene glycol) within the bath to a suitable temperature set-point of -5°C. In order to avoid any loss of material within the condenser, the running of the equipment will only commence once the set-point has been reached. Approximately 90 ml of pure component was injected into the clean VLE still via the liquid or vapour sample trap. It was of importance to note that this ensured that the VLE still was charged with pure component to a level approximately 4 cm higher than the top of the boiling chamber. This enabled ease of boil-up during dynamic operation, allowing the vapour-liquid mixture to reach the temperature sensor completely in turn creating accurate measurement in equilibrium temperature. Poor boil-up was noted to create erroneous and unstable temperature readings.

The vacuum pump was switched on to induce vacuum pressure in the still below atmospheric and also to maintain pressure below atmospheric during runs. The pressure controller was set to the operating pressure required. This action then allowed the pressure within the still to be decreased toward the set-point pressure via the actuation of the solenoid valves. The internal and external heaters were switched on to boil the liquid in the boiling chamber. The external heater was switched on first in order to compensate for environmental heat losses due to varying temperature conditions within the

laboratory throughout the course of each day. The internal heater was the primary source of heating the liquid. Adequate heating being supplied is of great significance during the boil-up process as it provides vigorous pumping in the Cottrell tube and a satisfactory circulation rate. A good circulation rate is observed by noticing the drop-rate of condensed liquid from the condenser in conjunction with the vaporisation rate from the boiling chamber. The heat supply of the internal heater to the liquid was then increased in various increments until the plateau region was reached. When the plateau region had been acquired, the system was then allowed to reach equilibrium.

At equilibrium the temperature and composition will be constant. For the systems measured in this study, an equilibrium time of approximately 50 minutes was found to be adequate. There have been many cases where systems studied elsewhere found an equilibrium time of 40 to 45 minutes to be sufficient. Once equilibrium was reached the temperature was logged. The vapour and liquid samples were withdrawn via the respective sample septa using a 1μl gas-tight liquid chromatography syringe. The samples were then analysed by a gas chromatograph. The phase compositions of the components were calculated from GC peak areas.

Once samples have been analysed, a volume of approximately 2 ml was removed from the vapour or liquid sample septum to measure the proceeding equilibrium data point. Thereafter a similar volume of the second component was added to the still in order to adjust the system phase composition. The mixture was then allowed to reach equilibrium. The vapour and liquid samples were then withdrawn and analysed as previously done. The entire phase composition range was covered by repeating this procedure. By covering both ends of the composition range, a greater allowance for accuracy becomes possible. This essentially tests the experimental technique as both sides of the equilibrium curves should smoothly meet in the middle when generated. Should the curves meet in a contrary position, the experimental technique could be erroneous.

5.3.6. Isothermal Operation

Proper operation of the still isobarically is critical, as isothermal operation is dependent on the accurate and successful operation of the still in isobaric mode. Therefore, start-up procedure is carried out in the same manner as it would be for isobaric operation. Procedures where the same for determination of equilibrium and composition analysis, with the difference in operation being, that pressure was varied to maintain constant system temperature. To acquire isothermal measurements, the pressure in the still was set to a value such that when equilibrium was obtained, the equilibrium temperature was close as possible to the operating temperature required. Isobaric operation was thereafter stopped and the temperature was manually adjusted to the desired value. This was done by increasing or decreasing the pressure manually. This had the effect of raising or lowering the temperature. (See Section 4.1.3).

5.3.7. Composition Analysis

When the binary mixture within the still was operating within the plateau region and equilibrium had been reached, vapour and liquid samples were withdrawn. 2 ml samples were collected from the vapour and liquid sample traps respectively using a standard 10ml syringe. The collected samples were placed into well sealed sample vials, each having a maximum volume of 2 ml. A 1 µl gas tight liquid syringe was then used to draw the samples from the vials and inject them directly into the Shimadzu 2014 GC. The GC was equipped with a thermal conductivity detector (TCD). A Porapak® Q packed column (OV-17) or a Chromosorb (W-HP) packed column (obtained from Trilab Support - South Africa) was used. The type of packed column used depends on the chemistry of the system being measured i.e. how well the components in the mixture separate and react to the phase of the columns packing (regarding the uniform shape of peaks).

5.3.8. Shutdown Procedure of VLE apparatus

It is important to render a safe and precise shut down procedure of the VLE apparatus after the acquisition of data. This will ensure the longevity of the equipment in the long run, and avoid electrical fires together with other safety hazards such as breakage of the glass, resulting in potentially hazardous chemical spillage. The heaters were switched off first. The cooling unit remained on to ensure that all vapours formed during experimentation were condensed. The system was then brought to cool to approximately 40^{o}C before turning off the control program. Pressure was returned to atmospheric by using the bypass line on the side of the ballast tank.

5.3.9. Shutdown Procedure of the Gas Chromatograph

The bridge current of the TCD was switched off. Next the injector temperature, column temperature, detector (TCD) and pre-heater temperature were all lowered to 25°C. The carrier gas flow rate was lowered to conserve gas. The carrier gas was only switched off once the detector temperature was cooled down to its set-point and switched off. This was done because the detector cannot be turned off without gas flowing through it as this will cause damage to it.

6

Chapter Six

EXPERIMENTAL RESULTS

In the preceding chapter, the experimental procedure described was developed as a result of several experimental runs carried out on a *test system*. The accuracy of the experimental data obtained is influenced by the accuracy and precision at which pressure, temperature and composition measurement is undertaken. The purity of the reagents used also impact the accuracy of experimental results.

Therefore, the test system was measured to ensure the correct operation of the vapour-liquid equilibrium (VLE) apparatus was performed and that the experimental method was acceptable pertaining to precision and accuracy. An isothermal VLE test system was measured: (cyclohexane + ethanol) at 323.15 K. The main criterion for selection of this system (which this particular system satisfies), was that it should be non-ideal and that consistent literature data for the system be available. In addition, this system is entirely miscible over the entire composition range. It is also difficult to measure making it an ideal subject to test an optimal experimental method on. Purities of the test chemicals used (as well as all chemicals used in this work), were also determined experimentally to ensure the reliability of the measured data. The test chemicals were available at high purity and reasonable costs, which are favourable attributes desired in any test chemical. VLE data were measured for the test system mentioned above and the results obtained were plotted against the literature data of the same system.

This chapter contains the experimental results obtained during the duration of this project and includes the phase equilibrium data measured. Calibrations for the pressure and temperature sensors, including the GC detectors are also presented. Measured variables for the systems under investigation, namely, pressure, temperature and composition, possess an uncertainty due to factors surrounding measurement. The uncertainty of measured variables also greatly influences the accuracy of the experimental results obtained. Hence, uncertainty along with the other factors mentioned above (pertaining to precision and reliability of experimental data), will be expanded upon within the preliminary sections of this chapter.

6.1. Purity of materials

Chemicals of the highest purity available were obtained and used in this study. It is imperative that all impurities from the chemicals and apparatus are removed prior to experimental work.

All of the chemicals used in all experimental work were liquids at room temperature and pressure. Prior to chemicals being used, their purities were checked against the manufacturer's stated purities printed on the product label. This was done with the utilisation of GC analyses, of the pure components, as well as the measurement of their refractive indices. Refractive indices were checked and verified using the ATAGO® 7000α refractometer with an indicated accuracy of ±0.00001. Measured values were then compared to literature values, with the absolute deviation (between measured and literature values) being noted, providing an appropriate indication of the chemical purity. A Shimadzu GC 2014 (TCD), with Porapak® Q and Chromosorb columns (both used on different occasions due to the chemistry of the different systems measured), was used to verify the purity of the chemicals; the stated had to be close to values specified by the supplier.

Following the method of Raal and Mühlbauer, (1998) for gas chromatographic analysis, no significant impurities were revealed for all chemicals used in this project. Furthermore, the agreement between the measured refractive indices of each chemical with those found in the literature, were all satisfactory in this study as shown in Table 6-1. Therefore, all chemicals were used directly without the need for further purification. Table 6-1 below lists all the chemicals used in the experimental work including the chemical suppliers, stated purities, GC analyses and refractive index results.

Table 6-1: Chemicals used and their Purities

Chemical (IUPAC name)	CAS number	Supplier	Minimum Purity mass (%)[a]	GC analysis Peak area (%)	Refractive Indices (at 298.15K) Literature[b]	This work
Methyl *tert*-butyl ether	1634-04-4	Merck	≥ 99.85	99.99	1.36630	1.36632
1-pentanol	71-41-0	Capital Laboratories	≥ 99.00	100.00	1.40770	1.40764
2, 2, 4-trimethylpentane	540-84-1	Lab Scan Analytical Sciences	≥ 99.50	99.99	1.38900	1.38910
Diisopropyl ether	108-20-3	Sigma-Aldrich	≥ 99.50	99.99	1.36551	1.36550
1-propanol	71-23-8	Sigma-Aldrich	≥ 99.50	100.00	1.3837	1.38368
2-butanol	78-92-2	Sigma-Aldrich	≥ 99.50	99.80	1.3978	1.39800
Cyclohexane	110-82-7	Merck	≥ 99.85	99.99	1.4235	1.42339
Ethanol	64-17-5	Merck	≥ 99.50	99.99	1.3594	1.35939

[a]Stated by supplier

[b]Yaws Handbook of Thermodynamic and Physical Properties of Chemical Compounds, Kovel, (Yaws and Gabbula, 2003).

6.2. Reporting Uncertainty in Measurements

An additional significant factor to be taken into account apart from checking the purity of chemicals used is the accuracy of all measurements that are undertaken. Uncertainty being reported in measurement is an important aspect of experimental data. This is mainly because quantification of uncertainty gives a reliable indication of the accuracy of the phase equilibrium measurements carried out, thus revealing the range wherein the 'true measured' value exists.

The difference between error and uncertainty is often times misunderstood. Error is computed as the difference between the measured value and the actual value of the particular variable being measured, whereas uncertainty is the calculation of the doubt regarding the experimentally measured result (Bell, 1999). The NIST standard method of computation of uncertainty is represented by the following standard equation (Taylor and Kuyatt, 1994):

$$u_c(\theta) = \pm\sqrt{\sum_i u_i\left(\theta\right)^2} \tag{6-1}$$

The combined standard uncertainty, u_c, is a combination of all the calculated uncertainty, taking into account all sources of error which includes calibration, measurement and instruments used. Identification of all possible sources that may contribute to uncertainty is essential to quantify uncertainty. The stability of the measured variable (symbol 'θ'), and the instruments used for measurements, are the most visible contributors to uncertainty. The variable, u_i represents the uncertainty resulting from any source possible such as the temperature or pressure calibration chart. For this particular project: pressure, temperature and composition uncertainties were computed.

6.2.1. Uncertainty in Pressure and Temperature

The pressure and temperature variables' uncertainty is a result of repeatability deviations of a single transducer reading and imperfections in the calibration plots. The standard representation of how to tabulate uncertainty for pressure and temperature are the following equations:

for pressure: $$u_c(P) = \pm\sqrt{u_{calib}(P)^2 + u_{rep}(P)^2} \tag{6-2}$$

for temperature: $$u_c(T) = \pm\sqrt{u_{calib}(T)^2 + u_{rep}(T)^2} \tag{6-3}$$

Subscripts *calib* and *rep* denote the calibration and repeatability respectively. Temperature will be taken into account for elaboration purposes in this section. The calibration curve provides the lower and upper limit of uncertainty which is derived for the temperature function in the equation (6-3). Temperature calibration plots clearly show (visually and computationally) the deviation from the set-point temperature. It is assumed that the temperature will always lie within the estimated range when calculating uncertainty. This is commonly designated as *Type B* (or random) uncertainty calculation method. The random approach utilises a rectangular distribution, outlined by the following equation:

$$u_{calib}(T) = \frac{b}{\sqrt{3}} \tag{6-4}$$

where '*b*' denotes the average length between the lower and upper limit of temperature uncertainty – the error quantity. When sampling of vapour and liquid takes place, the pressure and temperature at

the event of sampling is not stable. This behaviour results in the calculation of uncertainty for the repeatability of measurements performed. The measurements are assumed to lie close to the mean; hence this behaviour with respect to repeatability (called Gaussian type distribution) occurs. It is therefore referred to as a systematic uncertainty, otherwise known as *Type A* uncertainty evaluation method. The method uses statistical science to for analysis of data, and is conducted using the following expression:

$$u_{rep}(T) = \frac{\sigma}{\sqrt{n}} = \sqrt{\frac{1}{n(n-1)}\sum_{i=1}^{n}\left(T_i - \overline{T}\right)^2} \tag{6-5}$$

where *n* represents the number of duplicate measurements.

6.2.2. Uncertainty in Molar Composition

Accurate and precise quantification of the TCD calibration and the averaging of peak areas obtained from the sampling process are paramount. This holds true as these two factors can contribute greatly to the molar composition uncertainty.

Repeatability uncertainty for molar composition contributes to only about 1 % of the final uncertainty due to the low value of the standard deviation from the averaging of the repeated samples drawn and analysed, which is, 5 sample injections per data point. Therefore, it is encouraged that uncertainty on repeated samples be neglected (Soo, 2011). An additional point regarding neglecting of the repeatability uncertainty is because the VLE apparatus manual sampling technique is not ideal. The Molar composition uncertainty equation is parallel to that of pressure and temperature, thus the uncertainty of composition for all measurements is:

$$u_c(x_i) = \pm\sqrt{u_{calib}(x_i)^2 + u_{rep}(x_i)^2} \tag{6-6}$$

with '*i'* denoting the component *i.*

Errors that surface from the balance (or scale) used to weigh samples during the preparation of standard solutions before TCD calibration, also need to be accounted for. The symbol '*B*' represents this factor in the following equation:

$$u_{calib}(x_i) = \sqrt{u_B(x_i)^2 + u_{corr}(x_i)^2} \tag{6-7}$$

The mole fractions can be expressed in terms of the species mass. This is because the 'x_i' term is mass dependant with respect to the components in the chemical system being analysed. It is expressed as follows:

$$u_B(x_i) = \sqrt{\left[\left(\frac{\partial x_i}{\partial m_1}\right)_{m2} u(m_1)\right]^2 + \left[\left(\frac{\partial x_i}{\partial m_2}\right)_{m1} u(m_2)\right]^2} \tag{6-8}$$

By applying the following chemical relations:

$x_i = \frac{n_i}{(n_i + n_j)}$ where $n_i = \frac{m_i}{MM_i}$, we obtain the reduction of equation (6-8) as:

$$u_B(x_i) = x_1 x_2 \sqrt{\left[\frac{u(m_1)}{m_2}\right]^2 + \left[\frac{u(m_1)}{m_2}\right]^2} \tag{6-9}$$

The combined standard uncertainties in the measurements are reported in Table 6-2 below.

Table 6-2: Reported Uncertainties for Pressure, Temperature and Mole Fraction of Binary VLE systems.

Measured System	$u_c(P)$/kPa	$u_c(T)$/K	$u_c(x)$
MTBE + 1-pentanol	±0.10	±0.10	±0.006
MTBE + 2, 2, 4-trimethylpentane	±0.10	±0.10	±0.008
2, 2, 4-Trimethylpentane + 1-pentanol	±0.10	±0.10	±0.007
DIPE + 2,2,4-trimethylpentane	±0.03	±0.04	±0.012
DIPE + 1-propanol	±0.03	±0.04	±0.001
DIPE + 2-butanol	±0.03	±0.04	±0.018
Cyclohexane (1) + Ethanol (2)	±0.20	±0.11	±0.021

The higher uncertainties in DIPE + 2, 2, 4-trimethylpentane or 2-butanol and cyclohexane are due to a higher uncertainty in the GC calibrations of these systems, not necessarily the actual VLE analysis.

6.2.3. Statistical Analysis Equations

The root mean square deviation (rmsd) is an indication of the precision of a data correlation performed. It is represented by the following equation (6-10) below:

$$rmsd = \left\{ \frac{\sum_{a}\sum_{b}\sum_{c}\left[x_{abc}(\exp) - x_{abc}(calc)\right]^2}{6k} \right\} \tag{6-10}$$

where x is the mole fraction, k is the number of experimental points and the subscripts a and b represent the component and phase. c is the tie-line variable used for ternary systems and LLE.
Other basic equations used for statistical analysis are as follows:

$$\Delta = \frac{m_{\exp} - m_{calc}}{m_{\exp}} \tag{6-11}$$

$$AAD(\%) = \frac{100}{N}\sum_{i=1}^{N}\left|\Delta\right|_i \tag{6-12}$$

$$BIAS(\%) = \frac{100}{N}\sum_{i=1}^{N}\left(\Delta\right)_i \tag{6-13}$$

The deviation 'Δ' designates the relative deviation of a particular calculated thermodynamic property m from a corresponding experimentally measured value. The *AAD* is the average absolute deviation of a data set having N number of experimental points.

6.3. Equipment Calibrations and Accuracy of Measurements

The estimated accuracy of the measured variables temperature and pressure for this project is summarized in Table 6-3 below.

Table 6-3: Estimated accuracy of measured system variables

Variable	Apparatus of Ndlovu (2005)
Temperature/K	±0.042
Pressure/kPa	±0.034

6.3.1. Pressure and temperature sensor calibrations

The calibrations of the pressure and temperature sensors are discussed in greater detail in Chapter 5. The pressure transmitter used on the apparatus of Ndlovu (2005) had been calibrated by WIKA instruments such that the reading taken off the display unit was congruent to the actual system pressure. For the pressure transmitter on the apparatus the calibration plots were generated for the pressure range: 0 to 100 kPa. The calibration curves for the pressure sensor and for the temperature sensors located in the equilibrium chamber are presented in Figures 6-1 to 6-6.

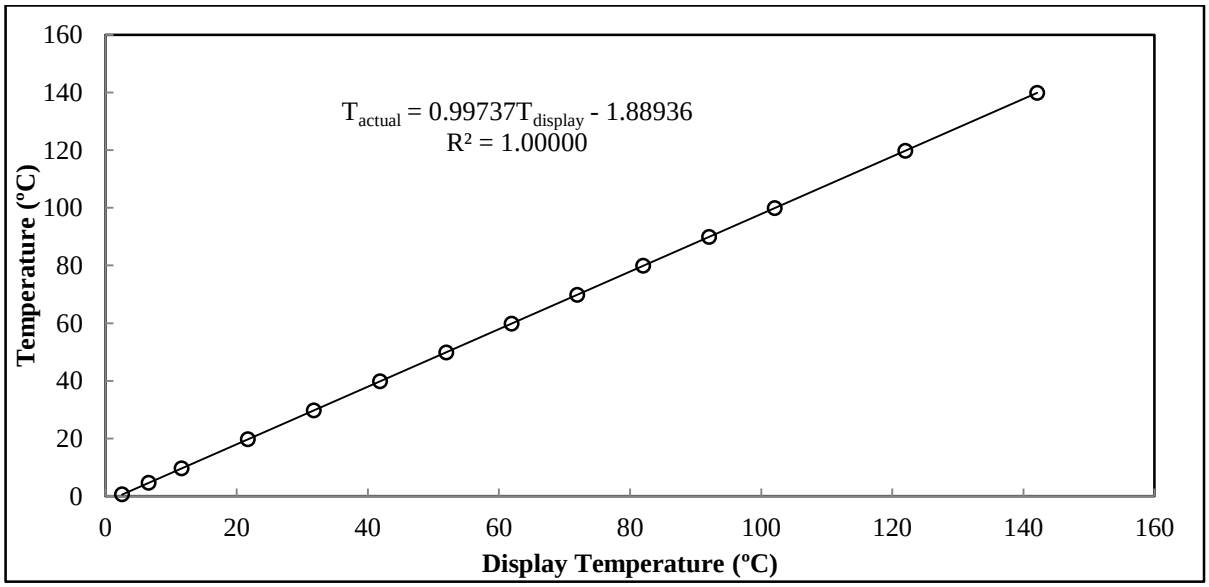

Figure 6-1: Calibration of the Pt-100 surface element for the VLE dynamic apparatus - linear relation between the actual and probe temperatures.

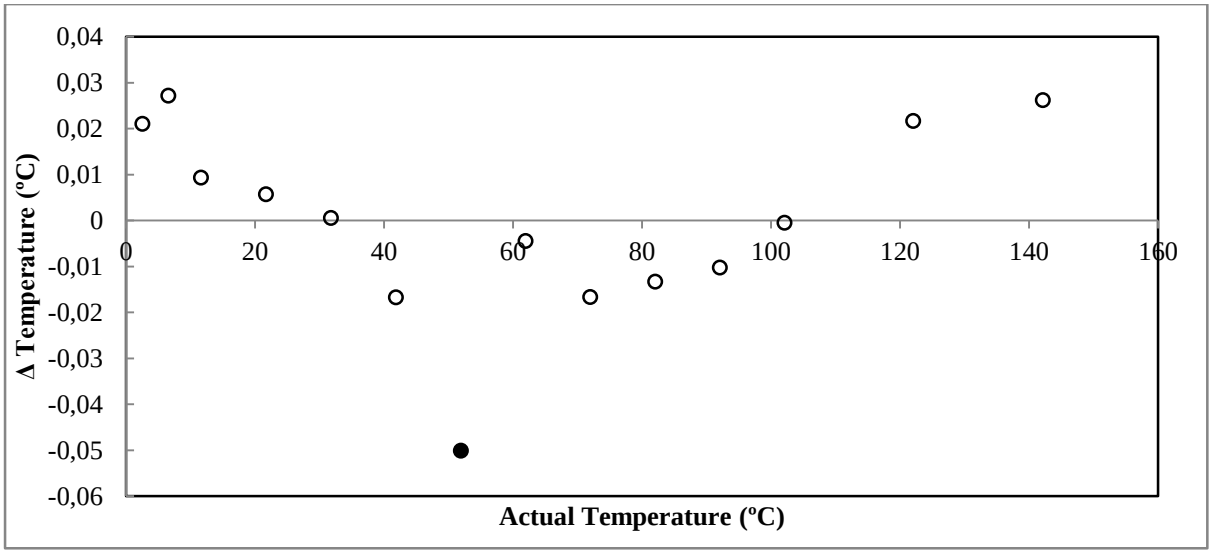

Figure 6-2: Deviations from the actual temperature, resulting from the use of a linear relation for dynamic analytic VLE apparatus: maximum deviation (●).

A comparison was made between the measured temperatures of the pt-100 temperature sensor and the calculated temperatures that were obtained by using the straight line polynomial generated from the calibration plot. This was done to test the accuracy of the calibration polynomial that was generated by the calibration plot, hence in turn resulting in a test of the accuracy of the overall temperature calibration. The graphical results can be seen in Figure 6-3 below.

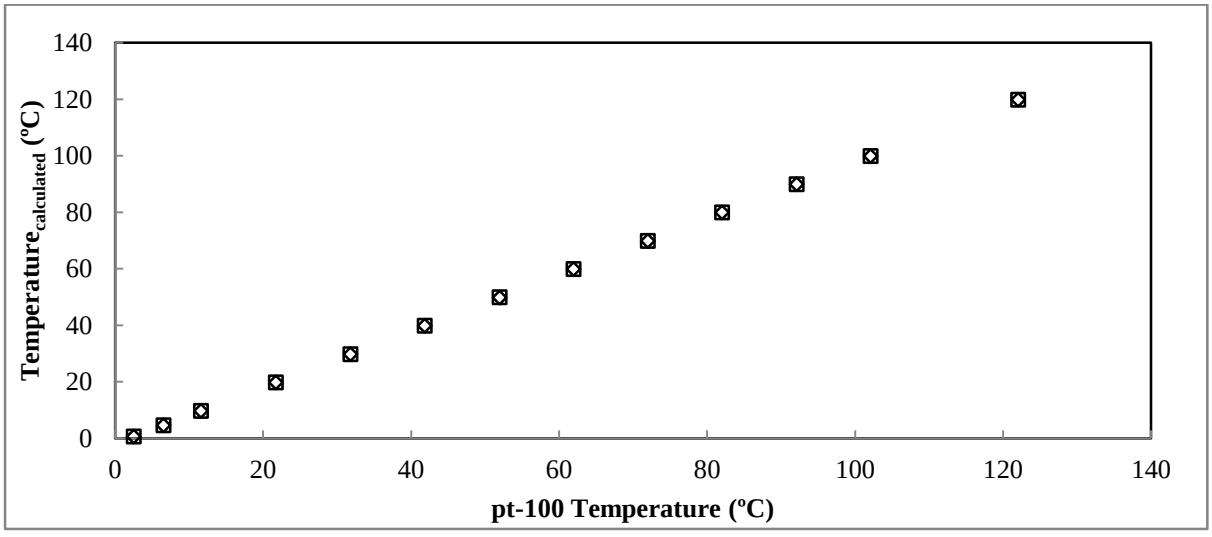

Figure 6-3: Measured pt-100 temperature (◊); calculated temperature using straight line polynomial equation (□).

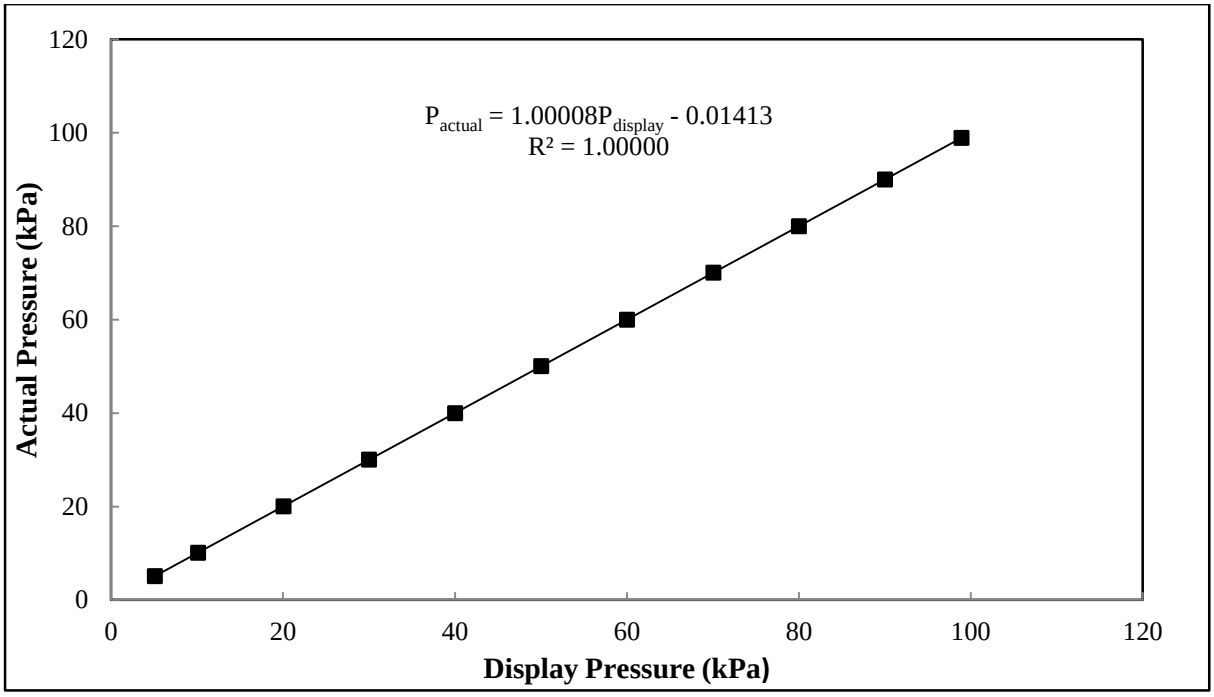

Figure 6-4: Calibration of pressure transducer for the VLE dynamic apparatus - linear relation between the actual and display pressure.

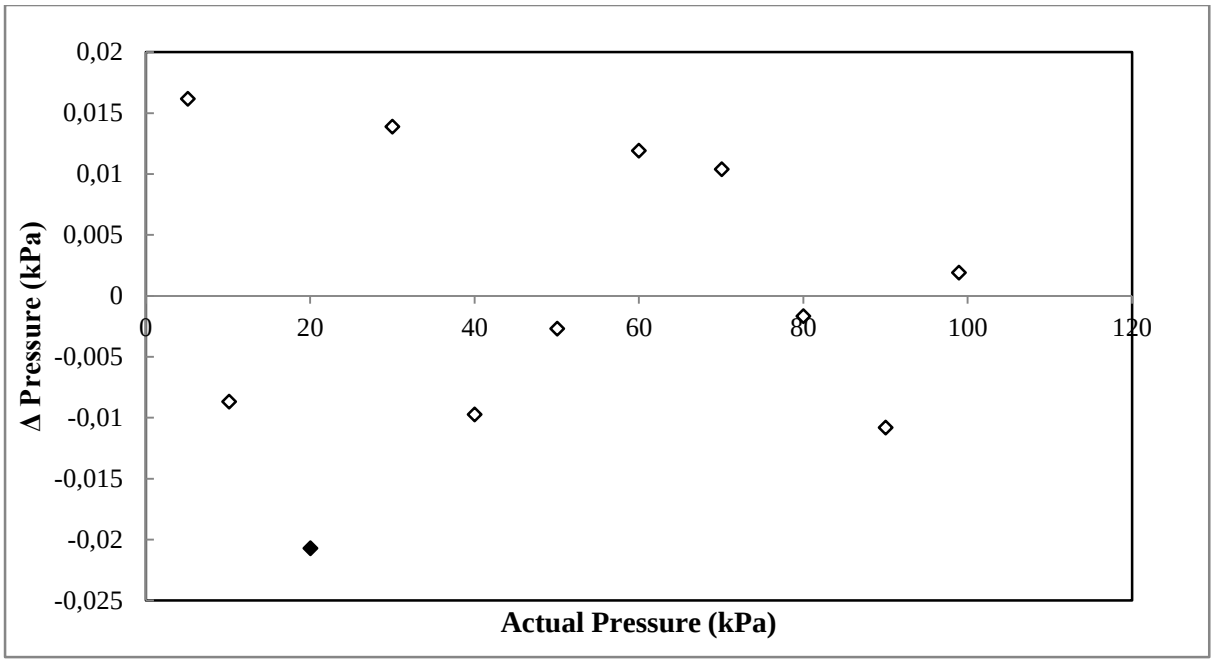

Figure 6-5: Deviations from the actual pressure, resulting from the use of a linear relation for the low pressure dynamic analytic VLE apparatus - maximum deviation (♦).

Similar to the temperature calibration, a comparison between the measured pressure (using the WIKA model P-10 pressure transducer) and the calibration polynomial generated from the pressure calibration plot was used to determine the accuracy of the calibration. The graphical results are seen below in Figure 6-6.

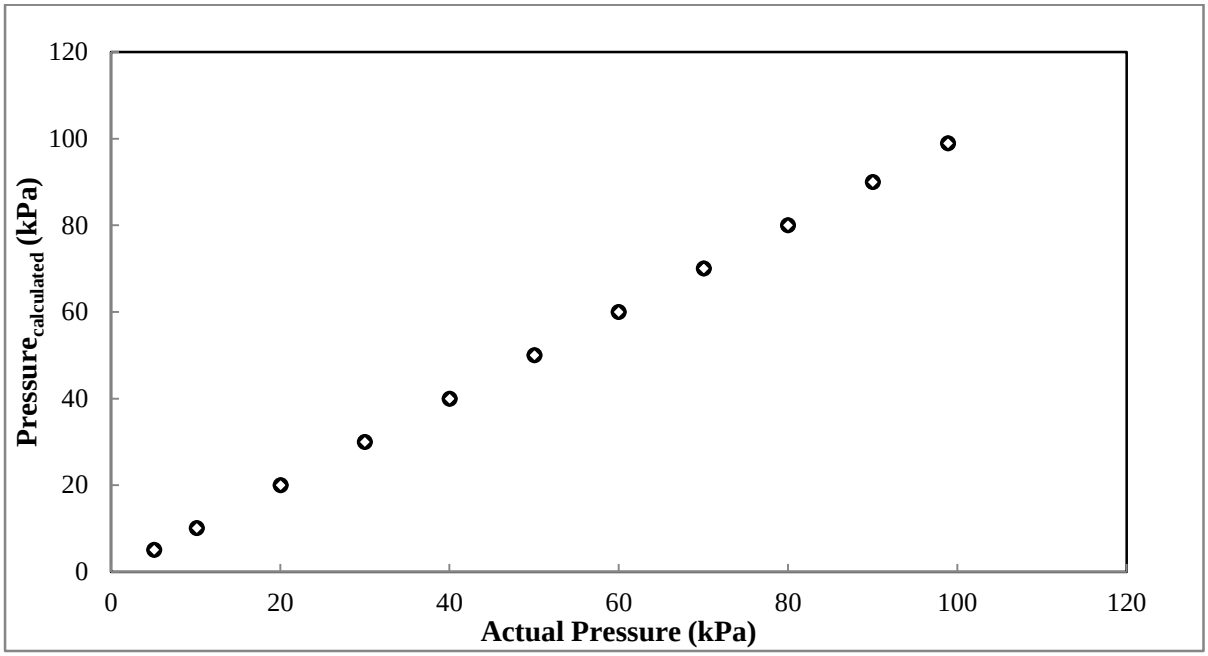

Figure 6-6: Measured transducer pressure (○)**; calculated pressure using straight line polynomial equation** (◊)**.**

6.3.2. GC calibrations and Operating Conditions

The GC operating conditions listed in Tables 6-4 and 6-5 ensured adequate separation of components of the chemical species and were the optimum instrument settings for the generation of separate sharp peaks for each system thus increasing the confidence level regarding measured molar compositions. These settings were utilized in obtaining the GC calibration graphs as well as the measured binary VLE results for all the systems. The details of the GC phase columns used for separation within the GC ovens are given in Table 6-6. Two different model gas chromatographs were used during sampling for this study.

Table 6-4: Shimadzu 2010 gas chromatograph operating conditions

Operation Conditions	GC Settings Utilised
System	cyclohexane + ethanol
Column used	HP-5 capillary
Injector Profile	
Injector temperature / °C	250
Carrier gas	Helium
Column pressure / kPa	35.6
Injection mode	Split less
Total flow / $mL.min^{-1}$	30
Detector Profile	
Detector type	TCD
Current / mA	80
Detector temperature / °C	250
Make up flow / $mL.min^{-1}$	4
Oven Profile	
Temperature control mode	Isothermal
Oven temperature / °C	135
Elution Time / min	
cyclohexane	1.022
ethanol	2.010

Table 6-5: Shimadzu 2014 gas chromatograph operating conditions

Operation Conditions	**GC Settings Utilised**					
System	MTBE + 1-pentanol	MTBE + 2, 2, 4-trimethylpentane	2, 2, 4-Trimethylpentane + 1-pentanol	DIPE + 2,2,4-trimethylpentane	DIPE + 1-propanol	DIPE + 2-butanol
Column used	Porapak® Q	Porapak® Q	Porapak® Q	Chromosorb	Chromosorb	Chromosorb
Injector Profile						
Injector temperature / °C	250	250	250	250	275	275
Carrier gas	Helium	Helium	Helium	Helium	Helium	Helium
Column pressure / kPa	25.6	25.6	25.5	25.7	32.2	33.1
Injection mode	Split less	Split less	Split less	Split less	Split less	Split less
Total flow / $mL.min^{-1}$	30	30	30	30	20	20
Detector Profile						
Detector type	TCD	TCD	TCD	TCD	TCD	TCD
Current / mA	60	60	60	75	65	60
Detector temperature / °C	250	250	250	250	250	250
Make up flow / $mL.min^{-1}$	2	2	2	2	2	2
Oven Profile						
Temperature control mode	Isothermal	Isothermal	Isothermal	Isothermal	Isothermal	Isothermal
Oven temperature / °C	100	95	100	100	55	55
Elution Time / min						
Methyl *tert*-butyl ether	1.272	1.300	-	-	-	-
1-pentanol	3.014	-	3.101	-	-	-
2, 2, 4-trimethylpentane	-	1.965	1.973	1.949	-	-
Diisopropyl ether	-	-	-	1.170	1.171	1.169
1-propanol	-	-	-	-	2.602	-
2-butanol	-	-	-	-	-	2.312

Table 6-6: Specifications for GC columns used for analyses

Column	Porapak® Q	Chromosorb	HP-5 capillary
Serial number	-	13284	19091J-413
Type	packed	packed	capillary
max temperature	250	300	250
Column length / m	2.5	4	30
Material	Stainless steel	Stainless steel	
OD / mm	3.2	-	-
ID / mm	2.2	2.20	0.32
mesh range	50/80		-

As discussed in Section 5.1.2.3, two linear graphs were plotted for each binary system. This was done to account for each end of the composition range of analysis, i.e., determination of the gradient of each of the two components in their respective dilute regions.

Should the gradient (known as the response factor) of the first plot (F_2/F_1) be equivalent to the mathematical inverse of the slope of the second plot ($1/(F_1/F_2)$), this would allow the response factor ratios to be assumed to remain constant. In turn a linear relationship can be assumed between the area ratios and mole fraction ratios across the entire mole fraction range. The response factors should be the mathematical inverse of each other to within approximately 1% according to common practice. If the inverse exceeds 1%, the response factor calculated for the two dilute regions for that particular region should be used. The inverse of each region being used interchangeably is considered incorrect.

All of the systems measured (with the exception of the cyclohexane (1) + ethanol (2) system),responded linearly and the gradients of A_1/A_2 versus x_2/x_1 were shown to be sufficiently close in value to the reciprocal of the gradient of A_2/A_1 versus x_2/x_1. Therefore, the values within 1% of each other were assumed adequate enough to represent a linear relationship.
All system calibration plots are located in section 6.5. Figures 6-7 to 6-8 displays the GC calibration plots for the test system cyclohexane + ethanol.

6.4. Systems analysed

All of binary systems for which isothermal phase equilibrium data were measured in this project were mentioned in Chapter 1. The (test) system of cyclohexane + ethanol was measured for the

confirmation the accuracy of the apparatus along with calibrations and the experimental procedure of phase equilibrium measurements. The remaining binary measured systems constitute new VLE data: some at previously unmeasured isotherm temperatures only, whilst other systems being entirely new. Pure component vapour pressure data was also measured for all systems in this study.

6.5. Pure Component Vapour Pressure Data

Vapour pressure measurements were undertaken for all pure components used in this study. These type of measurements can serve as a sort of preliminary test for the purity of a component used; hence deeming vapour pressure measurements crucial.

Literature data was used as a comparison for the measured vapour pressure data in order to scrutinise the accuracy and reliability of the measured data. It becomes most useful to become acquainted with the experimental procedure of the VLE apparatus by performing vapour pressure measurements. Equally important is the verification of the proper functioning of the VLE equipment by these measurements e.g., pressure, temperature and compositional calibrations as well as location of leakages. The deviation of the experimental vapour pressure data from that of the literature for quantification of the accuracy is calculated by using the equations:

for % deviation of pressure: $$\left(\frac{\Delta P}{P}\right) = 100 \times \frac{P^{\exp} - P^{lit}}{P^{\exp}} \tag{6-14}$$

for % deviation of temperature: $$\left(\frac{\Delta T}{T}\right) = 100 \times \frac{T^{\exp} - T^{lit}}{T^{\exp}} \tag{6-15}$$

Superscripts: "*exp*" and "*lit*" denote the experimental and literature data respectively. The measured data along with the percentage deviations from literature data are shown in tables 6-7 to 6-12. Graphical representations of the data are represented by Figures 6-7 to 6-12.

Table 6-7: Vapour pressure data for 1-pentanol

This work		ΔT (ºC)		ΔT (%)	
P_{exp} (kPa)	T_{exp} (ºC)	Lit[a]	Lit[b]	Lit[a]	Lit[b]
1.12	44.21	0.21	0.63	0.473	1.803
5.01	68.18	-0.03	-0.23	-0.045	-0.705
10.00	81.31	0.06	0.31	0.073	0.973
20.01	95.81	-0.05	-0.18	-0.056	-0.452
30.02	105.29	0.05	0.25	0.045	0.685

[a]Ambrose et al.(Ambrose and Sprake, 1970) (NIST Chemistry WebBook)

[b]Poling et al. (Poling et al., 2001)

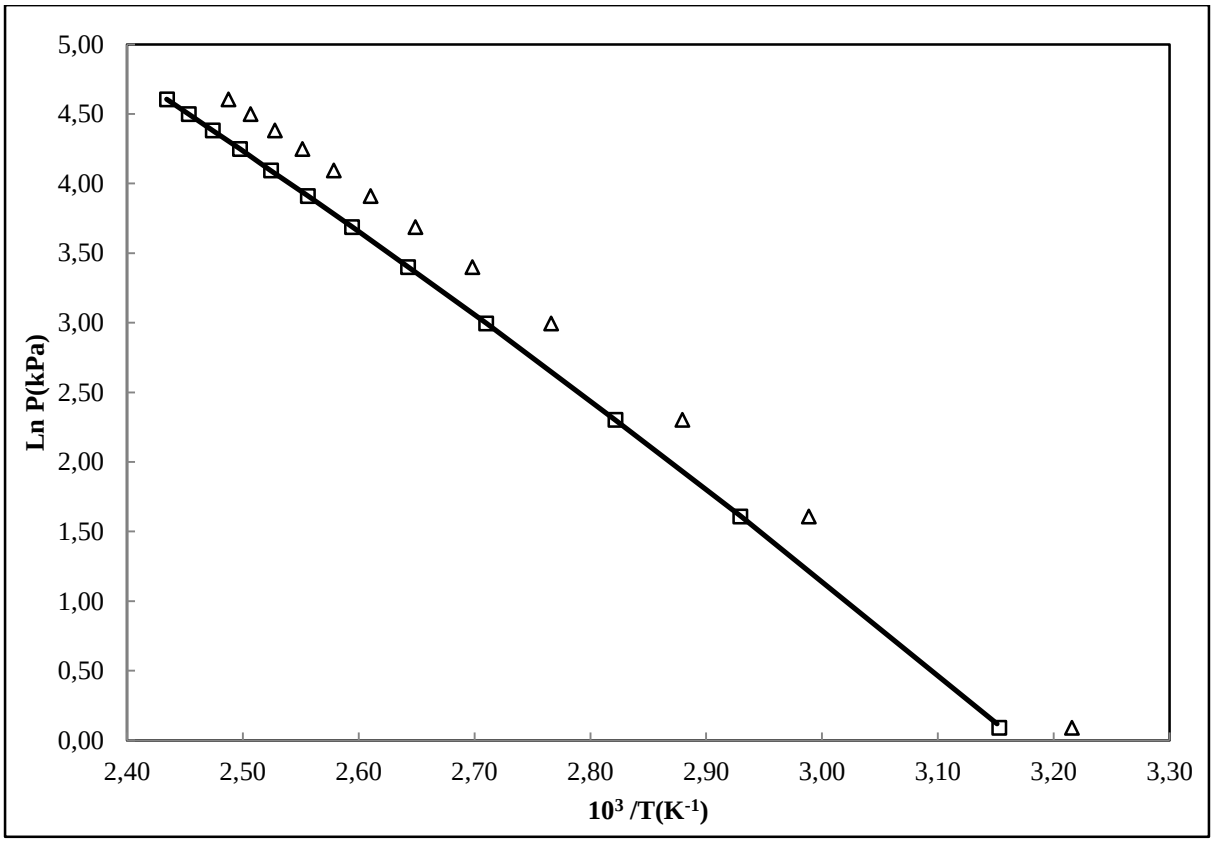

Figure 6-7: Experimental vapour pressure data plot for 1-pentanol: This work —; NIST standards (□); Poling et al., 2001 (Δ).

The large deviation between the measured data and the literature data of Poling et al., 2001 can be attributed to the choice of comparison data in this case. However, the data of Poling et al., 2001 does not affect the reliability of the measured data as the NIST standards data is widely considered more favourable.

Table 6-8: Vapour pressure data for 2, 2, 4-trimethylpentane

This work		ΔT (ºC)		ΔT (%)	
P_{exp} (kPa)	T_{exp} (ºC)	Lit[a]	Lit[b]	Lit[a]	Lit[b]
10.03	33.97	-0.08	-0.07	-0.249	-0.211
20.00	50.64	0.04	0.06	0.088	0.109
30.00	61.34	0.03	0.04	0.049	0.063
40.02	69.47	0.03	0.04	0.044	0.055
50.02	76.08	0.00	0.01	0.005	0.014

[a]Ambrose et al.(Ambrose and Sprake, 1970) (NIST Chemistry WebBook)

[b]Poling et al. (Poling et al., 2001)

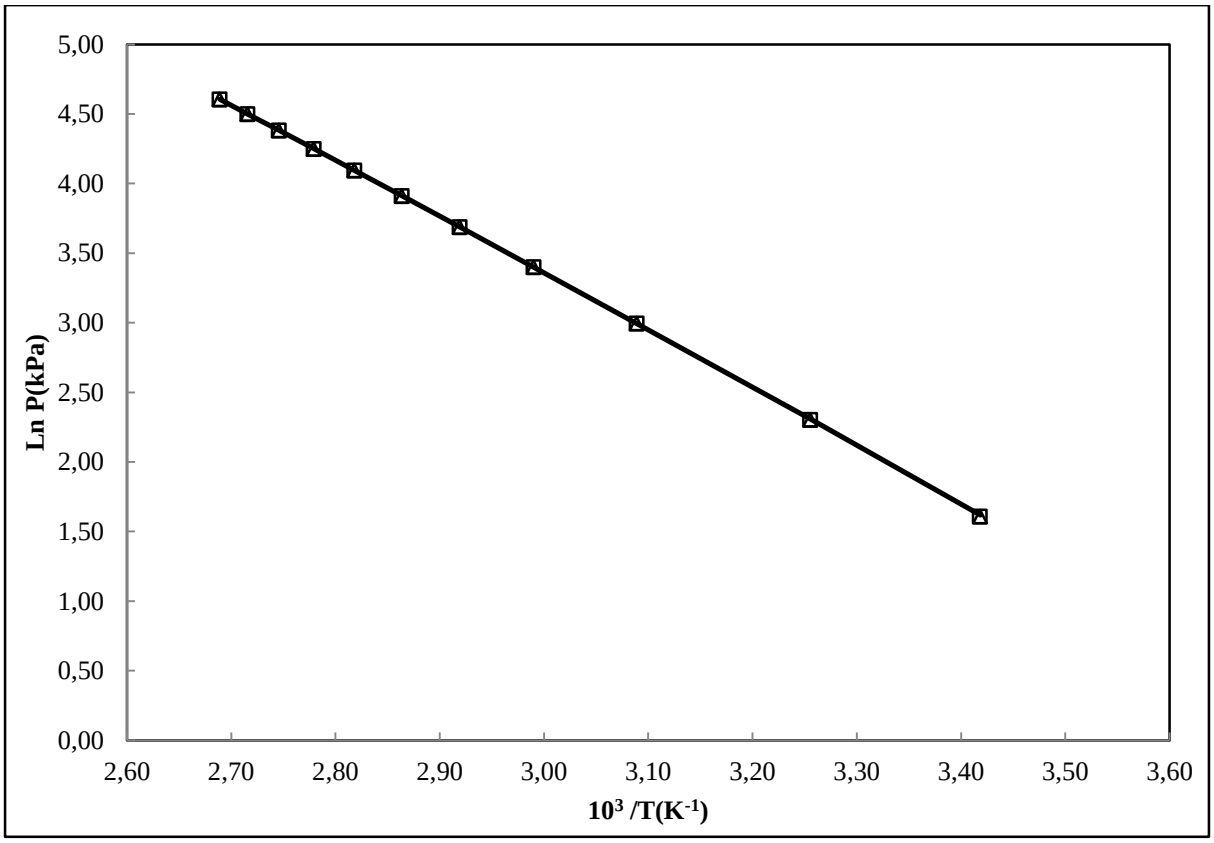

Figure 6-8: Experimental vapour pressure data plot for 2, 2, 4-trimethylpentane: This work —; NIST standards (□); Poling et al., 2001 (Δ).

Table 6-9: Vapour pressure data for MTBE

This work		ΔT (ºC)	ΔT (%)
P_{exp} (kPa)	T_{exp} (ºC)	Lit[a]	Lit[a]
40.03	29.46	0.01	0.031
50.02	35.27	0.04	0.115
60.01	40.18	0.04	0.094
69.97	44.42	-0.02	-0.038
79.92	48.32	0.06	0.116
89.99	51.74	0.02	0.038
100.00	54.91	0.02	0.040

[a]DDB, 2013

*out of range of source data

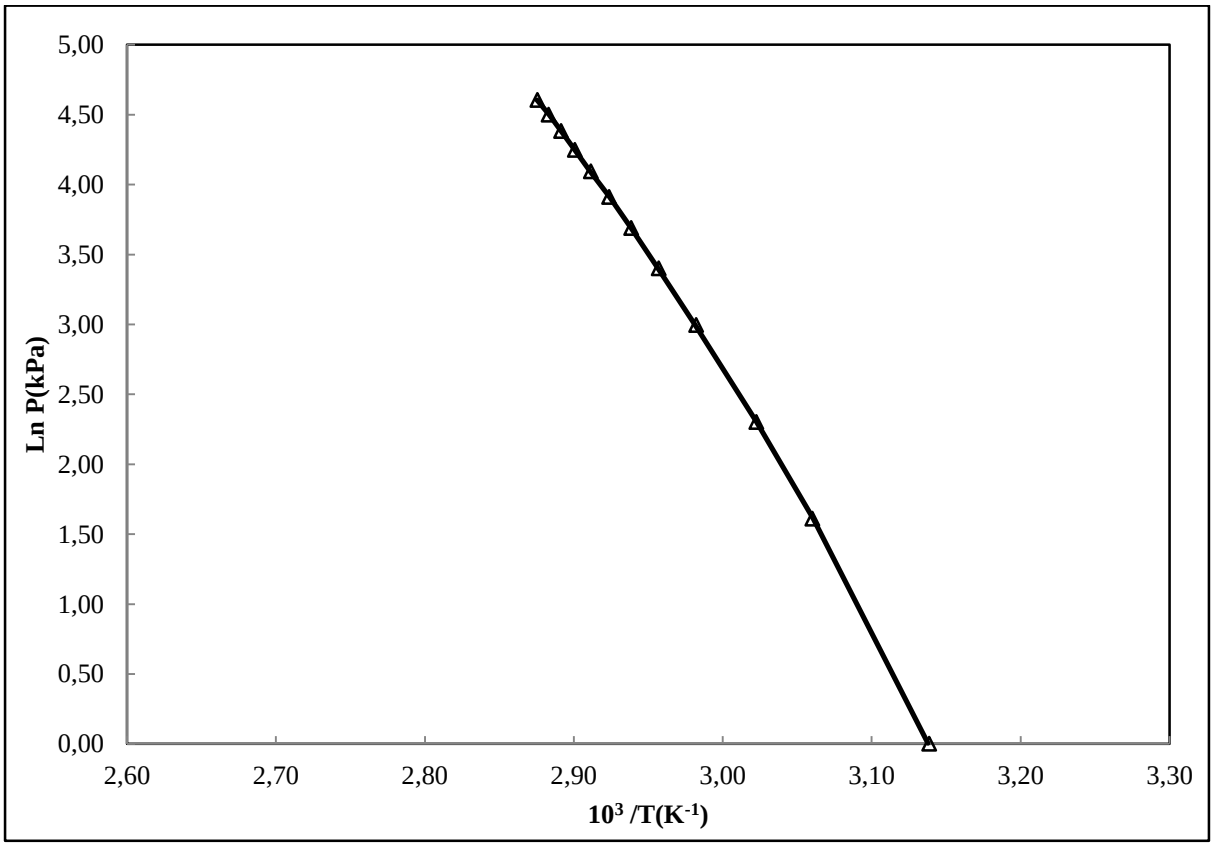

Figure 6-9: Experimental vapour pressure data plot for MTBE: This work —; DDB 2013 (Δ).

Table 6-10: Vapour pressure data for DIPE

This work		ΔT (ºC)		ΔT (%)	
P_{exp} (kPa)	T_{exp} (ºC)	Lit[a]	Lit[b]	Lit[a]	Lit[b]
40.00	41.95	0.11	-0.27	0.266	-0.632
49.97	47.85	0.11	-0.20	0.226	-0.409
59.97	52.88	0.11	-0.12	0.210	-0.227
69.93	57.27	0.10	-0.05	0.182	-0.093
79.94	61.14	0.04	-0.05	0.061	-0.078
89.94	64.70	0.03	0.02	0.052	0.031
100.08	67.86	-0.07	-0.01	-0.098	-0.016

[a]Cidlinsky et al. (Cidlinský and Polak, 1969) (NIST Chemistry WebBook)

[b]Reid et al.(Reid et al., 1977)

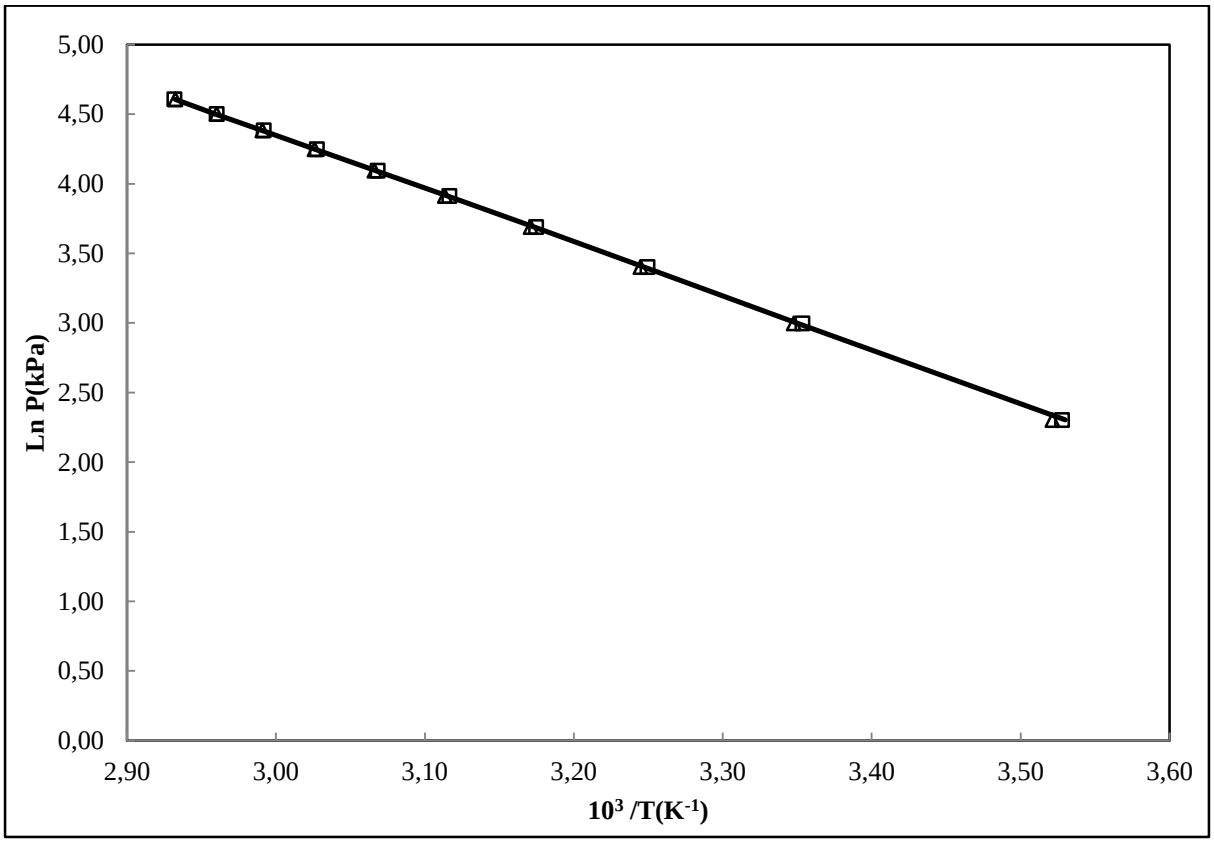

Figure 6-10: Experimental vapour pressure data plot for DIPE: This work —; NIST standards (□); Reid et al., 1977 (Δ).

Table 6-11: Vapour pressure data for 1-propanol

This work		ΔT (ºC)		ΔT (%)	
P_{exp} (kPa)	T_{exp} (ºC)	Lit[a]	Lit[b]	Lit[a]	Lit[b]
10.00	46.43	-0.03	0.08	-0.059	0.164
20.02	59.91	0.05	0.24	0.078	0.398
29.98	68.40	0.05	0.27	0.080	0.389

[a]Kemme et al.(Kemme and Kreps, 1969) (NIST Chemistry WebBook)

[b]Poling et al.(Poling et al., 2001)

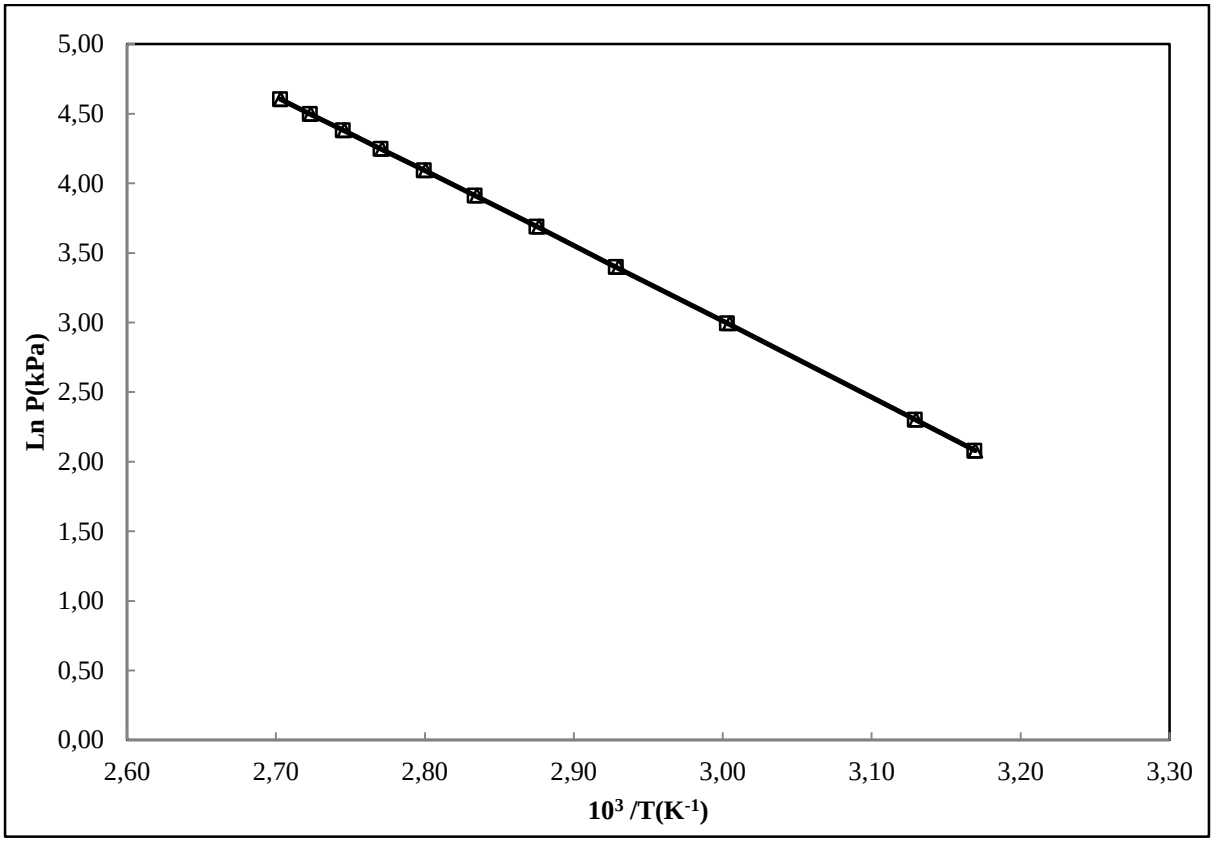

Figure 6-11: Experimental vapour pressure data plot for 1-propanol: This work —; NIST standards (□); Poling et al., 2001 (Δ).

Table 6-12: Vapour pressure data for 2-butanol

This work		ΔT (ºC)	ΔT (%)
P_{exp} (kPa)	T_{exp} (ºC)	Lit[a]	Lit[a]
4.99	37.32	0.00	-0.005
9.99	48.97	0.02	0.045
19.99	61.92	-0.04	-0.069
30.02	70.35	0.03	0.042

[a]Biddiscombe, Collerson et al., 1963

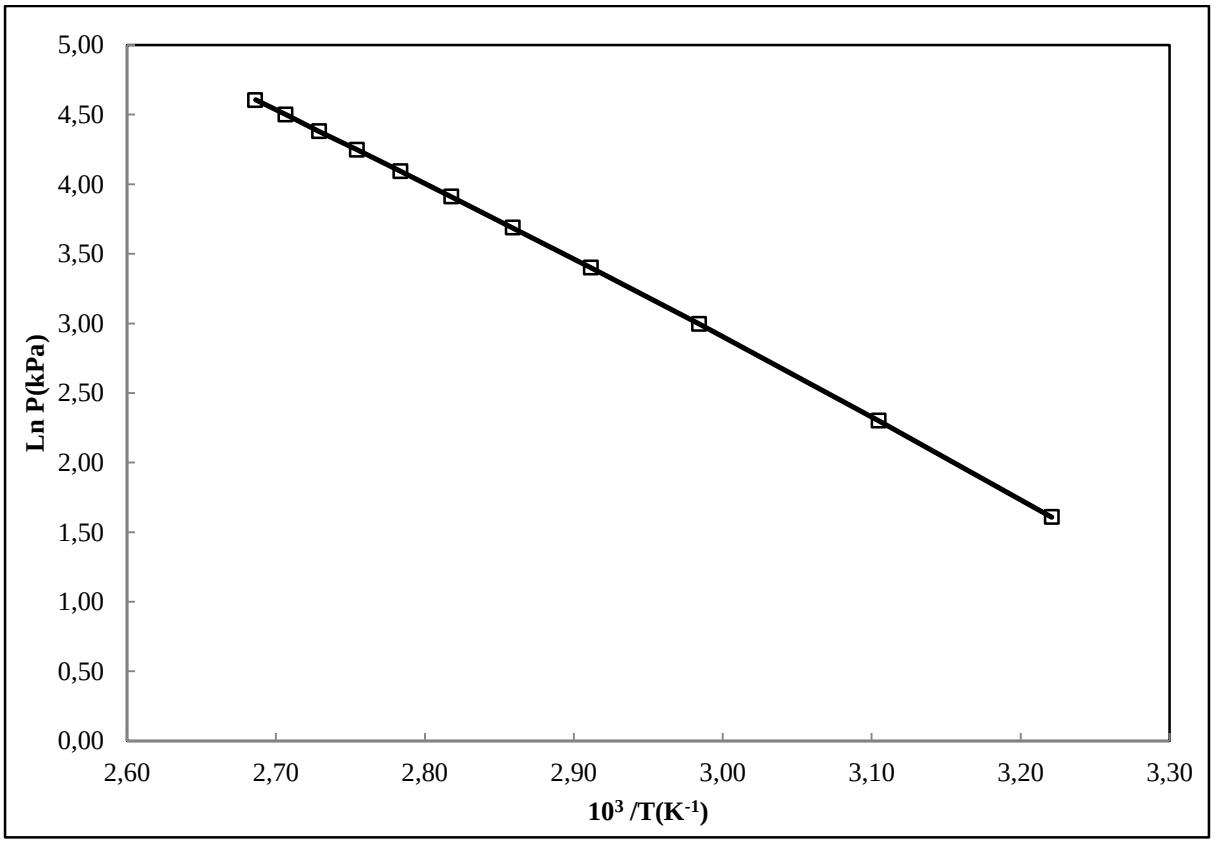

Figure 6-12: Experimental vapour pressure data plot for 2-butanol: This work —; NIST standards (□); DDB 2013 (Δ).

6.6. Binary Vapour-Liquid Equilibrium Data

6.6.1. Test System Results for cyclohexane (1) + ethanol (2)

A cyclohexane (1) + ethanol (2) test system at 323.15 K (Joseph et al., 2002) was measured in order to test the experimental procedure and reproducibility in this work.

Test systems have been previously done at isobaric conditions, however in this case, since all of the new data being measured is at isothermal conditions, it was decided that the test system be performed similarly. In addition, isothermal VLE data is more difficult and tedious to perform, hence rendering the test system conditions optimal for the continued success of the new systems to be measured. The composition analysis for the test system was undertaken utilising the Shimadzu 2010 GC fitted with a packed column (Porapak® Q). The GC settings for this system are outlined in Table 6-4. Figures 6-7 and 6-8 present the GC calibration plots. The literature data of Joseph *et al*. (2001) was used as a comparison for the experimental P-x-y and x-y data plots. The measured data was plotted against the literature data rendering Figures 6-9 and 6-10.

The aforementioned figures provide a visual representation of the excellent agreement between the literature and the experimental data.

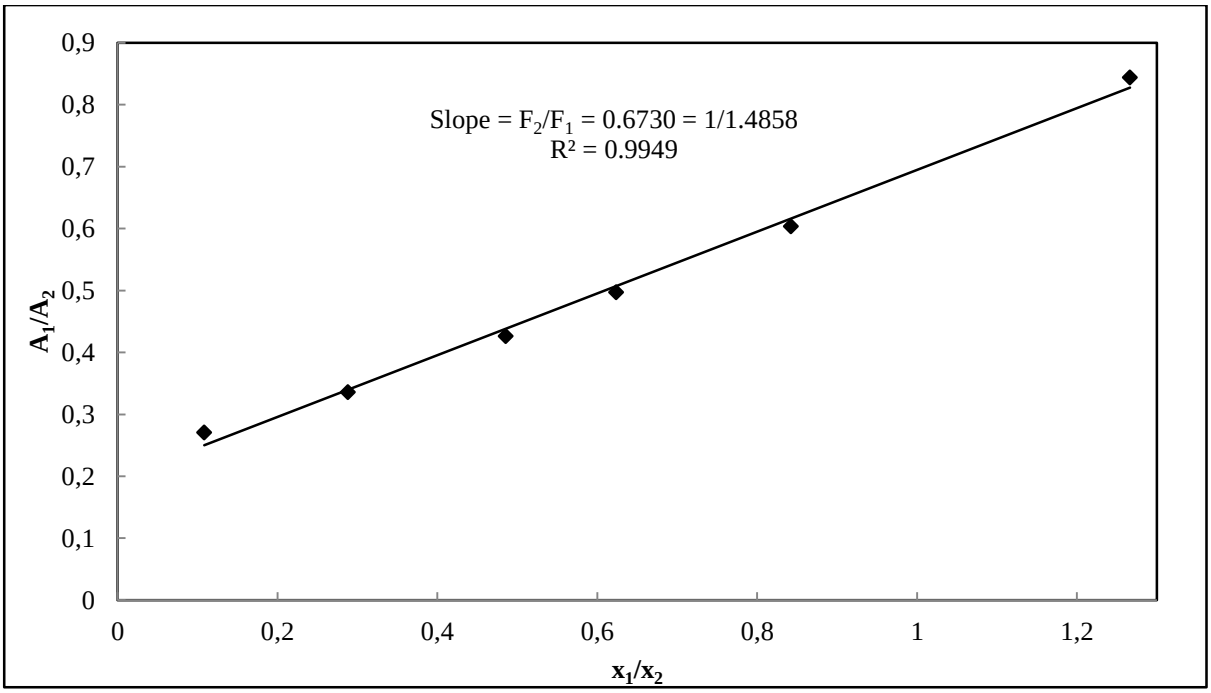

Figure 6-7: TCD Calibration plot for the cyclohexane (1) + ethanol (2) system (ethanol dilute region).

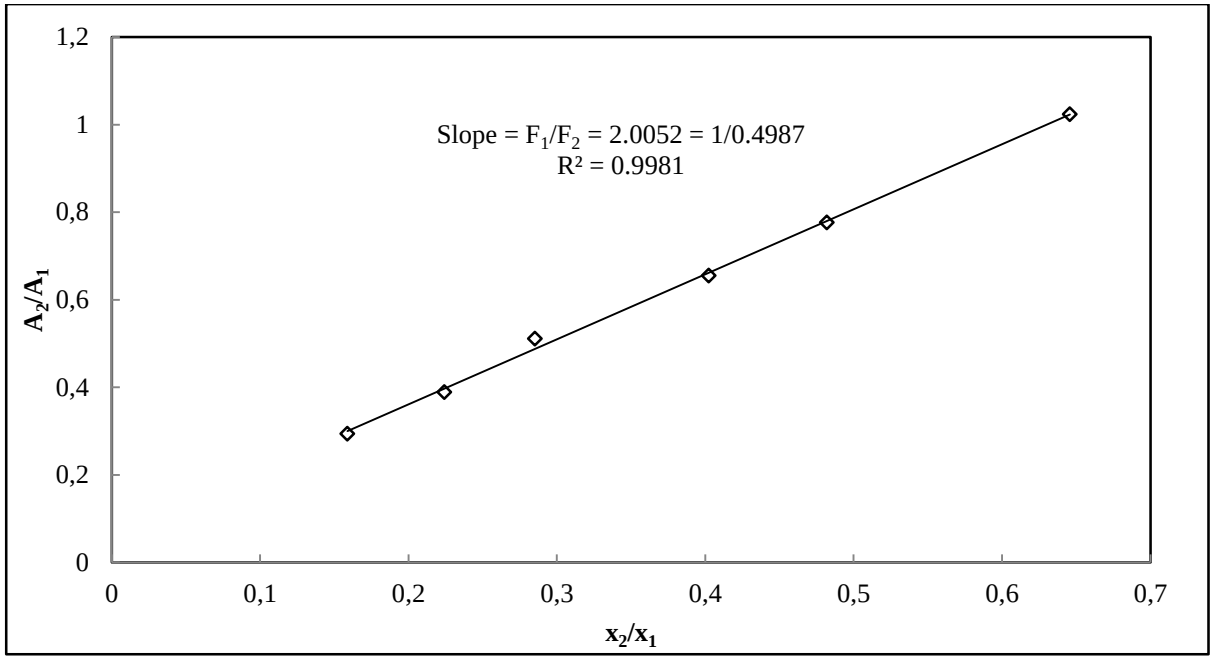

Figure 6-8: TCD Calibration plot for the cyclohexane (1) + ethanol (2) system (cyclohexane dilute region).

Table 6-13: Isothermal VLE data for cyclohexane (1) + ethanol (2) at T = 323.15 K.

P (kPa)	x_1	y_1	P (kPa)	x_1	y_1
29.97	0.000	0.000	57.73	0.669	0.603
35.97	0.021	0.160	57.20	0.812	0.621
39.65	0.043	0.250	56.30	0.882	0.633
53.65	0.200	0.509	54.79	0.906	0.649
56.55	0.440	0.558	51.10	0.957	0.718
57.44	0.536	0.570	45.88	0.982	0.824
57.67	0.591	0.592	36.21	1.000	1.000
57.68	0.593	0.595			

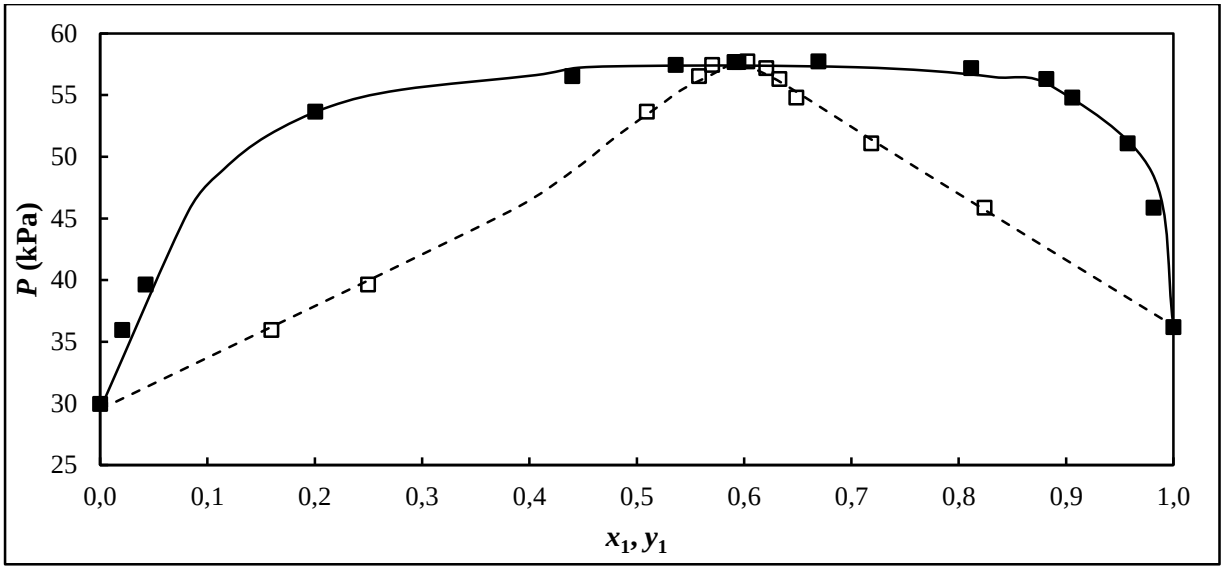

Figure 6-9: P-x_1-y_1 diagram for cyclohexane (1) + ethanol (2) at 323.15 K: (■, □), experimental values; (—), Joseph et al. (2001).

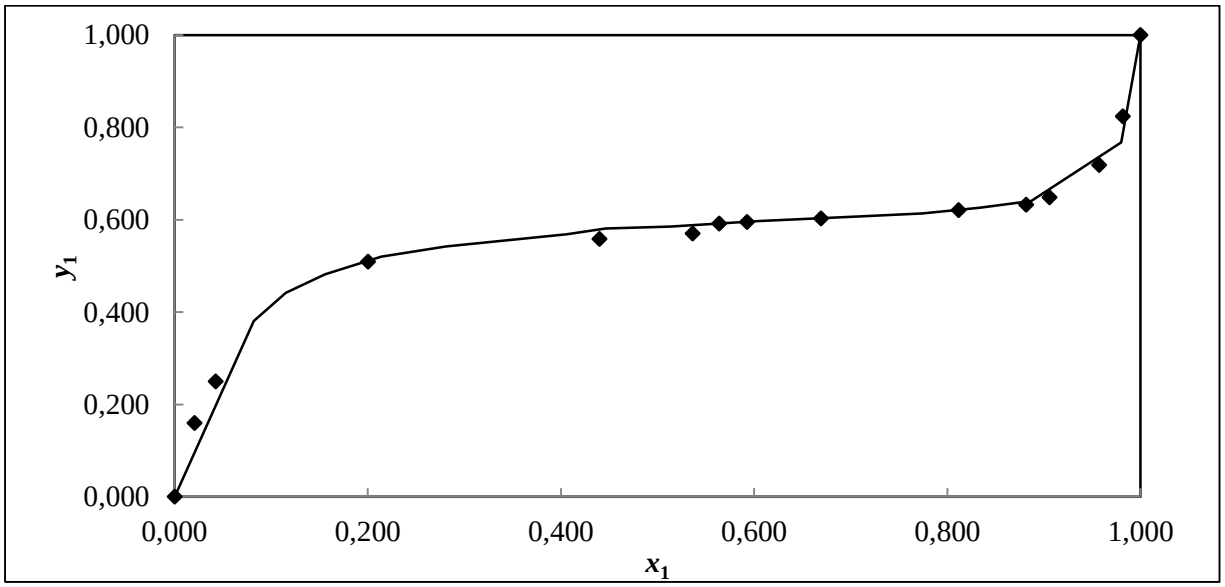

Figure 6-10: x_1-y_1 data for the cyclohexane (1) + ethanol (2) system at 323.15K: (♦), experimental values; (—), Joseph et al. (2001).

6.6.2. Results 2, 2, 4-trimethylpentane (1) + 1-pentanol (2) System

Measurements were undertaken at 350.15K, 360.15K and 370.15K, with all three sets of data representing new VLE data, previously unmeasured at these temperatures in literature. The composition analysis of this system was performed using the Shimadzu GC 2014 gas chromatograph. The GC was fitted with the Porapak®Q packed column (described in Tables 6-6), using the running conditions presented in table 6-5. Figures 6-11 and 6-12 represent the GC calibration plots. Experimental VLE data points are listed in Tables 6-14 to 6-16; with the graphical representations of the experimental data for all three isotherms shown in Figures 6-13 and 6-14.

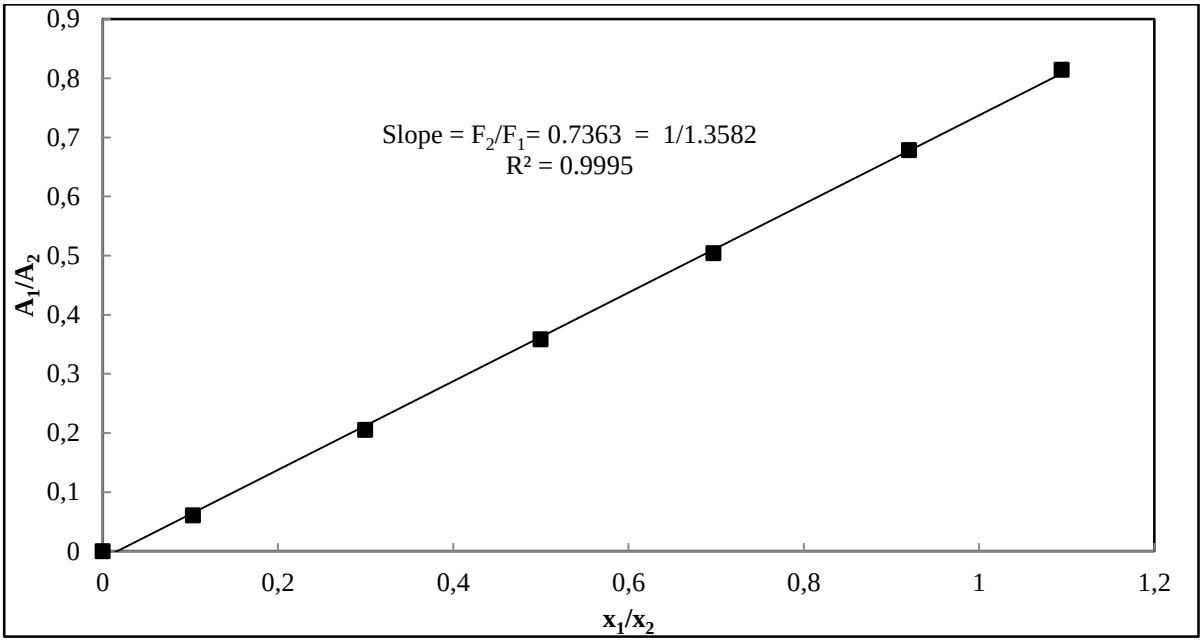

Figure 6-11: TCD Calibration plot for the 2, 2, 4-trimethylpentane (1) + 1-pentanol (2) system (1-pentanol dilute region).

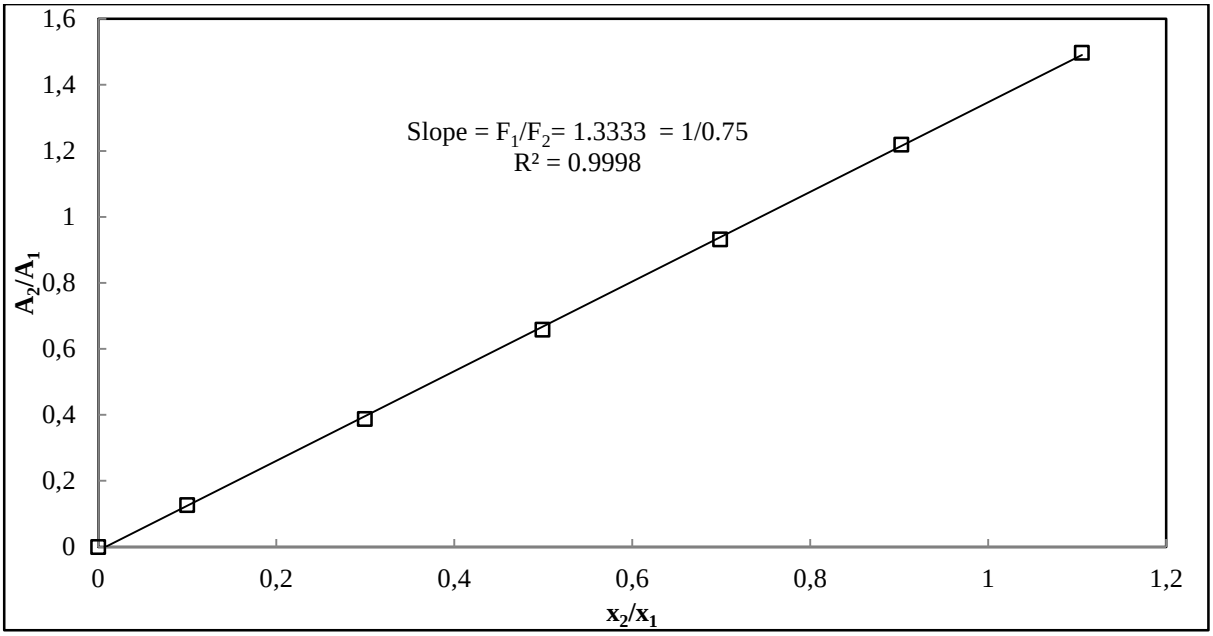

Figure 6-12: TCD Calibration plot for the 2, 2, 4-trimethylpentane (1) + 1-pentanol (2) system (2, 2, 4-trimethylpentane dilute region).

Table 6-14: P-x_1-y_1 data for 2, 2, 4-trimethylpentane (1) + 1-pentanol (2) at 350.15K, 360.15K and 370.15K.

P/kPa	x_1	y_1	P/kPa	x_1	y_1	P/kPa	x_1	y_1
	T/K			T/K			T/K	
	350.15			360.15			370.15	
8.04	0.000	0.000	13.26	0.000	0.000	21.04	0.000	0.000
10.02	0.010	0.172	18.47	0.019	0.253	25.33	0.010	0.122
13.03	0.029	0.376	24.83	0.051	0.449	30.87	0.030	0.292
18.04	0.061	0.542	30.21	0.086	0.555	38.38	0.061	0.446
25.03	0.121	0.690	37.80	0.132	0.662	47.06	0.100	0.562
33.03	0.213	0.780	45.05	0.192	0.728	59.21	0.172	0.666
38.03	0.284	0.816	51.50	0.263	0.776	68.33	0.240	0.729
46.03	0.525	0.871	59.01	0.393	0.821	75.20	0.313	0.766
50.01	0.814	0.914	67.11	0.664	0.872	87.76	0.536	0.829
51.01	0.899	0.930	68.58	0.737	0.877	90.40	0.616	0.843
51.41	0.949	0.955	69.40	0.796	0.892	93.70	0.748	0.868
51.56	0.969	0.970	70.12	0.839	0.902	96.54	0.939	0.938
51.55	0.990	0.988	70.95	0.869	0.917	96.51	0.949	0.945
51.54	1.000	1.000	71.09	0.931	0.938	95.76	0.989	0.986
			71.06	0.97	0.966	95.02	1.000	1.000
			70.69	1.000	1.000			

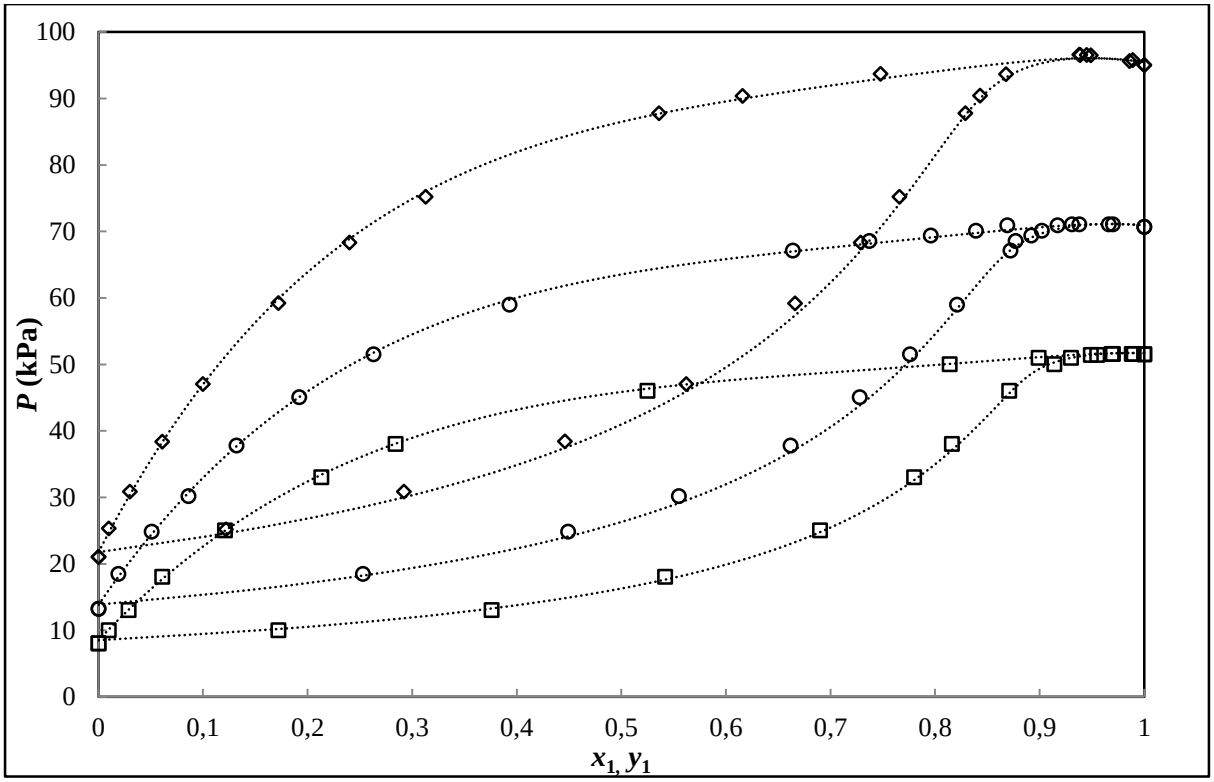

Figure 6-13: Experimental P-x_1-y_1 data for the 2, 2, 4-trimethylpentane (1) + 1-pentanol (2) system: 350.15K (◊); 360.15K (○); 370.15K (□); fitted trend line (….).

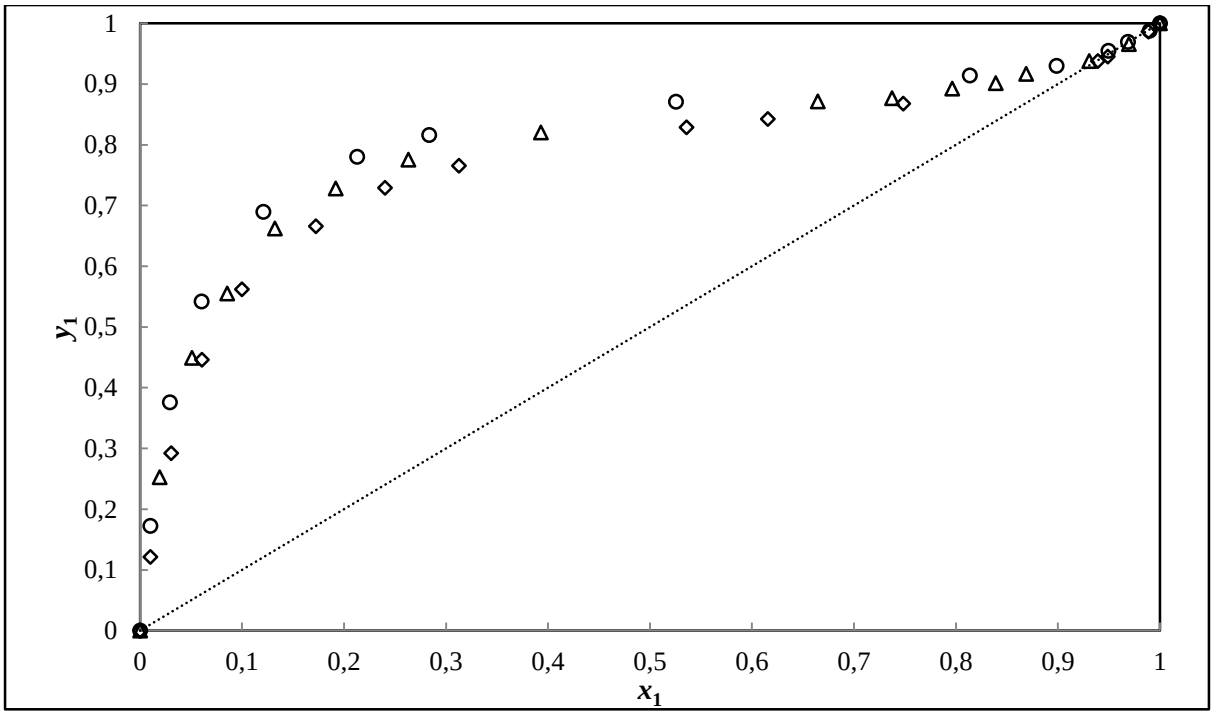

Figure 6-14: Experimental x_1-y_1 data for the 2, 2, 4-trimethylpentane (1) + 1-pentanol (2) system: 350.15K (○); 360.15K (Δ); 370.15K (◊); y=x (….).

6.6.3. Results Methyl *tert*-butyl ether (1) + 1-pentanol (2) System

For this system only two isotherms were investigated at 317.15 and 327.15K. Both the data sets are representative of new previously unmeasured data. A complete data set of three measured isotherms (in the case of this project) was originally planned; however the pure component pressure of MTBE was lower than 1 kPa for the temperature of 307.15K. This condition rendered the isotherm temperature immeasurable due to the limitations placed upon pressure stability within the VLE apparatus regarding such a minimal pressure. Compositional analysis for this system was carried out by utilising the Shimadzu 2014 GC fitted with a Porapak®Q packed column using the settings outlined in table 6-5. Figures 6-15 and 6-16 represent the GC calibration plots. Table 6-15 below shows the measured data for this system ad is graphically represented in Figures 6-17 to 6-18.

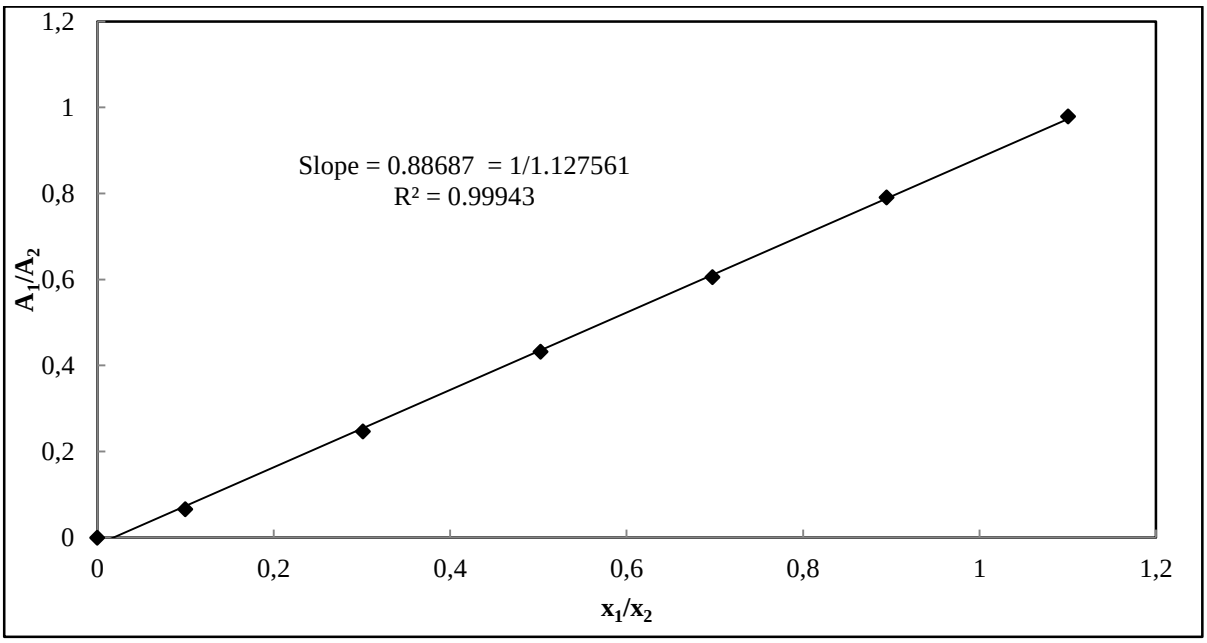

Figure 6-15: TCD Calibration plot for the MTBE (1) + 1-pentanol (2) system (1-pentanol dilute region).

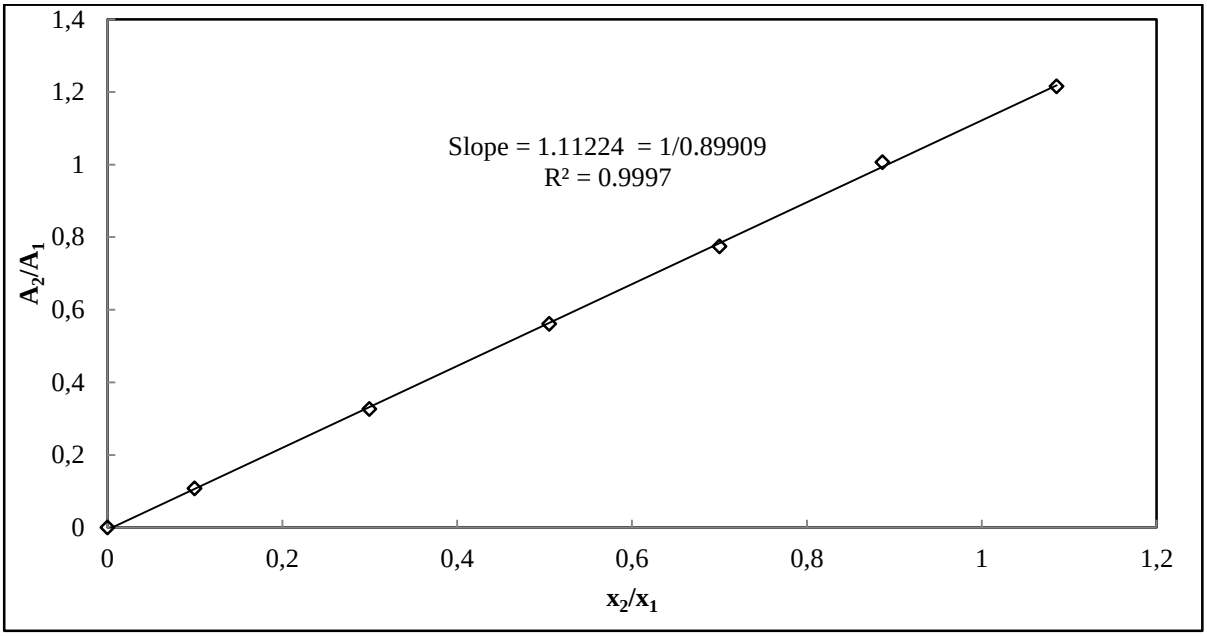

Figure 6-16: TCD Calibration plot for the MTBE (1) + 1-pentanol (2) system (MTBE dilute region).

Table 6-15: P-x_1-y_1 data for MTBE (1) + 1-pentanol (2) at 317.15K and 327.15K.

P/kPa	x_1	y_1	P/kPa	x_1	y_1
	T/K			T/K	
	317.15			327.15	
1.12	0.000	0.000	2.14	0.000	0.000
2.66	0.010	0.296	3.83	0.010	0.215
4.01	0.020	0.627	5.03	0.018	0.451
9.59	0.065	0.860	10.49	0.045	0.750
18.66	0.152	0.937	14.06	0.071	0.833
26.89	0.242	0.960	17.18	0.091	0.866
34.62	0.343	0.972	25.31	0.141	0.910
42.96	0.475	0.981	33.47	0.212	0.939
49.38	0.596	0.986	41.47	0.273	0.952
55.23	0.717	0.990	52.63	0.394	0.968
60.34	0.838	0.994	60.95	0.495	0.975
64.06	0.899	0.996	68.83	0.596	0.981
67.11	0.960	0.998	77.30	0.707	0.986
68.93	1.000	1.000	83.95	0.808	0.990
			88.54	0.879	0.993
			94.06	0.960	0.998
			97.13	1.000	1.000

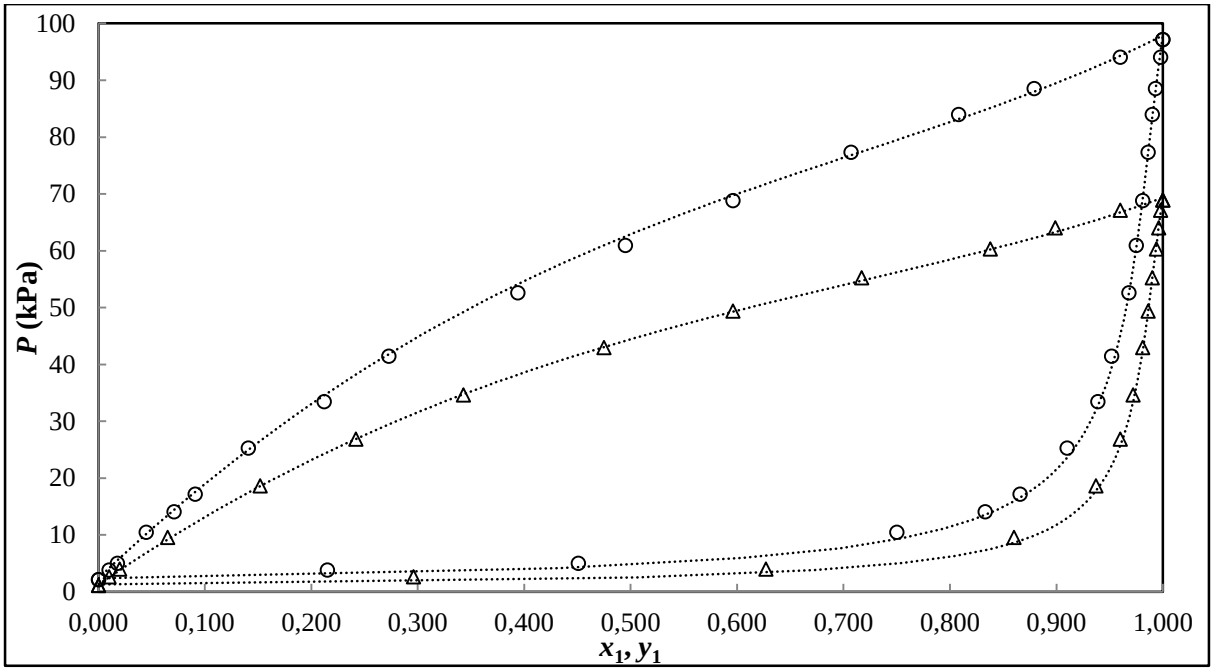

Figure 6-17: Experimental P-x_1-y_1 data for the MTBE (1) + 1-pentanol (2) system: 307.15K (Δ); 317.15K (○); fitted trend line (….).

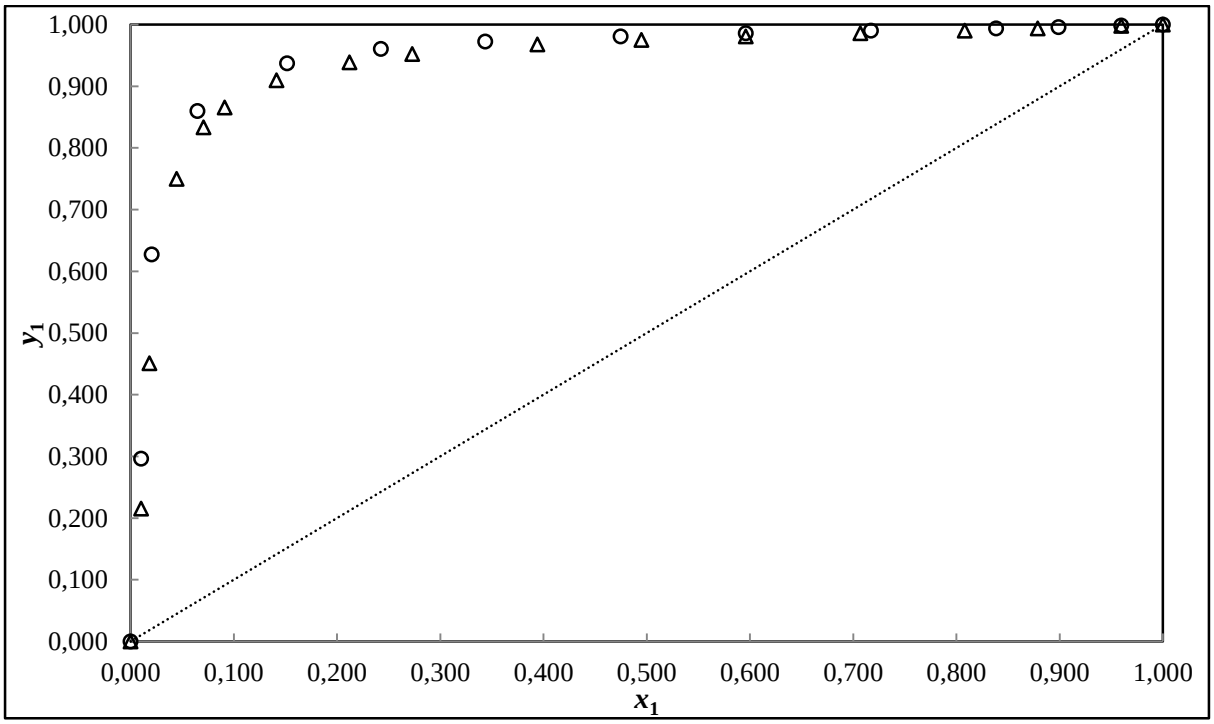

Figure 6-18: Experimental x_1-y_1 data for the MTBE (1) + 1-pentanol (2) system: 307.15K (Δ); 317.15K (○); y=x (….).

6.6.4. Results Methyl *tert*-butyl ether (1) + 2, 2, 4-trimethylpentane (2) System

The MTBE (1) + 2, 2, 4-trimethylpentane (2) system has been measured at an isotherm temperature of 313.15 K by Chamorro et al. (Chamorro et al., 2004). The data produced by Chamorro et al. (2004) however was only P-x_i data due to their utilisation of a static VLE apparatus. Therefore, in order to extend the data to other previously unmeasured temperatures, the VLE data for this study were measured at 307.15, 317.15 and 327.15K for P-x_i and P-y_i. The composition analysis of this system was carried out using the Shimadzu GC2014 GC with a Porapak®Q packed column using the operating conditions presented in Table 6-5. Figures 6-19 and 6-20 present the GC calibration plots. The experimental VLE data are listed in Table 6-16with the P-x-y and x-y plots being shown in Figures 6-21 and 6-22 respectively.

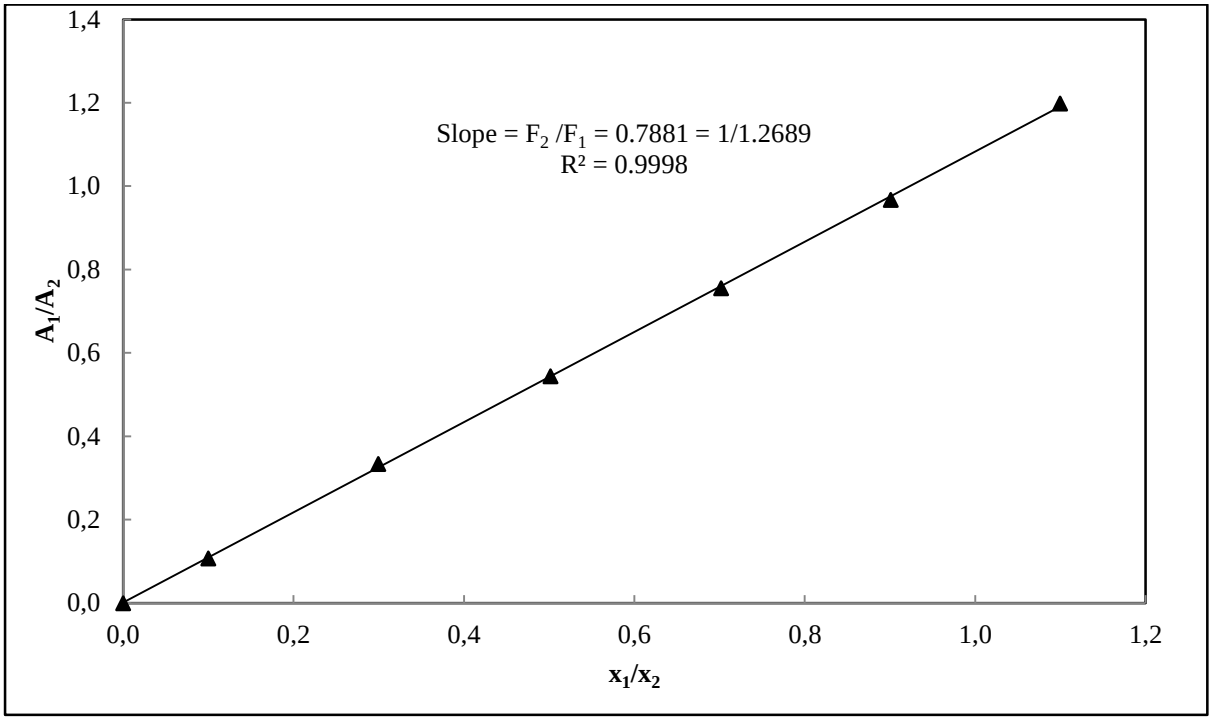

Figure 6-19: TCD Calibration plot for the MTBE (1) + 2, 2, 4-trimethylpentane (2) system (2, 2, 4-trimethylpentane dilute region).

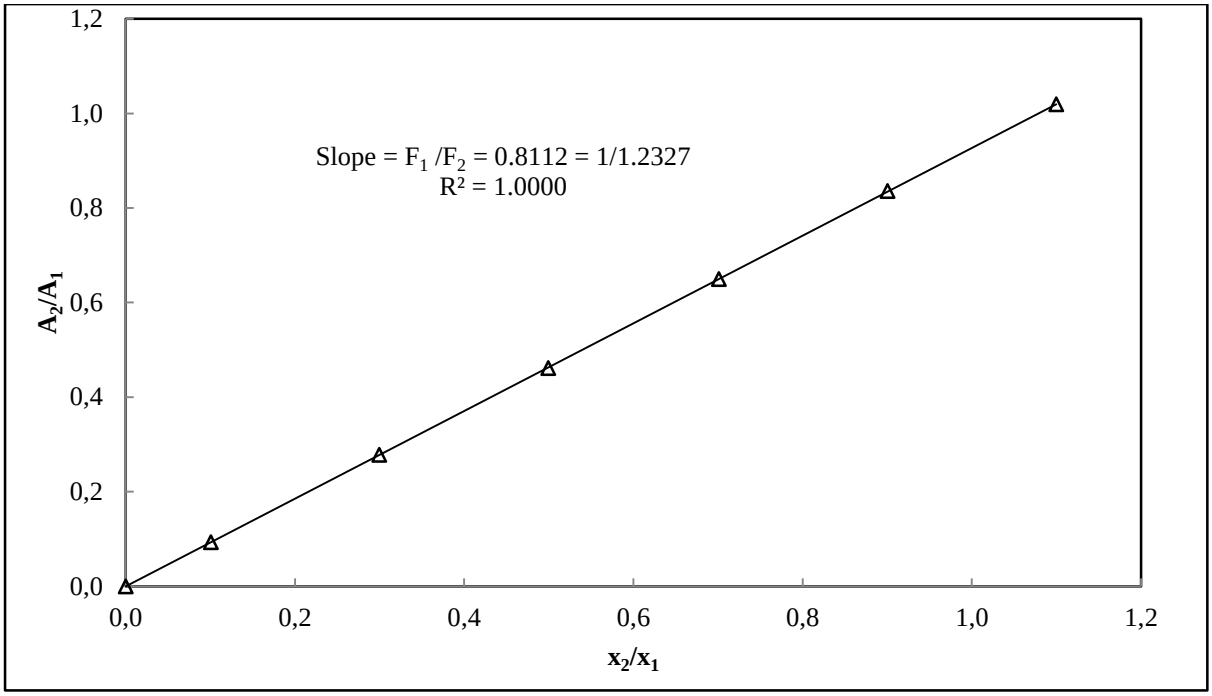

Figure 6-20: TCD Calibration plot for the MTBE (1) + 2, 2, 4-trimethylpentane (2) system (DIPE dilute region).

Table 6-16: P-x_1-$y_1$data for MTBE (1) + 2, 2, 4-trimethylpentane (2) at 307.15K, 317.15K and 327.15K.

P/kPa	x_1	y_1	P/kPa	x_1	y_1	P/kPa	x_1	y_1
	T/K			T/K			T/K	
	307.15			317.15			327.15	
10.10	0.000	0.000	15.38	0.000	0.000	22.95	0.000	0.000
11.80	0.028	0.174	17.86	0.023	0.167	25.55	0.015	0.122
14.64	0.077	0.369	20.25	0.050	0.267	29.65	0.052	0.272
18.78	0.156	0.547	24.82	0.111	0.449	34.68	0.101	0.406
24.01	0.266	0.688	28.45	0.166	0.545	40.58	0.165	0.524
28.08	0.364	0.767	32.46	0.225	0.623	48.68	0.257	0.644
34.44	0.540	0.854	37.23	0.306	0.703	55.94	0.343	0.719
37.67	0.638	0.887	42.89	0.402	0.776	60.83	0.410	0.763
40.32	0.722	0.917	45.10	0.447	0.800	65.77	0.477	0.800
41.94	0.770	0.932	53.03	0.605	0.872	70.00	0.543	0.833
43.85	0.829	0.953	58.97	0.737	0.917	75.20	0.622	0.866
45.24	0.892	0.973	63.34	0.838	0.953	82.20	0.739	0.914
46.60	0.936	0.987	65.44	0.899	0.973	87.85	0.833	0.945
47.53	0.980	0.997	67.48	0.949	0.988	92.69	0.913	0.973
47.71	1.000	1.000	67.93	0.966	0.990	95.22	0.960	0.989
			68.67	0.990	0.997	97.13	1.000	1.000
			68.93	1.000	1.000			

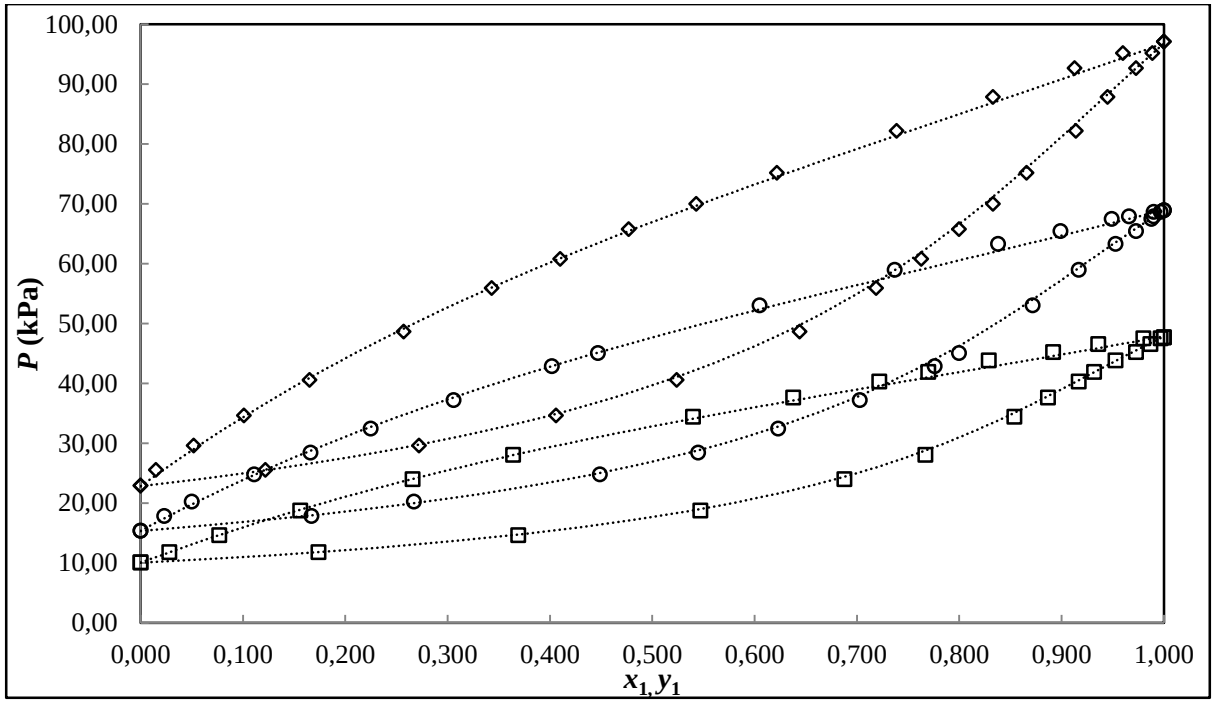

Figure 6-21: Experimental P-x_1-y_1 data for the MTBE (1) + 2, 2, 4-trimethylpentane (2) system: 307.15K (□); 317.15K (○); 327.15K (◊); fitted trend line (….).

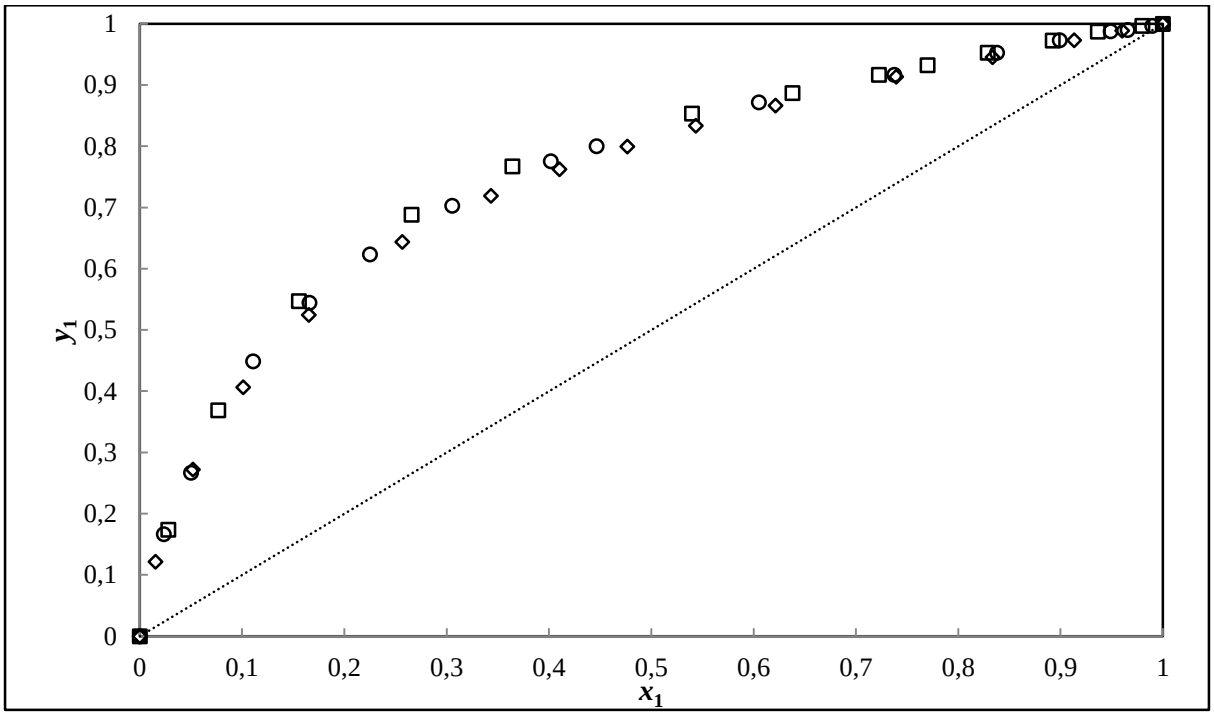

Figure 6-22: Experimental x_1-y_1 data for the MTBE (1) + 2, 2, 4-trimethylpentane (2) system: 307.15K (□); 317.15K (○); 327.15K (◊); $y=x$ (….).

6.6.5. Results Diisopropyl ether (1) + 2, 2, 4-trimethylpentane (2) System

The system of DIPE (1) + 2, 2, 4-trimethylpentane (2) was previously measured by Hwang (Hwang et al., 2008) at only one isotherm temperature of 303.15K. Hence the three isotherm temperatures measured in this study (i.e., 320.15, 330.15 and 340.15K) are previously unmeasured data and are to be used for the extension of the literature data range regarding this system. Compositional analysis of this system was performed using the Shimadzu GC 2014 GC which was fitted with a Chromosorb packed column (described in Table 6-6). The operating conditions used for the column are available in Table 6-5. The GC calibration plots are represented by Figures 6-23 and 6-24. The experimental VLE data are listed in Table 6-17 and shown graphically in Figures 6-24 and 6-25.

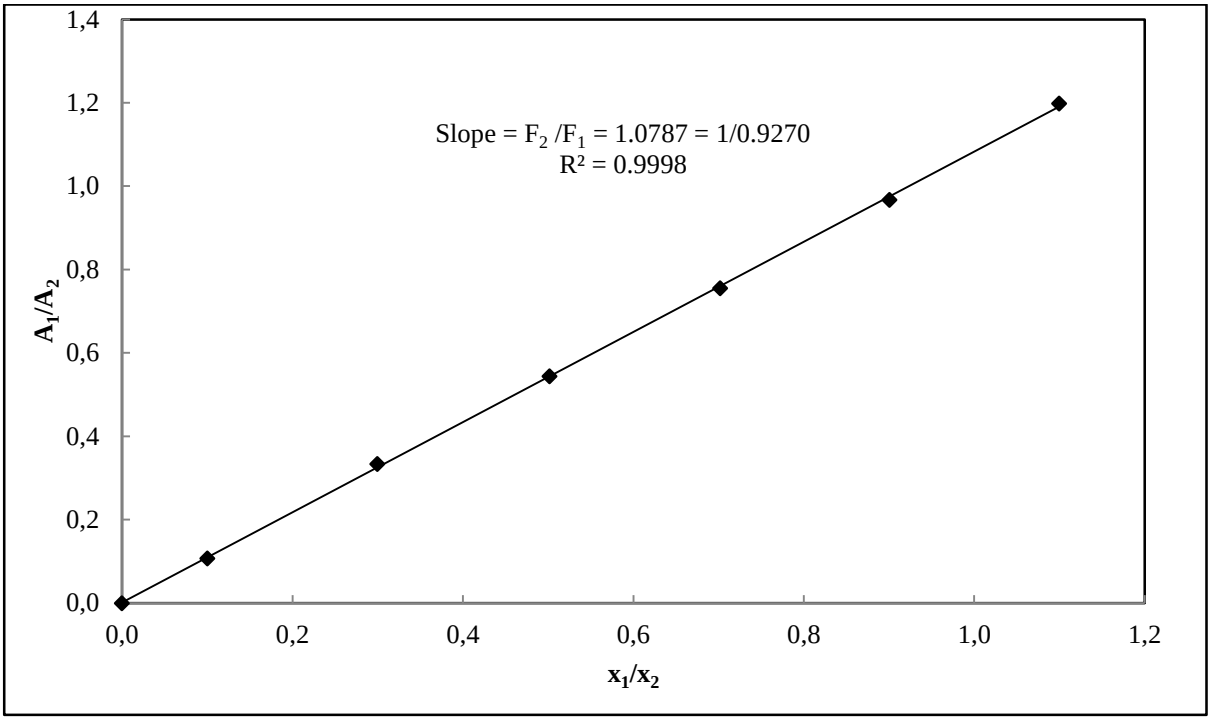

Figure 6-23: TCD Calibration plot for the DIPE (1) + 2, 2, 4-trimethylpentane (2) system (2, 2, 4-trimethylpentane dilute region).

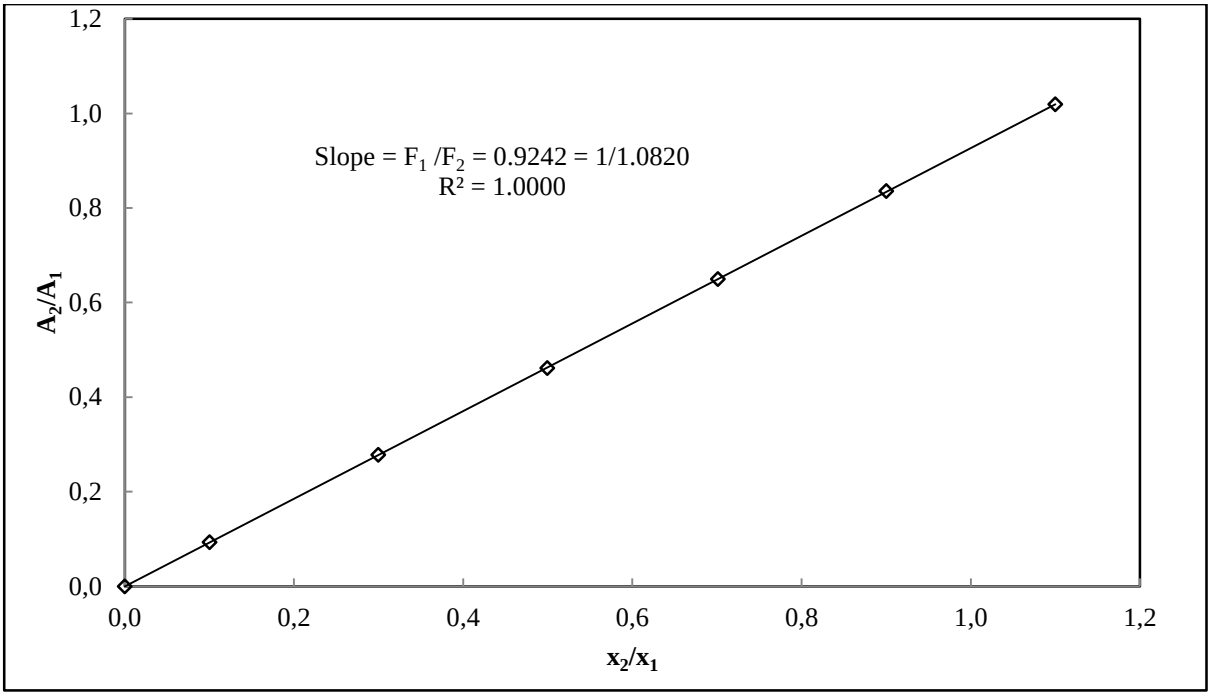

Figure 6-23: TCD Calibration plot for the DIPE (1) + 2, 2, 4-trimethylpentane (2) system (DIPE dilute region).

Table 6-17: P-x_1-y_1 data for DIPE (1) + 2, 2, 4-trimethylpentane (2) at 320.15K, 330.15K and 340.15K.

P/kPa	x_1	y_1	P/kPa	x_1	y_1	P/kPa	x_1	y_1
	T/K			T/K			T/K	
	320.15			330.15			340.15	
17.32	0.000	0.000	25.72	0.000	0.000	37.22	0.000	0.000
18.83	0.030	0.086	26.32	0.008	0.022	39.52	0.022	0.050
20.18	0.071	0.180	29.21	0.059	0.147	43.73	0.080	0.185
22.67	0.146	0.332	35.22	0.211	0.347	54.73	0.219	0.437
25.87	0.241	0.477	43.25	0.390	0.566	62.45	0.339	0.632
27.46	0.301	0.542	47.50	0.431	0.663	67.06	0.420	0.689
29.35	0.353	0.602	51.00	0.516	0.733	72.04	0.511	0.740
31.22	0.421	0.666	56.87	0.664	0.832	79.94	0.661	0.849
33.29	0.487	0.722	62.40	0.806	0.906	87.42	0.804	0.919
35.02	0.545	0.759	67.07	0.940	0.973	93.69	0.939	0.973
37.05	0.613	0.812	69.17	1.000	1.000	97.08	1.000	1.000
39.59	0.697	0.860						
41.40	0.752	0.890						
43.01	0.810	0.922						
45.22	0.878	0.956						
47.03	0.943	0.979						
47.89	0.976	0.992						
48.43	1.000	1.000						

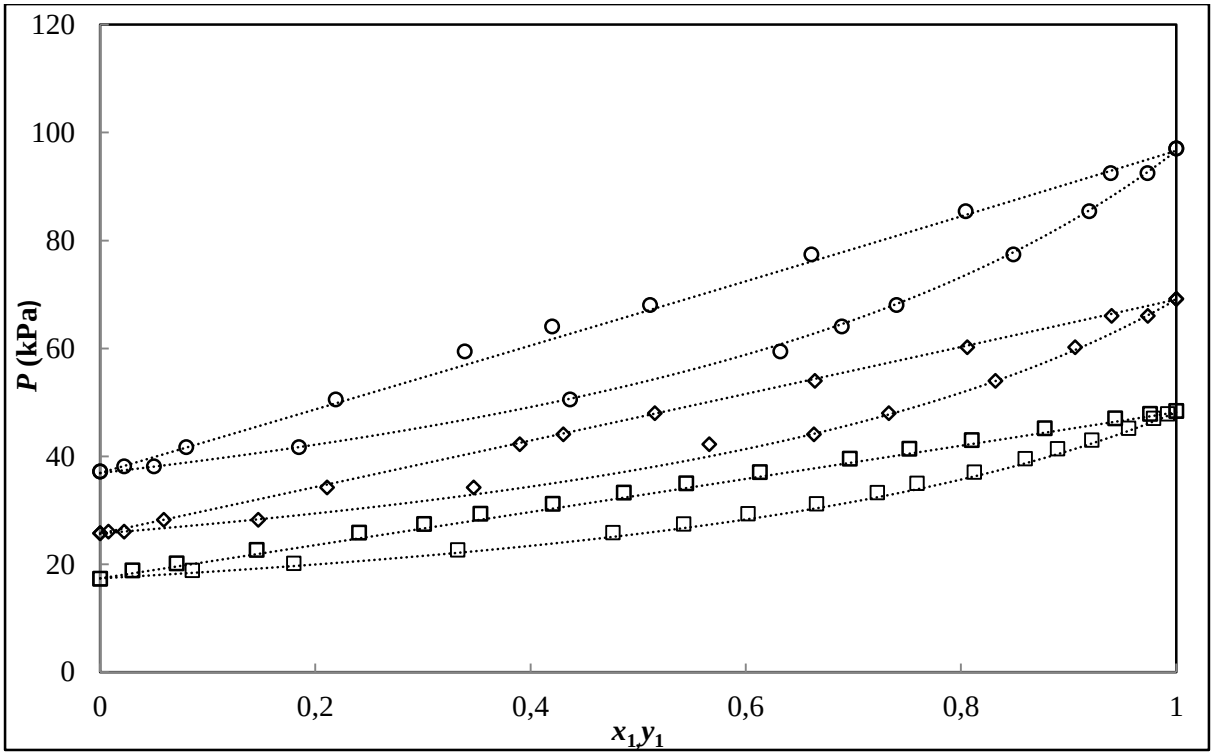

Figure 6-24: Experimental P-x_1-y_1 data for the DIPE (1) + 2, 2, 4-trimethylpentane (2) system: 320.15K (□); 330.15K (◊); 340.15K (○); fitted trend line (….).

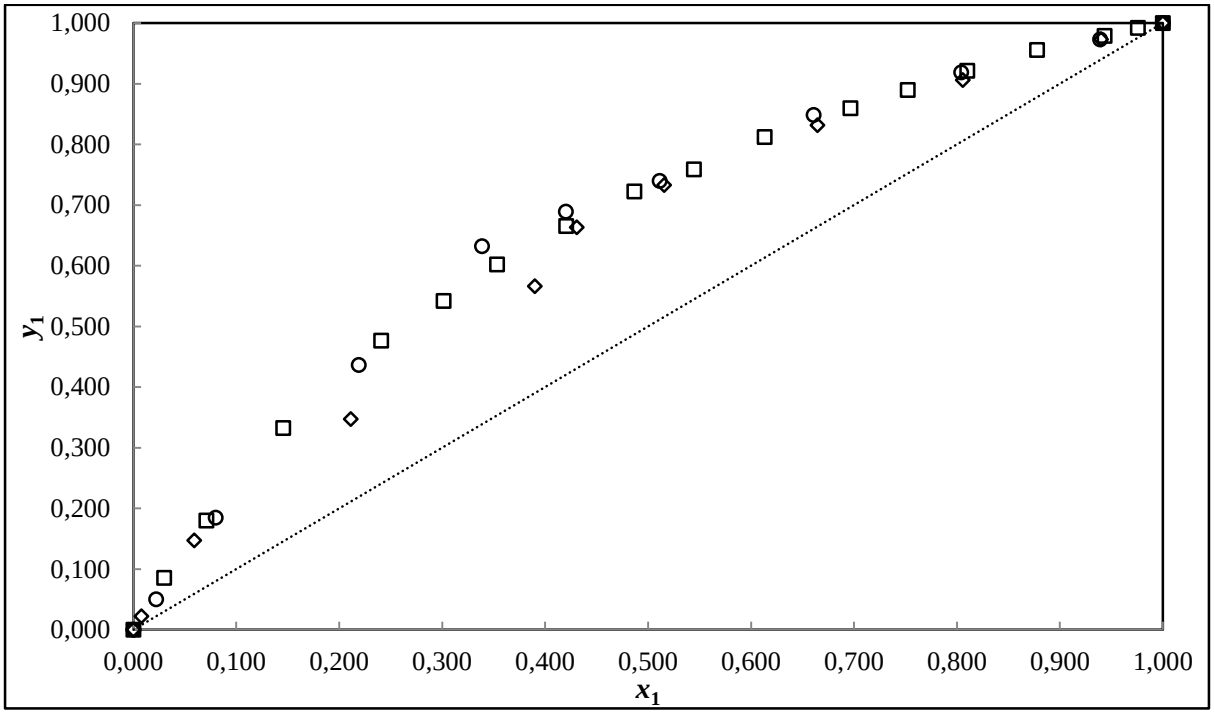

Figure 6-25: Experimental x_1-y_1 data for the DIPE (1) + 1-propanol (2) system: 320.15K (□); 330.15K (◊); 340.15K (○); y=x (….).

6.6.6. Results Diisopropyl ether (1) + 1-propanol (2) System

This system was investigated at isotherm temperatures of 320.15, 330.15 and 340.15K, all of which are representative of new data. Similar to the previous system mentioned above, the DIPE (1) + 1-propanol (2) system was measured by Hwang et al. (2008) at one isotherm temperature of 303.15K. The Shimadzu GC 2014 GC with a Chromosorb packed column was used in determining the compositional analysis. The settings used in this column to successfully obtain the required separation are outlined in Table 6-5 above. The GC calibration plots are given by Figures 6-27 and 6-28. Table 6-18 exhibits the experimental data whilst Figures 6-25 and 6-26 show the plots of the data.

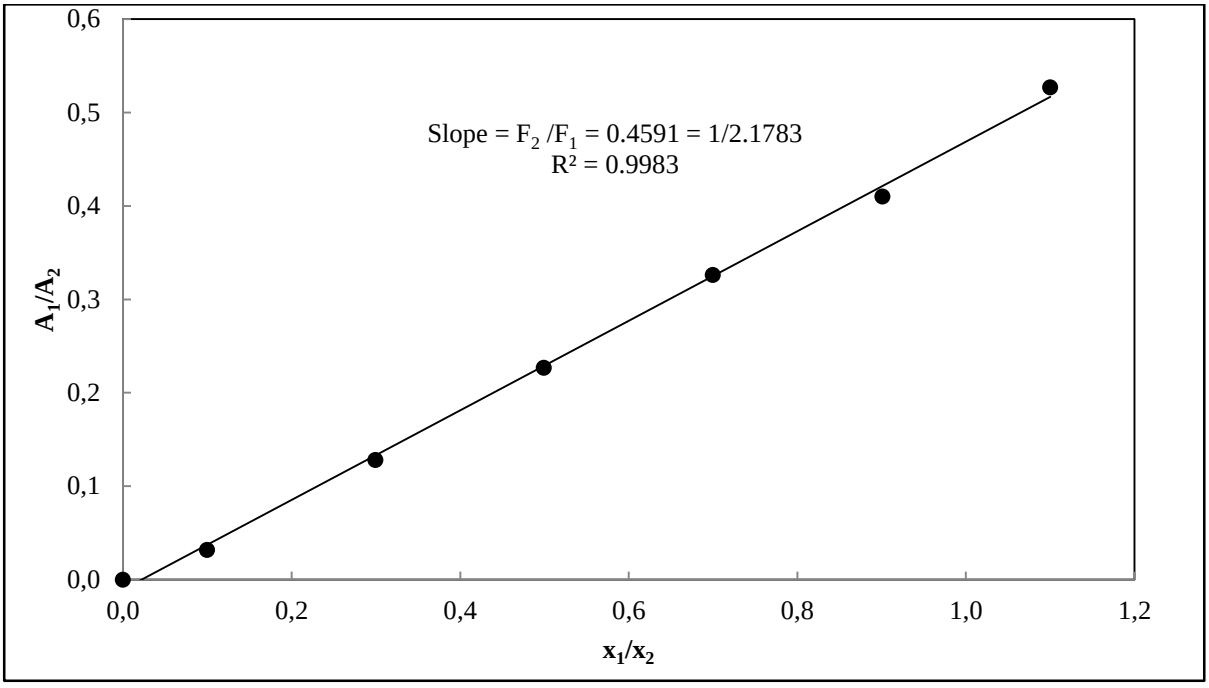

Figure 6-27: TCD Calibration plot for the DIPE (1) + 1-propanol (2) system (1-propanol dilute region).

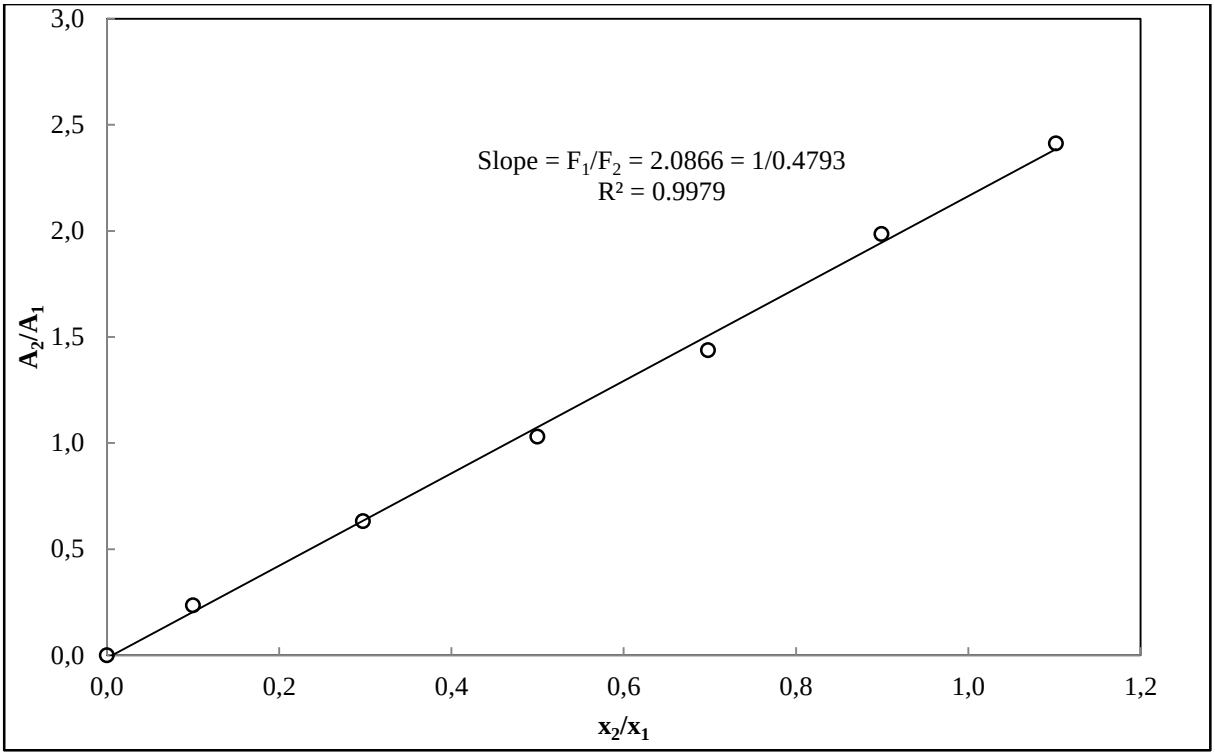

Figure 6-28: TCD Calibration plot for the DIPE (1) + 1-propanol (2) system (DIPE dilute region).

Table 6-18: P-x_1-y_1 data for DIPE (1) + 1-propanol (2) at 320.15K, 330.15K and 340.15K.

P/kPa	x_1	y_1	P/kPa	x_1	y_1	P/kPa	x_1	y_1
	T/K			T/K			T/K	
	320.15			330.15			340.15	
10.29	0.000	0.000	17.33	0.000	0.000	28.16	0.000	0.000
17.31	0.069	0.430	26.95	0.066	0.376	45.92	0.091	0.419
23.38	0.145	0.609	42.04	0.209	0.655	64.37	0.225	0.638
27.96	0.198	0.689	52.11	0.351	0.749	74.18	0.356	0.715
31.61	0.261	0.745	55.38	0.415	0.778	79.54	0.450	0.755
36.88	0.386	0.803	59.95	0.532	0.817	85.89	0.578	0.798
40.35	0.486	0.835	64.09	0.680	0.858	91.74	0.740	0.852
42.74	0.596	0.857	65.86	0.764	0.880	93.68	0.807	0.876
44.51	0.690	0.876	67.75	0.851	0.903	95.21	0.862	0.899
45.86	0.780	0.895	69.13	0.933	0.940	96.16	0.929	0.935
46.74	0.842	0.911	69.25	0.954	0.956	97.05	0.988	0.990
47.59	0.909	0.929	69.60	1.000	1.000	97.09	1.000	1.000
48.23	0.957	0.963						
48.52	0.979	0.980						
48.53	0.991	0.990						
48.49	1.000	1.000						

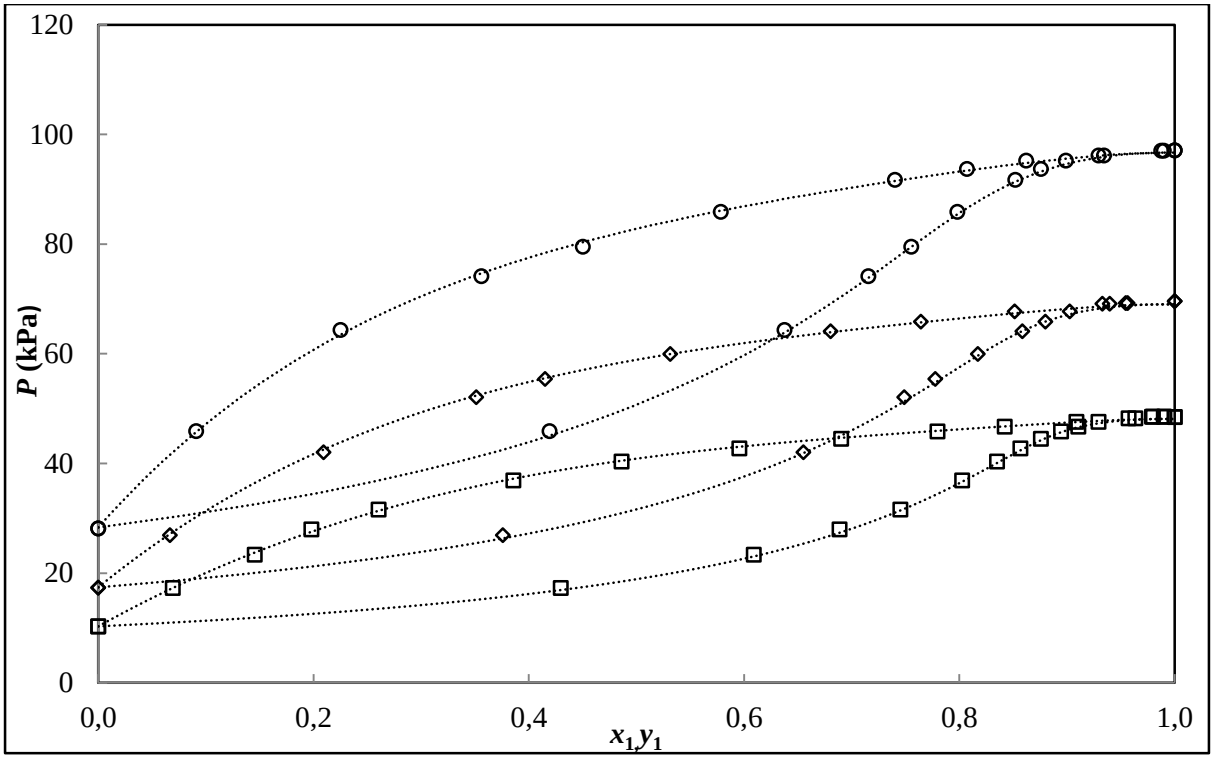

Figure 6-29: Experimental P-x_1-y_1 data for the DIPE (1) + 1-propanol (2) system: 320.15K (□); 330.15K (◊); 340.15K (○); fitted trend line (….).

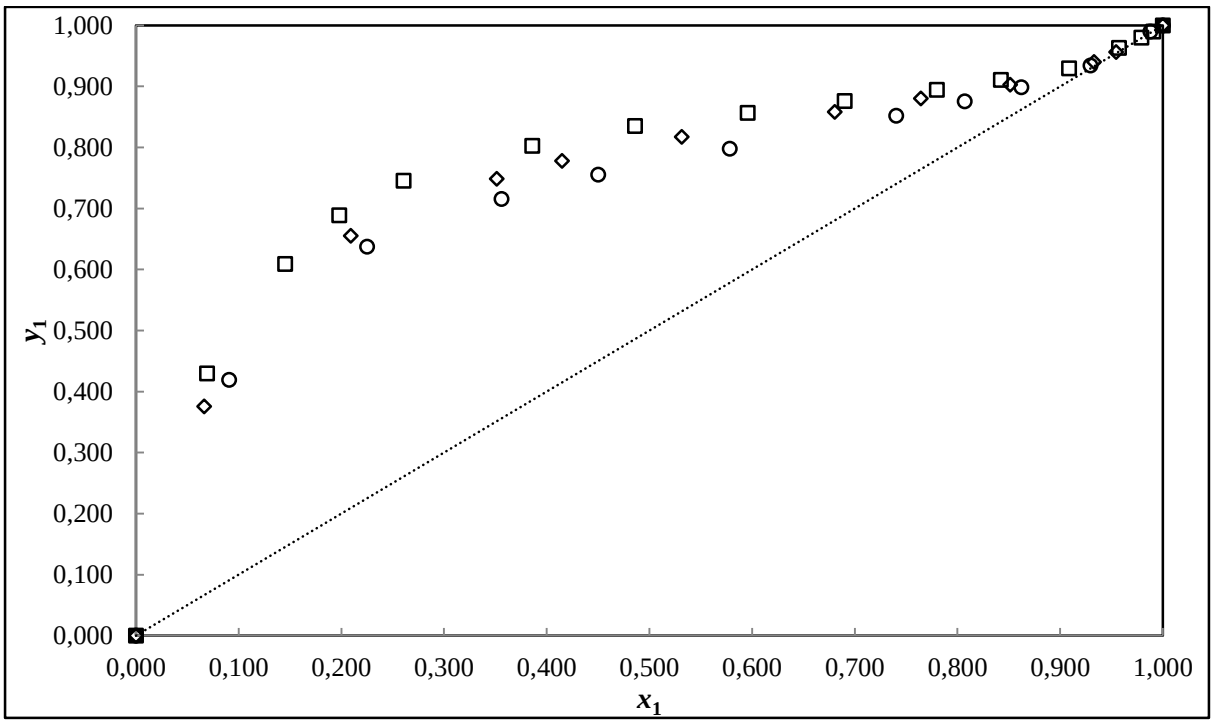

Figure 6-30: Experimental x_1-y_1 data for the DIPE (1) + 1-propanol (2) system: 320.15K (□); 330.15K (◊); 340.15K (○); y=x (….).

6.6.7. Results Diisopropyl ether (1) + 2-butanol (2) System

This system was previously investigated at an isotherm temperature of 313.15K by Villamañán (Villamañán et al., 2006b). All data measured for this system in this project are new temperature isotherms at 320.15, 330.15 and 340.15K. Much like the previous two systems discussed above comprising of the component DIPE, the Chromosorb packed column in conjunction with the Shimadzu GC 2014 model GC provided the most optimum separation. Along with the settings described in Table 6-5, the desirable separation was achieved. The GC calibration plots are visible in Figures 6-31 and 6-32. The experimental VLE data are given in Table 6-19 and Figures 6-33 and 6-34 shows the data graphically.

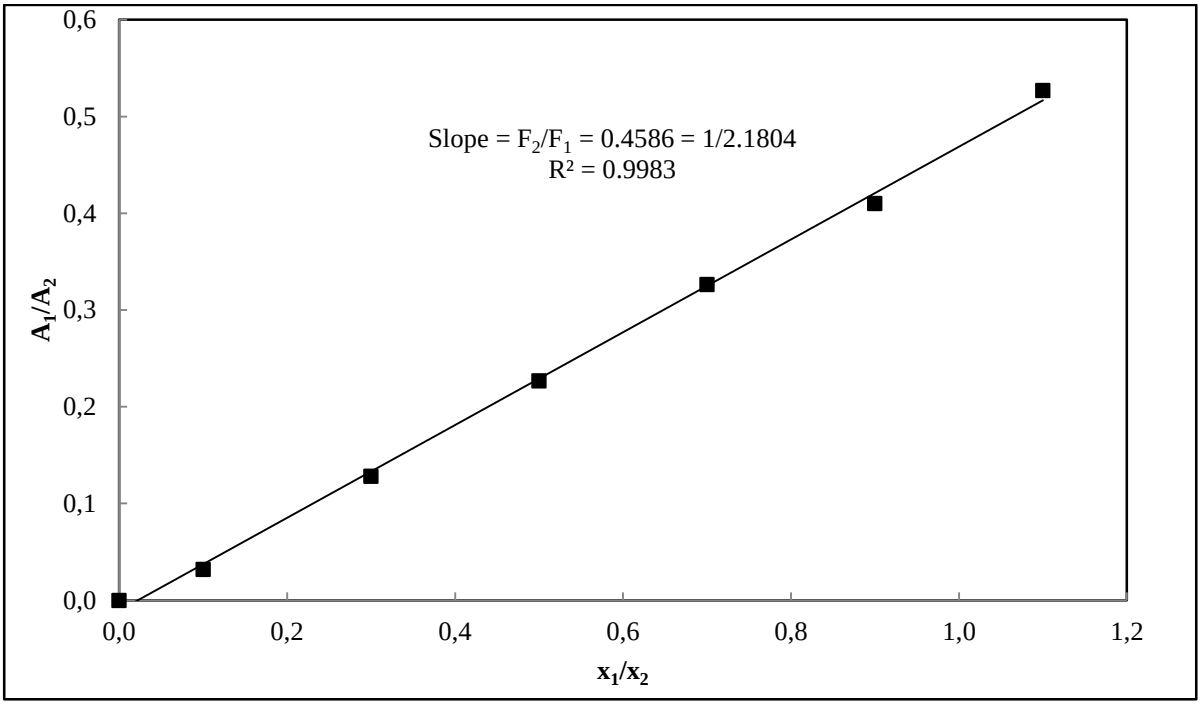

Figure 6-31: TCD Calibration plot for the DIPE (1) + 2-butanol (2) system (2-butanol dilute region).

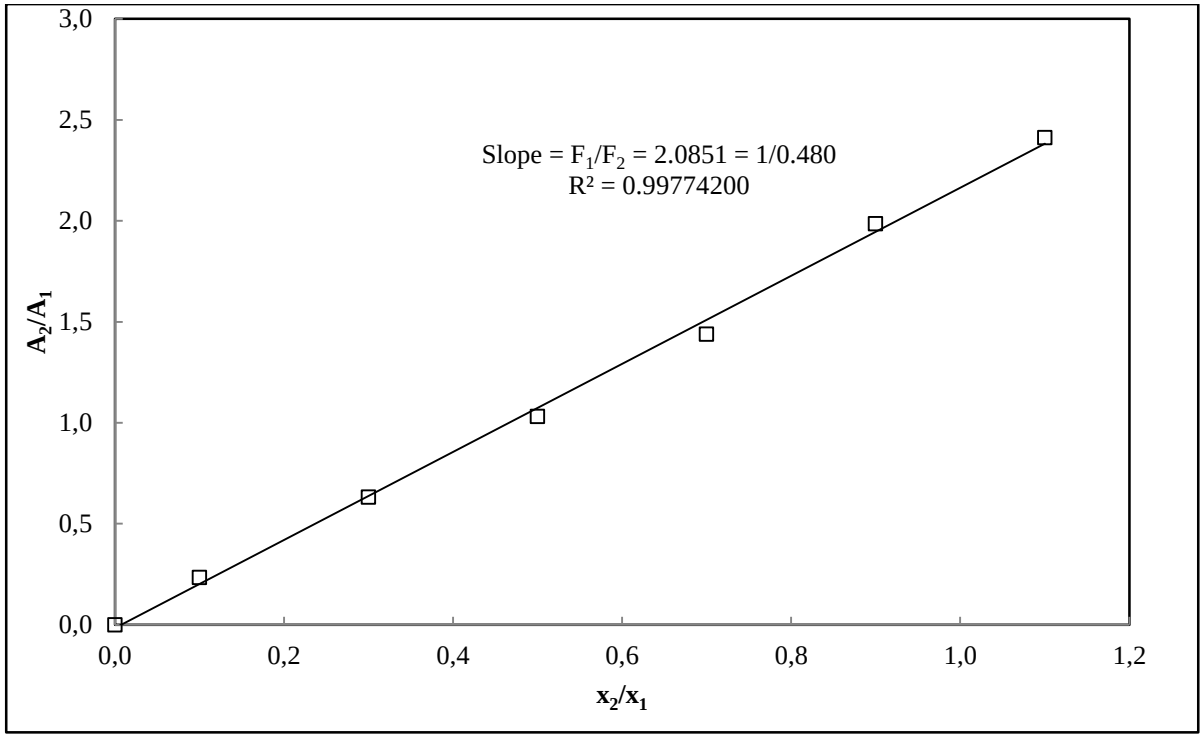

Figure 6-32: TCD Calibration plot for the DIPE (1) + 2-butanol (2) system (DIPE dilute region).

Table 6-19: P-x_1-y_1 data for DIPE (1) + 2-butanol (2) at 320.15K, 330.15K and 340.15K.

P/kPa	x_1	y_1	P/kPa	x_1	y_1	P/kPa	x_1	y_1
	T/K			T/K			T/K	
	320.15			330.15			340.15	
8.94	0.000	0.000	15.49	0.000	0.000	25.61	0.000	0.000
16.49	0.061	0.470	25.99	0.066	0.426	38.89	0.062	0.369
17.31	0.068	0.497	28.97	0.086	0.497	47.96	0.116	0.512
23.78	0.143	0.659	32.53	0.118	0.563	50.25	0.134	0.542
27.66	0.198	0.723	35.82	0.146	0.611	55.21	0.173	0.595
31.39	0.266	0.767	39.76	0.188	0.665	60.12	0.211	0.642
36.78	0.388	0.821	42.15	0.210	0.690	67.37	0.275	0.698
39.92	0.487	0.845	52.12	0.352	0.780	74.01	0.356	0.744
42.34	0.596	0.869	55.40	0.421	0.806	79.94	0.450	0.781
44.11	0.690	0.888	59.97	0.547	0.840	86.14	0.578	0.825
45.56	0.780	0.909	64.18	0.700	0.877	91.74	0.740	0.874
46.64	0.842	0.933	65.87	0.767	0.895	94.00	0.827	0.900
47.55	0.909	0.954	67.95	0.889	0.929	95.91	0.892	0.939
48.23	0.955	0.964	69.23	0.967	0.970	96.97	0.970	0.985
48.41	0.979	0.980	69.55	0.985	0.986	97.00	0.988	0.990
48.60	0.991	0.992	69.59	1.000	1.000	97.06	1.000	1.000
48.69	1.000	1.000						

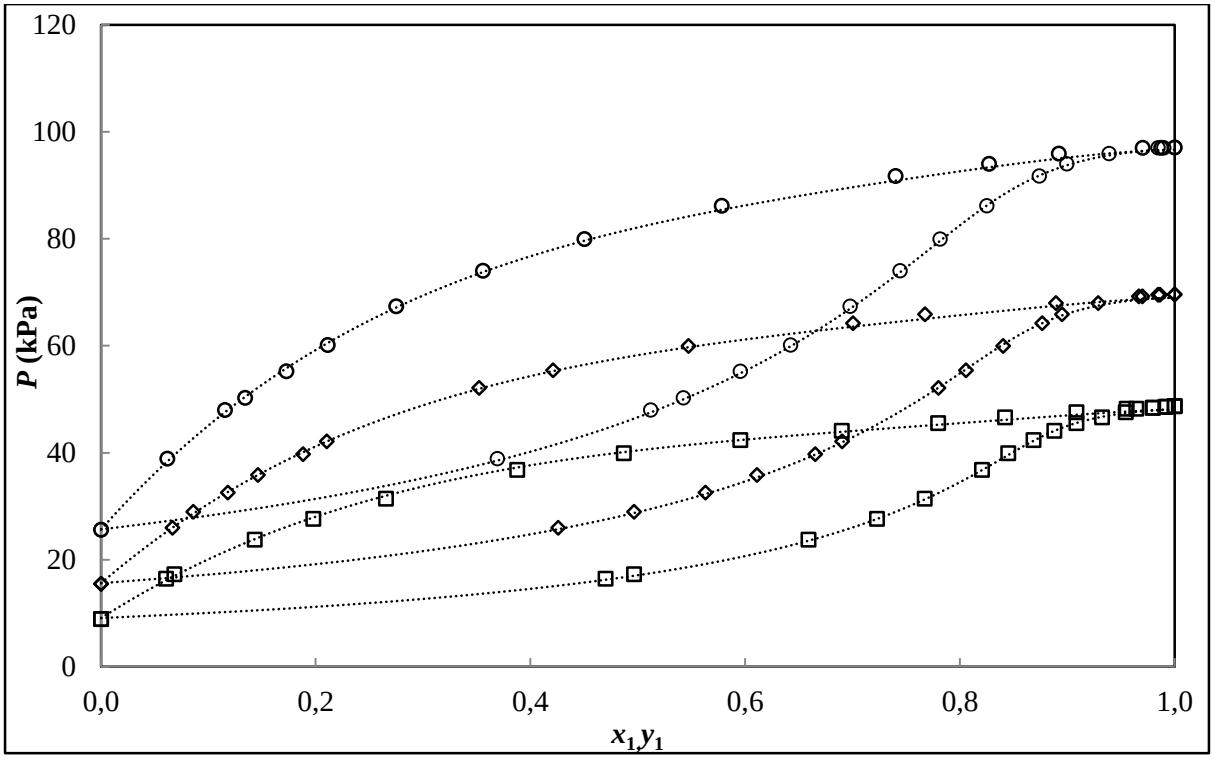

Figure 6-33: Experimental P-x_1-y_1 data for the DIPE (1) + 2-butanol (2) system: 320.15K (□); 330.15K (◊); 340.15K (○); fitted trend line (….).

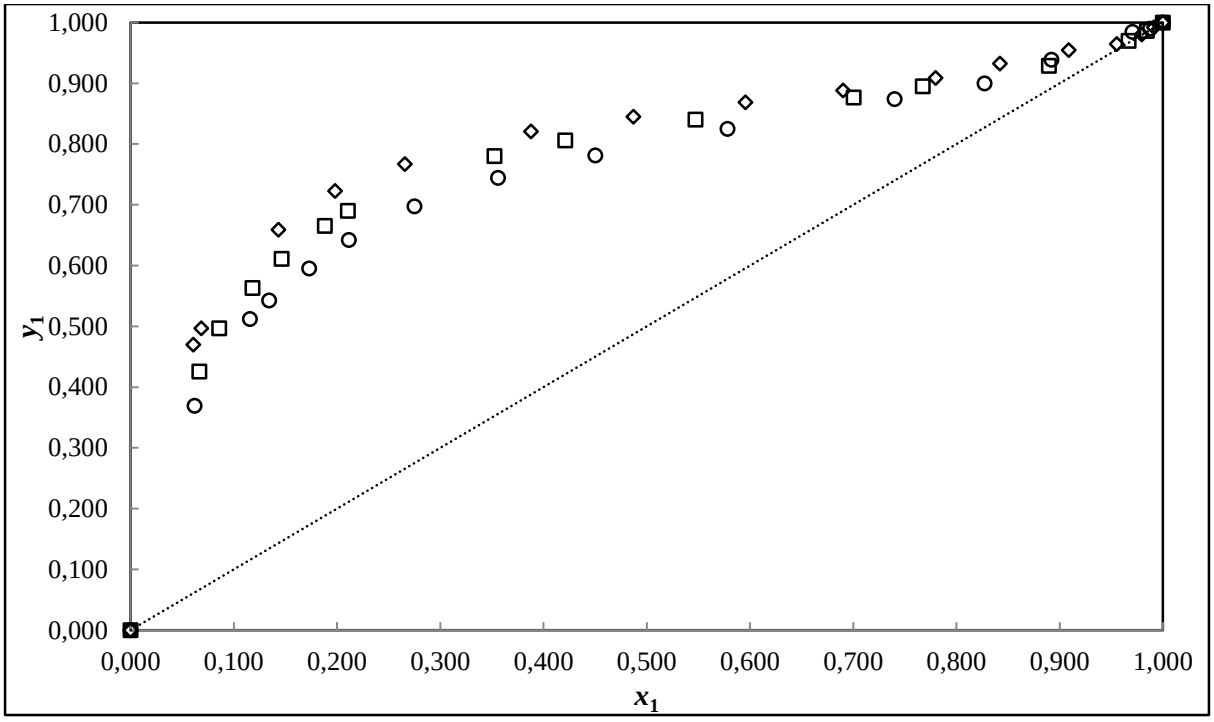

Figure 6-34: Experimental x_1-y_1 data for the DIPE (1) + 2-butanol (2) system: 320.15K (□); 330.15K (◊); 340.15K (○); y=x (….).

7

Chapter Seven

DATA ANALYSIS AND DISCUSSION

This chapter deals with reduction of all the measured experimental VLE data using the theoretical aspects of phase equilibria and thermodynamic consistency previously discussed at length in chapter 2. The formulation of a basis for the application of the measured data for industrial purposes and situations is the core rational for the analysis of experimental data by utilising the appropriate thermodynamic models. This can also provide an enhanced understanding of a particular system's phase behaviour. This chapter includes the vapour pressure data analysis with the Antoine type equation, the determination of experimental activity coefficients and the VLE data reduction employing the combined $\lambda - \phi$ and direct $\phi - \phi$ methods and thermodynamic consistency testing for all measured VLE systems. VLE data were regressed using the appropriate models available in Aspen Plus®. All measured VLE data were subjected to thermodynamic consistency testing in order to show the quality of the data and the extent to which the measured data fit the mathematical models.

7.1. Correlation of Experimental Vapour Pressure data for Pure Components

Accurately measured vapour pressure data are crucial in the modeling of binary VLE systems. Vapour pressures were therefore measured in this investigation for all the pure components that were used with this data tabulated and plotted in Section 6.4. The general form of the Antoine equation was used for the regression of the vapour pressure data shown below in equation (7-1):

$$\ln P_i^{sat}(kPa) = A_i + \frac{B_i}{T(^\circ C) + C_i} \qquad (7\text{-}1)$$

Table 7-1 below presents the regressed parameters along with the absolute average error for the Antoine equation. The low absolute average error values for the expression provides an indication that the equation fitted the experimental vapour pressure data exceptionally well.

Table 7-1: Regressed Parameters for the Antoine equation

Parameter	Pure Components					
	MTBE	**1-pentanol**	**Isooctane**	**DIPE**	**1-propanol**	**2-butanol**
A	57.604	114.063	84.710	19.336	86.338	121.937
B	-5555.140	-10041.891	-6625.912	-4111.658	-9490.087	-9750.057
C	11.987	-12.792	0.247	1.142	23.354	-9.463
AAD% $_{(\Delta P)}$	0.01	0.10	0.10	0.16	0.13	0.15

Pure component vapour pressure data can also be correlated by using an equation of state (EOS). The temperature dependent alpha function (α) impacts on the pure component parameter used in an EOS. Therefore, the reduction of experimental vapour pressure data results in these pure component parameters being obtained from an empirical correlation or EOS. Pure component parameters from the empirical correlations and the temperature dependent alpha function of Mathias and Copeman (1983) were regressed to improve the accuracy of vapour pressure correlations in VLE investigations. The Soave-Redlich- Kwong (SRK) and Peng-Robinson (PR) equations of state with the temperature dependent alpha function (α) of Mathias and Copeman (1983) were utilised as the thermodynamic models of choice for the direct method portion of binary VLE regression in this investigation.

7.1.1. Pure Component Regression with Equations of State

The SRK and PR equations of state can produce favourable phase equilibrium predictions and vapour pressure predictions (for non-polar components only) by requiring very little input information. It is for this reason that they are the two most widely used cubic equations of state for industrial design and optimisation applications, and also beneficial for use in this project. In this project however, the temperature dependent function (α) of Mathias and Copeman (Mathias and Copeman, 1983) was used with the SRK and PR equations of state because of the polar components that were used in experiments. For polar components, the temperature dependent function (α) of Mathias and Copeman (1983) produces a higher degree of complexity by utilization of adjustable parameters. In addition this also improves the accuracy of vapour pressure predictions – which influences the accuracy of VLE calculations significantly (Twu et al., 1991). Therefore, the experimental vapour pressure data were also reduced to obtain the parameters of the temperature dependent function (α) of Mathias and Copeman (1983), resulting in a more accurate vapour pressure predictions. Tables 7-2 and 7-3 respectively show the pure component parameters from the regression with the temperature dependent function (α) of Mathias and Copeman (1983) in the SRK and PR equations of state.

Table 7-2: Reduced pure component parameters for the α-function of Mathias and Copeman (1983) with the SRK EOS.

Component	κ_1	κ_2	κ_3	RMSD
				P/kPa
2,2,4-trimethylpentane	0.997	-0.525	1.080	0.29
1-pentanol	1.359	-0.414	2.297	0.36
MTBE	0.929	-0.441	1.147	0.30
DIPE	0.921	0.801	-2.226	0.11
1-propanol	1.277	0.958	-1.592	0.43
2-butanol	1.149	1.221	-0.931	0.52

Table 7-3: Reduced pure component parameters for the α-function of Mathias and Copeman (1983) with the PR EOS.

Component	κ_1	κ_2	κ_3	RMSD
				P/kPa
2,2,4-trimethylpentane	0.826	-0.1700	0.622	0.27
1-pentanol	1.165	-0.037	-1.779	0.39
MTBE	0.764	-0.111	0.724	0.19
DIPE	0.750	1.122	-2.600	0.24
1-propanol	1.080	1.337	-2.079	0.28
2-butanol	0.961	1.562	-1.394	0.13

7.2. Vapour Pressure Data Thermodynamic Consistency Testing

Researchers of the Design Institute for Physical Property Data (DIPPR) Compilation Project recommend that qualitative thermodynamic consistency testing be performed on experimental vapour pressure data also (Daubert et al., 1990).

It was therefore in the best interests of this project that this testing be undertaken by simply plotting the data in the form of ln *P* versus (*1 / T*). By representing the plot in this manner, a visual

examination for the decomposition or polymerization with an increase in temperature can be performed. The data are considered thermodynamically consistent if the plot shows a linear trend. This means that no decomposition or polymerization would have occurred with an increase in temperature. This exercise however is best performed by using wide temperature range as this is considered to produce a more definitive result.

Linear trends can be observed for all vapour pressure data measurements in this project presented in section 6.4, Figures 6-7 to 6-12. Provision of visual confirmation of the data passing the thermodynamic consistency testing within its temperature range therefore becomes apparent.

7.3. Experimental Activity Coefficients for Binary VLE systems

Experimental activity coefficients can be determined (in theory) by using the second virial coefficients by the vapour phase correction factor, Φ_i given by the virial EOS Equation (2-25), and substituting it into Equation (2-23). The methods for calculating second virial coefficients are discussed in detail in section 2.4.2. Assuming ideal gas behaviour for the vapour phase $(\Phi_i = 1)$ is another manner of obtaining experimental activity coefficients.

The correlations of Hayden and O'Connell (1975) and Nothnagel *et al*. (1973) were selected to compute second virial coefficients for this work. These methods cover a large range of compounds including associating, non-polar and polar compounds, especially the method of Hayden and O'Connell (1975). The pure component properties for these correlations were located in Aspen Plus®; both methods are discussed further also in section 2.4.2. When/once the activity coefficients were calculated from the experimental values of the vapour composition (y_i), liquid composition (x_i) and the calculated values of Φ_i by substitution into Equation (2-23), *experimental* activity coefficients were obtained. The activity coefficients are called *experimental* because they were calculated directly from VLE data by omitting the use of an activity coefficient model.

The calculated activity coefficients are typically poor in quality when encountering systems with components exhibiting high levels of association. This is because these models usually do not take into account the effect that the association between the molecules causes when calculating the activity coefficients (Sewpersad, 2012). The logarithmic plot of the activity coefficients for the system of MTBE (1) + 1-pentanol (1) is represented below in Figure (7-1). These are the logarithms of the experimental and calculated versus the liquid composition of MTBE.

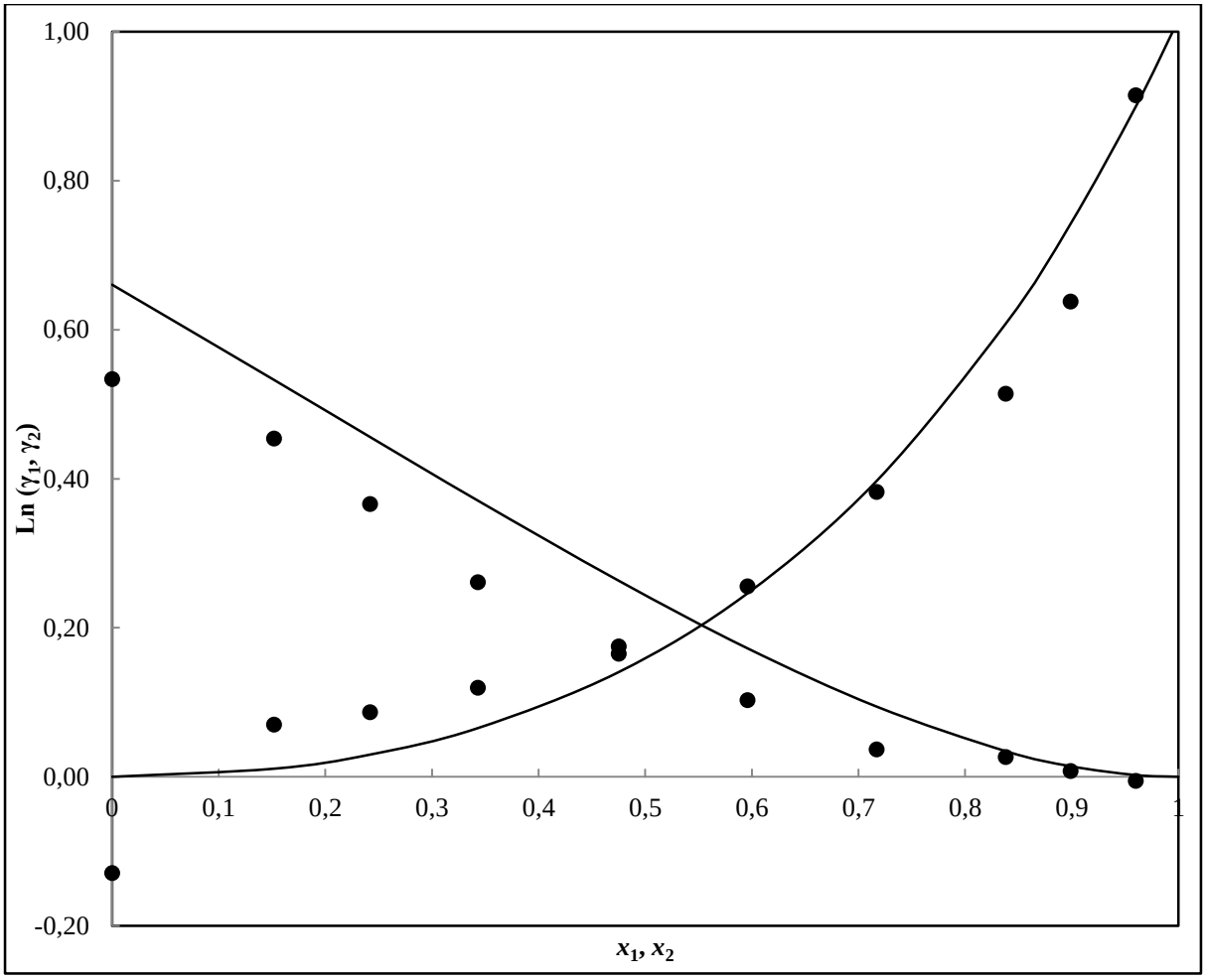

Figure 7-1: The comparison of experimentally determined liquid-phase activity coefficients (using Modified Raoult's Law) and those calculated from the model for the MTBE (1) + 1-pentanol (2) system at 317.15 K: ● this work, — HOC-NRTL model.

The large deviations that can be seen in Figure 7-1 are attributed to the strong association that occurs. Association aspects pertaining to the ether-alcohol chemical systems under investigation in this study are outlined in more detail in Chapter 1. This occurs even at low pressures, a region where strong association having an impact on poor computed activity coefficients should be insignificant. Therefore, it is vital to utilise models that take into account strong association between molecules in chemical systems.

7.4. Measured Binary VLE data Regression

The reduction of binary VLE data and the techniques used were discussed extensively in Chapter 2 Section 2.6. Experimental VLE data were correlated by placing emphasis on the non-ideality in both the vapour and liquid phases. The techniques used in the reduction involved determining the optimal parameters for each thermodynamic model that was used by utilising both the combined $(\gamma - \phi)$ and

direct methods $(\phi - \phi)$ in conjunction with bubble point pressure calculations. Model parameters were optimized by minimizing the deviations between the pressure and vapour composition from the experimental data. The predictive values (obtained by iteration using the model selected) were then used to correlate the experimental data. By solving for the optimal parameter solutions of each thermodynamic model, the difference between experimental and predicted values became minimized. This was achieved by utilisation of the *ordinary least squares method* objective function, which reduces to Barkers method when only *P*-x_i data is used.

A process simulator like Aspen Plus® is the most popular and widely used tool for modeling and predicting industrial process performance. It is for this reason that Aspen Plus® was used as the process simulation package of choice with the combined and direct methods for VLE data regression. The Aspen Plus® process simulator is also equipped with numerous models that include those which are capable of describing association and solvation in chemical systems. Three local-composition based activity coefficient models were chosen to account for the liquid phase non-ideality: viz., the Wilson (1964), NRTL (Renon and Prausnitz, 1968) and the UNIQUAC (Abrams and Prausnitz, 1975). The vapour phase fugacity coefficients for describing non-ideality were calculated using methods of Hayden and O'Connell (1975) and Nothnagel *et al*. (1973), capable of describing associating and non-associating systems available. The direct method required a mixing rule to accurately model the experimental VLE data. Hence, the Soave-Redlich-Kwong (Redlich and Kwong, 1949, Soave, 1972) and Peng Robinson (1976) equations of state was combined using the temperature dependent function (α) of Mathias and Copeman (1983) with the Wong-Sandler (1992) mixing rule. The Wong and Sandler (1992) mixing rule was held in high esteem for selection in this study specifically because of its applicability in a wide range of mixtures. These mixtures include the contents of hydrocarbons, inorganic gases, mixtures containing aromatic, along with polar and associating systems. The Wong and Sandler (1992) mixing rule required an activity coefficient model to reduce the experimental VLE data, therefore, the Wilson (Wilson, 1964), NRTL (Renon and Prausnitz, 1968) and the UNIQUAC (Abrams and Prausnitz, 1975) activity coefficient models were employed. All three activity coefficient models were employed in order to reflect the versatility of each model pertaining to various systems regressed and the lowest deviations that can be produced from experimental data correlation. For ease of comprehension and to illustrate the combinations used for the combined and direct methods, Tables 7-4 and 7-5 respectively, provide a summary of the abbreviated model names and combinations used in data regression.

Table 7-4: Regression Model Combinations used for the Combined Method.

Correlation for Second Virial Coefficient	Activity Coefficient Model	Abbreviation of Model Combination
Nothnagel (1973)	Wilson	Wilson-NTH
Nothnagel (1973)	NRTL	NRTL-NTH
Nothnagel (1973)	UNIQUAC	UNIQUAC-NTH
Hayden and O'Connell (1975)	Wilson	Wilson-HOC
Hayden and O'Connell (1975)	NRTL	NRTL-HOC
Hayden and O'Connell (1975)	UNIQUAC	UNIQUAC-HOC

Table 7-5: Regression Model Combinations used for the Direct Method.

Equation of State	α-Function Correlation	Mixing Rule	Activity Coefficient Model for Mixing Rule	Abbreviated Model Combination
Redlich-Kwong, (1949) and Soave, (1972)	Mathias and Copeman (1983)	Wong and Sandler (1992)	Wilson	RKS-MC-WS-Wilson
Redlich-Kwong, (1949) and Soave, (1972)	Mathias and Copeman (1983)	Wong and Sandler (1992)	NRTL	RKS-MC-WS-NRTL
Redlich-Kwong, (1949) and Soave, (1972)	Mathias and Copeman (1983)	Wong and Sandler (1992)	UNIQUAC	RKS-MC-WS-UNIQUAC
Peng and Robinson (1976)	Mathias and Copeman (1983)	Wong and Sandler (1992)	Wilson	PR-MC-WS-Wilson
Peng and Robinson (1976)	Mathias and Copeman (1983)	Wong and Sandler (1992)	NRTL	PR-MC-WS-NRTL
Peng and Robinson (1976)	Mathias and Copeman (1983)	Wong and Sandler (1992)	UNIQUAC	PR-MC-WS-UNIQUAC

7.4.1. Objective function for Parameter Optimisation

Both the combined and direct method model parameters were optimised by the minimisation of the pressure deviations for isotherms between the experimentally measured pressures and the calculated values given by the model used for regression. Previously discussed in section 2.6.1, the minimisation of the error in the difference between the experimental and calculated data (the residual, δ) becomes the basis for the regression algorithm. According to Van Ness (1995), the minimisation of the pressure residuals (ΔP) supplies a fit that is at least as good as any other that could be obtained by minimising another such as the vapour composition residuals (Δy). Equations (2-120) and (2-121) are the two residuals (pressure and vapour composition) that were used to correlate each set of data in this study; they are referred to as the primary residuals (Abbott and Van Ness, 1982).

Aspen Plus® contains and employs a three step procedure to perform all data reductions. These three steps consist of:

- the initialisation – uses the Deming method; an approximate solution method
- the middle loop – uses the Britt-Luecke algorithm
- the end loop – runs the data regression iterative process to completion supplying the residuals along with pure component and the binary interaction parameters

The Britt-Luecke algorithm is a rigorous *maximum-likelihood* method. The maximum-likelihood method insures a global optimum with regards to parameter estimation, and was utilised instead of the approximate solution method of Deming (1943). The aforementioned methods supplied a more superior convergence as opposed to the approximate solution method of Deming (1943). The Deming method is however used for initialisation of iterations and is recommended by Aspen to be selected as an alternative should the Britt-Luecke provide no convergence. The objective function used for ordinary least squares method for determining the G^E model and binary interaction parameters with respect to the binary VLE computations was:

$$S = \frac{1}{n}\sum_{i}^{n}\left[\left(\frac{\left|P_i^{\exp} - P_i^{calc}\right|}{P_i^{\exp}}\right) + \left(\left|y_i^{\exp} - y_i^{calc}\right|\right)\right] \tag{7-2}$$

7.4.2. Parameter Estimation for VLE Modeling

Parameter estimation for VLE modeling with the use of local composition models proves to be a troublesome global optimization problem, with their characteristics posing a challenge to any kind of optimization technique (Bonilla-Petriciolet et al., 2009). Although the three NRTL model parameters: τ_{ij}, τ_{ji} and the non-randomness parameter α_{ij} are adjustable, many authors suggest that superior results are obtained by fixing the non-randomness parameter between 0.2 and 0.47 (as discussed in more detail in section 2.5.1.2). The NRTL α_{ij} parameter was set to 0.3 for all regressions based on the recommendation of Walas (1985) for non-aqueous mixtures (discussed further also in section 2.5.1.2); with the systems that were measured in this study being non-aqueous. Only the a_{ij} and b_{ij} parameters in equation (2-108) for activity coefficient models were included in the data reductions, with all other parameters (besides the non-randomness parameter α_{ij}) being set to zero.

7.5. Comparison with Literature Data

In this section, the systems previously measured that were located in literature were MTBE + 2, 2, 4-trimetylpentane; DIPE + 2, 2, 4-trimetylpentane; DIPE + 1-propanol and DIPE + 2-butanol. These were located by using the NIST TDE (ThermoData Engine) function in Aspen Plus®. All the literature data systems mentioned were regressed using Aspen Plus® regardless of what program or simulation package was used by the original authors. Subsequently, all authors mentioned in this section have not specified what simulation package or program was used to reduce their experimental data. Additionally, nowadays it has become the standard practice in all publications to use the NIST guidelines for evaluating and expressing the uncertainty. All authors mentioned here have not specified whether they have done so. All *AAD* values calculated in Aspen Plus® for this section, are for the best fitted model from the extrapolated literature data to the data of this work. All literature data have been regressed with temperature dependence in order to predict different temperature isotherms, as with the data of this work.

7.5.1. The MTBE + 2, 2, 4-trimetylpentane system Literature Data Comparison

The literature data for this system was by Bernatová et al. 2001. Their data was measured at isotherm temperatures of T = (318.13, 328.20 and 339.28) K.

In their study, only the compositional analysis of the MTBE + 2, 2, 4-trimetylpentane was performed using a vibrating-tube densimeter (A. Paar Australia). The other two system compositions in their

work were analysed in a Hewlett-Packard gas chromatograph HP5890 (Bernatová and Wichterle, 2001). The reason for this manner of analysing the samples using a different technique for only the one system is not specified or justified in their paper, which is somewhat unusual. Another discrepancy that can be noted with their work is that they had stated that the composition was obtained with accuracy of 0.0001 mol%. In addition to this, the accuracy of their density determination is estimated to be better than ±0.00002 g cm^{-3}. These uncertainty estimates appear to be rather low and therefore perceived as an underestimation of uncertainty. Furthermore the authors have not specified what method of uncertainty calculation (NIST or otherwise) used. Hence, this renders their uncertainty estimations unreliable. It can be deduced that since this paper was published in 2001 that it was not as strict a practice to use the NIST guidelines for evaluating and expressing the uncertainty as is the standard practise to do so in recent years. Furthermore, the two literature isotherms of T = (318.13 and 328.20) K, were found to be thermodynamically inconsistent. Both literature isotherms fail the point test (Van Ness et al., 1973) in Aspen Plus® whereas all three isotherms of this work pass and where found to be thermodynamically consistent according to the point test.

Therefore, this thermodynamic inconsistency in the lietrature data could most likely be the reason for the poor extrapolation results of their correlated data to the measured isotherms in this project. Unfortunately this data of Bernatová et al. 2001 is the only available in literature for this system. The three data sets of Bernatová et al. 2001 were simultaneously regressed with the Wilson and NRTL models using the same experimental uncertainties in the maximum likelihood approach used by the authors. Although the data was correlated well by the models, the regression of their data was performed using the without their experimental vapour pressures which were not stated in the publication of Bernatová et al. 2001. Instead the literature vapour pressures within the Aspen Plus® database were used. The $AAD\%_{(\Delta P)}$ and $AAD\%_{(\Delta y)}$ values (for the Wilson model) calculated in Aspen Plus® for their data is 0.43 and 0.71 respectively. The Wilson model in their study had correlated their data best. So was the case when the regression was run for the literature data in this study. Figures 7-74 and 7-75 show the extrapolation results pertaining to this study's data and this data extrapolated to the data of Bernatová et al. 2001 respectively.

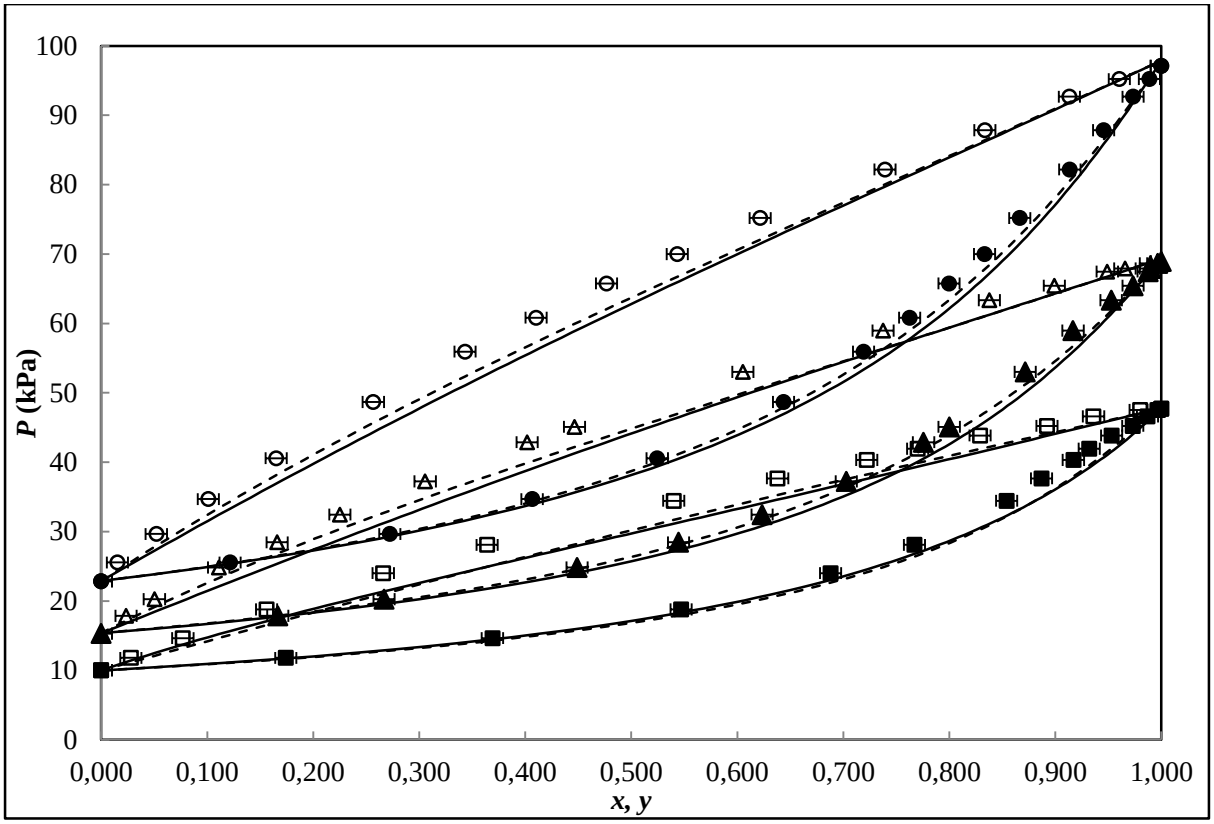

Figure 7-2: Experimental VLE and modeling extrapolation of Bernatová et al. 2001 data: *P-x-y* data for the MTBE (1) + 2, 2, 4-trimethylpentane (2) system at 307.15K (□); 317.15K (△); 327.15K (○); — extrapolated HOC-NRTL; - - - extrapolated HOC-Wilson.

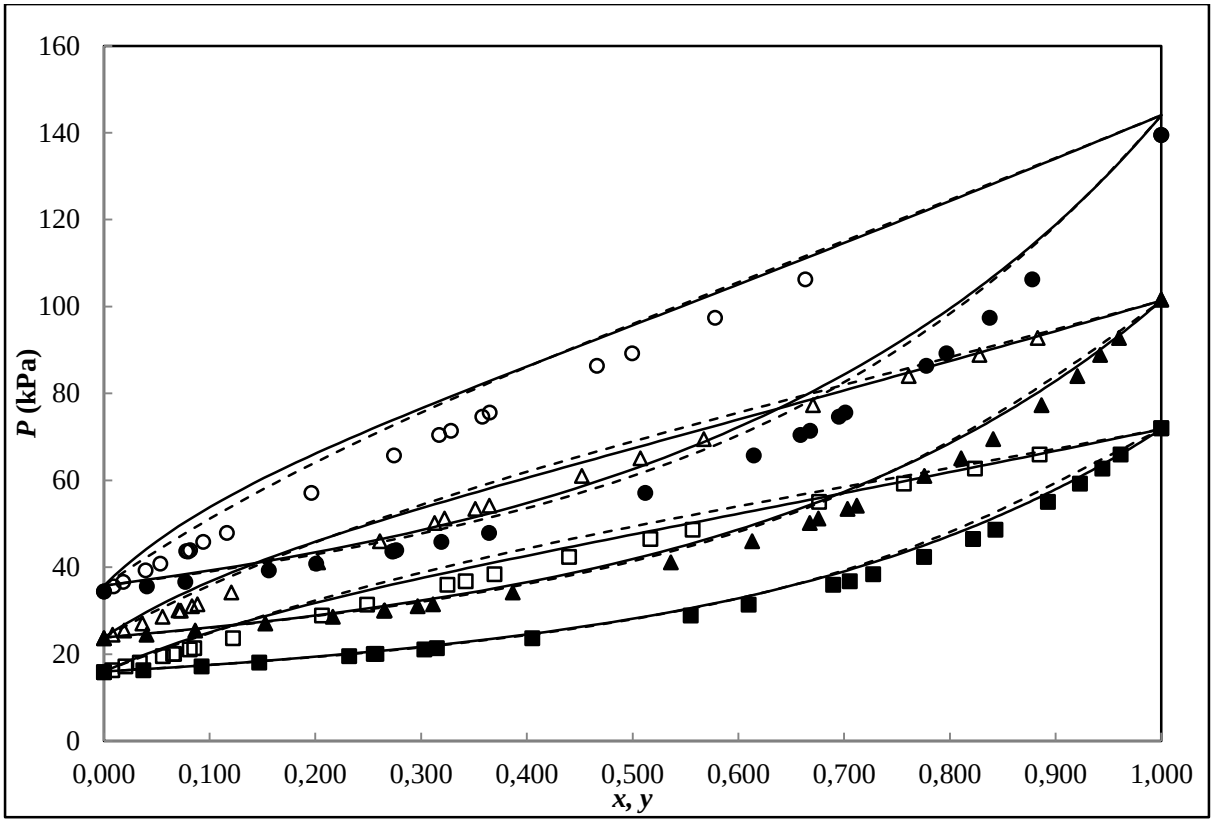

Figure 7-3: Experimental VLE and modeling extrapolation of this work: *P-x-y* data for the MTBE (1) + 2, 2, 4-trimethylpentane (2) system of Bernatová et al. 2001 at 318.13K (□); 328.20K (△); 339.28K (○); — extrapolated HOC-NRTL; - - - extrapolated HOC-Wilson.

7.5.2. The DIPE + 2, 2, 4-trimetylpentane system Literature Data Comparison

The literature data extrapolated for this system was by Hwang et al. (2007 and 2009). Their data was measured at isotherm temperatures of T = (303.15 and 333.15) K.

The technique of headspace gas chromatography (HSGC) was used to measure their isotherms in both papers. For the work of Hwang et al. 2007 and Hwang et al. 2009, the uncertainty of the measured equilibrium mole fraction for is about ±0.00001. It has not been specified by the authors (for both publications) as to what method of uncertainty calculation has been utilised here. It can therefore be deduced that this stated uncertainty is an underestimation as the NIST standards method of uncertainty calculation could not yield such a low uncertainty if applied correctly.

The literature data was correlated simultaneously in this study with the Wilson and NRTL models. The method reduction was not mentioned by the authors. Therefore, the maximum likelihood method was used in conjunction with their reported uncertainty for the regression of their data here. The $AAD\%_{(\Delta P)}$ and $AAD\%_{(\Delta y)}$ values calculated (for the Wilson model) in Aspen Plus® for their data is

0.41 and 1.22 respectively. The data of Hwang et al. (2007 and 2009), was correlated well by the Wilson model. It gave the best fit also when regressed in this work for extrapolation. The literature vapour pressures within the Aspen Plus® database were used to reduce the data of Hwang et al. (2007 and 2009). In both cases, their experimental vapour pressure data were not specified. Figure 7-76 exhibits the correlated data of Hwang et al. 2007 and Hwang et al. 2009 extrapolated simultaneously to the data of this work. The Wilson model had correlated the data more accurately to the data of this work, shown in Figure 7-76. Model dependency is therefore displayed for this system.

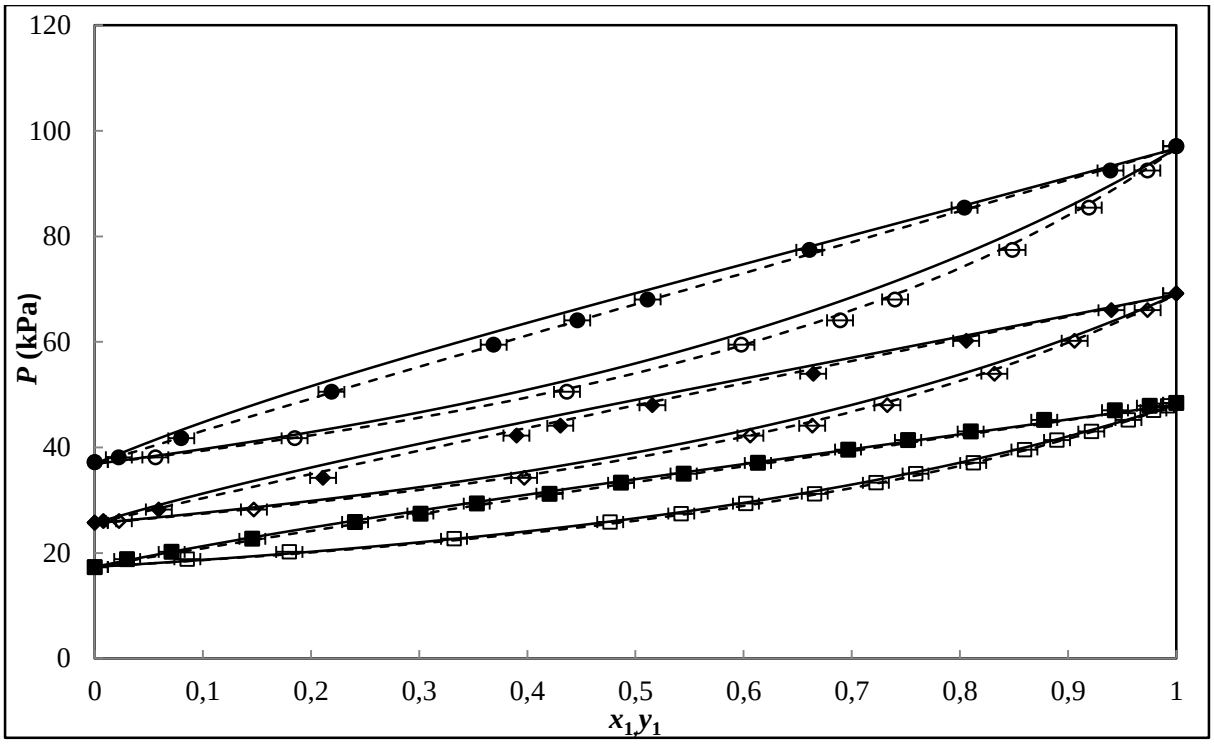

Figure 7-4: Experimental VLE and modeling extrapolation of this work: *P-x-y* data for the DIPE (1) + 2, 2, 4-trimethylpentane (2) system at 320.15K (□); 330.15K (△); 340.15K (○); — extrapolated HOC-NRTL; - - - extrapolated HOC-Wilson.

7.5.3. The DIPE + 1-propanol system Literature Data Comparison

The literature data extrapolated for this system was from the work of Hwang et al. 2007. This is the same publication expounded on in section 7.7.2, having the same uncertainty in the measurement etc. Their data was measured at an isotherm temperatures of T = 303.15 K for this system.

The Hwang et al. 2007 data was correlated in this work well by the Wilson and NRTL models for their data. The NRTL model $AAD\%_{(\Delta P)}$ and $AAD\%_{(\Delta y)}$ values calculated in Aspen Plus® were 0.66 and 0.56 respectively. The same regression conditions apply for section 7.5.2. Their binary interaction parameters were then extrapolated to predict data for all three isotherms measured in this work. The

NRTL model provided the best fit result for this project's experimental data to the extrapolated data of Hwang et al. 2007. However the result of the extrapolation of their data to the higher temperature isotherm (T = 340.15 K) of this work, was not as accurate toward the dilute region of DIPE. The Wilson model prediction however provides a more accurate fit in this region only. This could be attributed to the fact that the data of Hwang et al. 2007 is measured at a temperature of 303.15 K, much lower than 340.15 K. This kind of occurrence has been noted before with extrapolation after data reduction with temperature dependence. It can also depend sometimes on the model used in the data regression.

Figure 7-77 shows the correlated data of Hwang et al. 2007 extrapolated to the experimental data of this work.

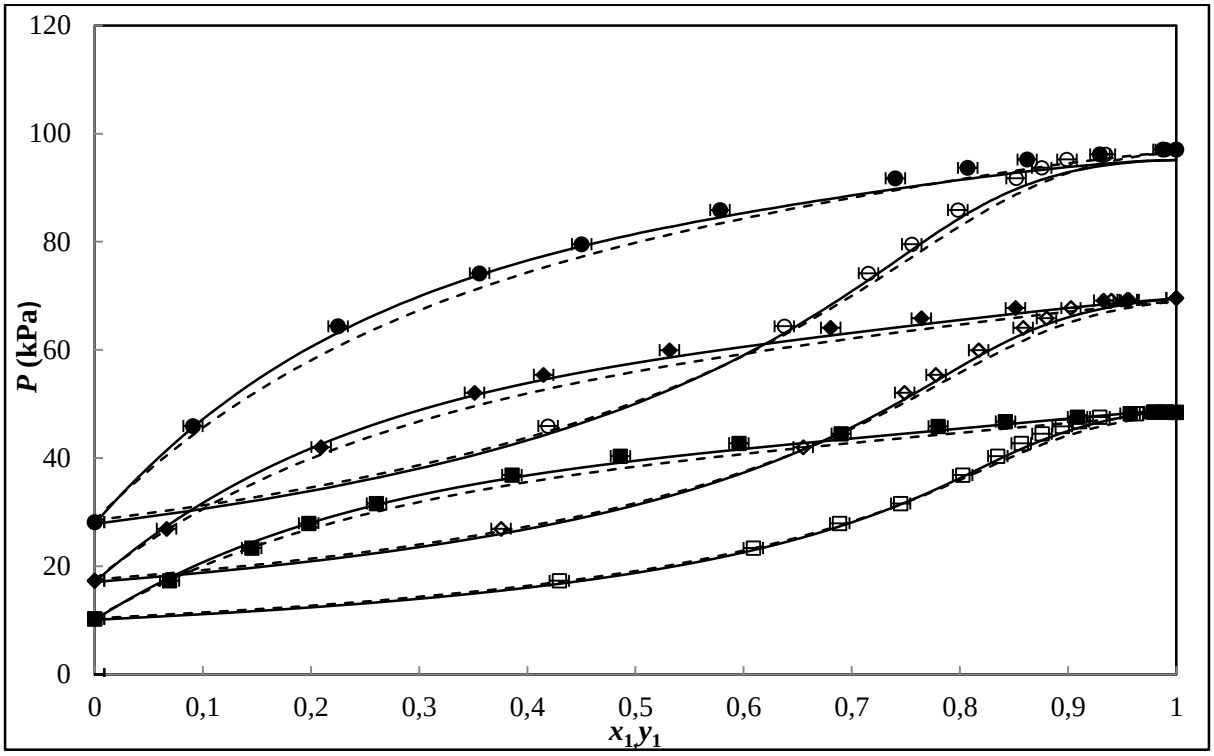

Figure 7-5: Experimental VLE and modeling extrapolation of this work: *P-x-y* data for the DIPE (1) + 1-propanl (2) system at 320.15K (□); 330.15K (△); 340.15K (○); — extrapolated HOC-NRTL; - - - extrapolated HOC-Wilson.

7.5.4. The DIPE + 2-butanol system Literature Data Comparison

The literature data extrapolated for this system was by Villamañán et al. 2006. Their data was measured at an isotherm temperature of T = 313.15 K.

A static technique consisting of an isothermal total pressure cell was used for their measurements (Villamañán et al., 2006a). They estimated uncertainties in mole fraction of ±0.0005. With this publication also the authors have not specified the method of uncertainty calculation used.
The data was correlated well by the Wilson and NRTL models in this study for their data. The Wilson model *AAD%* $_{(\Delta P)}$ and *AAD%* $_{(\Delta y)}$ calculated in Aspen Plus® for their data was 0.21 and 0.076 respectively. Data reduction for the binary and ternary mixtures was done by Barker's method in Villamañán et al. 2006. Therefore, the same method (using their experimental uncertainty) was used in this study to regress their data. The literature vapour pressures from the Aspen Plus® database were used to reduce the data of Villamañán et al. 2006 - their experimental vapour pressure data were not specified. The extrapolation results were less than satisfactory for the work of Villamañán et al. 2006 to that of the three measured isotherms of this work. The NRTL model gave the best fit for the lowest temperature isotherm (T = 320.15 K). This is closest to their measured isotherm (T = 313.15 K) for this system. The NRTL deviation becomes visibly worse with an increase in temperature, developing an azeotrope from the predicted NRTL isotherm for temperatures T = (330.15 and 340.15) K. The Wilson model however, had the lowest overall *AAD%* $_{(\Delta P)}$ reported in Villamañán et al. 2006. Similar was the case when their data was reduced and extrapolated to the temperature isotherms of this study. As mentioned previously in section 7.5.3, extrapolation after data reduction with temperature dependence, can result in the deviation of the model prediction from the experimental data being larger for the higher temperature isotherms. The Wilson model however, exhibits somewhat larger deviations for the lower temperature isotherms namely T = (320.15 and 330.15) K. It can be seen that the isotherm of T = 340.15 K is extrapolated much closer to this study's measured data from the Wilson model prediction.

Figure 7-78 shows the correlated data of Villamañán et al. 2006 extrapolated to the experimental data of this work. The model dependency on the overall result can clearly be observed here, favouring the Wilson model overall.

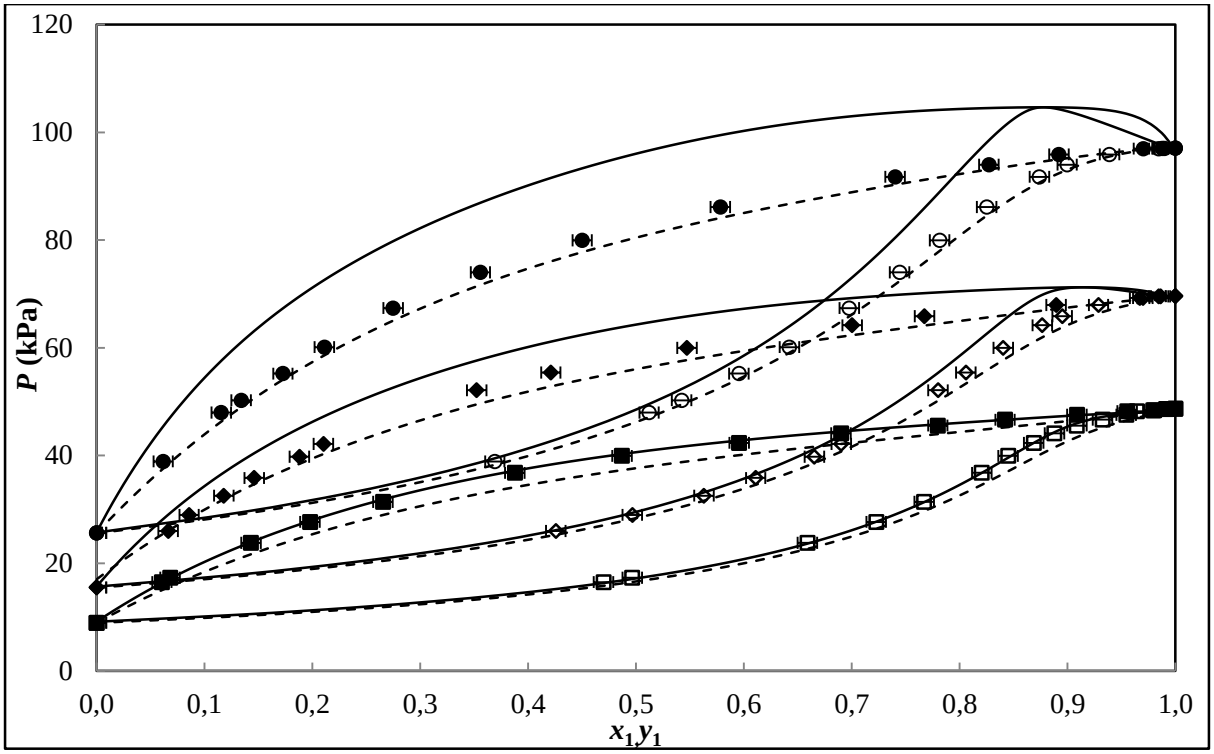

Figure 7-6: Experimental VLE and modeling extrapolation of this work: *P-x-y* data for the DIPE (1) + 2-butanol (2) system at 320.15K (□); 330.15K (△); 340.15K (○); — extrapolated HOC-NRTL; - - - extrapolated HOC-Wilson.

7.6. Previously Unmeasured Isotherms

In this section the data analysis was performed for the previously unmeasured isotherms of their specified temperatures. These isotherm temperatures were not found in literature.

7.6.1. Modeling Results for 2, 2, 4-trimethylpentane (1) + 1-pentanol (2)

The adjustable binary interaction parameters for the different models used in the regression of the 2, 2, 4-trimethylpentane (1) + 1-pentanol (2) system are given in Tables 7-6 to 7-8. The average deviations of pressure (ΔP/kPa), vapour molar compositions (Δy_1) and the average absolute deviation (AAD %) of the vapour mole fraction are also in Tables 7-6 to 7-8.

There were no significant differences observed between the models, with both HOC-Wilson and NTH-Wilson models showing the least deviations for the data set at 350.15 K. Typically the combination of the equations of in state with the NRTL model mostly gave a better fit than combinations with the Wilson and UNIQUAC models. The effect of temperature dependant modeling results is shown significantly by the increase in deviations with temperature. The (AAD %) increases with temperature with the lowest value of 0.47 % (< 0.5%) observed in the PR-Wilson equation, while highest value at 0.80 % (< 0.5%) for the PR-UNIQUAC equation for the 370.15 K data set. It could be possible to attribute this behaviour (with increase in temperature) to the significance of stronger short range association and dipole effects of pentan-1-ol to pentan-1-ol molecules within the vapour phase. The mobility of molecules with an increase in temperature therefore becomes imminent, which further promotes this effect. The system exhibited a minimum boiling azeotrope with the azeotrope shifting away from the iso-octane rich region with an increase in isotherm temperature. Table B-7 (Appendix B) provides the calculated azeotropic conditions. The Figures 7-7 to 7-12 represent the comparison of the model fits to the measured VLE data. Figure D-1 in Appendix D shows the relative volatility plots for this system. Experimental activity coefficients are given in the Appendix C.

The observance of the predicted activity coefficients deviating from the experimental activity coefficients becomes more pronounced upon approaching the dilute regions. This behaviour can be attributed to the fact that the models represent thermodynamic behaviour poorly at infinite dilution (Mqondisi, 2012).

Table 7-6: Combined Method Modeling results using Hayden-O'Connell method for 2, 2, 4-trimethylpentane (1) + 1-pentanol (2)

Model	**T±0.10/K**	α_{12}	$^{a}A_{12}$ **J/mol**	$^{a}A_{21}$ **J/mol**	**(Δ*P*) AAD**	**AAD% (Δ*P*)**	**(Δy_1) AAD**	**AAD%(Δy_1)**
NRTL-HOC								
	350.15	0.30	-3274	2239	0.26	1.10	0.003	0.30
	360.15	0.30	-3206	2182	0.27	0.74	0.003	0.37
	370.15	0.30	-3184	2164	0.30	0.55	0.003	0.38
Wilson-HOC								
	350.15	-	-1881	3387	0.29	1.15	0.002	0.17
	360.15	-	-1820	3312	0.20	0.62	0.004	0.30
	370.15	-	-1776	3254	0.31	0.63	0.003	0.22
UNIQUAC-HOC								
	350.15	-	1227	-595.7	0.24	1.08	0.002	0.32
	360.15	-	1195	-575.7	0.30	0.78	0.003	0.39
	370.15	-	1189	-571.6	0.35	0.66	0.003	0.42

[a]Wilson: $A_{12} = a_{12} - a_{22}$ and $A_{21} = a_{21} - a_{11}$; NRTL: $A_{12} = g_{12} - g_{22}$ and $A_{21} = g_{21} - g_{11}$; UNIQUAC: $A_{12} = u_{12} - u_{22}$ and $A_{21} = u_{21} - u_{11}$; A_{12}: binary interaction parameters representation for the models in Aspen Plus®. k_{ij}: parameter for fitting with Wong and Sandler mixing rule.

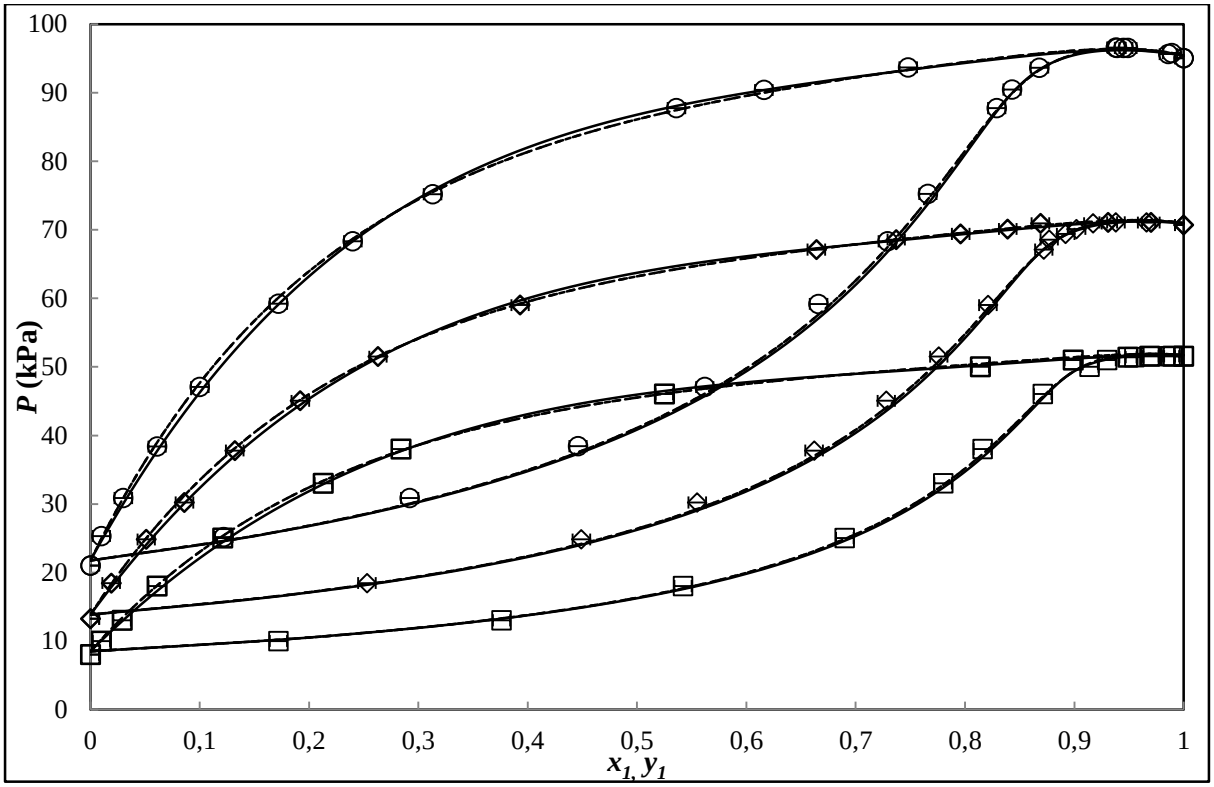

Figure 7-7: Experimental VLE and modeling results: P-*x*-*y* data for the 2, 2, 4-trimethylpentane (1) + 1-pentanol (2) system at 350.15K (□); 360.15K (◊); 370.15K (●); — HOC-NRTL; - - - HOC-Wilson; ... HOC-UNIQUAC.

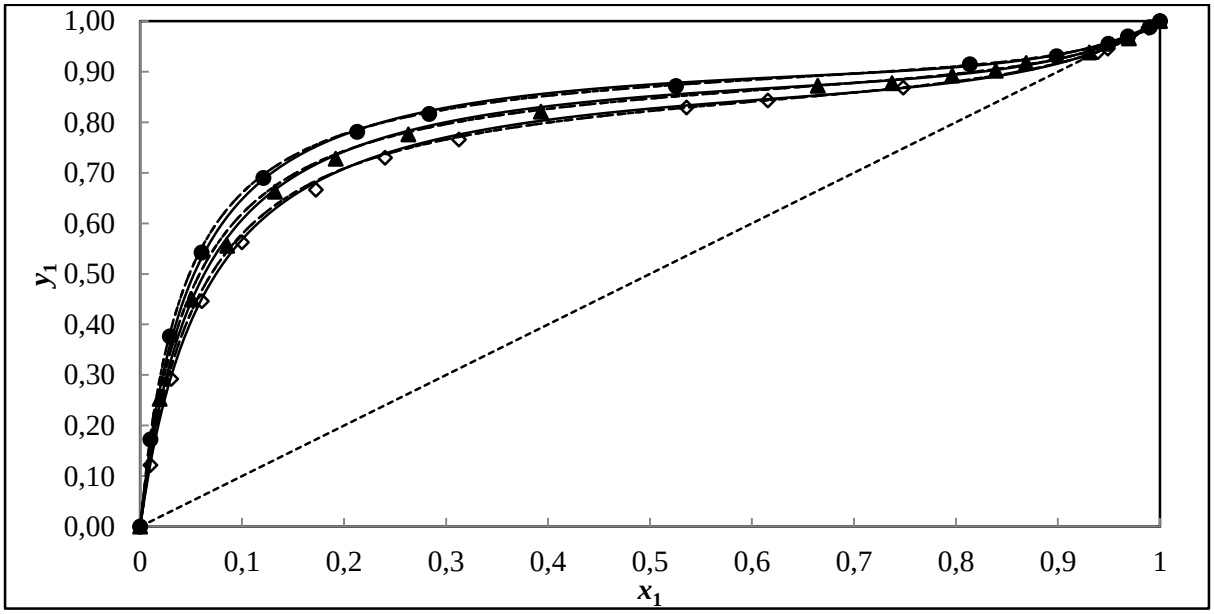

Figure 7-8: Experimental VLE and modeling results: x-y data for the 2, 2, 4-trimethylpentane (1) + 1-pentanol (2) system at 350.15K (◊); 360.15K (▲); 370.15K (●); — HOC-NRTL; - - - HOC-Wilson; ... HOC-UNIQUAC.

Table 7-7: Combined Method Modeling results using Nothnagel et al. method (NTH) for 2, 2, 4-trimethylpentane (1) + 1-pentanol (2)

Model	**T±0.10/K**	α_{12}	A_{12} **J/mol**	A_{21} **J/mol**	**(Δ*P*) AAD**	**AAD% (Δ*P*)**	**(Δy_1) AAD**	**AAD%(Δy_1)**
NRTL-NTH								
	350.15	0.30	-3190	2223	0.22	1.02	0.003	0.30
	360.15	0.30	-3123	2163	0.29	0.74	0.003	0.36
	370.15	0.30	-3136	2158	0.31	0.56	0.003	0.40
Wilson-NTH								
	350.15	-	-1878	3389	0.22	0.99	0.002	0.17
	360.15	-	-1815	3313	0.20	0.63	0.004	0.29
	370.15	-	-1769	3253	0.17	0.46	0.003	0.27
UNIQUAC-NTH								
	350.15	-	1227	-595.0	0.22	1.02	0.002	0.32
	360.15	-	1194	-574.9	0.29	0.78	0.003	0.39
	370.15	-	1187	-569.7	0.34	0.66	0.003	0.42

[a]Wilson: $A_{12} = a_{12} - a_{22}$ and $A_{21} = a_{21} - a_{11}$; NRTL: $A_{12} = g_{12} - g_{22}$ and $A_{21} = g_{21} - g_{11}$; UNIQUAC: $A_{12} = u_{12} - u_{22}$ and $A_{21} = u_{21} - u_{11}$; A_{12}: binary interaction parameters representation for the models in Aspen Plus®. k_{ij}: parameter for fitting with Wong and Sandler mixing rule.

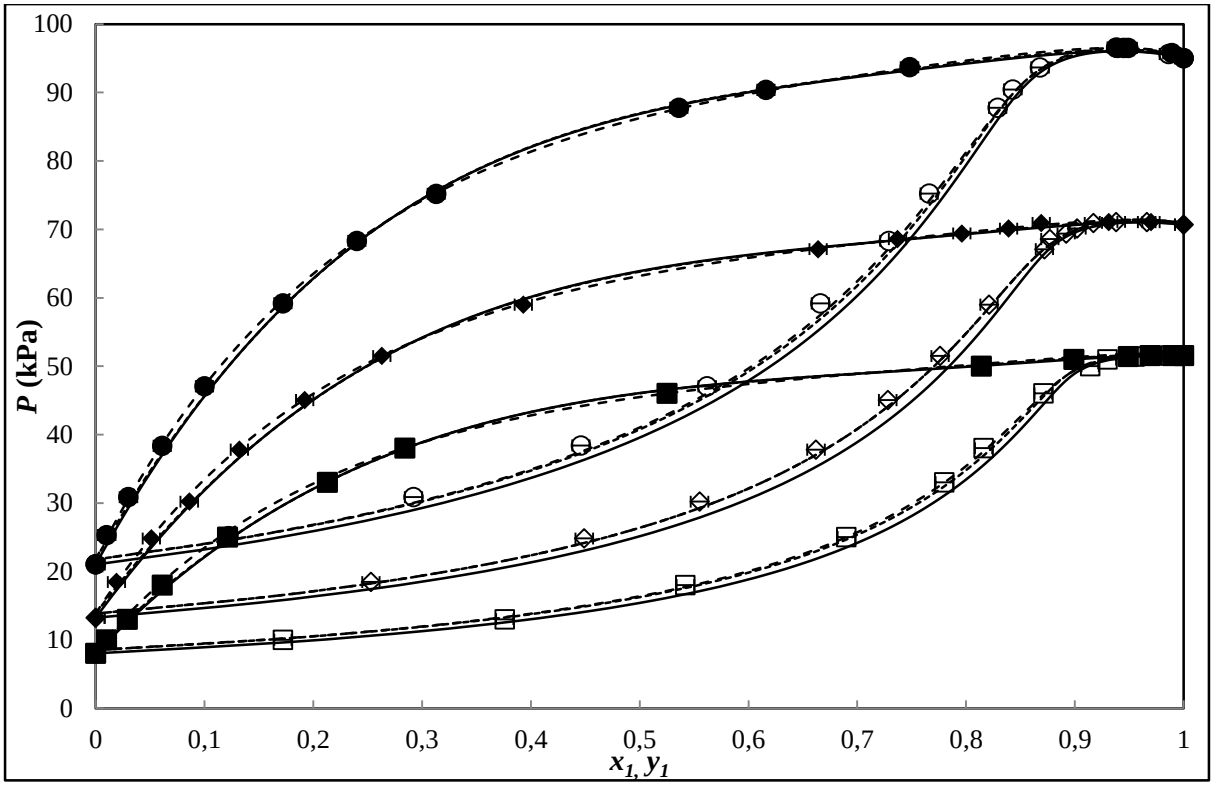

Figure 7-9: Experimental VLE and modeling results: P-*x*-*y* data for the 2, 2, 4-trimethylpentane (1) + 1-pentanol (2) system at 350.15K (□); 360.15K (◊); 370.15K (●); — NTH-NRTL; - - - NTH-Wilson; ... NTH-UNIQUAC.

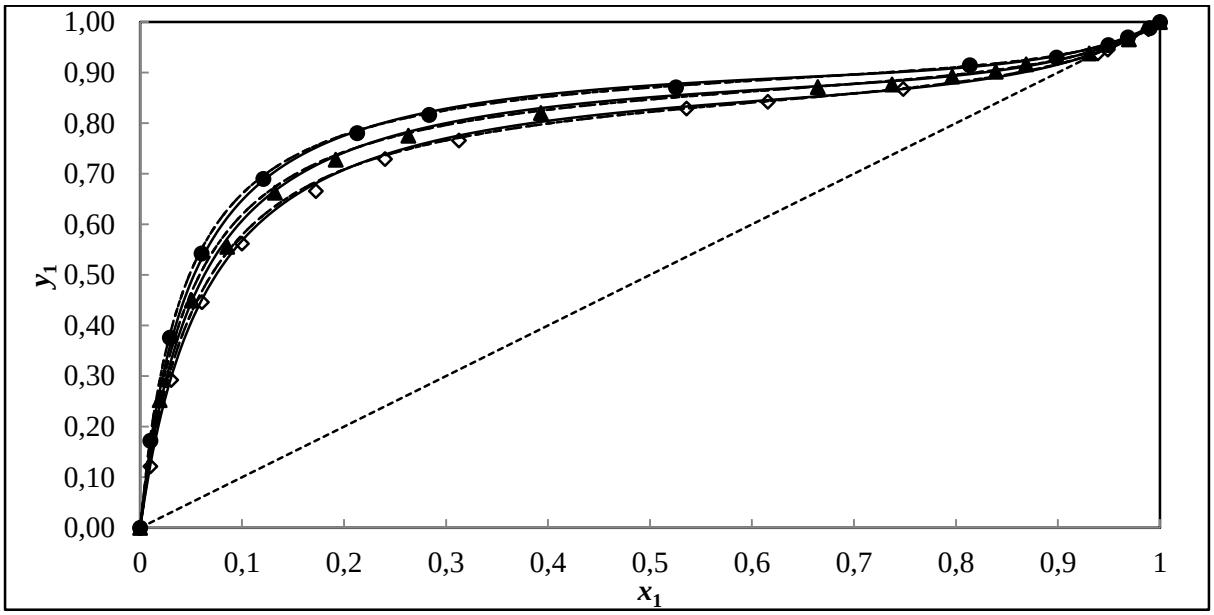

Figure 7-10: Experimental VLE and modeling results: *x*-*y* data for the 2, 2, 4-trimethylpentane (1) + 1-pentanol (2) system at 350.15K (◊); 360.15K (▲); 370.15K (●); — NTH-NRTL; - - - NTH-Wilson; ... NTH-UNIQUAC.

Table 7-8: Direct Method Modeling results for 2, 2, 4-trimethylpentane (1) + 1-pentanol (2)

Model	**T±0.10/K**	α_{12}	k_{ij}	A_{12} **J/mol**	A_{21} **J/mol**	**(Δ*P*) AAD**	**AAD% (Δ*P*)**	**(Δy_1) AAD**	**AAD%(Δy_1)**
PR-MC-WS-NRTL									
	350.15	0.30	-0.343	799.4	2500	0.28	0.75	0.004	0.43
	360.15	0.30	-0.351	827.7	2544	0.22	0.38	0.003	0.64
	370.15	0.30	-0.225	657.9	2140	0.18	0.21	0.003	0.73
PR-MC-WS-Wilson									
	350.15	-	0.144	298.5	-2406	0.41	1.00	0.002	0.28
	360.15	-	0.082	48.43	-2429	0.31	0.52	0.002	0.50
	370.15	-	0.168	349.4	-2323	0.48	0.57	0.003	0.47
PR-MC-WS-UNIQUAC									
	350.15	-	-0.329	-207.7	-246.9	0.29	0.76	0.003	0.47
	360.15	-	-0.310	-204.5	-241.6	0.24	0.42	0.003	0.67
	370.15	-	-0.363	-225.8	-264.4	0.23	0.29	0.003	0.79

[a]Wilson: $A_{12} = a_{12} - a_{22}$ and $A_{21} = a_{21} - a_{11}$; NRTL: $A_{12} = g_{12} - g_{22}$ and $A_{21} = g_{21} - g_{11}$; UNIQUAC: $A_{12} = u_{12} - u_{22}$ and $A_{21} = u_{21} - u_{11}$; A_{12}: binary interaction parameters representation for the models in Aspen Plus®. k_{ij}: parameter for fitting with Wong and Sandler mixing rule.

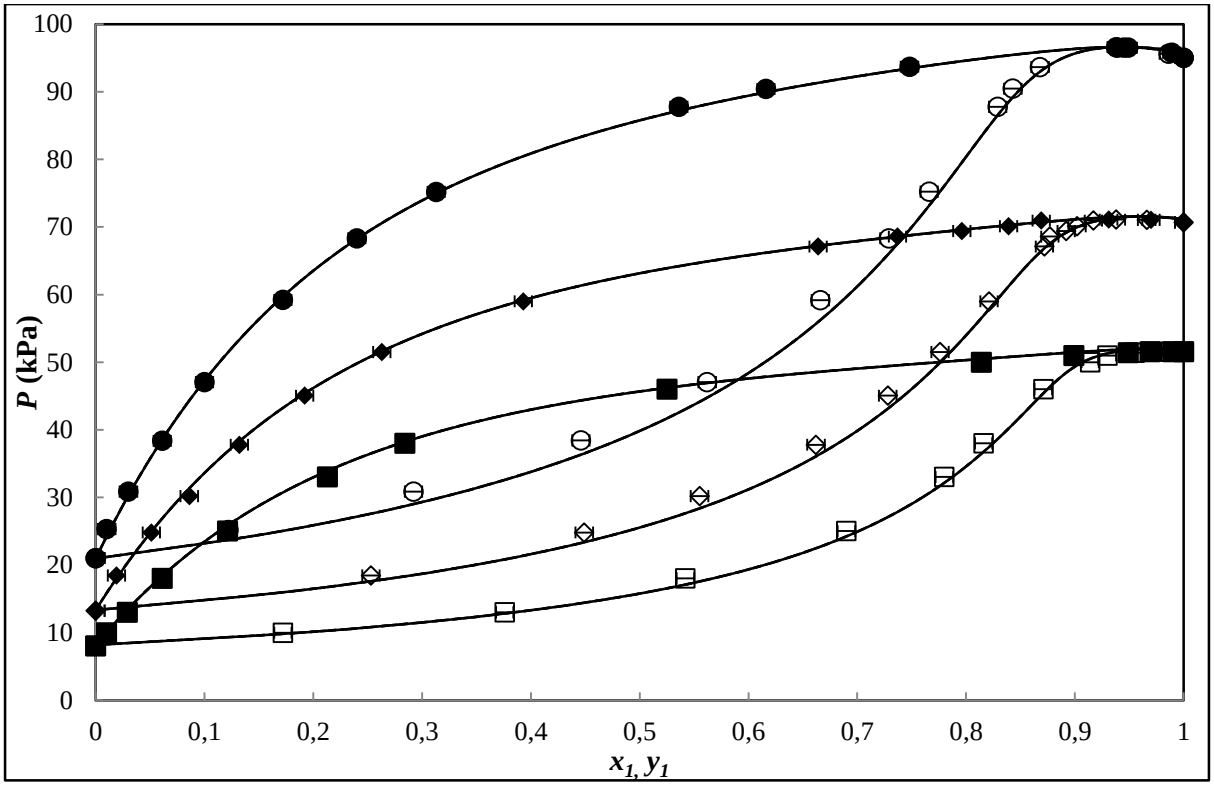

Figure 7-11: Experimental VLE and modeling results: P-*x*-*y* data for the 2, 2, 4-trimethylpentane (1) + 1-pentanol (2) system at 350.15K (□); 360.15K (◊); 370.15K (●); — PR-NRTL; - - - PR-Wilson; ... PR-UNIQUAC.

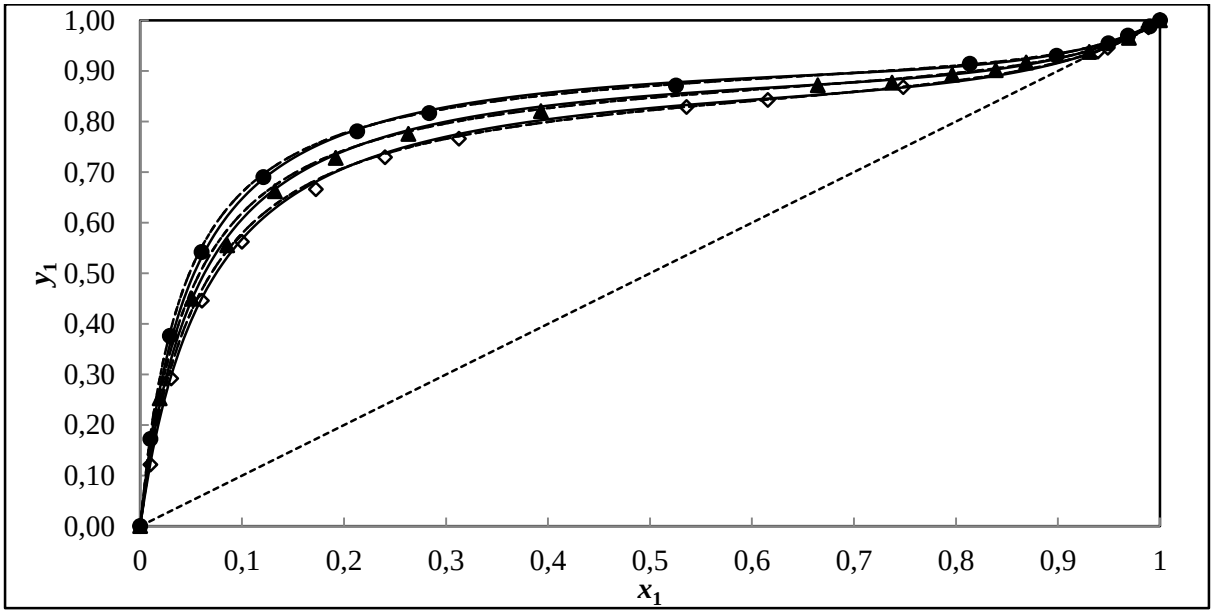

Figure 7-12: Experimental VLE and modeling results: *x*-*y* data for the 2, 2, 4-trimethylpentane (1) + 1-pentanol (2) system at 350.15K (◊); 360.15K (▲); 370.15K (●); — PR-NRTL; - - - PR-Wilson; ... PR-UNIQUAC.

7.6.2. Modeling Results for the MTBE (1) + 1-pentanol (2) System

Tables 7-9 to 7-11 provide the adjustable binary interaction parameters for the different models used in the modeling of the MTBE (1) + 1-pentanol (2) system. The average deviations of pressure (ΔP/kPa), vapour molar compositions (Δy_1) and the average absolute deviation (AAD %) of the vapour mole fraction are also given in Tables 7-9 to 7-11. The models fitted the data fairly well with the minimum and maximum vapour mole fraction AAD% of 0.07 and 0.35 respectively. The NRTL-NTH model gave the best fit for both 317.15 K and 327.15 K data sets; while PR-MC-WS-NRTL gave the highest deviations of vapour phase mole fraction for both temperature isotherms. The model fit results to the *P-x-y* data are shown graphically from Figures 7-13 to 7-15. Figures D-2 relative volatility plots for each data set with experimental activity coefficients given in Appendix C.

Table 7-9: Combined Method Modeling results for MTBE (1) + 1-pentanol (2)

Model	**T±0.10/K**	α_{12}	A_{12} **J/mol**	A_{21} **J/mol**	**(ΔP) AAD**	**AAD% (ΔP)**	**(Δy_1) AAD**	**AAD%(Δy_1)**
NRTL-HOC								
	317.15	0.30	1204	-178.6	0.39	2.07	0.001	0.07
	327.15	0.30	1045	-110.0	0.59	1.07	0.005	0.19
Wilson-HOC								
	317.15	-	-35.89	-1020	0.36	2.03	0.001	0.07
	327.15	-	-71.86	-892.1	0.55	1.04	0.005	0.19
UNIQUAC-HOC								
	317.15	-	-577.2	257.3	0.38	2.06	0.001	0.07
	327.15	-	-494.9	211.5	0.58	1.06	0.005	0.19

[a]Wilson: $A_{12} = a_{12} - a_{22}$ and $A_{21} = a_{21} - a_{11}$; NRTL: $A_{12} = g_{12} - g_{22}$ and $A_{21} = g_{21} - g_{11}$; UNIQUAC: $A_{12} = u_{12} - u_{22}$ and $A_{21} = u_{21} - u_{11}$; A_{12}: binary interaction parameters representation for the models in Aspen Plus®. k_{ij}: parameter for fitting with Wong and Sandler mixing rule.

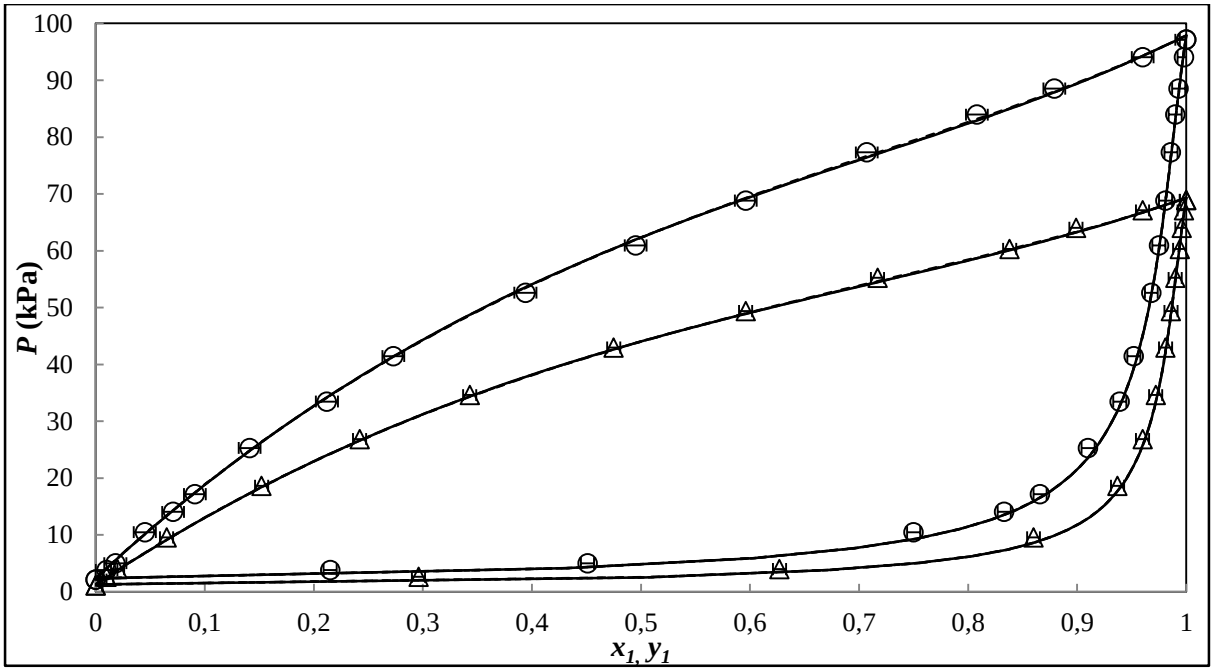

Figure 7-13: Experimental VLE and modeling results: P-*x*-*y* data for the MTBE (1) + 1-pentanol (2) system at 317.15K (△); 327.15K (○); — HOC-NRTL; - - - HOC-Wilson; ... HOC-UNIQUAC.

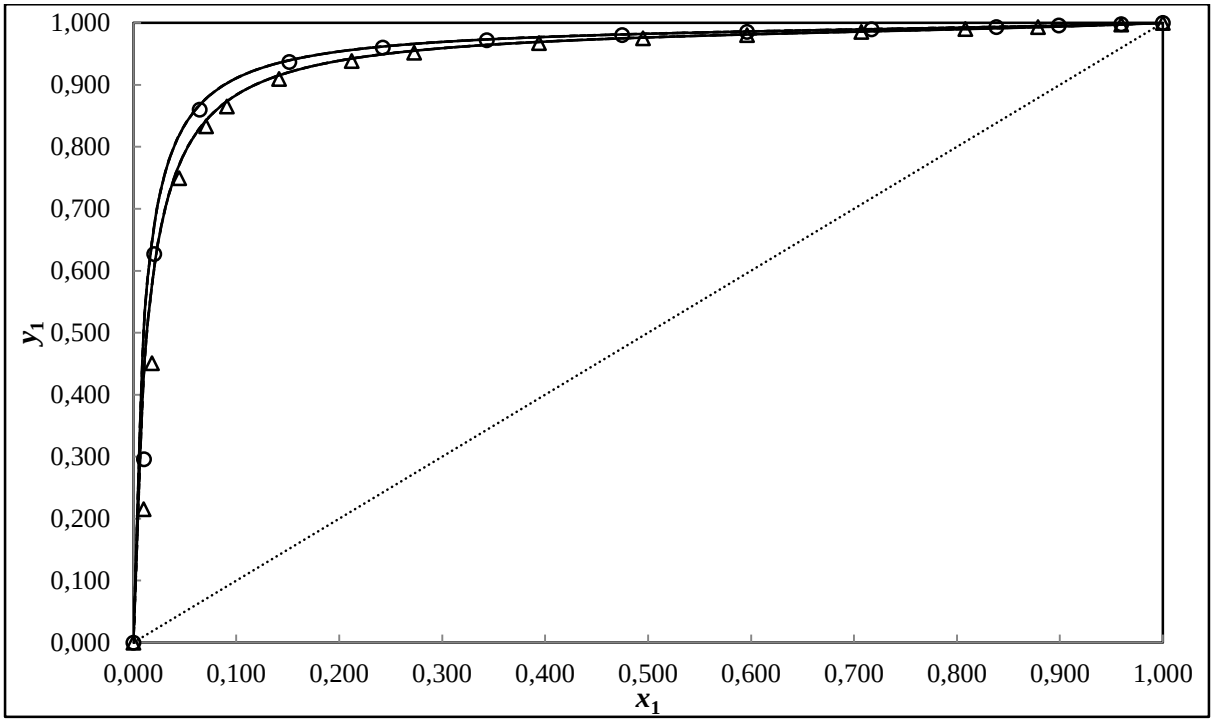

Figure 7-14: Experimental VLE and modeling results: *x*-*y* data for the MTBE (1) + 1-pentanol (2) system at 317.15K (△); 327.15K (○); — HOC-NRTL; - - - HOC-Wilson; ... HOC-UNIQUAC.

Table 7-10: Combined Method Modeling results using Nothnagel et al. method (NTH) for MTBE (1) + 1-pentanol (2)

Model	**T±0.10/K**	α_{12}	A_{12} **J/mol**	A_{21} **J/mol**	**(Δ*P*) AAD**	**AAD% (Δ*P*)**	**(Δy_1) AAD**	**AAD%(Δy_1)**
NRTL-NTH								
	317.15	0.30	1198	-177.2	0.24	1.67	0.001	0.08
	327.15	0.30	1035	-107.2	0.56	1.00	0.005	0.17
Wilson-NTH								
	317.15	-	-36.51	-1014	0.19	1.57	0.001	0.08
	327.15	-	-73.13	-882.1	0.51	0.95	0.005	0.17
UNIQUAC-NTH								
	317.15	-	-574.1	256.0	0.23	1.65	0.001	0.08
	327.15	-	-489.5	209.0	0.55	0.99	0.005	0.17

[a]Wilson: $A_{12} = a_{12} - a_{22}$ and $A_{21} = a_{21} - a_{11}$; NRTL: $A_{12} = g_{12} - g_{22}$ and $A_{21} = g_{21} - g_{11}$; UNIQUAC: $A_{12} = u_{12} - u_{22}$ and $A_{21} = u_{21} - u_{11}$; A_{12}: binary interaction parameters representation for the models in Aspen Plus®. k_{ij}: parameter for fitting with Wong and Sandler mixing rule.

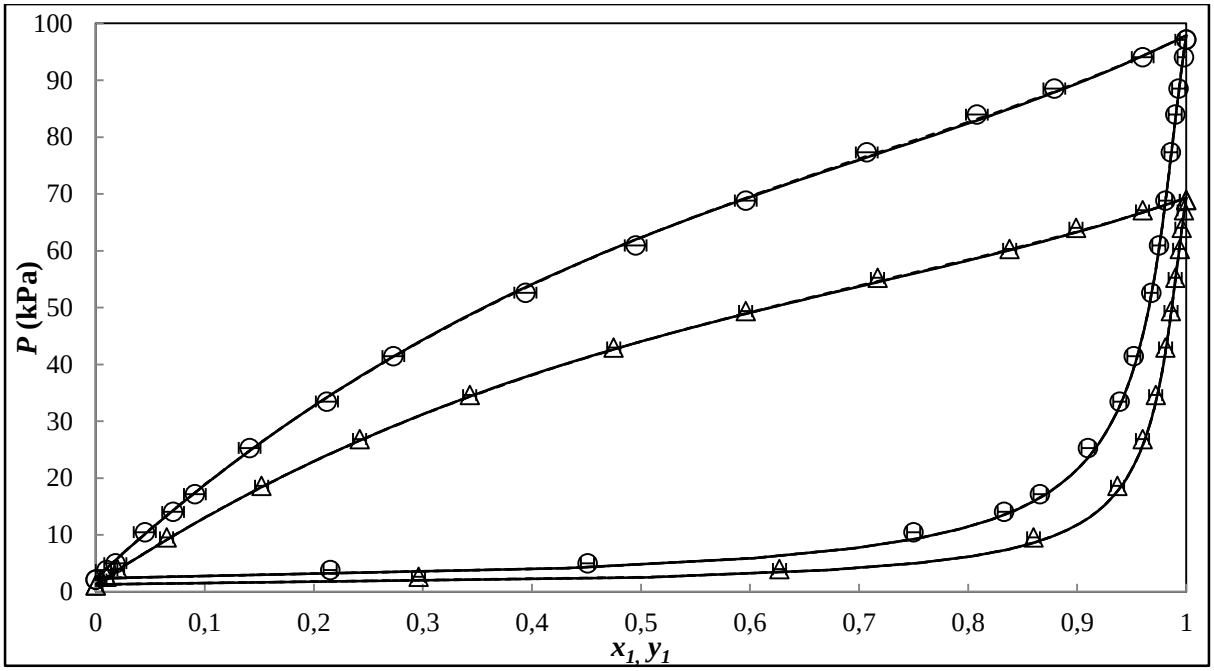

Figure 7-15: Experimental VLE and modeling results: P-*x*-*y* data for the MTBE (1) + 1-pentanol (2) system at 317.15K (△); 327.15K (○); — NTH-NRTL; - - - NTH-Wilson; ... NTH-UNIQUAC.

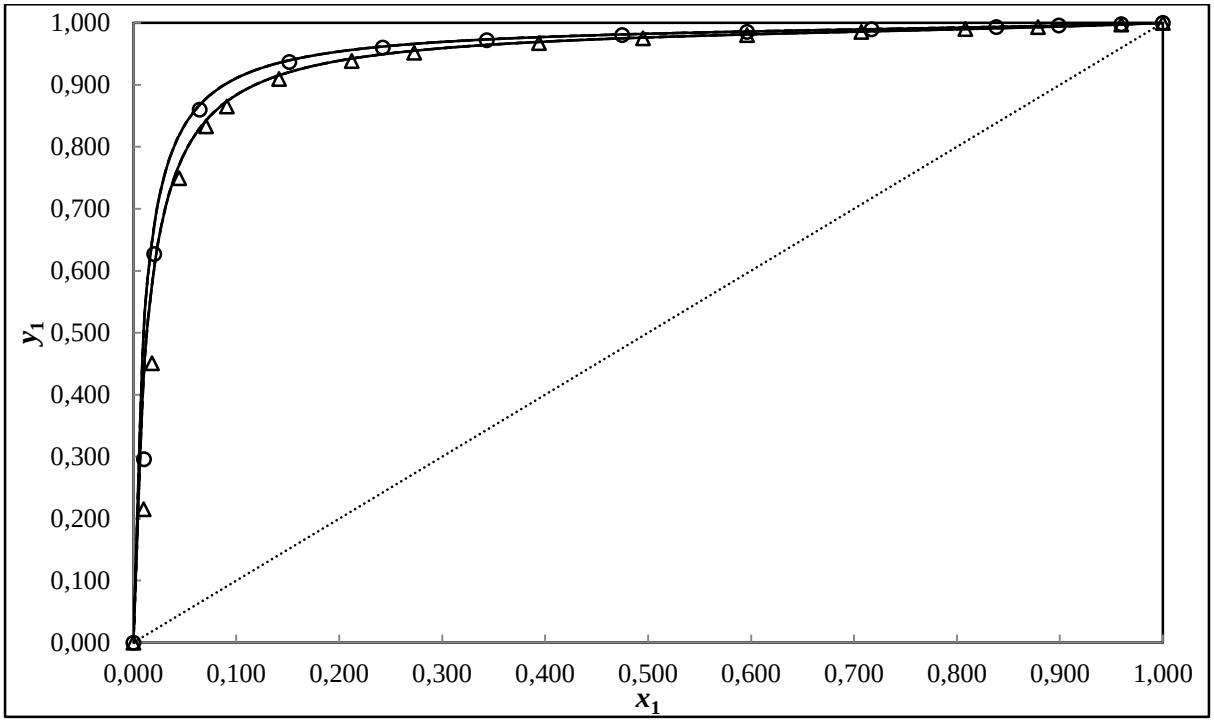

Figure 7-16: Experimental VLE and modeling results: *x*-*y* data for the MTBE (1) + 1-pentanol (2) system at 317.15K (△); 327.15K (○); — NTH-NRTL; - - - NTH-Wilson; ... NTH-UNIQUAC.

Table 7-11: Direct Method Modeling results for MTBE (1) + 1-pentanol (2)

Model	T±0.10/K	α_{12}	k_{ij}	A_{12} J/mol	A_{21} J/mol	(ΔP) AAD	AAD% (ΔP)	(Δy_1) AAD	AAD%(Δy_1)
PR-MC-WS-NRTL									
	317.15	0.30	-0.132	-4023	1873	1.17	2.56	0.002	0.20
	327.15	0.30	-0.073	-4117	1770	1.62	2.18	0.004	0.35
PR-MC-WS-Wilson									
	317.15	-	-0.339	-1877	-1955	0.94	2.16	0.002	0.20
	327.15	-	-0.349	-1846	-1955	1.39	1.91	0.004	0.35
PR-MC-WS-UNIQUAC									
	317.15	-	-0.069	2090	-865.9	1.11	2.45	0.002	0.20
	327.15	-	-0.056	2090	-857.9	1.54	2.09	0.004	0.35

[a]Wilson: $A_{12} = a_{12} - a_{22}$ and $A_{21} = a_{21} - a_{11}$; NRTL: $A_{12} = g_{12} - g_{22}$ and $A_{21} = g_{21} - g_{11}$; UNIQUAC: $A_{12} = u_{12} - u_{22}$ and $A_{21} = u_{21} - u_{11}$; A_{12}: binary interaction parameters representation for the models in Aspen Plus®. k_{ij}: parameter for fitting with Wong and Sandler mixing rule.

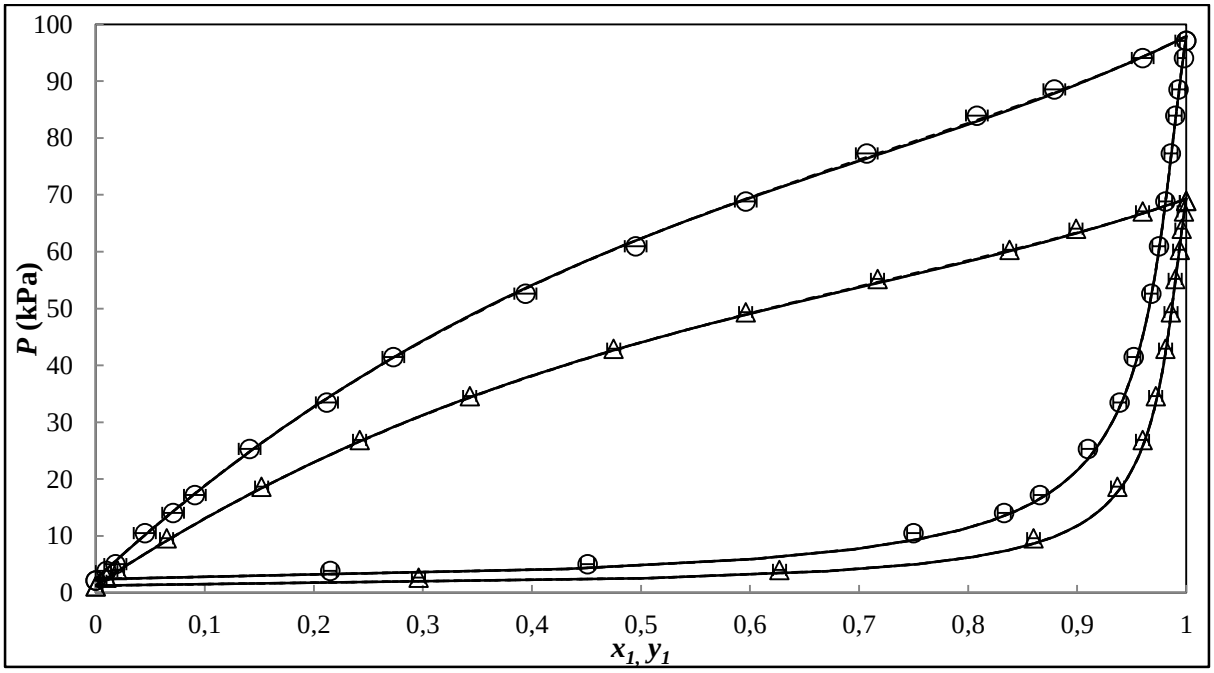

Figure 7-17: Experimental VLE and modeling results: P-*x*-*y* data for the MTBE (1) + 1-pentanol (2) system at 317.15K (△); 327.15K (○); — PR-NRTL; - - - PR-Wilson; ... PR-UNIQUAC.

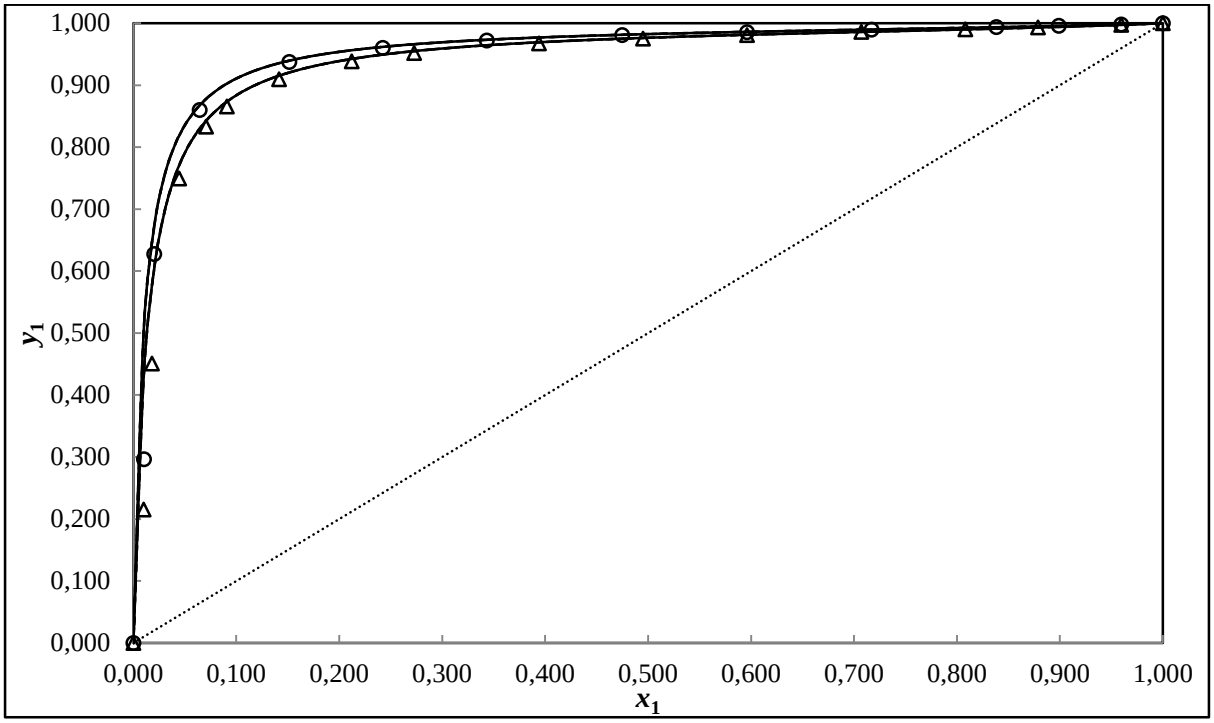

Figure 7-18: Experimental VLE and modeling results: *x-y* data for the MTBE (1) + 1-pentanol (2) system at 317.15K (△); 327.15K (○); — PR-NRTL; - - - PR-Wilson; ... PR-UNIQUAC.

7.6.3. Modeling Results for the MTBE (1) + 2, 2, 4-trimethylpentane (2) System

Tables 7-12 to 7-15 provide the adjustable binary interaction parameters for the different models used in the modeling of the MTBE (1) + 2, 2, 4-trimethylpentane (2) system. The average deviations of the pressure (ΔP/kPa), vapour molar compositions (Δy_1) and the average absolute deviation (AAD %) of the vapour mole fraction are also presented in Tables 7-12 to 7-15. Figures 7-19 to 7-24 display the graphical representation of model to *P-x-y* data for this system. The relative volatilities for this data set are graphically represented on Figure D-3 in Appendix D and the experimental activity coefficient values are listed in the appendix C. All the models gave a satisfactory representation of the data for this system. The best fit was given by the NRTL-HOC and the NRTL-NTH models, both with an AAD of the vapour mole fraction 1.04% at the isotherm temperature of T = 307.15 K. The cubic equation of state models however gave the least favourable results particularly for the T = 327.15 K isotherm from the PR-MC-WS-UNIQUAC model having a significantly higher AAD value of 3.63 %.

Table 7-12: Combined Method Modeling results for MTBE (1) + 2, 2, 4-trimethylpentane (2)

Model	**T±0.10/K**	α_{12}	A_{12} **J/mol**	A_{21} **J/mol**	**(Δ*P*) AAD**	**AAD% (Δ*P*)**	**(Δy_1) AAD**	**AAD%(Δy_1)**
NRTL-HOC								
	307.15	0.30	1012	-345.0	0.21	0.63	0.007	1.04
	317.15	0.30	118.6	382.3	0.47	1.16	0.008	2.18
	327.15	0.30	141.6	344.7	0.53	0.92	0.009	2.97
Wilson-HOC								
	307.15	-	-4062	3672	0.28	0.72	0.007	1.18
	317.15	-	-4430	4186	0.47	1.17	0.008	2.20
	327.15	-	-4280	4041	0.61	1.03	0.010	2.80
UNIQUAC-HOC								
	307.15	-	-1971	56.33	0.20	0.60	0.007	1.32
	317.15	-	242.0	-421.7	0.52	1.25	0.008	2.09
	327.15	-	231.1	-403.3	0.57	0.96	0.010	2.89

[a]Wilson: $A_{12} = a_{12} - a_{22}$ and $A_{21} = a_{21} - a_{11}$; NRTL: $A_{12} = g_{12} - g_{22}$ and $A_{21} = g_{21} - g_{11}$; UNIQUAC: $A_{12} = u_{12} - u_{22}$ and $A_{21} = u_{21} - u_{11}$; A_{12}: binary interaction parameters representation for the models in Aspen Plus®. k_{ij}: parameter for fitting with Wong and Sandler mixing rule.

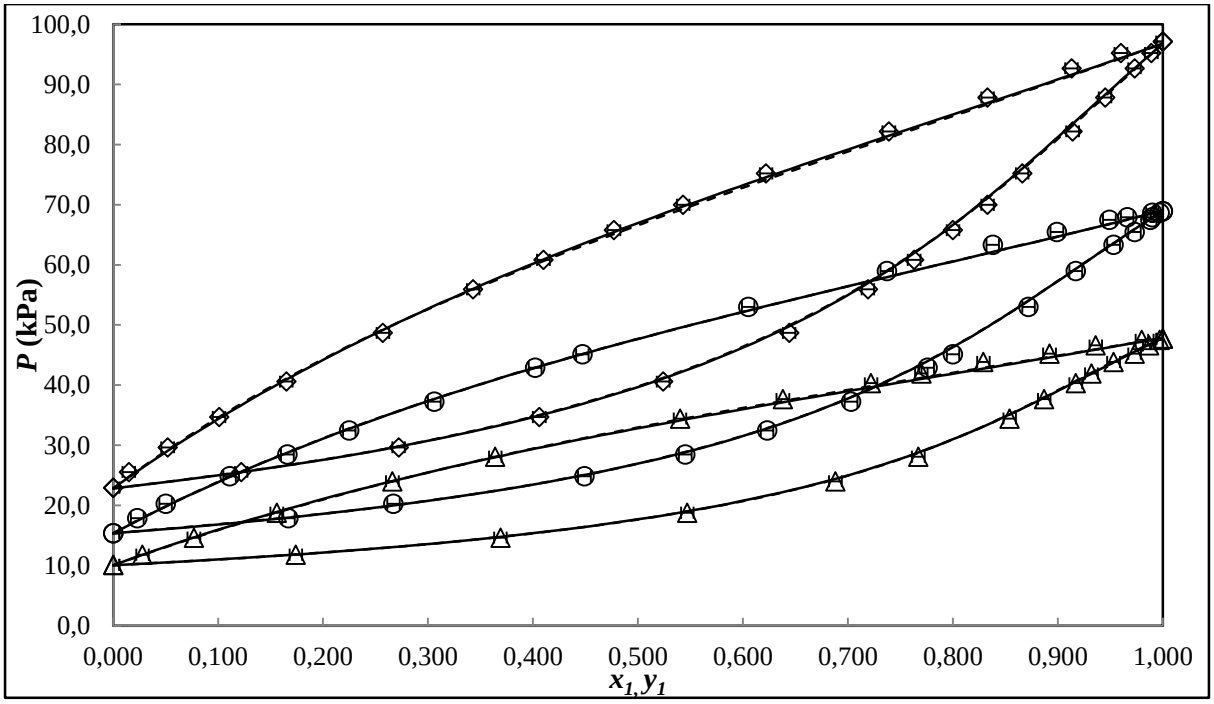

Figure 7-19: Experimental VLE and modeling results: P-*x*-*y* data for the MTBE (1) + 2, 2, 4-trimethylpentane (2) system at 307.15K (△); 317.15K (◊); 327.15K (○); — HOC-NRTL; - - - HOC-Wilson; ... HOC-UNIQUAC.

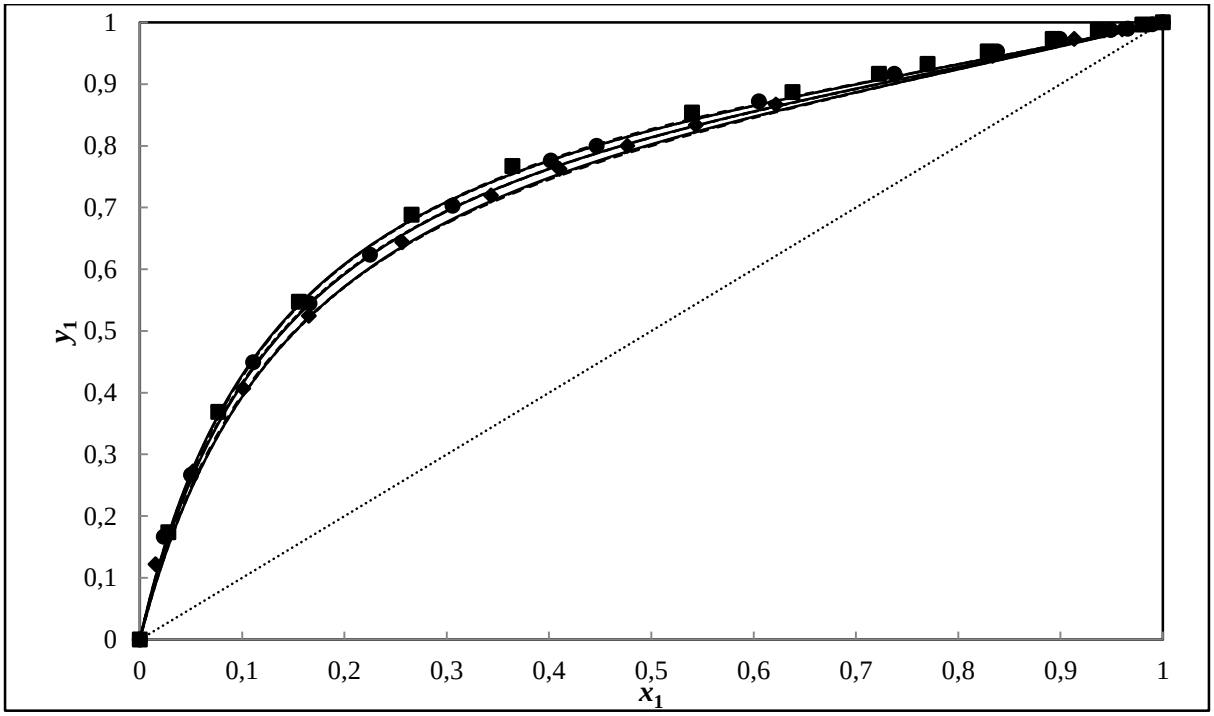

Figure 7-20: Experimental VLE and modeling results: *x*-*y* data for the MTBE (1) + 2, 2, 4-trimethylpentane (2) system at 307.15K (♦); 317.15K (●); 327.15K (■); — HOC-NRTL; - - - HOC-Wilson; ... HOC-UNIQUAC.

Table 7-13: Combined Method Modeling results using Nothnagel et al. method (NTH) for MTBE (1) + 2, 2, 4-trimethylpentane (2)

Model	**T±0.10/K**	α_{12}	A_{12} **J/mol**	A_{21} **J/mol**	**(Δ*P*) AAD**	**AAD% (Δ*P*)**	**(Δy_1) AAD**	**AAD%(Δy_1)**
NRTL-NTH								
	307.15	0.30	-1967	2018	0.35	0.92	0.007	1.04
	317.15	0.30	-2658	2644	0.41	1.08	0.008	2.22
	327.15	0.30	-2551	2535	0.48	0.88	0.009	3.09
Wilson-NTH								
	307.15	-	-4428	1547	0.28	0.72	0.007	1.17
	317.15	-	-4377	2129	0.41	1.07	0.008	2.15
	327.15	-	-4241	2050	0.59	0.98	0.010	2.89
UNIQUAC-NTH								
	307.15	-	-3427	-5397	0.37	0.96	0.007	1.12
	317.15	-	-3387	-5439	0.43	1.14	0.008	2.04
	327.15	-	-3392	-5433	0.55	0.96	0.010	3.11

[a]Wilson: $A_{12} = a_{12} - a_{22}$ and $A_{21} = a_{21} - a_{11}$; NRTL: $A_{12} = g_{12} - g_{22}$ and $A_{21} = g_{21} - g_{11}$; UNIQUAC: $A_{12} = u_{12} - u_{22}$ and $A_{21} = u_{21} - u_{11}$; A_{12}: binary interaction parameters representation for the models in Aspen Plus®. k_{ij}: parameter for fitting with Wong and Sandler mixing rule.

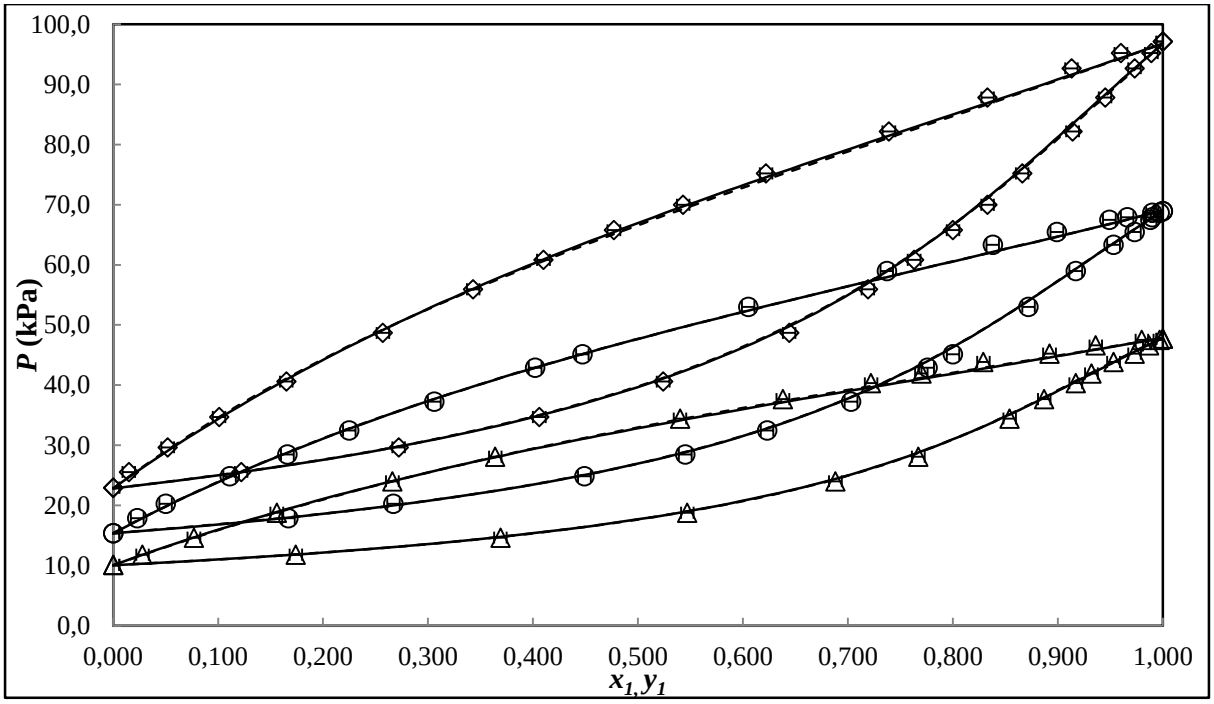

Figure 7-21: Experimental VLE and modeling results: P-*x*-*y* data for the MTBE (1) + 2, 2, 4-trimethylpentane (2) system at 307.15K (△); 317.15K (◊); 327.15K (○); — NTH-NRTL; - - - NTH-Wilson; ... NTH-UNIQUAC.

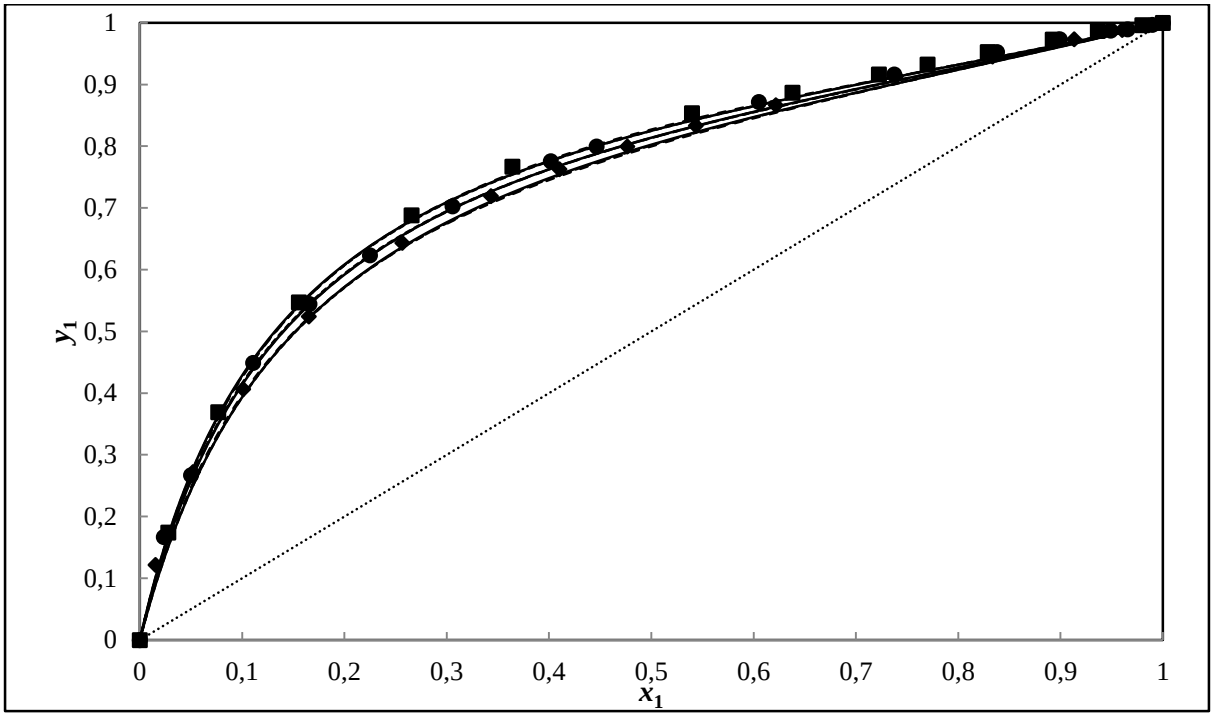

Figure 7-22: Experimental VLE and modeling results: *x*-*y* data for the MTBE (1) + 2, 2, 4-trimethylpentane (2) system at 307.15K (♦); 317.15K (●); 327.15K (■); — NTH-NRTL; - - - NTH-Wilson; ... NTH-UNIQUAC.

Table 7-14: Direct Method Modeling results for MTBE (1) + 2, 2, 4-trimethylpentane (2)

Model	**T±0.10/K**	α_{12}	k_{ij}	A_{12} **J/mol**	A_{21} **J/mol**	**(Δ*P*) AAD**	**AAD% (Δ*P*)**	**(Δy_1) AAD**	**AAD%(Δy_1)**
PR-MC-WS-NRTL									
	307.15	0.30	-0.121	-7992	4439	0.60	1.66	0.009	1.57
	317.15	0.30	0.431	-1167	7591	0.17	0.35	0.010	2.76
	327.15	0.30	0.449	-1145	7768	0.19	0.27	0.012	3.48
PR-MC-WS-Wilson									
	307.15	-	-0.404	-2339	-4803	0.59	1.45	0.008	1.34
	317.15	-	0.328	-3834	6758	1.13	2.29	0.010	2.81
	327.15	-	0.336	-4243	6678	1.11	1.57	0.011	3.51
PR-MC-WS-UNIQUAC									
	307.15	-	0.028	3748	-2846	0.62	1.55	0.009	1.53
	317.15	-	0.491	5303	-4670	1.18	2.44	0.010	2.73
	327.15	-	0.021	4037	-3038	1.19	1.67	0.012	3.63

[a]Wilson: $A_{12} = a_{12} - a_{22}$ and $A_{21} = a_{21} - a_{11}$; NRTL: $A_{12} = g_{12} - g_{22}$ and $A_{21} = g_{21} - g_{11}$; UNIQUAC: $A_{12} = u_{12} - u_{22}$ and $A_{21} = u_{21} - u_{11}$; A_{12}: binary interaction parameters representation for the models in Aspen Plus®. k_{ij}: parameter for fitting with Wong and Sandler mixing rule.

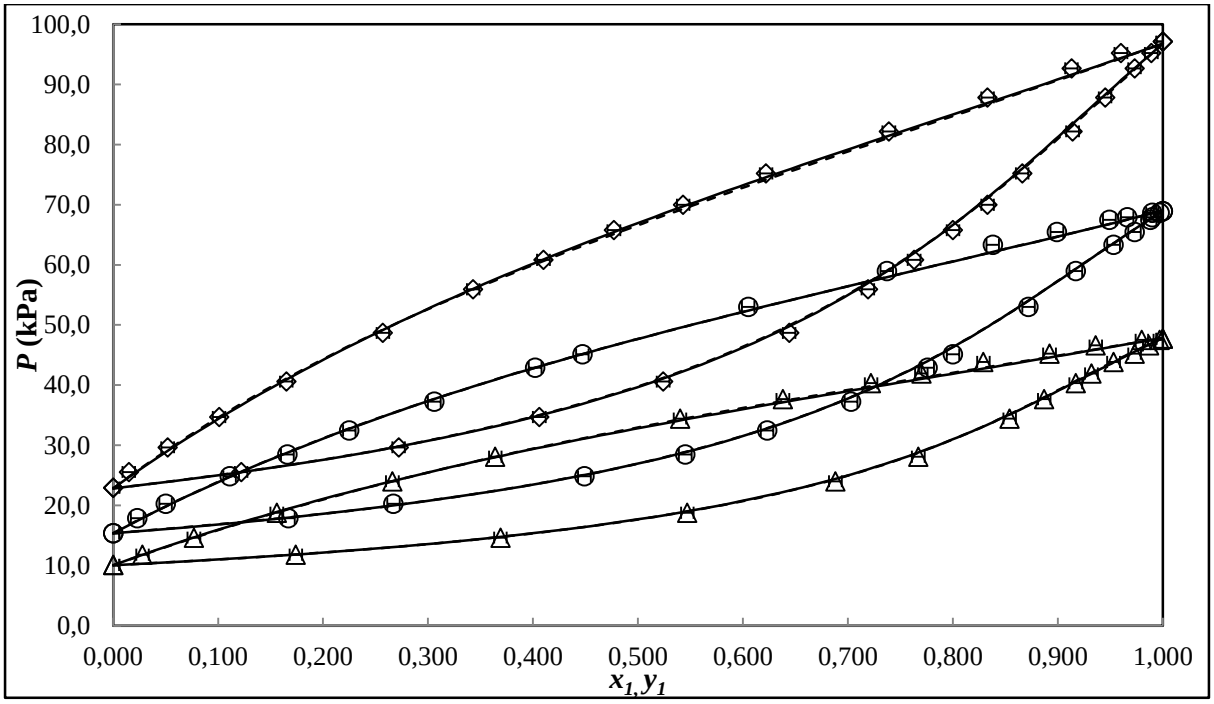

Figure 7-23: Experimental VLE and modeling results: P-*x*-*y* data for the MTBE (1) + 2, 2, 4-trimethylpentane (2) system at 307.15K (△); 317.15K (◊); 327.15K (○); — PR-NRTL; - - - PR-Wilson; ... PR-UNIQUAC.

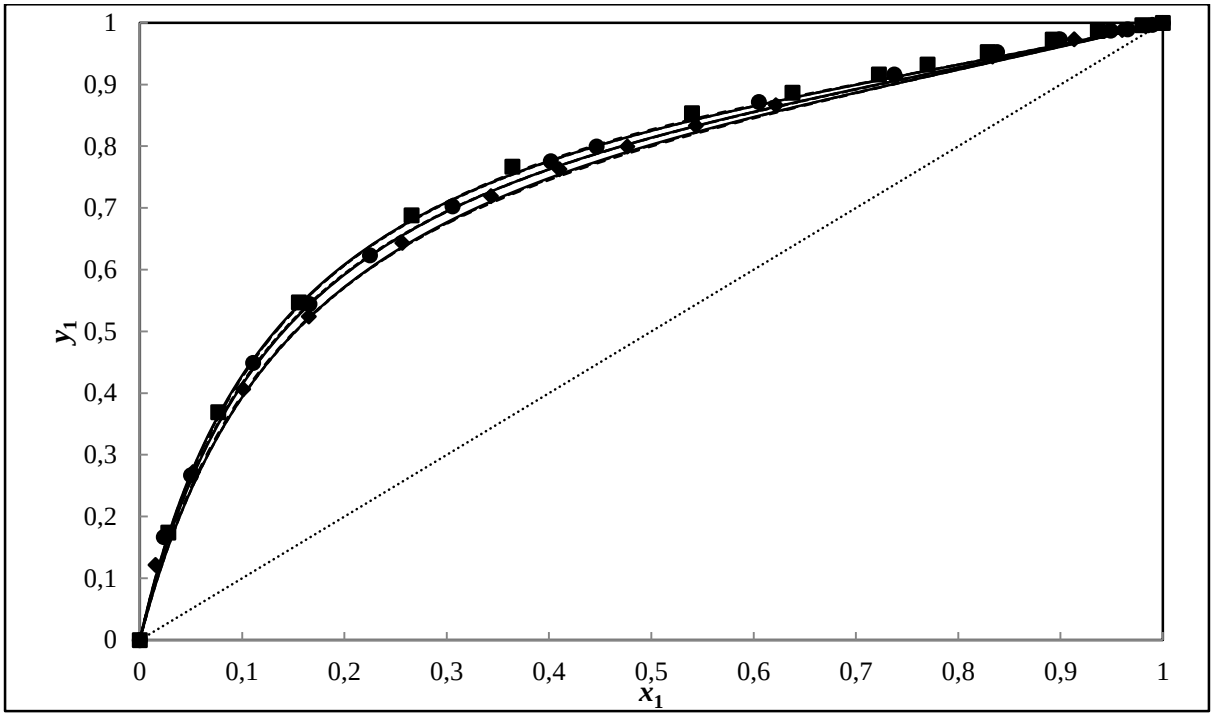

Figure 7-24: Experimental VLE and modeling results: *x*-*y* data for the MTBE (1) + 2, 2, 4-trimethylpentane (2) system at 307.15K (♦); 317.15K (●); 327.15K (■); — PR-NRTL; - - - PR-Wilson; ... PR-UNIQUAC.

7.6.4. Modeling Results for the DIPE (1) + 2, 2, 4-trimethylpentane (2) System

Tables 7-15 to 7-17 give the adjustable binary interaction parameters for the different models used for the modeling DIPE (1) + 2, 2, 4-trimethylpentane (2). The average deviations of the pressure (ΔP/kPa), vapour molar compositions (Δy_1) and the vapour mole fraction average absolute deviation (AAD %) are also given here. Figures 7-25 and 7-30 show the graphical representation of model to *P x-y* data for this system. The relative volatilities for this data set are graphically shown on figure D-4 and the experimental activity coefficient values are given in the appendix C. The NRTH-NTH model gave poor fits for this system for the 340.15K isotherm, with vapour mole fraction AAD at almost 3 %. A more pronounced deviation was observed in iso-octane dilute region.

Table 7-15: Combined Method Modeling results for DIPE (1) + 2, 2, 4-trimethylpentane (2)

Model	**T±0.10/K**	α_{12}	A_{12} **J/mol**	A_{21} **J/mol**	**(Δ*P*) AAD**	**AAD% (Δ*P*)**	**(Δy_1) AAD**	**AAD%(Δy_1)**
NRTL-HOC								
	320.15	0.30	-1010	-649.2	0.20	0.64	0.003	0.83
	330.15	0.30	-1096	-608.4	0.56	1.22	0.006	1.55
	340.15	0.30	187.7	-1860	0.51	0.80	0.007	1.14
Wilson-HOC								
	320.15	-	472.8	1111	0.24	0.64	0.004	0.93
	330.15	-	423.9	1209	0.56	1.26	0.006	1.62
	340.15	-	1520	1365	0.51	0.80	0.007	1.13
UNIQUAC-HOC								
	320.15	-	-1859	1324	0.96	2.39	0.007	1.24
	330.15	-	-2014	1412	1.15	2.11	0.008	2.05
	340.15	-	-1983	1381	1.40	1.79	0.009	2.00

[a]Wilson: $A_{12} = a_{12} - a_{22}$ and $A_{21} = a_{21} - a_{11}$; NRTL: $A_{12} = g_{12} - g_{22}$ and $A_{21} = g_{21} - g_{11}$; UNIQUAC: $A_{12} = u_{12} - u_{22}$ and $A_{21} = u_{21} - u_{11}$; A_{12}: binary interaction parameters representation for the models in Aspen Plus®. k_{ij}: parameter for fitting with Wong and Sandler mixing rule.

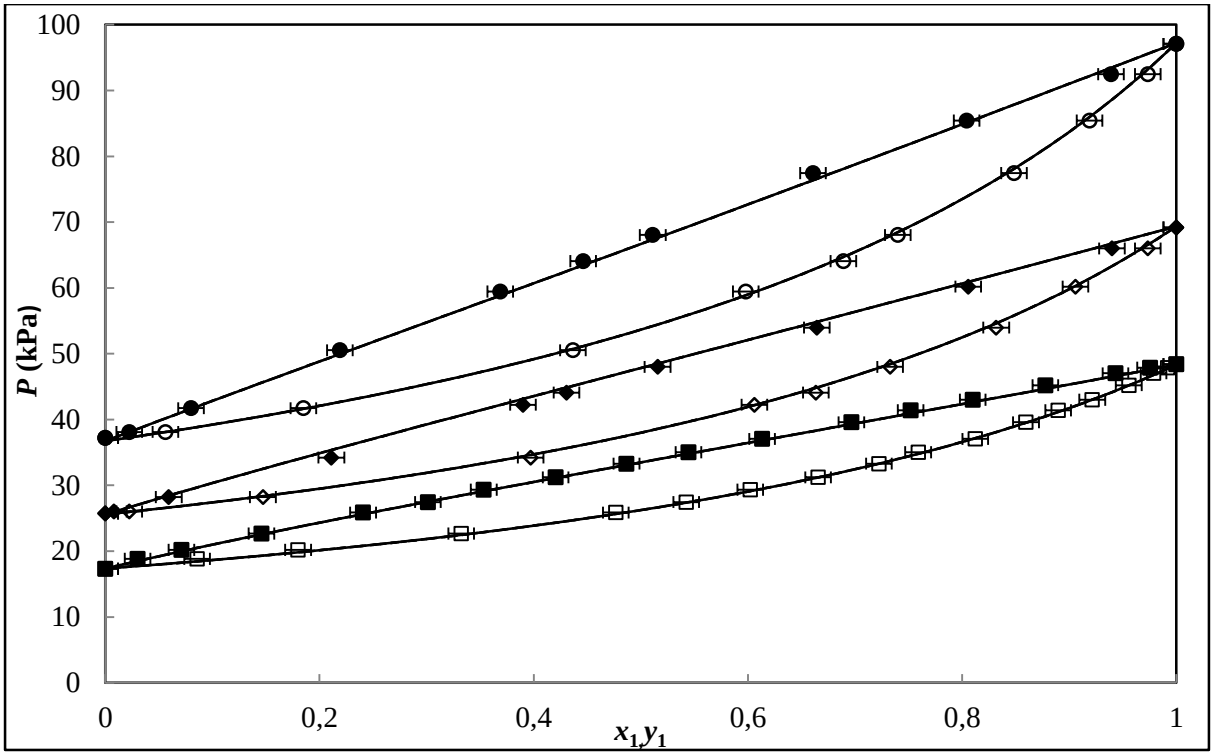

Figure 7-25: Experimental VLE and modeling results: P-*x*-*y* data for the DIPE (1) + 2, 2, 4-trimethylpentane (2) system at 320.15K (□); 330.15K (◊); 340.15K (○); — HOC-NRTL; - - - HOC-Wilson; ... HOC-UNIQUAC.

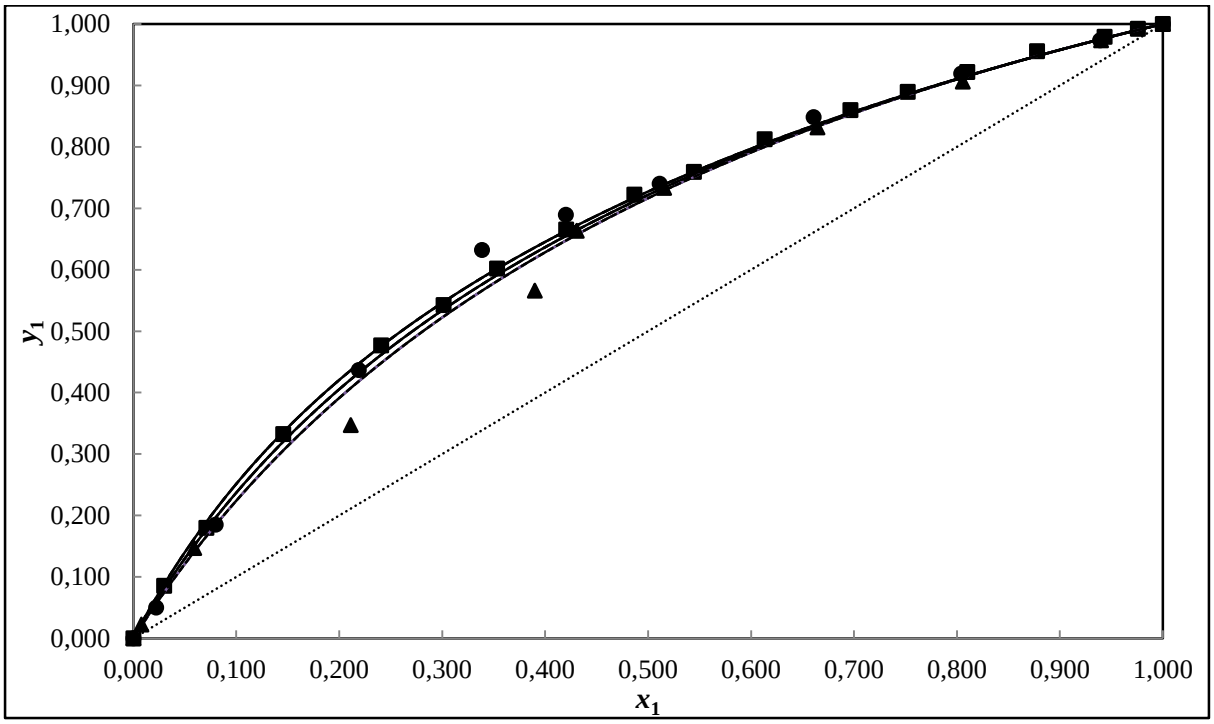

Figure 7-26: Experimental VLE and modeling results: *x*-*y* data for the DIPE (1) + 2, 2, 4-trimethylpentane (2) system at 320.15K (▲); 330.15K (●); 340.15K (■); — HOC-NRTL; - - - HOC-Wilson; ... HOC-UNIQUAC.

Table 7-16: Combined Method Modeling results using Nothnagel et al. method (NTH) for DIPE (1) + 2, 2, 4-trimethylpentane (2)

Model	**T±0.10/K**	α_{12}	A_{12} **J/mol**	A_{21} **J/mol**	**(Δ*P*) AAD**	**AAD% (Δ*P*)**	**(Δy_1) AAD**	**AAD%(Δy_1)**
NRTL-NTH								
	320.15	0.30	-554.7	2213	0.52	1.67	0.003	0.65
	330.15	0.30	336.0	1004	0.58	1.35	0.006	2.14
	340.15	0.30	936.1	615.2	0.61	1.09	0.010	2.96
Wilson-NTH								
	320.15	-	-336.5	189.0	0.47	1.27	0.003	0.59
	330.15	-	-22.09	26.64	0.59	1.33	0.006	1.55
	340.15	-	299.9	-418.2	0.38	0.64	0.008	1.79
UNIQUAC-NTH								
	320.15	-	341.8	-456.0	0.47	1.43	0.003	0.59
	330.15	-	29.32	-32.89	0.59	1.33	0.006	1.50
	340.15	-	-423.0	335.2	0.63	0.38	0.008	1.73

[a]Wilson: $A_{12} = a_{12} - a_{22}$ and $A_{21} = a_{21} - a_{11}$; NRTL: $A_{12} = g_{12} - g_{22}$ and $A_{21} = g_{21} - g_{11}$; UNIQUAC: $A_{12} = u_{12} - u_{22}$ and $A_{21} = u_{21} - u_{11}$; A_{12}: binary interaction parameters representation for the models in Aspen Plus®. k_{ij}: parameter for fitting with Wong and Sandler mixing rule.

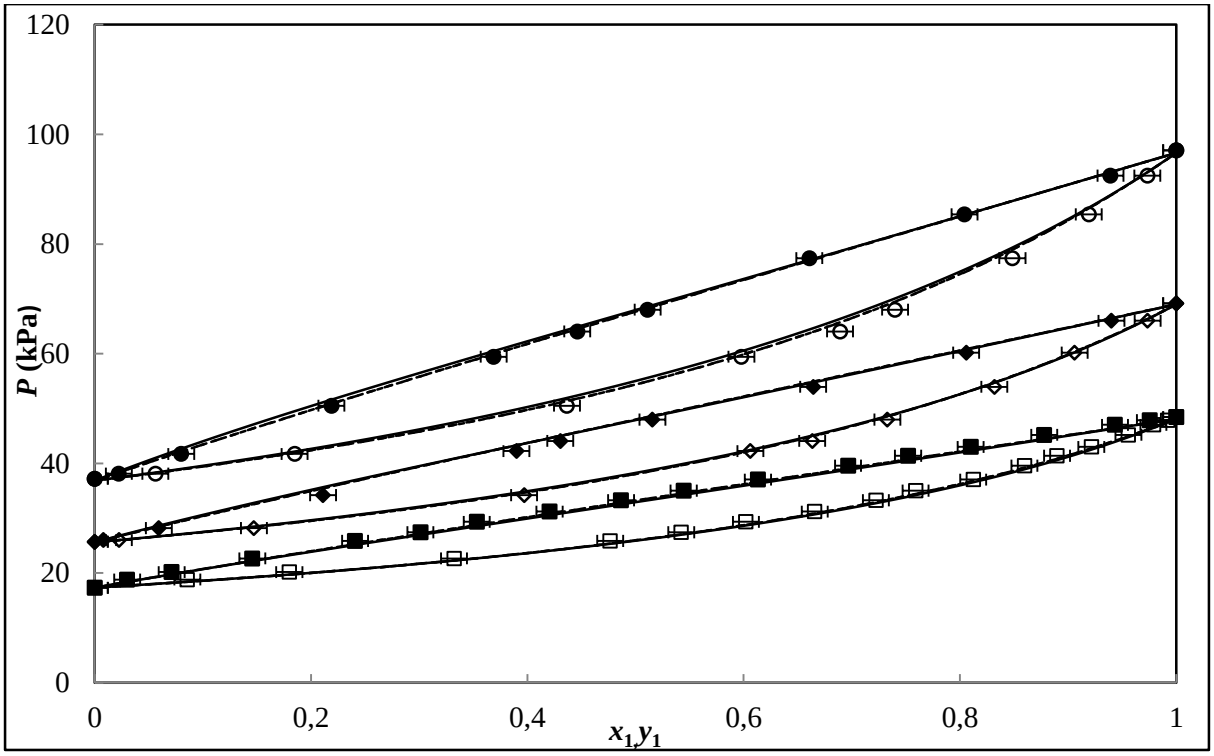

Figure 7-27: Experimental VLE and modeling results: P-*x*-*y* data for the DIPE (1) + 2, 2, 4-trimethylpentane (2) system at 320.15K (□); 330.15K (◊); 340.15K (○); — NTH-NRTL; - - - NTH-Wilson; ... NTH-UNIQUAC.

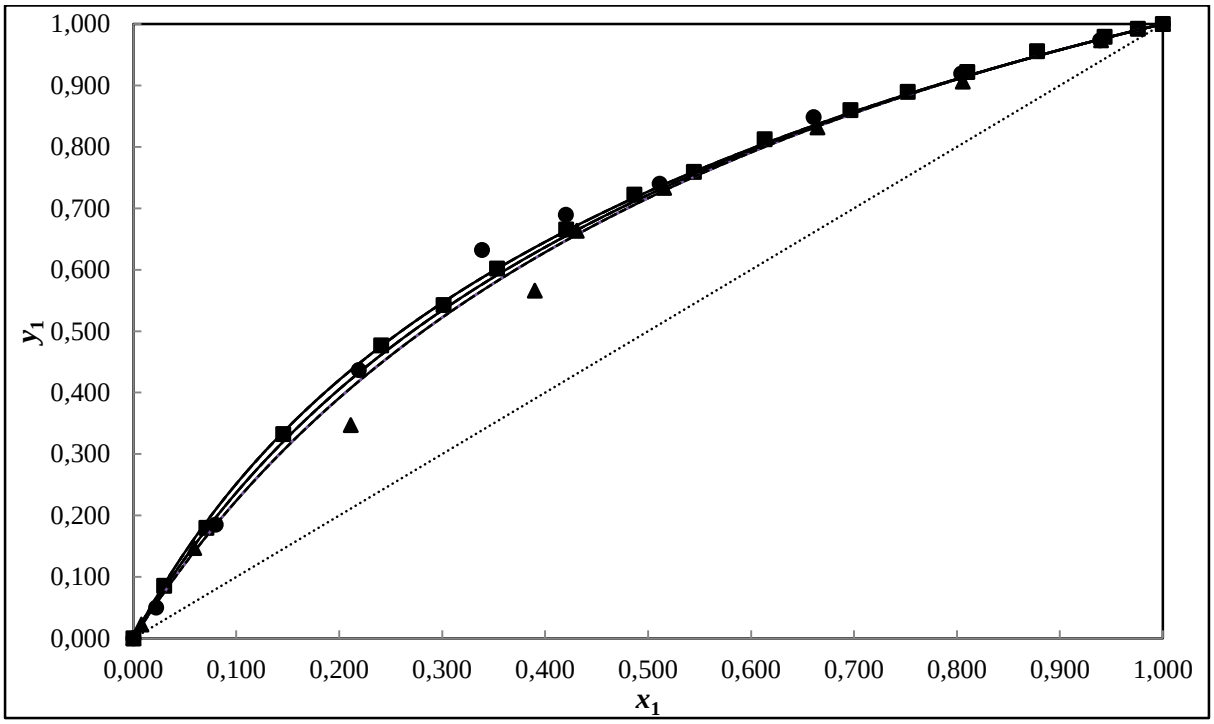

Figure 7-28: Experimental VLE and modeling results: *x*-*y* data for the DIPE (1) + 2, 2, 4-trimethylpentane (2) system at 320.15K (▲); 330.15K (●); 340.15K (■); — NTH-NRTL; - - - NTH-Wilson; ... NTH-UNIQUAC.

Table 7-17: Direct Method Modeling results for DIPE (1) + 2, 2, 4-trimethylpentane (2)

Model	**T±0.10/K**	α_{12}	k_{ij}	A_{12} **J/mol**	A_{21} **J/mol**	**(Δ*P*) AAD**	**AAD% (Δ*P*)**	**(Δy_1) AAD**	**AAD%(Δy_1)**
PR-MC-WS-NRTL									
	320.15	0.30	0.053	-385426	105444	0.21	0.67	0.003	0.55
	330.15	0.30	0.028	811726	-244396	0.53	1.20	0.005	1.02
	340.15	0.30	0.053	-256160	845184	0.53	0.79	0.008	1.56
PR-MC-WS-Wilson									
	320.15	-	0.035	-823919	165374	0.28	0.67	0.003	0.58
	330.15	-	0.026	-667653	98965	0.53	1.23	0.005	1.02
	340.15	-	0.035	-379838	-358647	0.52	0.79	0.008	1.56
PR-MC-WS-UNIQUAC									
	320.15	-	0.204	-155.72	-109511	0.28	0.82	0.003	0.58
	330.15	-	-0.212	34655	-201014	0.53	1.23	0.005	1.04
	340.15	-	0.242	-242656	19969	0.52	0.79	0.008	1.56

[a]Wilson: $A_{12} = a_{12} - a_{22}$ and $A_{21} = a_{21} - a_{11}$; NRTL: $A_{12} = g_{12} - g_{22}$ and $A_{21} = g_{21} - g_{11}$; UNIQUAC: $A_{12} = u_{12} - u_{22}$ and $A_{21} = u_{21} - u_{11}$; A_{12}: binary interaction parameters representation for the models in Aspen Plus®. k_{ij}: parameter for fitting with Wong and Sandler mixing rule.

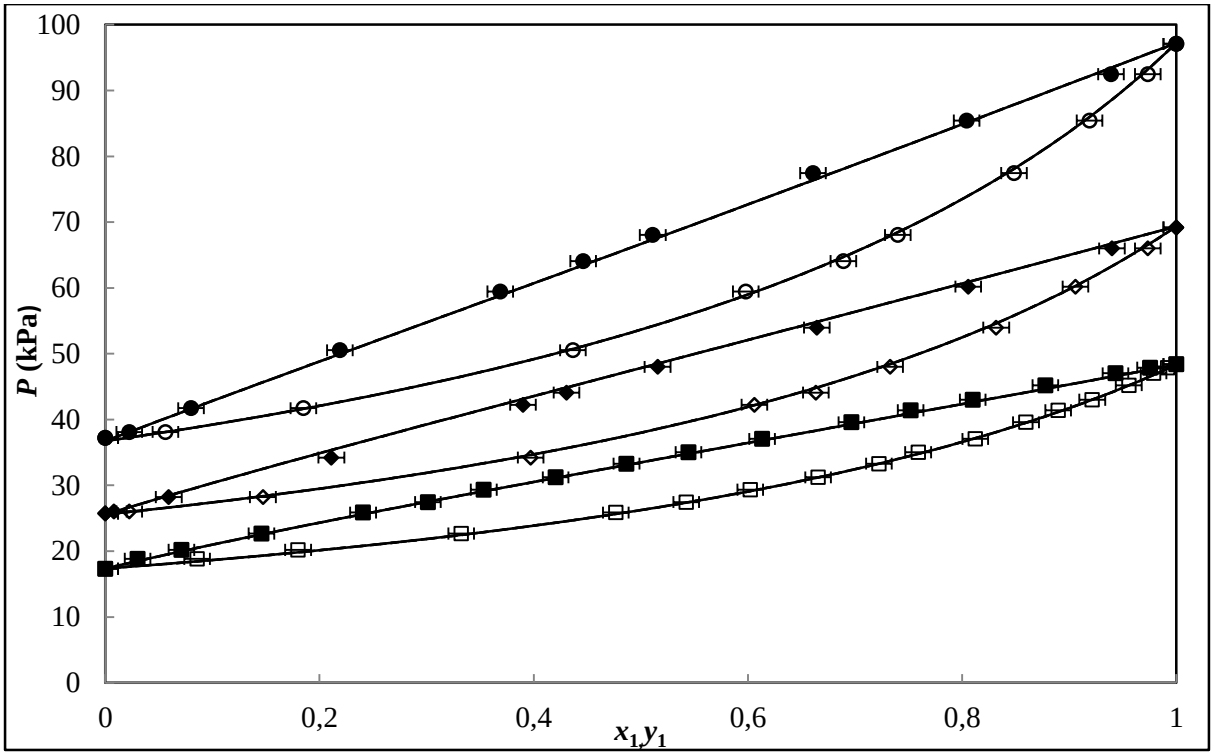

Figure 7-29: Experimental VLE and modeling results: P-*x*-*y* data for the DIPE (1) + 2, 2, 4-trimethylpentane (2) system at 320.15K (□); 330.15K (◊); 340.15K (○); — PR-NRTL; - - - PR-Wilson; ... PR-UNIQUAC.

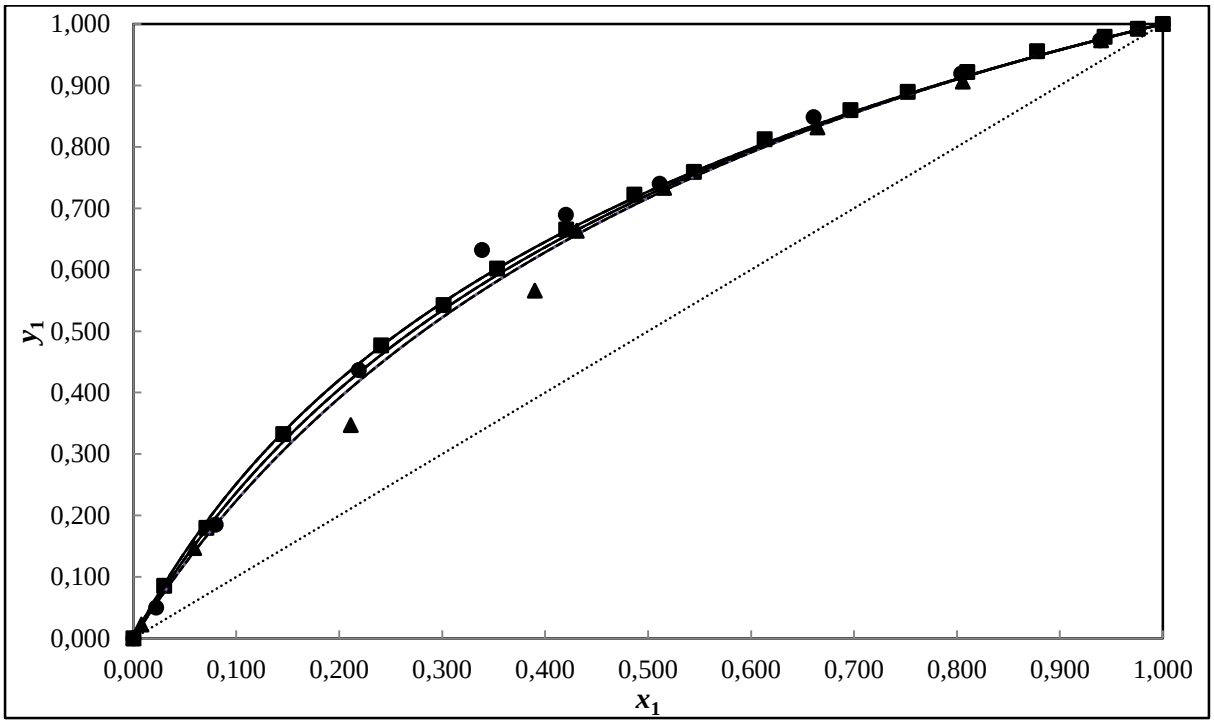

Figure 7-30: Experimental VLE and modeling results: *x*-*y* data for the DIPE (1) + 2, 2, 4-trimethylpentane (2) system at 320.15K (▲); 330.15K (●); 340.15K (■); — PR-NRTL; - - - PR-Wilson; ... PR-UNIQUAC.

7.6.5. Modeling Results for the DIPE (1) + 1-propanol (2) System

Tables 7-18 to 7-20 show the adjustable binary interaction parameters for the various models used in the reduction of this system with the average deviations of pressure (ΔP/kPa), the vapour molar compositions (Δy_1) and the vapour mole fraction average absolute deviation (AAD %). Figures 7-31 to 7-36 display the graphical representation of model to *P-x-y* data for this system. The relative volatilities for this data set are graphically represented on Figure D-5 in Appendix D and the experimental activity coefficient values are given in Table C5 Appendix C. The models used to regress this system supplied reasonable representation of the data for this system with no significant difference observed between the models. The best fit was given by the PR-MC-WS-Wilson model, having an AAD 0.35% for the vapour mole fraction for the isotherm temperature of T = 340.15 K. The lower temperature isotherms of 320.15 K and 330.15 K for the PR-MC-WS-Wilson model however, gave the highest AAD deviations of 1.59% and 1.33% respectively. This shows a decrease in the deviation with an increase in temperature with the PR-MC-WS-Wilson model exhibiting the effect of temperature dependence modeling.

Table 7-18: Combined Method Modeling results for DIPE (1) + 1-propanol (2)

Model	**T±0.10/K**	α_{12}	A_{12} **J/mol**	A_{21} **J/mol**	**(Δ*P*) AAD**	**AAD% (Δ*P*)**	**(Δy_1) AAD**	**AAD%(Δy_1)**
NRTL-HOC								
	320.15	0.30	1630	-78.60	0.43	1.14	0.004	0.58
	330.15	0.30	1420	-308.3	0.27	0.41	0.004	0.68
	340.15	0.30	922.2	296.9	1.15	1.44	0.005	0.75
Wilson-HOC								
	320.15	-	-182.8	-148.0	0.45	1.17	0.005	0.70
	330.15	-	-223.2	-1299	0.17	0.35	0.004	0.65
	340.15	-	-434.1	-874.2	1.16	1.43	0.005	0.75
UNIQUAC-HOC								
	320.15	-	-1214	446.4	0.46	1.19	0.004	0.54
	330.15	-	-1105	410.1	0.32	0.60	0.005	0.69
	340.15	-	-865.5	301.7	1.13	1.44	0.005	0.76

[a]Wilson: $A_{12} = a_{12} - a_{22}$ and $A_{21} = a_{21} - a_{11}$; NRTL: $A_{12} = g_{12} - g_{22}$ and $A_{21} = g_{21} - g_{11}$; UNIQUAC: $A_{12} = u_{12} - u_{22}$ and $A_{21} = u_{21} - u_{11}$; A_{12}: binary interaction parameters representation for the models in Aspen Plus®. k_{ij}: parameter for fitting with Wong and Sandler mixing rule.

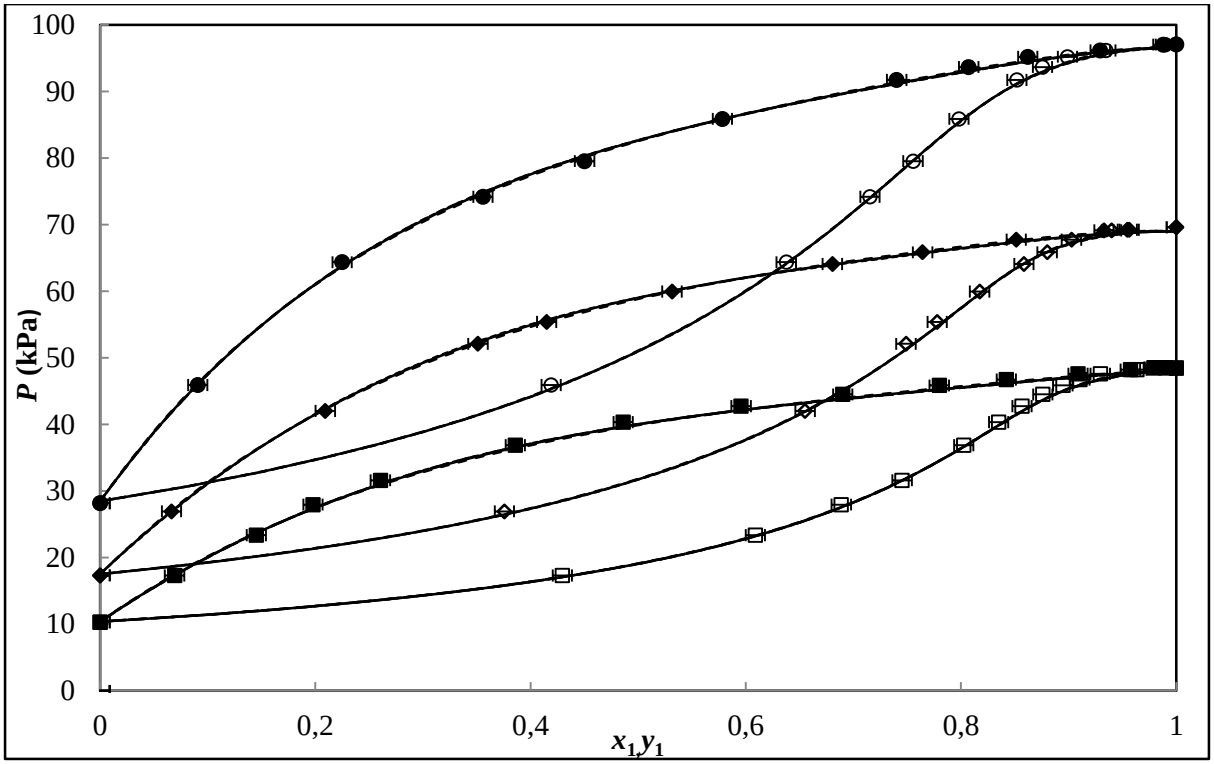

Figure 7-31: Experimental VLE and modeling results: P-*x*-*y* data for the DIPE (1) + 1-propanol (2) system at 320.15K (□); 330.15K (◊); 340.15K (○); — HOC-NRTL; - - - HOC-Wilson; ... HOC-UNIQUAC.

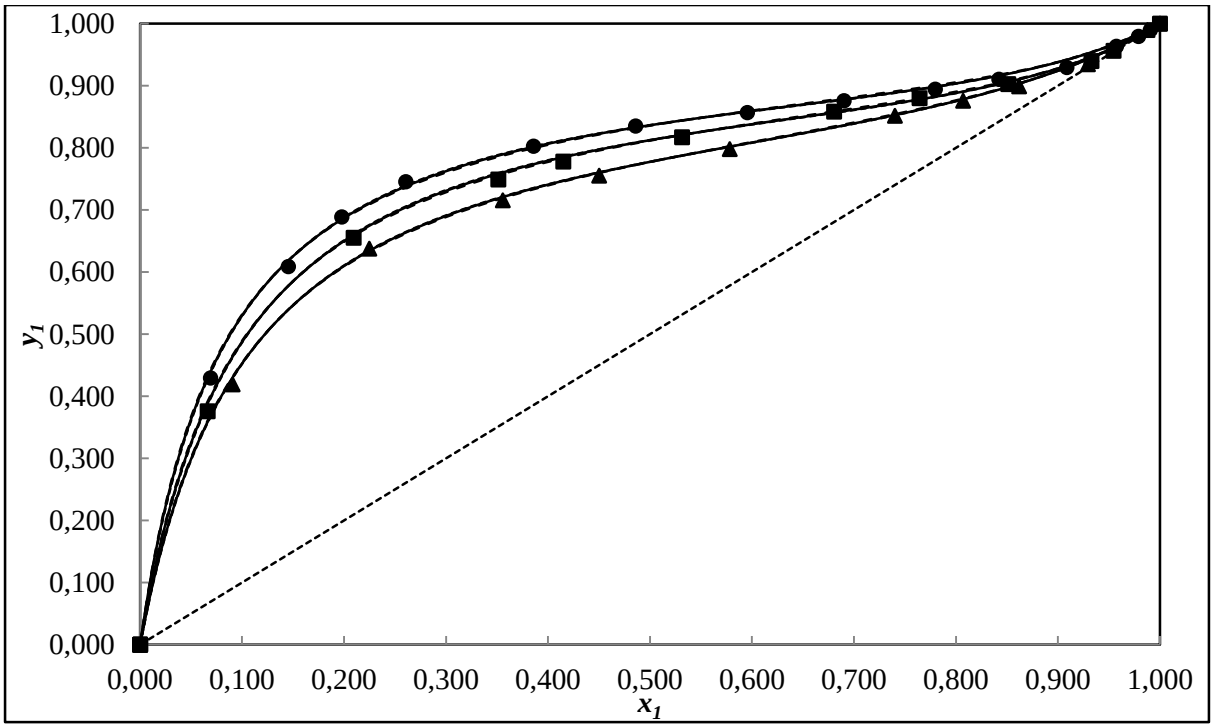

Figure 7-32: Experimental VLE and modeling results: *x*-*y* data for the DIPE (1) + 1-propanol (2) system at 320.15K (▲); 330.15K (■); 340.15K (●); — HOC-NRTL; - - - HOC-Wilson; ... HOC-UNIQUAC.

Table 7-19: Combined Method Modeling results using Nothnagel et al. method (NTH) for DIPE (1) + 1-propanol (2)

Model	**T±0.10/K**	α_{12}	A_{12} **J/mol**	A_{21} **J/mol**	**(Δ*P*) AAD**	**AAD% (Δ*P*)**	**(Δy_1) AAD**	**AAD%(Δy_1)**
NRTL-NTH								
	350.15	0.30	2109	6.144	0.30	0.81	0.004	0.65
	360.15	0.30	1900	77.58	0.19	0.29	0.004	0.68
	370.15	0.30	1350	368.9	0.96	1.26	0.004	0.61
Wilson-NTH								
	350.15	-	395.7	-284.1	0.32	0.88	0.005	0.69
	360.15	-	339.0	-141.4	0.17	0.33	0.004	0.68
	370.15	-	113.9	247.9	0.92	1.22	0.006	0.74
UNIQUAC-NTH								
	350.15	-	-499.0	285.3	0.36	0.94	0.004	0.53
	360.15	-	-412.5	254.3	0.32	0.60	0.005	0.71
	370.15	-	-195.7	151.8	0.92	1.22	0.005	0.70

[a]Wilson: $A_{12} = a_{12} - a_{22}$ and $A_{21} = a_{21} - a_{11}$; NRTL: $A_{12} = g_{12} - g_{22}$ and $A_{21} = g_{21} - g_{11}$; UNIQUAC: $A_{12} = u_{12} - u_{22}$ and $A_{21} = u_{21} - u_{11}$; A_{12}: binary interaction parameters representation for the models in Aspen Plus®. k_{ij}: parameter for fitting with Wong and Sandler mixing rule.

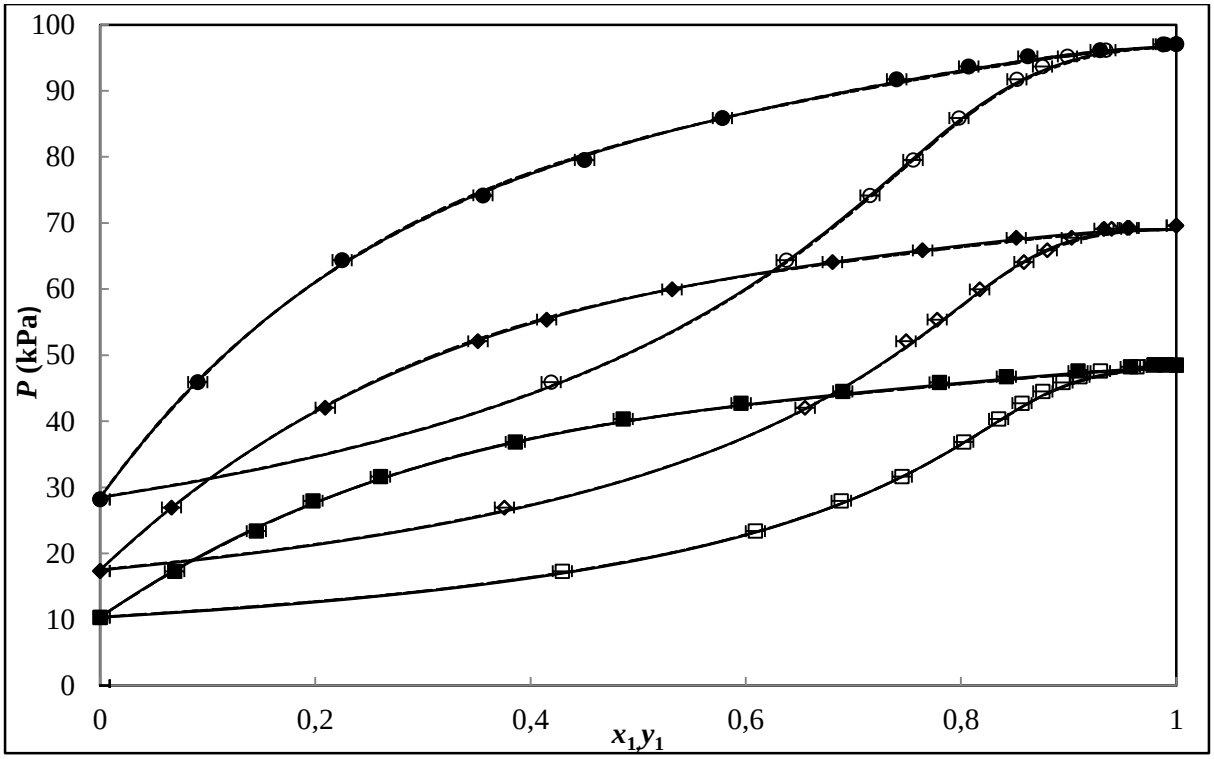

Figure 7-33: Experimental VLE and modeling results: P-*x*-*y* data for the DIPE (1) + 1-propanol (2) system at 320.15K (□); 330.15K (◊); 340.15K (○); — NTH-NRTL; - - - NTH-Wilson; ... NTH-UNIQUAC.

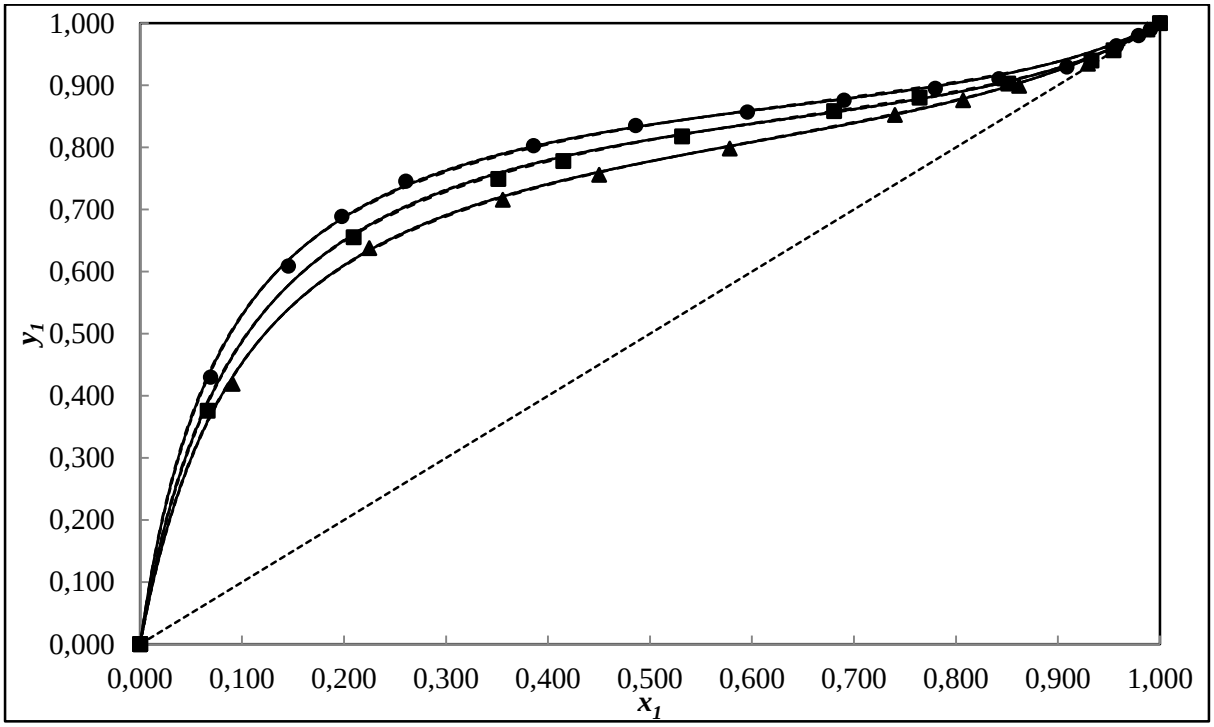

Figure 7-34: Experimental VLE and modeling results: *x*-*y* data for the DIPE (1) + 1-propanol (2) system at 320.15K (▲); 330.15K (■); 340.15K (●); — NTH-NRTL; - - - NTH-Wilson; ... NTH-UNIQUAC.

Table 7-20: Direct Method Modeling results for DIPE (1) + 1-propanol (2)

Model	**T±0.10/K**	α_{12}	k_{ij}	A_{12} **J/mol**	A_{21} **J/mol**	**(Δ*P*) AAD**	**AAD% (Δ*P*)**	**(Δy_1) AAD**	**AAD%(Δy_1)**
PR-MC-WS-NRTL									
	320.15	0.30	-0.559	-9404	5473	0.37	0.97	0.005	0.69
	330.15	0.30	-0.649	-8980	5703	0.19	0.34	0.003	0.55
	340.15	0.30	-0.383	-9529	5123	0.67	0.93	0.004	0.55
PR-MC-WS-Wilson									
	320.15	-	-0.374	-1657	-5043	0.89	2.29	0.012	1.59
	330.15	-	-0.372	-1676	-5043	1.30	2.20	0.008	1.33
	340.15	-	-0.488	-2525	-5043	2.20	2.55	0.011	0.35
PR-MC-WS-UNIQUAC									
	320.15	-	-0.023	4561	-1523	0.22	0.63	0.004	0.66
	330.15	-	0.002	4490	-1482	0.28	0.49	0.005	0.89
	340.15	-	-0.252	4548	-1702	0.42	0.58	0.004	0.62

[a]Wilson: $A_{12} = a_{12} - a_{22}$ and $A_{21} = a_{21} - a_{11}$; NRTL: $A_{12} = g_{12} - g_{22}$ and $A_{21} = g_{21} - g_{11}$; UNIQUAC: $A_{12} = u_{12} - u_{22}$ and $A_{21} = u_{21} - u_{11}$; A_{12}: binary interaction parameters representation for the models in Aspen Plus®. k_{ij}: parameter for fitting with Wong and Sandler mixing rule.

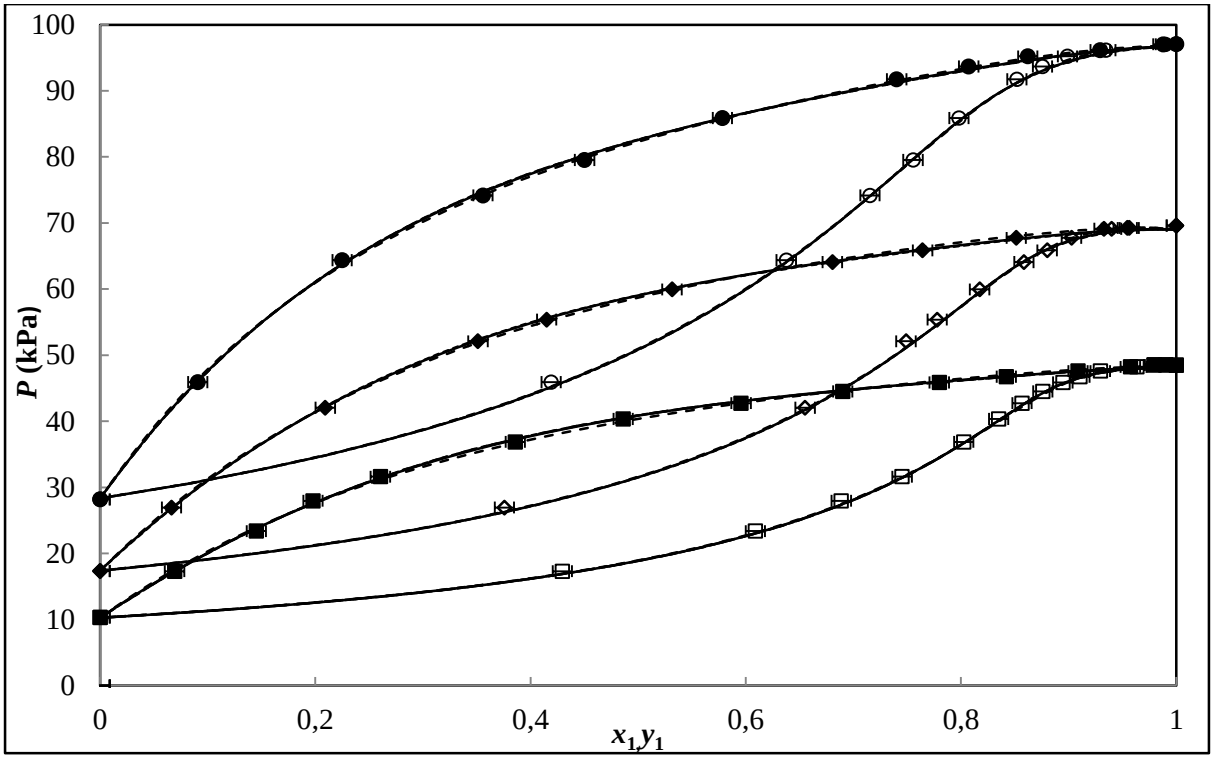

Figure 7-35: Experimental VLE and modeling results: P-*x*-*y* data for the DIPE (1) + 1-propanol (2) system at 320.15K (□); 330.15K (◊); 340.15K (○); — PR-NRTL; - - - PR-Wilson; ... PR-UNIQUAC.

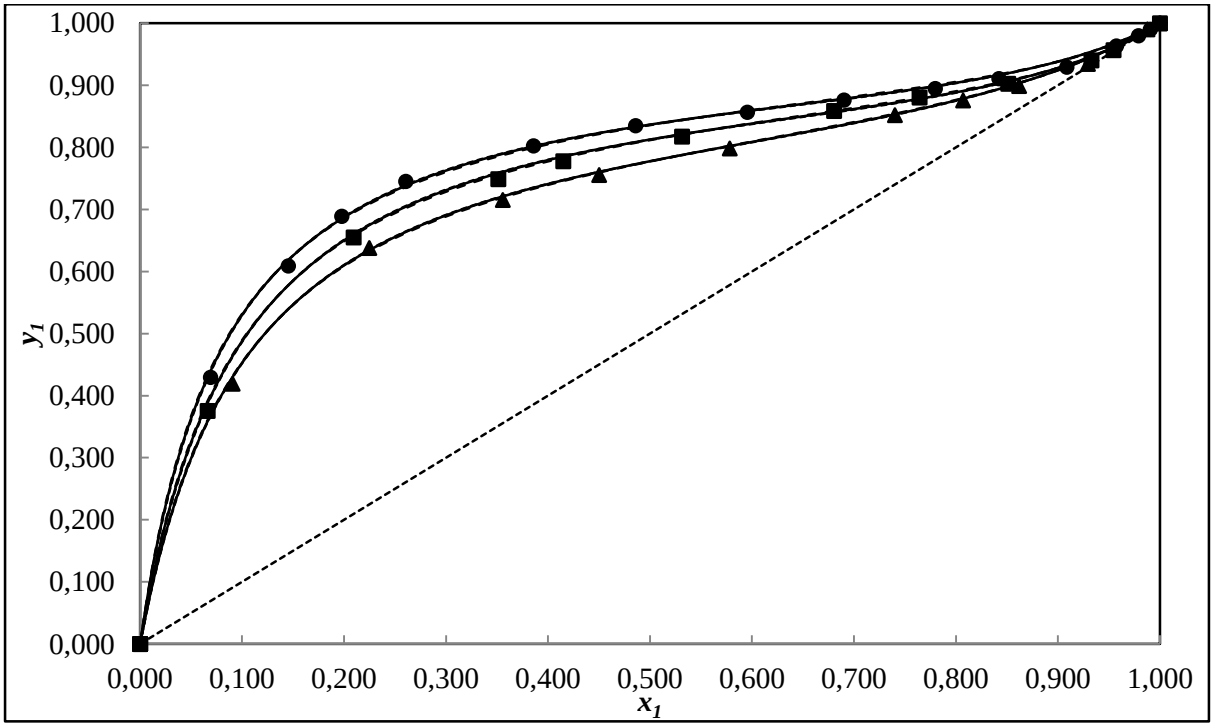

Figure 7-36: Experimental VLE and modeling results: *x*-*y* data for the DIPE (1) + 1-propanol (2) system at 320.15K (▲); 330.15K (■); 340.15K (●); — PR-NRTL; - - - PR-Wilson; ... PR-UNIQUAC.

7.6.6. Modeling Results for the DIPE (1) + 2-butanol (2) System

Tables 7-21 to 7-23 show the adjustable binary interaction parameters for the various models used in the reduction of the DIPE (1) + 2-butanol (2) system. These tables also show the average deviations of pressure (ΔP/kPa), the vapour molar compositions (Δy_1) and the average absolute deviation (AAD %) of the vapour mole fraction. Figures 7-26 and 7-27 display the graphical representation of model to *P-x-y* data for this system. Figures 7-37 and 7-42 display the graphical representation of model to *P-x-y* data for this system. The relative volatilities for this data set are represented graphically in Appendix D, Figure D-6. The experimental activity coefficient values are given in the Appendix C Table C-6. The models represented the experimental data for this system fairly well with the best fits given by the NRTL-HOC and the Wilson-NTH models. At an isotherm temperature of T = 330.15K, the Wilson-NTH model gave the lowest vapour mole fraction AAD of 0.44%. The NRTL-HOC model gave the lowest overall AAD for the vapour mole fraction of 0.46% and 0.49% for T = 320.15K and T = 330.15K respectively. The PR-MC-WS model produced the highest overall vapour mole fraction AAD with all three local composition combinations; PR-MC-WS-UNIQUAC having the highest at T = 1.17%.

Table 7-21: Combined Method Modeling results for DIPE (1) + 2-butanol (2)

Model	**T±0.10/K**	α_{12}	A_{12} **J/mol**	A_{21} **J/mol**	**(Δ*P*) AAD**	**AAD% (Δ*P*)**	**(Δy_1) AAD**	**AAD%(Δy_1)**
NRTL-HOC								
	320.15	0.30	1320	185.9	0.54	1.71	0.004	0.46
	330.15	0.30	1318	131.6	0.32	0.55	0.003	0.49
	340.15	0.30	1037	236.7	0.91	1.31	0.009	1.40
Wilson-HOC								
	320.15	-	-378.1	-1273	0.58	1.63	0.004	0.54
	330.15	-	-328.7	-1247	0.29	0.57	0.003	0.45
	340.15	-	-397.0	-969.5	0.89	1.37	0.012	1.35
UNIQUAC-HOC								
	320.15	-	-859.3	306.1	0.61	1.86	0.004	0.62
	330.15	-	-862.3	320.7	0.32	0.62	0.003	0.49
	340.15	-	-724.9	264.0	0.91	1.39	0.009	1.41

[a]Wilson: $A_{12} = a_{12} - a_{22}$ and $A_{21} = a_{21} - a_{11}$; NRTL: $A_{12} = g_{12} - g_{22}$ and $A_{21} = g_{21} - g_{11}$; UNIQUAC: $A_{12} = u_{12} - u_{22}$ and $A_{21} = u_{21} - u_{11}$; A_{12}: binary interaction parameters representation for the models in Aspen Plus®. k_{ij}: parameter for fitting with Wong and Sandler mixing rule.

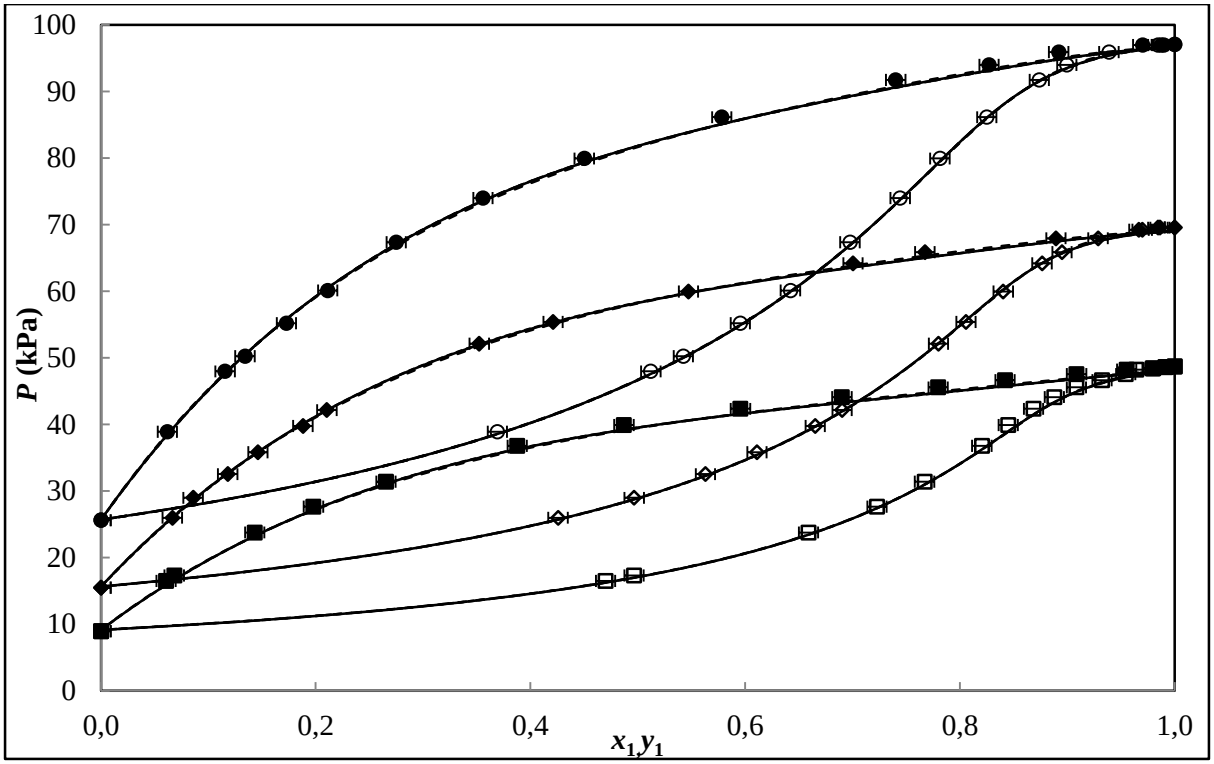

Figure 7-37: Experimental VLE and modeling results: P-*x*-*y* data for the DIPE (1) + 2-butanol (2) system at 320.15K (□); 330.15K (◊); 340.15K (○); — HOC-NRTL; - - - HOC-Wilson; ... HOC-UNIQUAC.

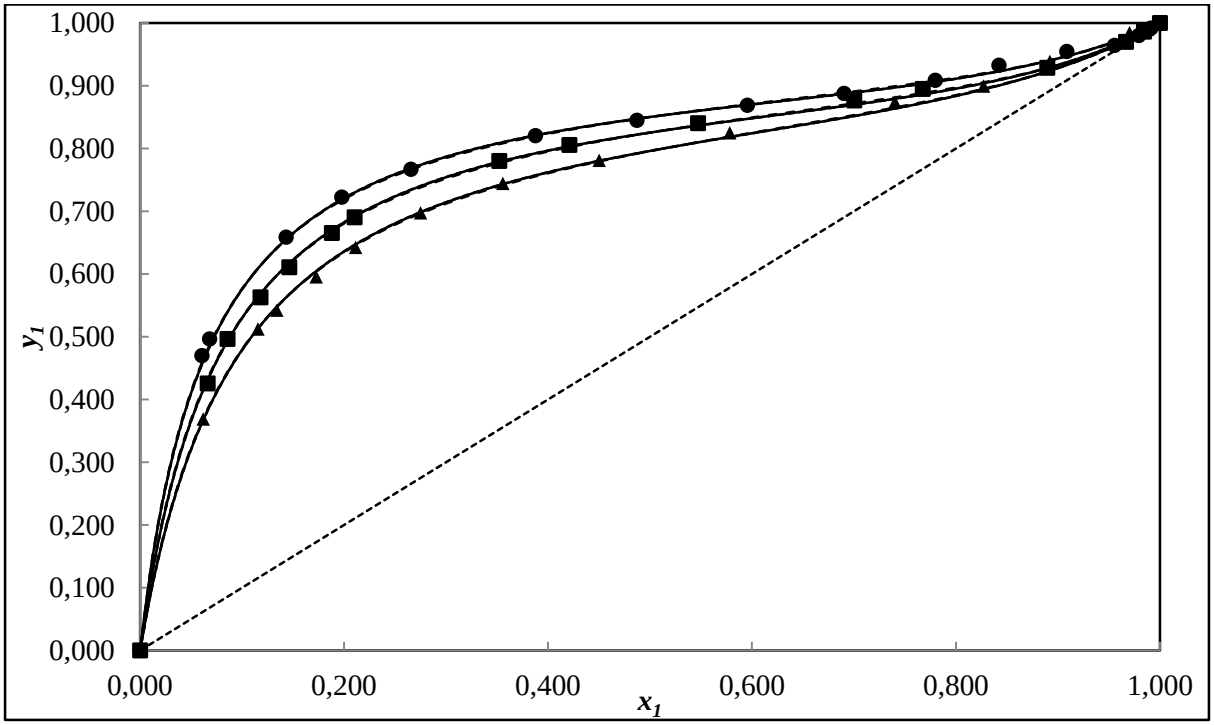

Figure 7-38: Experimental VLE and modeling results: *x*-*y* data for the DIPE (1) + 2-butanol (2) system at 320.15K (▲); 330.15K (■); 340.15K (●); — HOC-NRTL; - - - HOC-Wilson; ... HOC-UNIQUAC.

Table 7-22: Combined Method Modeling results using Nothnagel et al. method (NTH) for DIPE (1) + 2-butanol (2)

Model	**T±0.02/K**	α_{12}	A_{12} **J/mol**	A_{21} **J/mol**	**(Δ*P*) AAD**	**AAD% (Δ*P*)**	**(Δy_1) AAD**	**AAD%(Δy_1)**
NRTL-NTH								
	320.15	0.30	3270	196.1	0.74	2.37	0.005	0.82
	330.15	0.30	3211	139.9	0.27	0.50	0.003	0.46
	340.15	0.30	2879	241.7	1.46	2.19	0.013	1.91
Wilson-NTH								
	320.15	-	1220	3149	0.37	1.00	0.005	0.73
	330.15	-	1222	3039	0.26	0.52	0.003	0.44
	340.15	-	1110	3188	0.71	1.06	0.005	0.54
UNIQUAC-NTH								
	320.15	-	912.6	134.9	0.44	1.31	0.005	0.69
	330.15	-	854.4	155.3	0.30	0.60	0.003	0.48
	340.15	-	939.4	104.8	0.66	0.96	0.004	0.65

[a]Wilson: $A_{12} = a_{12} - a_{22}$ and $A_{21} = a_{21} - a_{11}$; NRTL: $A_{12} = g_{12} - g_{22}$ and $A_{21} = g_{21} - g_{11}$; UNIQUAC: $A_{12} = u_{12} - u_{22}$ and $A_{21} = u_{21} - u_{11}$; A_{12}: binary interaction parameters representation for the models in Aspen Plus®. k_{ij}: parameter for fitting with Wong and Sandler mixing rule.

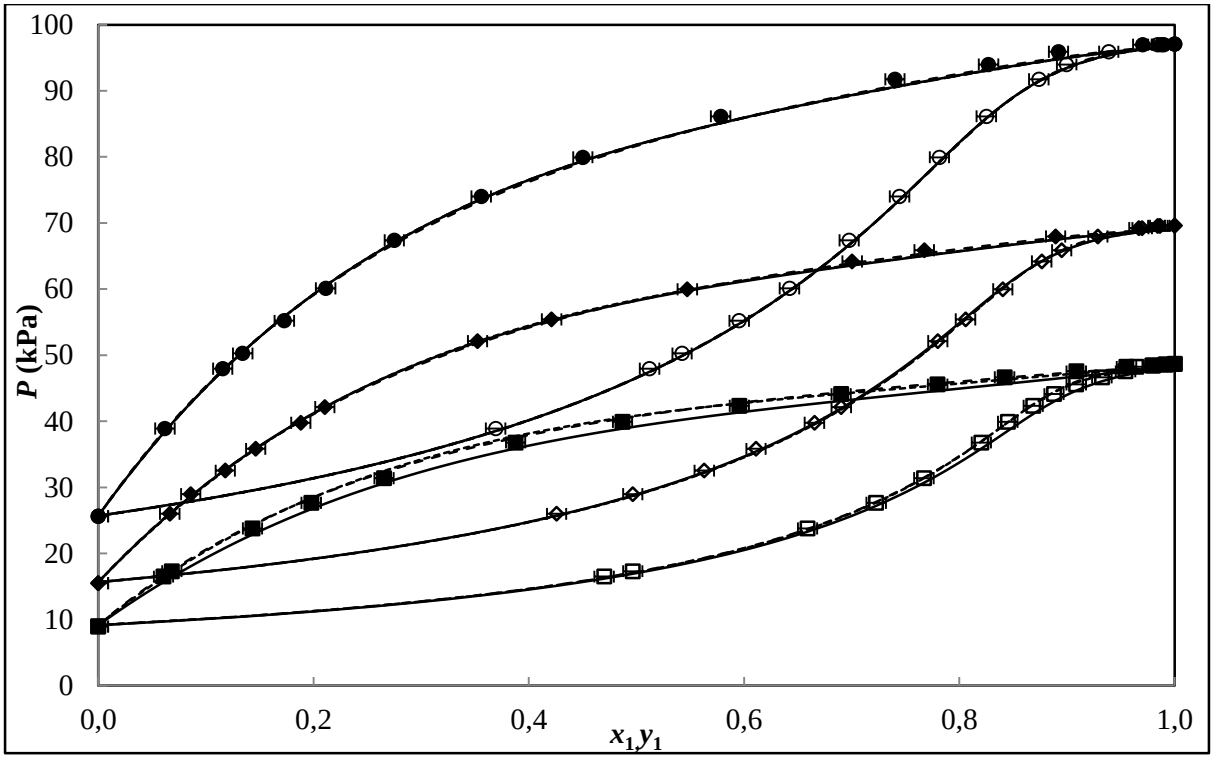

Figure 7-39: Experimental VLE and modeling results: P-*x*-*y* data for the DIPE (1) + 2-butanol (2) system at 320.15K (□); 330.15K (◊); 340.15K (○); — NTH-NRTL; - - - NTH-Wilson; ... NTH-UNIQUAC.

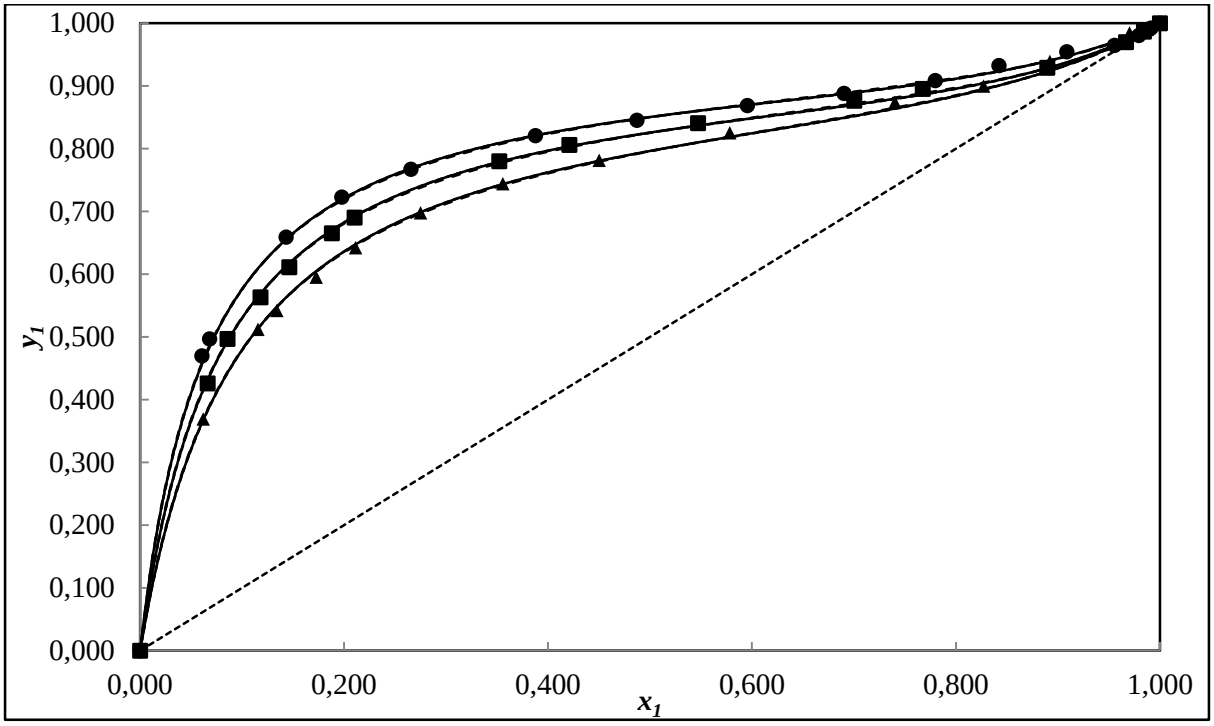

Figure 7-40: Experimental VLE and modeling results: *x*-*y* data for the DIPE (1) + 2-butanol (2) system at 320.15K (▲); 330.15K (■); 340.15K (●); — NTH-NRTL; - - - NTH-Wilson; ... NTH-UNIQUAC.

Table 7-23: Direct Method Modeling results for DIPE (1) + 2-butanol (2)

Model	**T±0.02/K**	α_{12}	k_{ij}	A_{12} **J/mol**	A_{21} **J/mol**	**(Δ*P*) AAD**	**AAD% (Δ*P*)**	**(Δy_1) AAD**	**AAD%(Δy_1)**
PR-MC-WS-NRTL									
	320.15	0.30	-0.603	-2239	3179	0.19	0.85	0.007	1.09
	330.15	0.30	0.015	-3052	1604	0.35	0.57	0.008	1.14
	340.15	0.30	0.303	-3074	765.0	0.44	0.76	0.008	1.16
PR-MC-WS-Wilson									
	320.15	-	0.016	-402.0	-1515	0.40	1.26	0.007	1.11
	330.15	-	0.140	-24.23	-1384	0.33	0.84	0.007	1.01
	340.15	-	0.140	-107.2	-952.8	0.52	0.95	0.008	0.83
PR-MC-WS-UNIQUAC									
	320.15	-	-0.024	-943.1	458.3	0.34	1.14	0.007	1.09
	330.15	-	0.055	-967.6	522.7	0.32	0.79	0.008	1.17
	340.15	-	0.294	-868.5	656.0	0.33	0.61	0.008	1.13

[a]Wilson: $A_{12} = a_{12} - a_{22}$ and $A_{21} = a_{21} - a_{11}$; NRTL: $A_{12} = g_{12} - g_{22}$ and $A_{21} = g_{21} - g_{11}$; UNIQUAC: $A_{12} = u_{12} - u_{22}$ and $A_{21} = u_{21} - u_{11}$; A_{12}: binary interaction parameters representation for the models in Aspen Plus®. k_{ij}: parameter for fitting with Wong and Sandler mixing rule.

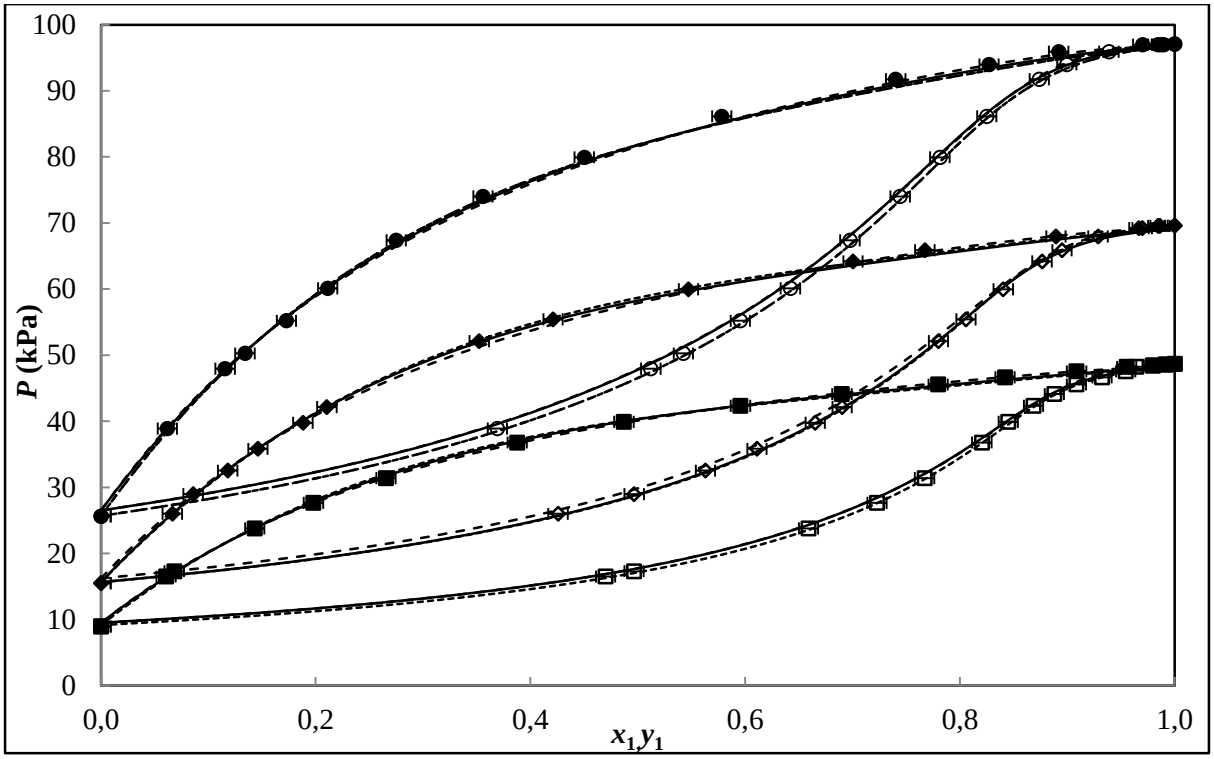

Figure 7-41: Experimental VLE and modeling results: P-*x*-*y* data for the DIPE (1) + 2-butanol (2) system at 320.15K (□); 330.15K (◊); 340.15K (○); — PR-NRTL; - - - PR-Wilson; ... PR-UNIQUAC.

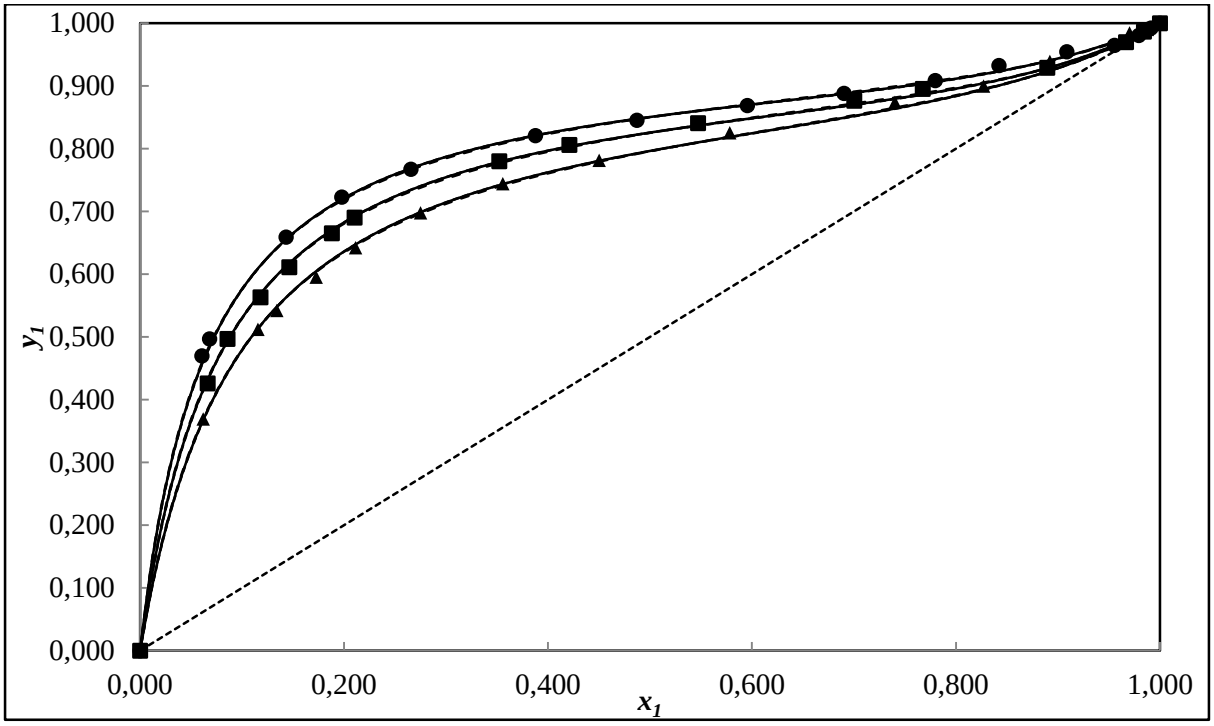

Figure 7-42: Experimental VLE and modeling results: *x*-*y* data for the DIPE (1) + 2-butanol (2) system at 320.15K (▲); 330.15K (■); 340.15K (●); — PR-NRTL; - - - PR-Wilson; ... PR-UNIQUAC.

7.7. Thermodynamic Consistency Testing of Experimental VLE Data

The testing of the thermodynamic consistency of experimental VLE data becomes the most significant aspect of data analysis. This testing represents the acceptability of the measured data according and whether the standard of the model parameters obtained via data regression may be utilised for future industrial design and literature purposes. As previously emphasised in Chapter 2 Section 2.7, the area test is not a sufficient condition for a consistency test as it is considered un-rigorous and too mild. Therefore, in this investigation, the focus was on the direct and point test were used to reflect quality experimental data.

Owing to the association that exists between ether-alcohol systems because of the alcohol molecule, the non-idealities within the vapour phase are still significantly noteworthy despite all systems being measured at low pressures. As a result of this the ideal gas law or even more importantly the truncated virial EOS becomes invalid. Although the results for the direct test have been computed and tabulated, they will not be utilised as the means of quality data assessment for all systems measured. More specifically because in this case the direct test can only use an activity coefficient model whereas the point test can use an EOS and activity coefficient model. The point test of Van Ness et al. (Van Ness et al., 1973, Van Ness et al., 1978, Abbott and Van Ness, 1982) however is more stringent. It analyses the consistency from the pressure and vapour composition residuals by using the total absolute error (*AE%*). This is the sum of the square of the absolute deviation in the pressure (ΔP_{AAD}) with the vapour phase composition (Δy_{AAD}). These two variables are used as the primary means of ascertaining which model/s best fit measured data. Hence, the point test was used to test the thermodynamic consistency of all systems measured in this project.

The point test has the distinction of being considered as a modeling test since a thermodynamically consistent model must be located that is able to fit the experimental data before the test can become applicable (discussed in depth in section 2.7.2). When the point test is applied, minimisation of the pressure deviations between experimental pressures and those calculated by the model occurs. This happens when the model chosen for data correlation is reduced to fit experimental P-x_i data to obtain value sets for the adjustable model parameters. As a result, the systematic errors then become transferred to the vapour composition y_i residual. The vapour composition from the model is then used to compute y_i values, which are then compared to the experimentally obtained y_i values. This is done because the experimental y_i data are not used in the data regression. The aforementioned residual then represents a measure of the thermodynamic consistency of the system. It is important to note that the mathematical model/s used in the regression/s is already thermodynamically consistent since it satisfies the Gibbs-Duhem equation. The average absolute deviation of the vapour composition,

(Δy_{AAD}) must be less than 0.01 for the system or experimental data set to be deemed thermodynamically consistent using the point test.

Application of the point test provides intricate details on the consistency of the measured data including the models used to fit them. The results obtained from the point test are highly sensitive to the selection of model employed for the data reduction. In light of this it can be seen that even though a particular data set may fail this consistency test, the data may not necessarily be guaranteed as inconsistent. This may in fact be attributed to the selection of the improper model for reduction analysis. Additionally, some data points may be omitted and the test re-run, as opposed to deeming the entire data set inconsistent. It is also possible for a data set to pass the point test and still be erroneous. Nevertheless, although these tests may inadvertently introduce errors, they still remain a dominant means for distinguishing the consistency of experimental data and a wealth of information that is challenging to acquire by any other means (Jackson and Wilsak, 1995).

The complexity of the vapour phase for the binary systems in this investigation called for the methodical approach of data analysis whereby the vapour phase models were varied initially. The ideal gas models and activity coefficient model was initially kept constant using the NRTL model. The HOC, NTH, PR and SRK equations of state were used in the regression of experimental data for determining the non-idealities in the vapour phase. More often than not (in most instances), it was seen that the NRTL activity coefficient model rendered the best fit to the experimental data by providing the lowest P and y_i residuals. The model combinations of NRTL-HOC, WILSON-HOC and UNIQUAC-HOC were only applied (to analyse consistency) once the best fit EOS was found. Thereafter the activity coefficient model could be varied to the aforementioned combinations (whilst fixing the EOS as with HOC) in order to observe whether the residuals improved with variation of activity coefficient model.

In the following sections, the consistency tests results for all systems measured are discussed. The point test requirements were met for all data points for certain temperature isotherms while at other temperatures, the test failed (for the same system).The results of the point test conducted over an entire compositional range for the whole data set has been illustrated in the tables below. Data points that had failed the point test were also included in these tables. The data points that resulted in the point test failing (for model combinations) however were strategically excluded one at a time. This allowed the point test to be re-initialised until the criterion of the test i.e. $\left|\Delta y_{i,avg}\right| \leq 0.01$could be fulfilled. Points that were excluded for a specific model combination to facilitate the passing of the test are designated by the ‘x’ symbol in the table within the appropriate column.

When certain data points were excluded from the final analysis, it was due to them rendering erroneous results; however these points could only be identified post execution of modeling. The rationale behind this is the fact that the points that proved to be problematic in the data regression could not merely be spotted and thereafter removed. It becomes much simpler to run the regression initially, and once complete, troubleshooting can commence with the complicated point/s being removed. It stands to good reasoning that the points under scrutiny for causing erroneous results may in fact not be faulty at all. Other models not used in the current investigation, could in fact correlate the measured data with greater ease providing a more optimum reduction outcome and better represent the system under investigation.

The binary interaction parameters for all temperature isotherms reduced were obtained by utilising the data that had passed the point test for at least one of the model combinations used in this study (previously discussed). The (ΔP_{AAD}) and (Δy_{AAD}) are given at the bottom of each table pertaining to cases where the full set of data points were used including where only the data points which passed the point test were used.

7.7.1. Consistency Test for the 2, 2, 4-trimethylpentane (1) + 1-pentanol (2)

The pressure and vapour phase composition absolute average deviations for each of the model combinations used for regression are given in Tables 7-24 to 7-26 for the data sets of 350.15K, 360.15K and 370.15K. A summary of the point test analysis for the three data sets is also shown in Tables 7-24. These pressure-residuals and y_i-residuals for this data set are plotted in Figures 7-43 to 7-48. This presents the varying activity coefficient with equation of state models for describing liquid and vapour phase non-idealities respectively for the point test results using the combined and direct methods of VLE reduction. The Wilson-HOC gave a vapour phase deviation of 0.012 in the 370.15 K data set, which falls out of the point test margin range of 0.01. However, varying the activity coefficient model for the NTH EOS model combinations provided more favourable for all three isotherms resulting in vapour phase deviations below 0.01. The same held true for the PR and RKS cubic EOS model combinations for all three isotherm data sets. The RKS EOS model results for the point test is shown in Appendix A. Five points in each of the isotherm data sets had to be excluded from the final regression for the data to be thermodynamically consistent according to the point test specifications. Thereafter, all model combinations used had correlated the data acceptably averse to anomalous behavioural patterns, with good scatter about the *x*-axis for the P-residuals, extending leeway for the y_i-residuals to have reasonable scatter.

Table 7-24: Results of the thermodynamic consistency testing for the 2, 2, 4-trimethylpentane (1) + 1-pentanol (2) systems at 350.15, 360.15 and 370.15 K – Combined method; HOC EOS.

Model	T±0.10/K	Total points measured	Consistent points	(ΔP) AAD	(Δy_1) AAD
NRTL-HOC					
	350.15	14	9	0.54	0.004
	360.15	16	11	0.32	0.003
	370.15	15	10	0.91	0.009
Wilson-HOC					
	350.15	14	9	0.58	0.004
	360.15	16	11	0.29	0.003
	370.15	15	10	0.89	0.012
UNIQUAC-HOC					
	350.15	14	9	0.61	0.004
	360.15	16	11	0.32	0.003
	370.15	15	10	0.91	0.009

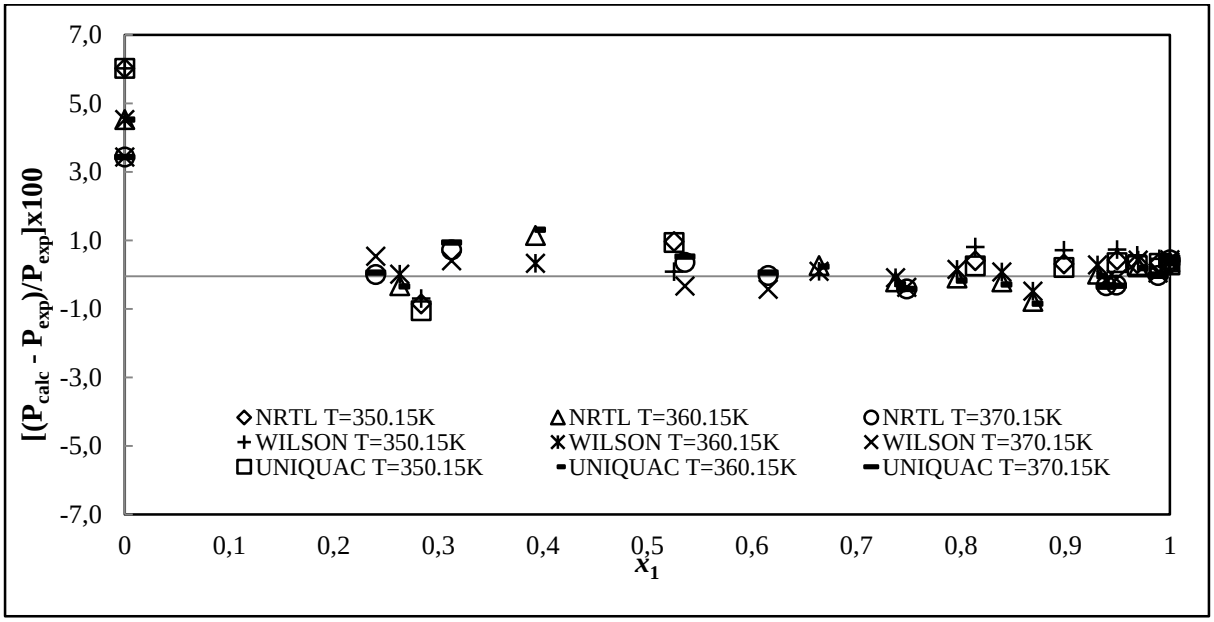

Figure 7-43: Point test for HOC EOS (activity coefficient model variation) P-residual for the 2, 2, 4-trimethylpentane (1) + 1-pentanol (2) system at: 350.15 K, 360.15K and 370.15K

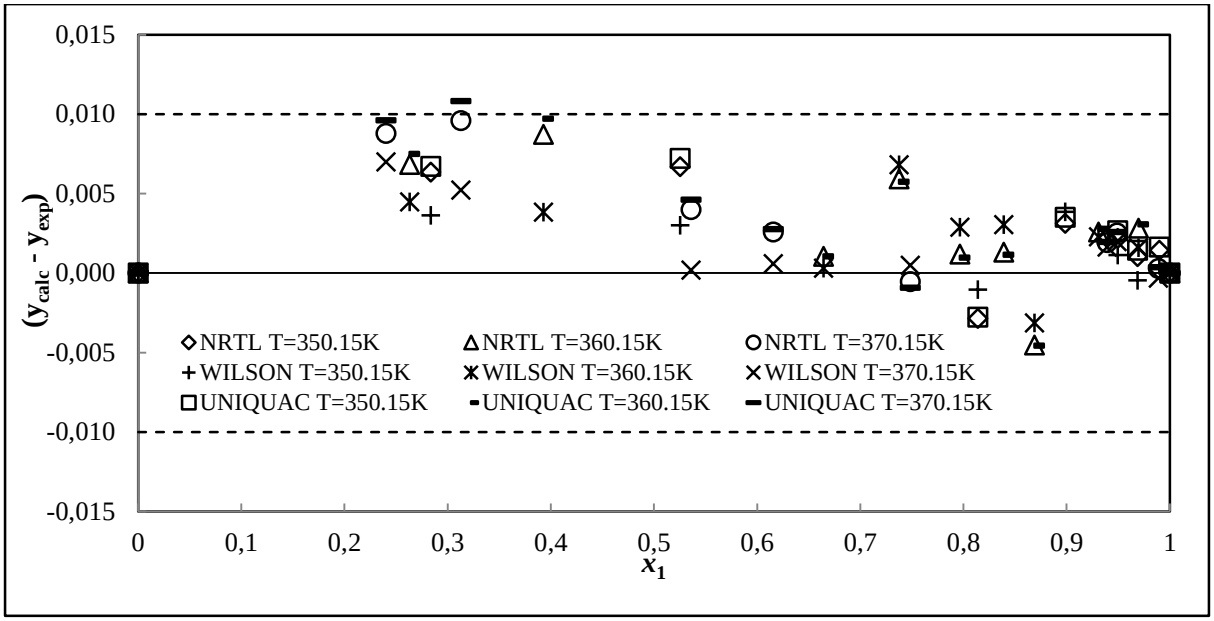

Figure 7-44: Point test for HOC EOS (activity coefficient model variation) y-residual for the 2, 2, 4-trimethylpentane (1) + 1-pentanol (2) system at: 350.15 K, 360.15K and 370.15K

Table 7-25: Results of the thermodynamic consistency testing for the 2, 2, 4-trimethylpentane (1) + 1-pentanol (2) systems at 350.15, 360.15 and 370.15 K – Combined method; NTH EOS.

Model	T±0.10/K	Total points measured	Consistent points	(ΔP) AAD	(Δy_1) AAD
NRTL-NTH					
	350.15	14	9	0.22	0.003
	360.15	16	11	0.29	0.003
	370.15	15	10	0.31	0.003
Wilson-NTH					
	350.15	14	9	0.22	0.002
	360.15	16	11	0.20	0.004
	370.15	15	10	0.17	0.003
UNIQUAC-NTH					
	350.15	14	9	0.22	0.002
	360.15	16	11	0.29	0.003
	370.15	15	10	0.34	0.003

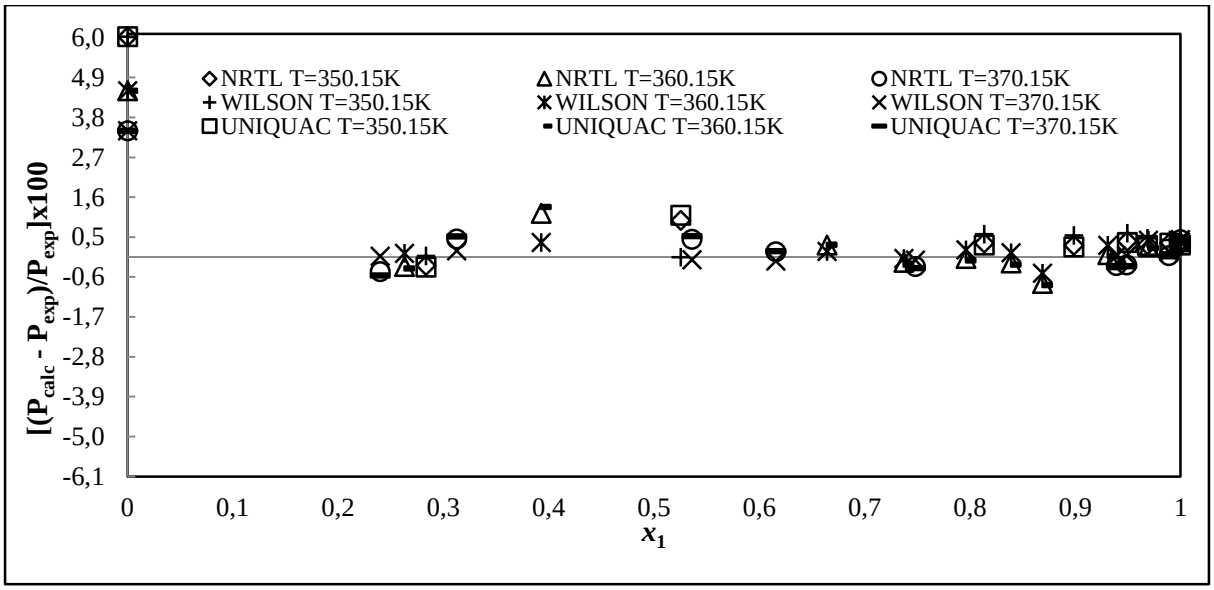

Figure 7-45: Point test for NTH EOS (activity coefficient model variation) P-residual for the 2, 2, 4-trimethylpentane (1) + 1-pentanol (2) system at: 350.15 K, 360.15K and 370.15K

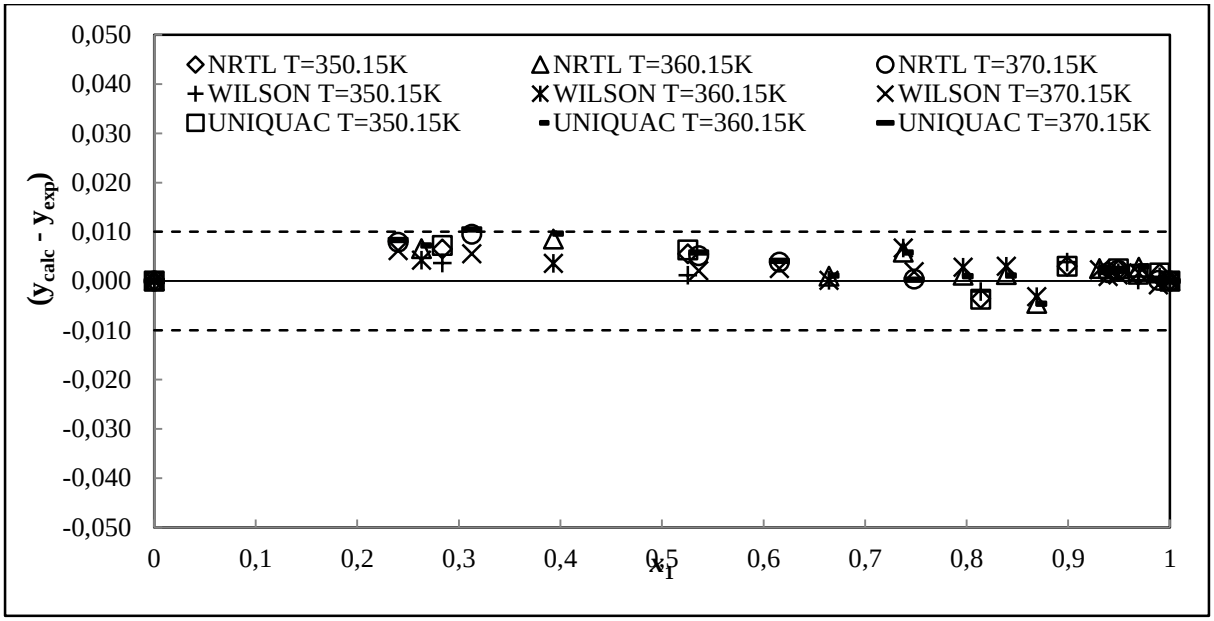

Figure 7-46: Point test for NTH EOS (activity coefficient model variation) y-residual for the 2, 2, 4-trimethylpentane (1) + 1-pentanol (2) system at: 350.15 K, 360.15K and 370.15K

Table 7-26: Results of the thermodynamic consistency testing for the 2, 2, 4-trimethylpentane (1) + 1-pentanol (2) systems at 350.15, 360.15 and 370.15 K – Direct method.

Model	T±0.10/K	Total points measured	Consistent points	(ΔP) AAD	(Δy_1) AAD
PR-MC-WS-NRTL					
	350.15	14	9	0.28	0.004
	360.15	16	11	0.22	0.003
	370.15	15	10	0.18	0.003
PR-MC-WS-WILSON					
	350.15	14	9	0.41	0.002
	360.15	16	11	0.31	0.002
	370.15	15	10	0.48	0.003
PR-MC-WS-UNIQUAC					
	350.15	14	9	0.29	0.003
	360.15	16	11	0.24	0.003
	370.15	15	10	0.23	0.003

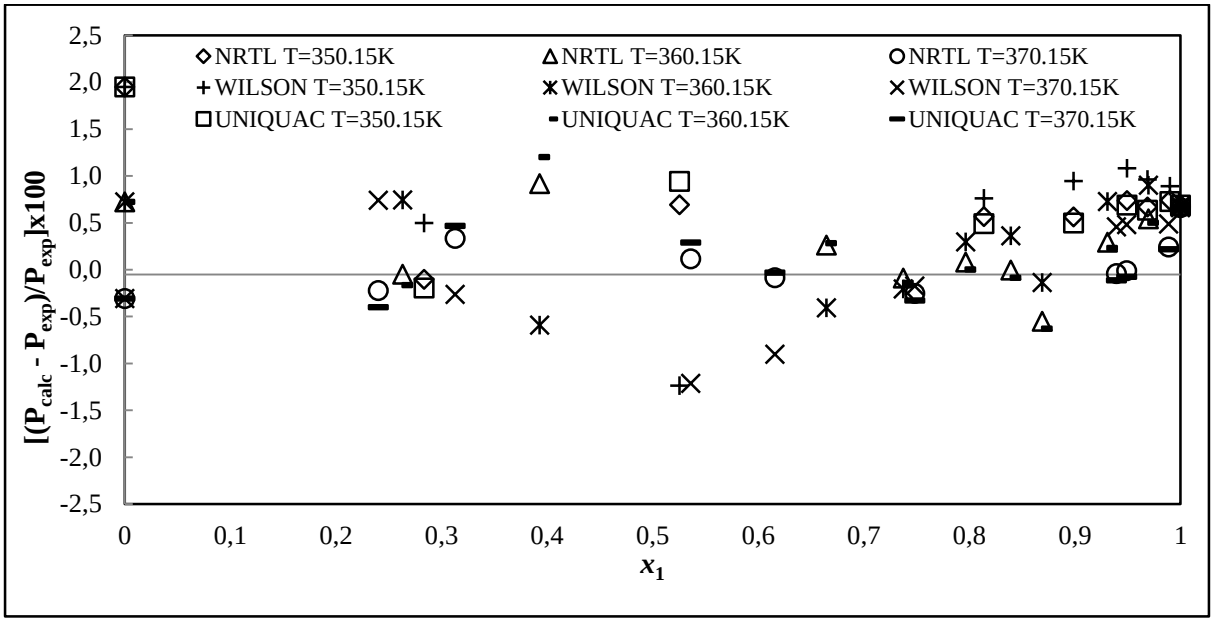

Figure 7-47: Point test for PR EOS (activity coefficient model variation) P-residual for the 2, 2, 4-trimethylpentane (1) + 1-pentanol (2) system at: 350.15 K, 360.15K and 370.15K

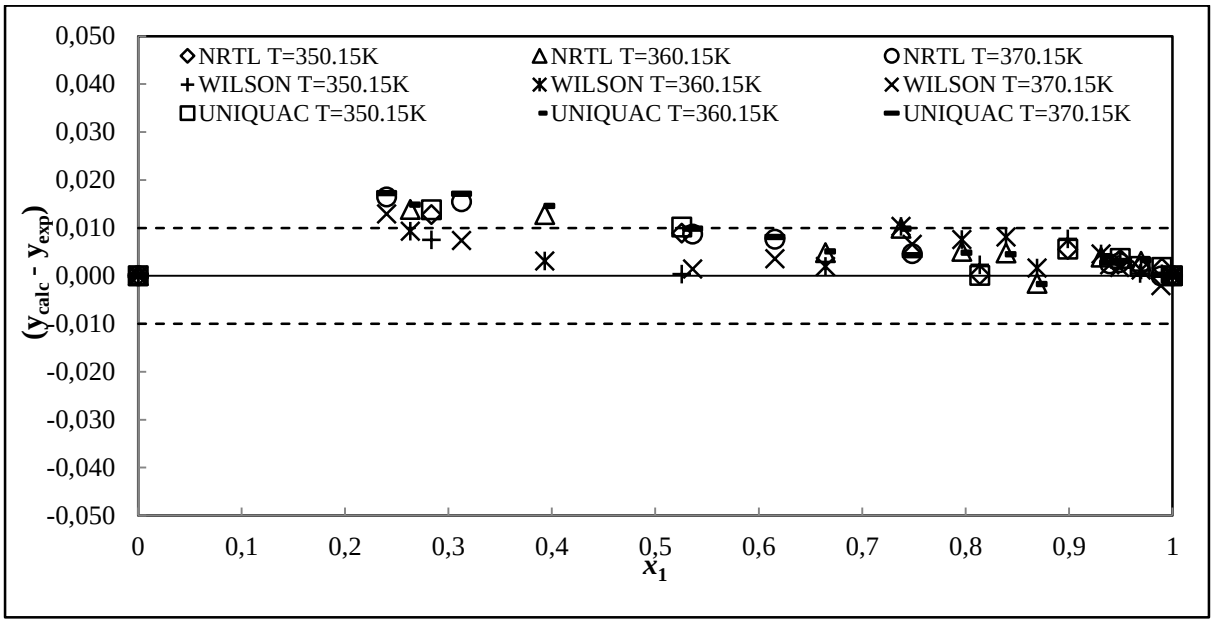

Figure 7-48: Point test for PR EOS (activity coefficient model variation) y-residual for the 2, 2, 4-trimethylpentane (1) + 1-pentanol (2) system at: 350.15 K, 360.15K and 370.15K

7.7.2. Consistency Test for the MTBE (1) + 1-pentanol (2) System

The models used provided satisfactory data fit for the MTBE (1) + 1-pentanol (2) system. The ΔP and Δ*y* values for this system are given in Tables 7-27 to 7-29 with a summary of the point test analysis

for the two data sets also presented. The average vapour phase deviations were found to be less than the point test margin of 0.01 for the 317.15 K and 327.15 K data sets for all the local activity coefficient model combinations with Hayden O' Connell and Nothnagel equations of state. These pressure-residuals and y_i-residuals for this data set are plotted in Figures 7-49 to 7-54. The 327.15 K data sets did not pass the point test margin for both the PR EOS and RKS EOS model combinations with all three local activity coefficient models. The pressure-residuals and y_i-residuals for the PR cubic EOS data set are plotted in Figures 7-53 to 7-54. The RKS model combination residuals are plotted in Appendix A. Changing the activity coefficient models made very insignificant changes to the ΔP and Δy values for the combined and direct method of regression. The pressure-residuals are scattered reasonably well about the x-axis with no significant bias trends. Five data points had to be excluded from the 317.15K data set and two were excluded from the 327.15K data set before the point test criterion was satisfied.

Table 7-27: Results of the thermodynamic consistency testing for the MTBE (1) + 1-pentanol (2) systems at 317.15 and 327.15 K – Combined method; HOC EOS.

Model	**T±0.10/K**	**Total points measured**	**Consistent points**	**(ΔP) AAD**	**(Δy_1) AAD**
NRTL-HOC					
	317.15	16	11	0.39	0.001
	327.15	15	13	0.59	0.005
Wilson-HOC					
	317.15	16	11	0.36	0.001
	327.15	15	13	0.55	0.005
UNIQUAC-HOC					
	317.15	16	11	0.38	0.001
	327.15	15	13	0.58	0.005

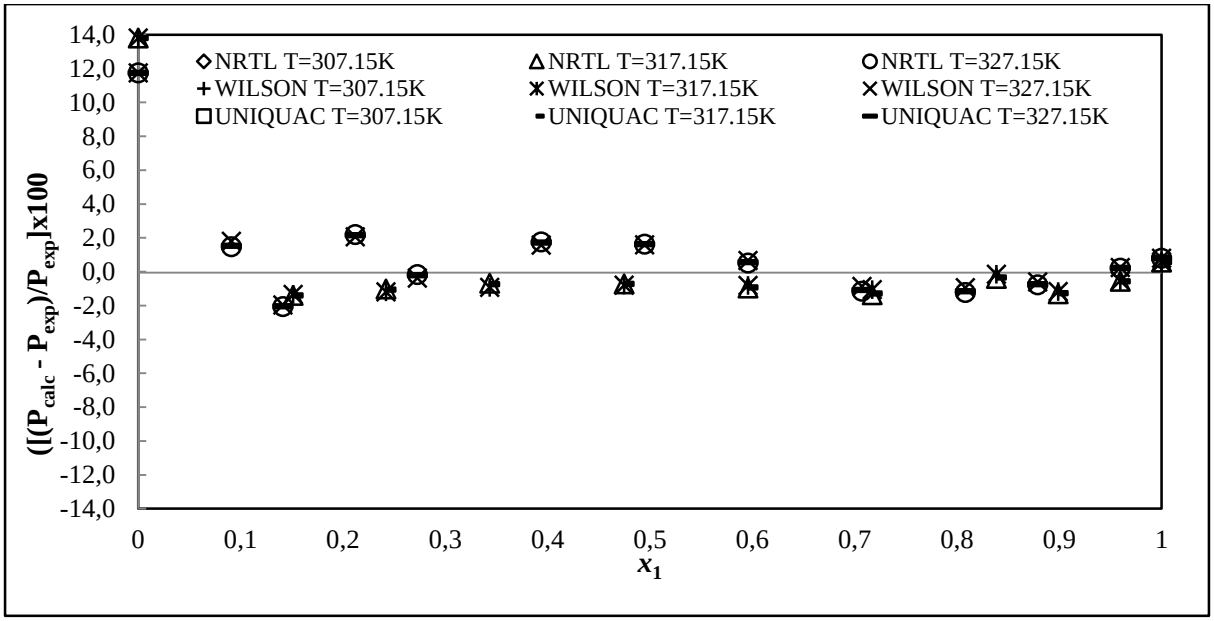

Figure 7-49: Point test for HOC EOS (activity coefficient model variation) P-residual for the MTBE (1) + 1-pentanol (2) system at: 317.15K and 327.15K

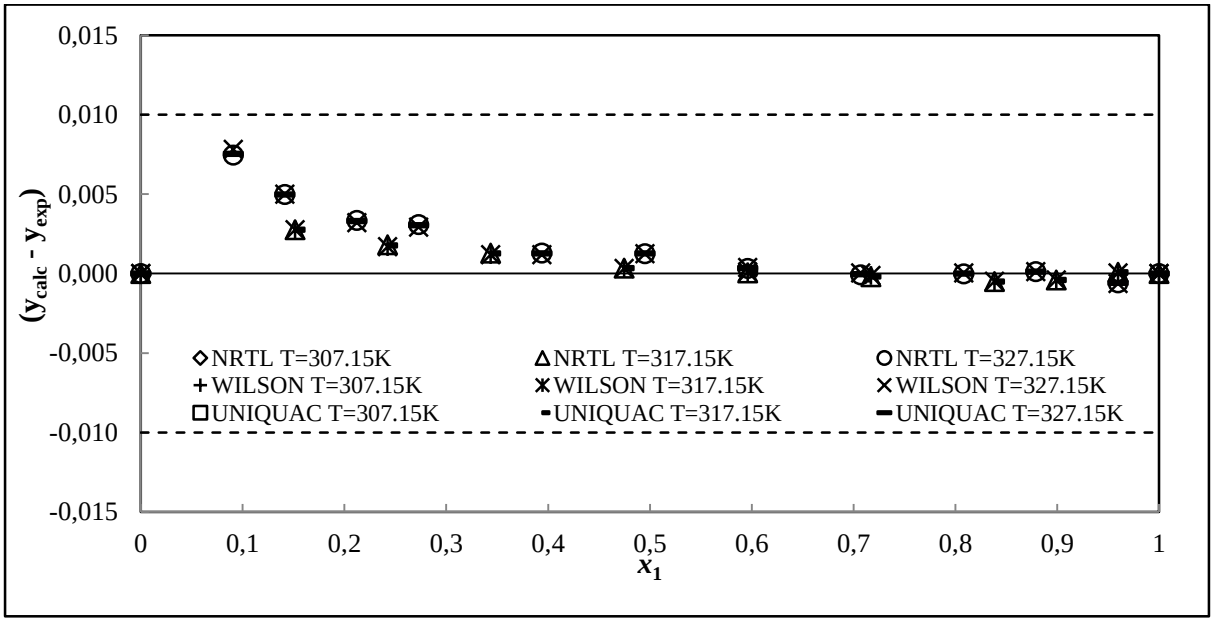

Figure 7-50: Point test for HOC EOS (activity coefficient model variation) y-residual for the MTBE (1) + 1-pentanol (2) system at: 317.15K and 327.15K

Table 7-28: Results of the thermodynamic consistency testing for the MTBE (1) + 1-pentanol (2) systems at 317.15 and 327.15 K – Combined method; NTH EOS.

Model	T±0.10/K	Total points measured	Consistent points	(ΔP) AAD	(Δy_1) AAD
NRTL-NTH					
	317.15	14	11	0.08	0.001
	327.15	17	13	0.17	0.005
Wilson-NTH					
	317.15	16	11	0.08	0.001
	327.15	15	13	0.17	0.005
UNIQUAC-NTH					
	317.15	16	11	0.08	0.001
	327.15	15	13	0.17	0.005

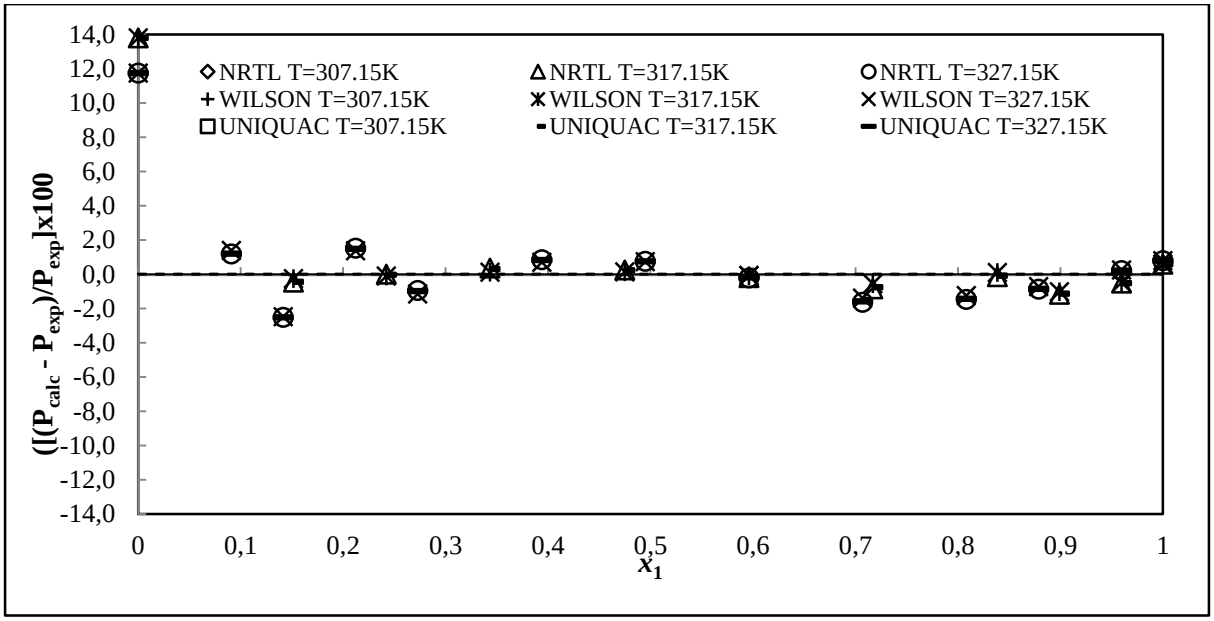

Figure 7-51: Point test for NTH EOS (activity coefficient model variation) P-residual for the MTBE (1) + 1-pentanol (2) system at: 317.15K and 327.15K

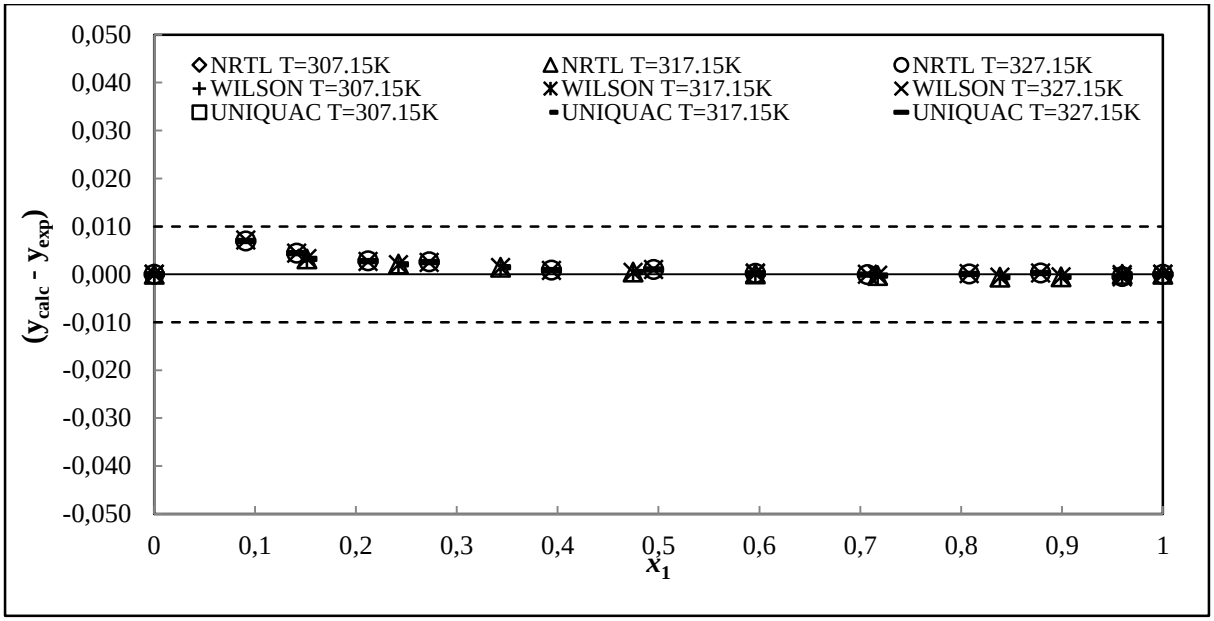

Figure 7-52: Point test for NTH EOS (activity coefficient model variation) y-residual for the MTBE (1) + 1-pentanol (2) system at: 317.15K and 327.15K

Table 7-29: Results of the thermodynamic consistency testing for the MTBE (1) + 1-pentanol (2) systems at 317.15 and 327.15 K – Direct method.

Model	T±0.10/K	Total points measured	Consistent points	(ΔP) AAD	(Δy_1) AAD
PR-MC-WS-NRTL					
	317.15	14	11	1.17	0.002
	327.15	17	13	1.62	0.004
PR-MC-WS-WILSON					
	317.15	16	11	0.94	0.002
	327.15	15	13	1.39	0.004
PR-MC-WS-UNIQUAC					
	317.15	16	11	1.11	0.002
	327.15	15	13	1.54	0.004

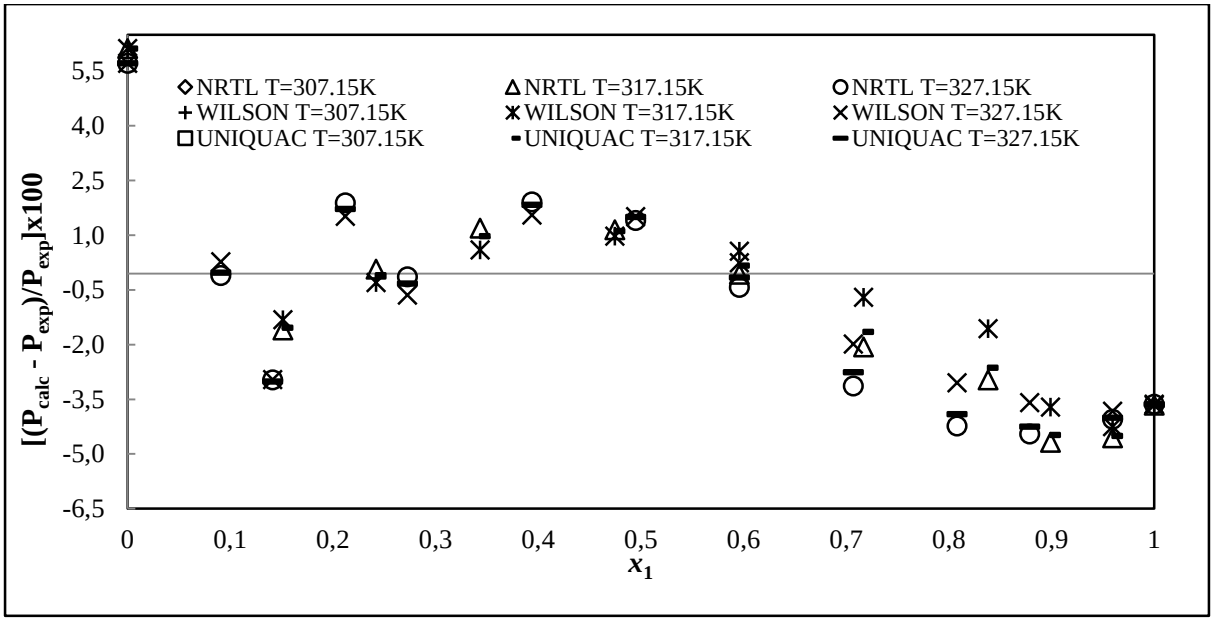

Figure 7-53: Point test for PR EOS (activity coefficient model variation) P-residual for the MTBE (1) + 1-pentanol (2) system at: 317.15K and 327.15K

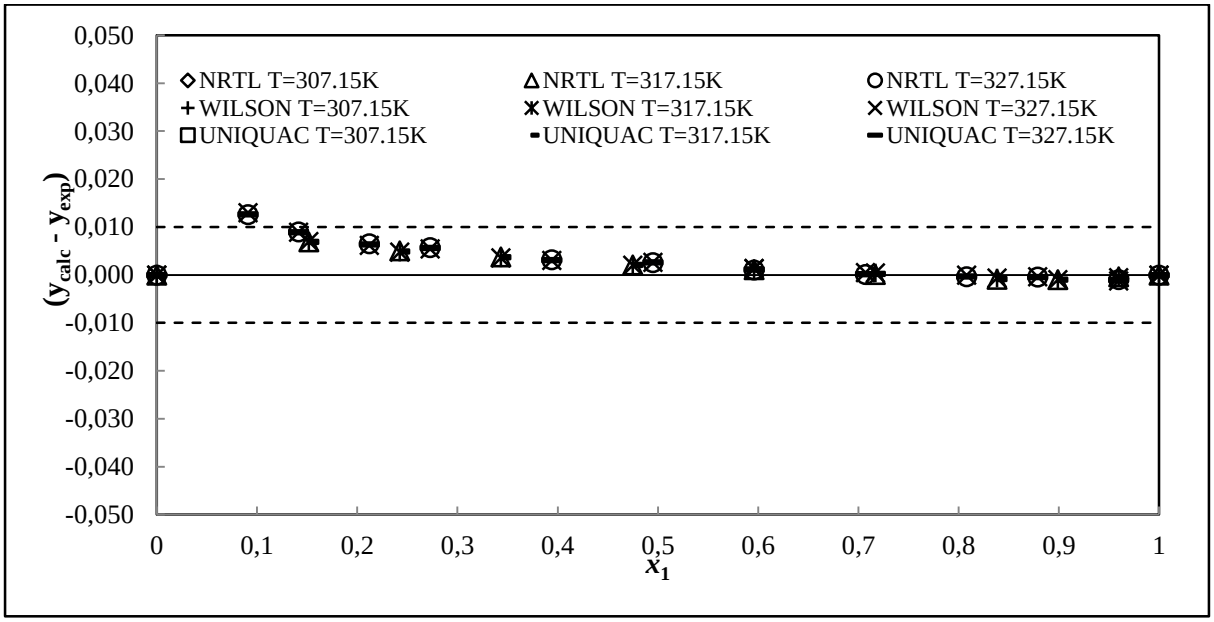

Figure 7-54: Point test for PR EOS (activity coefficient model variation) y-residual for the MTBE (1) + 1-pentanol (2) system at: 317.15K and 327.15K

7.7.3. Consistency Test for the MTBE (1) + 2, 2, 4-trimethylpentane (2) System

For this system the models provided satisfactory data fit for the MTBE (1) + 2, 2, 4-trimethylpentane (2) system. Tables 7-30 to 7-32 provide the ΔP and Δ*y* values for this system along with a summary of the point test analysis for the three isotherm measured data. The average vapour phase deviations

were found to be less than the point test margin of 0.01 for all the activity coefficient model combinations with Hayden O' Connell and Nothnagel equations of state for the combined method of VLE reduction. Regarding the direct method however, the PR-MC-WS-NRTL for the 327.15 K data set having a value of 0.012, with the PR-MC-WS-Wilson at 327.15 K data set having a value of 0.011. These results fall above the point test margin of 0.01. The RKS-MC-WS-NRTL and RKS-MC-WS-UNIQUAC models (both at isotherm data temperatures of 327.15 K), also had a value above the point test margin of 0.012. The pressure-residuals and y_i-residuals for the three data sets are plotted in Figures 7-55 to 7-60. It can be seen in the pressure-residual plots that there is a slight negative bias in the scatter for all the model combinations used for the combined and direct methods of regression. This bias in the scatter may suggest inconsistency. The y_i-residuals also show a negative bias in the plots for all model combinations. Oddly enough the data for all three isotherms had past the point test for all model combinations used for correlating the data in Aspen Plus®. For this reason all data points were included in the final reduction analyses except the two points that were excluded for the 307.15 K data set for all model combinations.

Table 7-30: Results of the thermodynamic consistency testing for the MTBE (1) + 2, 2, 4-trimethylpentane (2) systems at 307.15, 317.15 and 327.15 K – Combined method; HOC EOS.

Model	T±0.10/K	Total points measured	Consistent points	(ΔP) AAD	(Δy_1) AAD
NRTL-HOC					
	307.15	15	13	0.21	0.007
	317.15	17	17	0.47	0.008
	327.15	16	16	0.53	0.009
Wilson-HOC					
	307.15	15	13	0.28	0.007
	317.15	17	17	0.47	0.008
	327.15	16	16	0.61	0.010
UNIQUAC-HOC					
	307.15	15	13	0.20	0.007
	317.15	17	17	0.52	0.008
	327.15	16	16	0.57	0.010

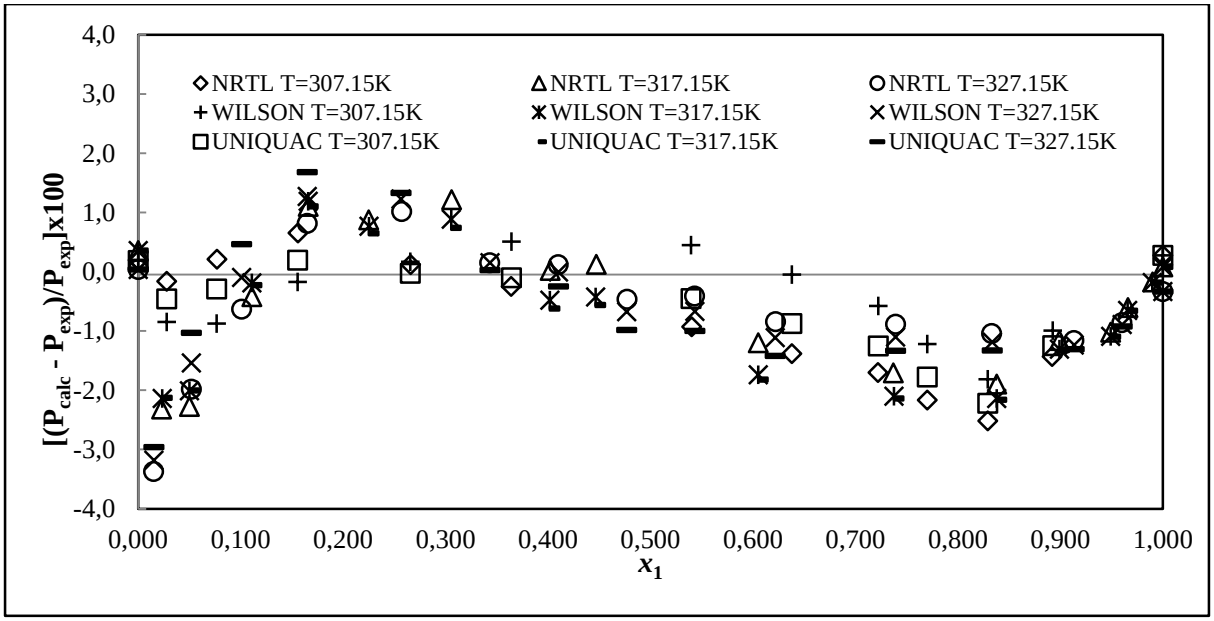

Figure 7-55: Point test for HOC EOS (activity coefficient model variation) P-residual for the MTBE (1) + 2, 2, 4-trimethylpentane (2) system at: 307.15K, 317.15K and 327.15K

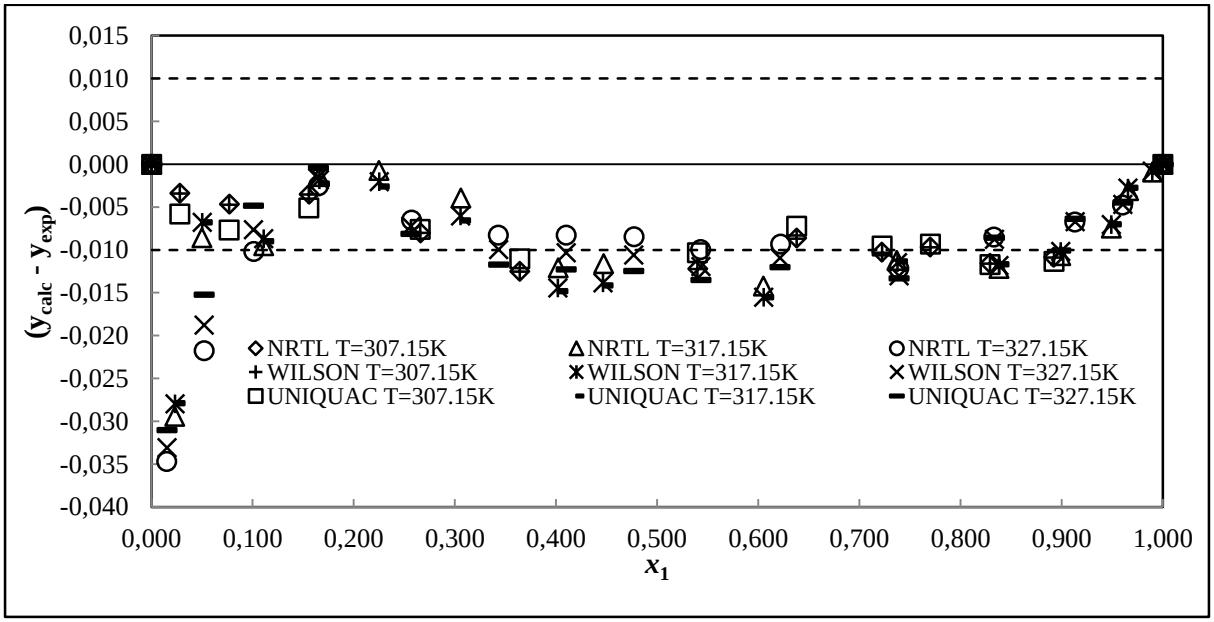

Figure 7-56: Point test for HOC EOS (activity coefficient model variation) y-residual for the MTBE (1) + 2, 2, 4-trimethylpentane (2) system at: 307.15K, 317.15K and 327.15K

Table 7-31: Results of the thermodynamic consistency testing for the MTBE (1) + 2, 2, 4-trimethylpentane (2) systems at 307.15, 317.15 and 327.15 K – Combined method; NTH EOS.

Model	T±0.10/K	Total points measured	Consistent points	(ΔP) AAD	(Δy_1) AAD
NRTL-NTH					
	307.15	15	13	0.35	0.007
	317.15	17	17	0.41	0.008
	327.15	16	16	0.48	0.009
Wilson-NTH					
	307.15	15	13	0.28	0.007
	317.15	17	17	0.41	0.008
	327.15	16	16	0.59	0.010
UNIQUAC-NTH					
	307.15	15	13	0.37	0.007
	317.15	17	17	0.43	0.008
	327.15	16	16	0.55	0.010

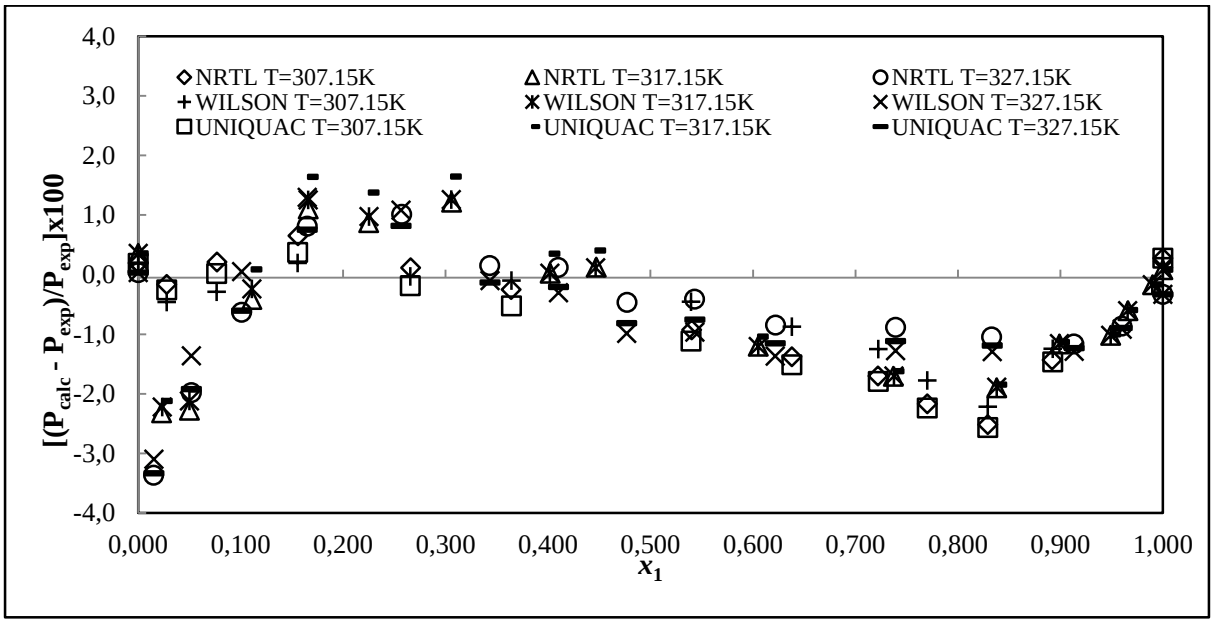

Figure 7-57: Point test for NTH EOS (activity coefficient model variation) P-residual for the MTBE (1) + 2, 2, 4-trimethylpentane (2) system at: 307.15K, 317.15K and 327.15K

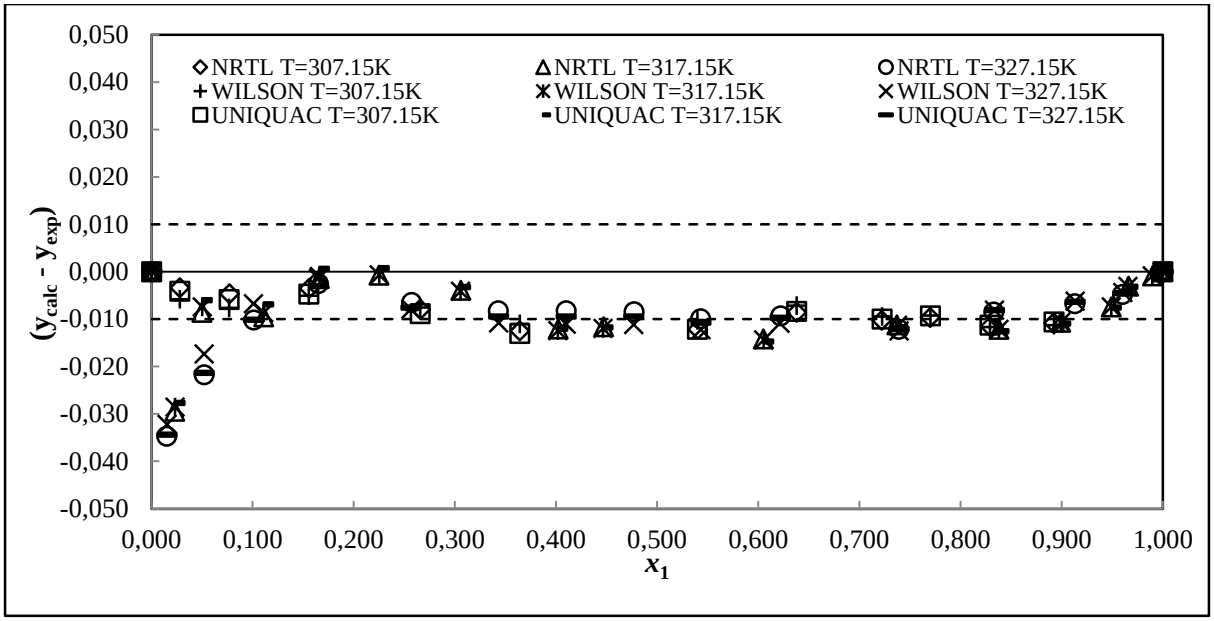

Figure 7-58: Point test for NTH EOS (activity coefficient model variation) y-residual for the MTBE (1) + 2, 2, 4-trimethylpentane (2) system at: 307.15K, 317.15K and 327.15K

Table 7-32: Results of the thermodynamic consistency testing for the MTBE (1) + 2, 2, 4-trimethylpentane (2) systems at 307.15, 317.15 and 327.15 K – Direct method.

Model	T±0.10/K	Total points measured	Consistent points	(ΔP) AAD	(Δy_1) AAD
PR-MC-WS-NRTL					
	307.15	15	13	0.60	0.009
	317.15	17	17	0.17	0.010
	327.15	16	16	0.19	0.012
PR-MC-WS-Wilson					
	307.15	15	13	0.59	0.008
	317.15	17	17	1.13	0.010
	327.15	16	16	1.11	0.011
PR-MC-WS-UNIQUAC					
	307.15	15	13	0.62	0.009
	317.15	17	17	1.18	0.010
	327.15	16	16	1.19	0.012

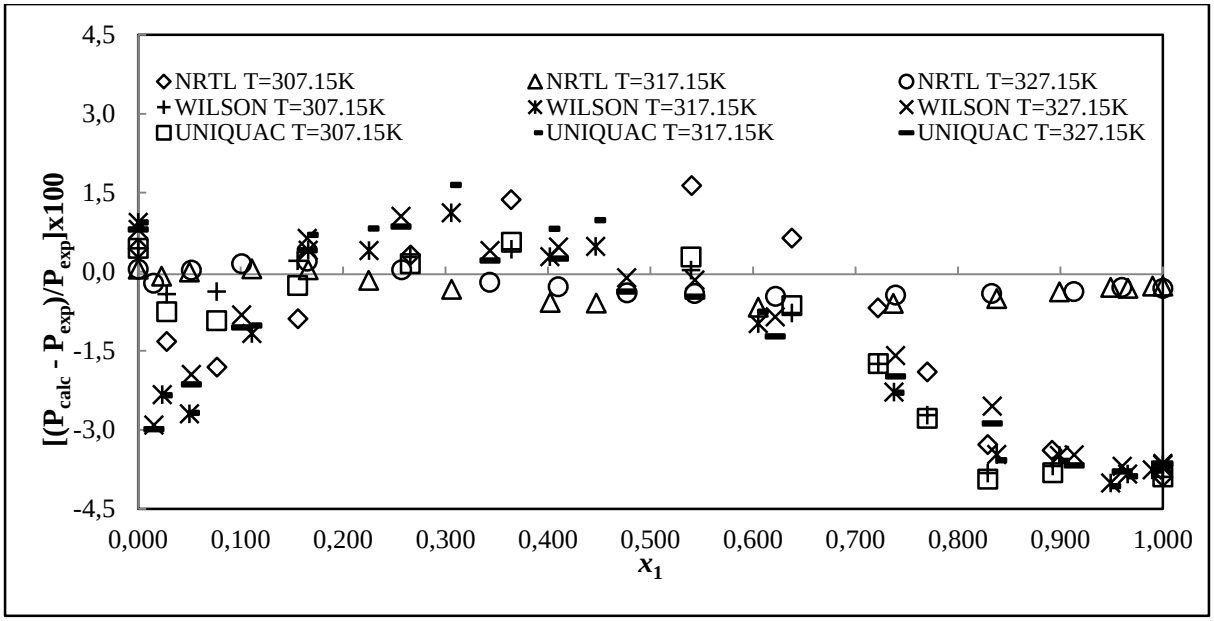

Figure 7-59: Point test for PR EOS (activity coefficient model variation) P-residual for the MTBE (1) + 2, 2, 4-trimethylpentane (2) system at: 307.15K, 317.15K and 327.15K

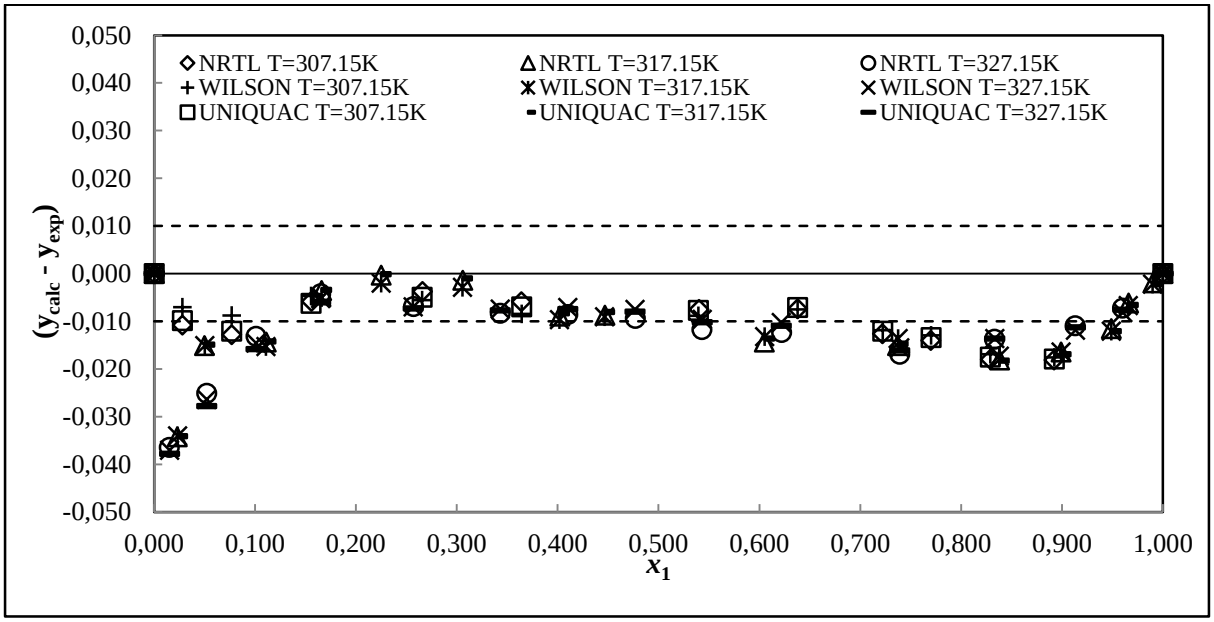

Figure 7-60: Point test for PR EOS (activity coefficient model variation) y-residual for the MTBE (1) + 2, 2, 4-trimethylpentane (2) system at: 307.15K, 317.15K and 327.15K

7.7.4. Consistency Test for the DIPE (1) + 2, 2, 4-trimethylpentane (2)

The diisopropyl ether (1) + 2, 2, 4-trimethylpentane (2) system was regressed fairly well to fit model parameters for the combined and direct method. Tables 7-33 to 7-35 summarises the results for the point test for this system. The ΔP and Δ*y* values for this system are also given in Table Tables 7-33 to

7-35. Figures 7-61 to 7-66 exhibit the pressure-residuals and y_i-residuals for the three data sets. The RKS EOS model combination residuals are plotted in Appendix A. The average vapour phase deviations were found to be less than the point test margin of 0.01 for all the activity coefficient model combinations at all three isotherm data sets. Only the NRTL-NTH model at 340.15 K had exhibited a value of 0.010 which is still reasonably acceptable for the point test criteria. The p-residuals scattered reasonably well around the *x*-axis suggesting thermodynamic consistency for all model combinations (combined and direct method). No data points had to be excluded from the three data sets before the test criterion was satisfied for the point test in Aspen Plus® for all model combinations.

Table 7-33: Results of the thermodynamic consistency testing for the DIPE (1) + 2, 2, 4-trimethylpentane (2) systems at 320.15, 330.15 and 340.15 K – Combined method; HOC EOS.

Model	**T±0.10/K**	**Total points measured**	**Consistent points**	**(ΔP) AAD**	**(Δy_1) AAD**
NRTL-HOC					
	320.15	18	18	0.20	0.003
	330.15	11	11	0.56	0.006
	340.15	11	11	0.51	0.007
Wilson-HOC					
	320.15	18	18	0.24	0.004
	330.15	11	11	0.56	0.006
	340.15	11	11	0.51	0.007
UNIQUAC-HOC					
	320.15	18	18	0.96	0.007
	330.15	11	11	1.15	0.008
	340.15	11	11	1.40	0.009

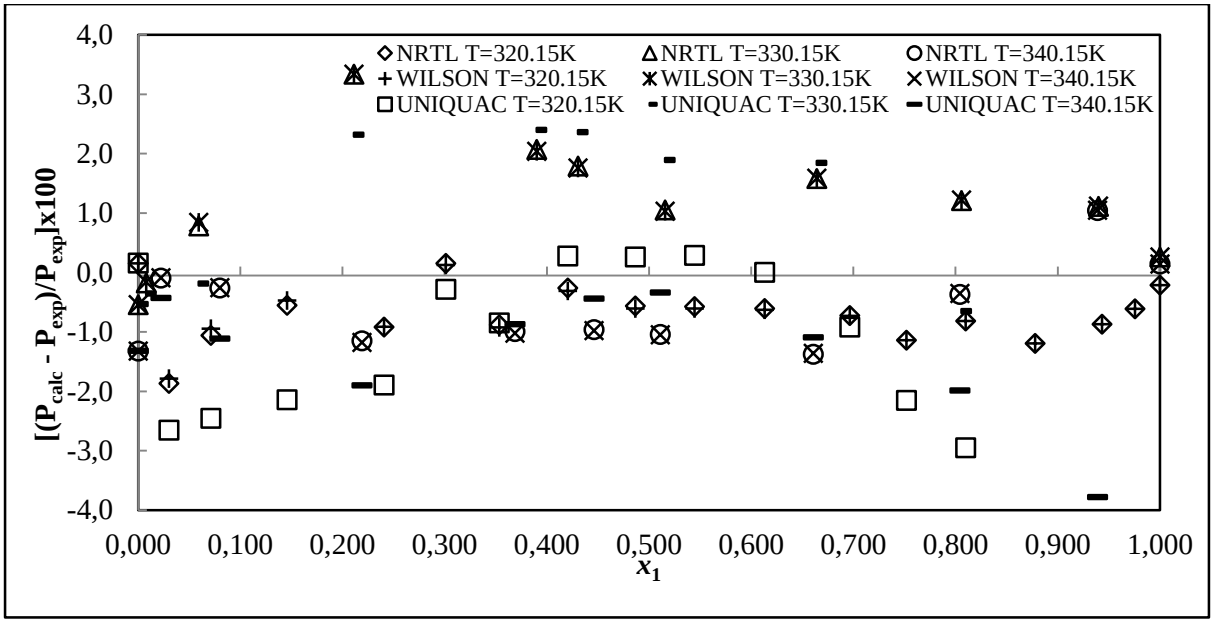

Figure 7-61: Point test for HOC EOS (activity coefficient model variation) P-residual for the DIPE (1) + 2, 2, 4-trimethylpentane (2) system at: 320.15K, 330.15K and 340.15K

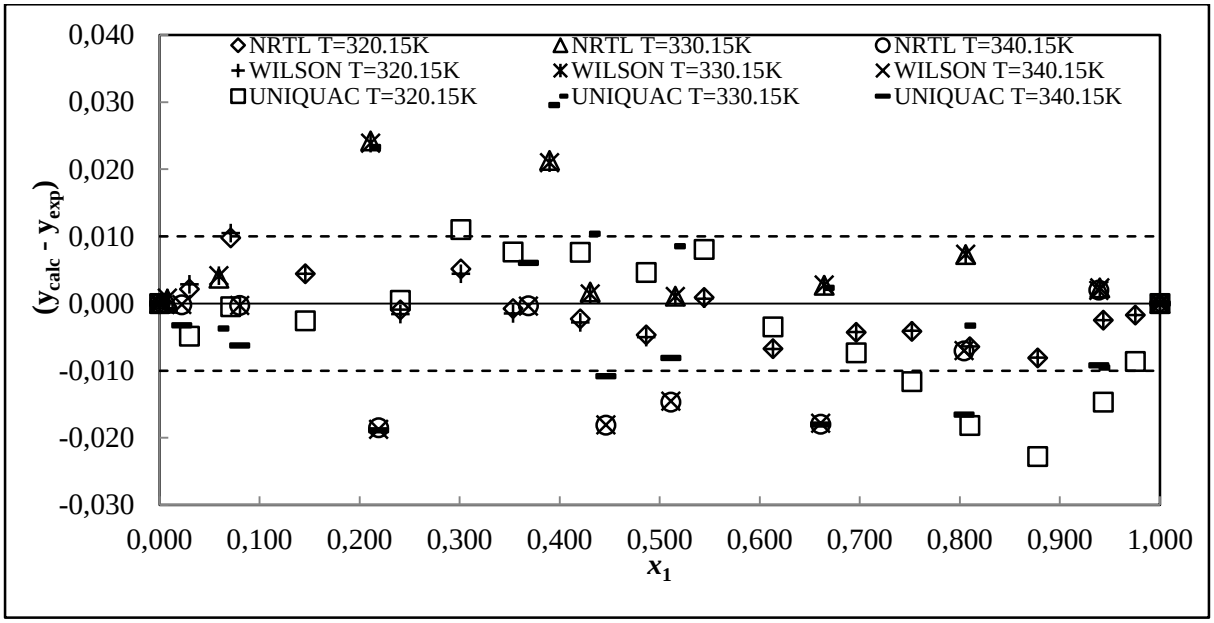

Figure 7-62: Point test for HOC EOS (activity coefficient model variation) y-residual for the DIPE (1) + 2, 2, 4-trimethylpentane (2) system at: 320.15K, 330.15K and 340.15K

Table 7-34: Results of the thermodynamic consistency testing for the DIPE (1) + 2, 2, 4-trimethylpentane (2) systems at 320.15, 330.15 and 340.15 K – Combined method; NTH EOS.

Model	T±0.10/K	Total points measured	Consistent points	(ΔP) AAD	(Δy_1) AAD
NRTL-NTH					
	320.15	18	18	0.52	0.003
	330.15	11	11	0.58	0.006
	340.15	11	11	0.61	0.010
Wilson-NTH					
	320.15	18	18	0.47	0.003
	330.15	11	11	0.59	0.006
	340.15	11	11	0.38	0.008
UNIQUAC-NTH					
	320.15	18	18	0.47	0.003
	330.15	11	11	0.59	0.006
	340.15	11	11	0.63	0.008

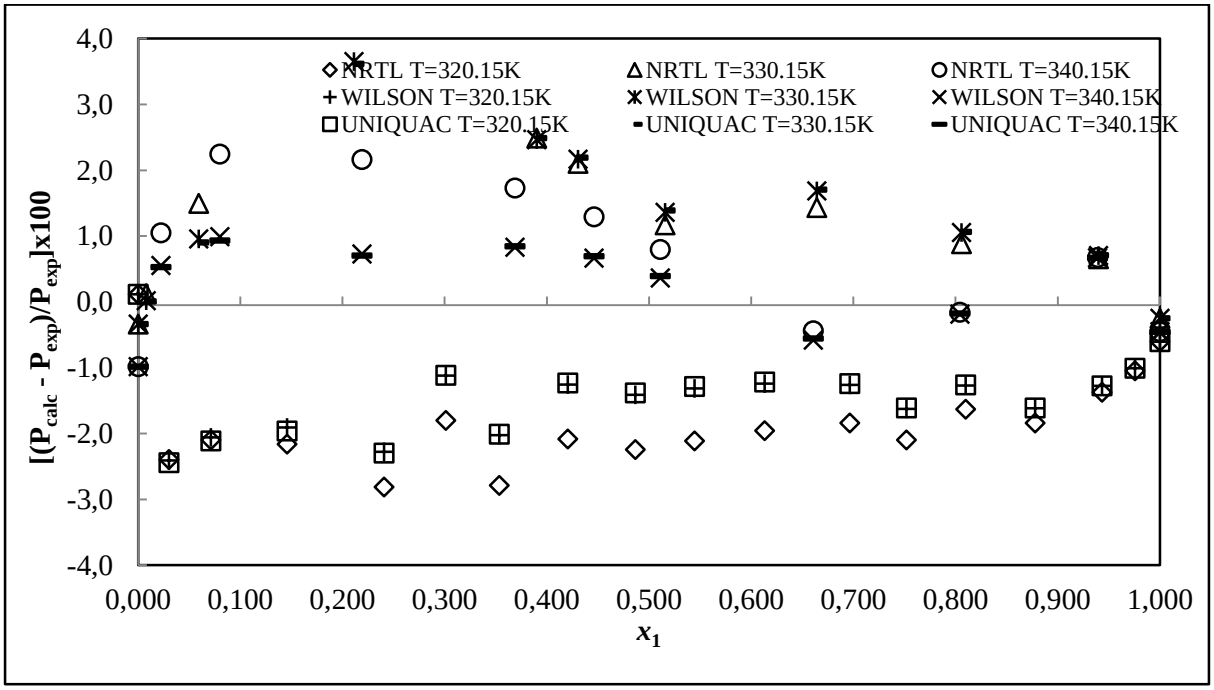

Figure 7-63: Point test for NTH EOS (activity coefficient model variation) P-residual for the DIPE (1) + 2, 2, 4-trimethylpentane (2) system at: 320.15K, 330.15K and 340.15K

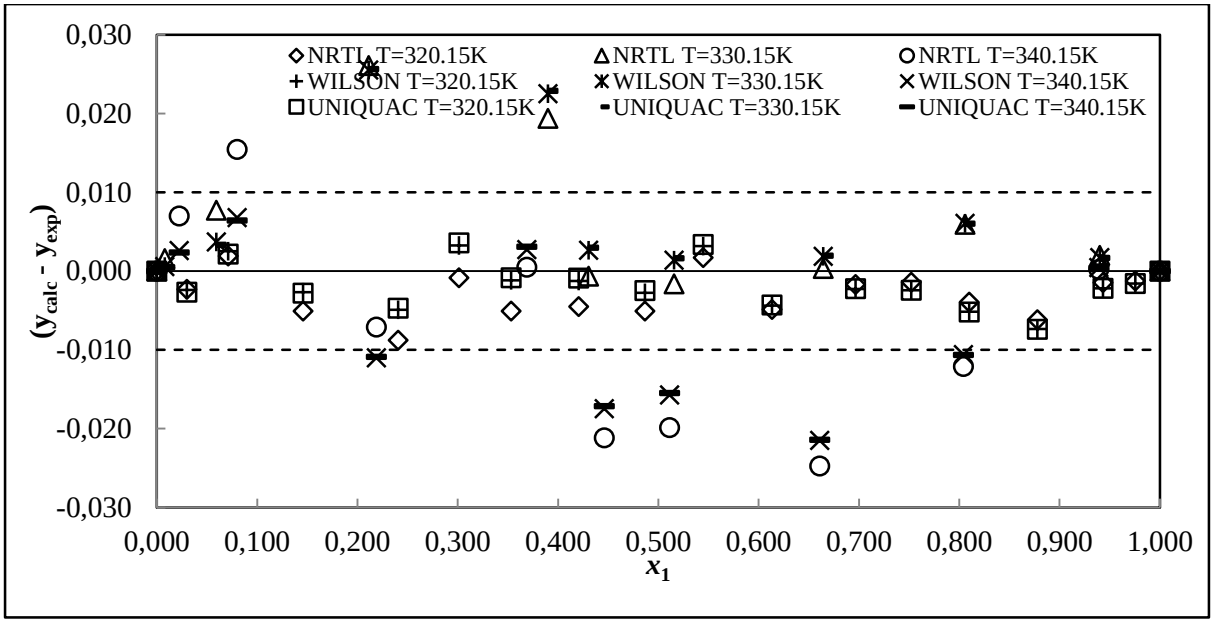

Figure 7-64: Point test for NTH EOS (activity coefficient model variation) y-residual for the DIPE (1) + 2, 2, 4-trimethylpentane (2) system at: 320.15K, 330.15K and 340.15K

Table 7-35: Results of the thermodynamic consistency testing for the DIPE (1) + 2, 2, 4-trimethylpentane (2) systems at 320.15, 330.15 and 340.15 K – Direct method.

Model	T±0.10/K	Total points measured	Consistent points	(ΔP) AAD	(Δy_1) AAD
PR-MC-WS-NRTL					
	320.15	18	18	0.21	0.003
	330.15	11	11	0.53	0.005
	340.15	11	11	0.53	0.008
PR-MC-WS-Wilson					
	320.15	18	18	0.28	0.003
	330.15	11	11	0.53	0.005
	340.15	11	11	0.52	0.008
PR-MC-WS-UNIQUAC					
	320.15	18	18	0.28	0.003
	330.15	11	11	0.53	0.005
	340.15	11	11	0.52	0.008

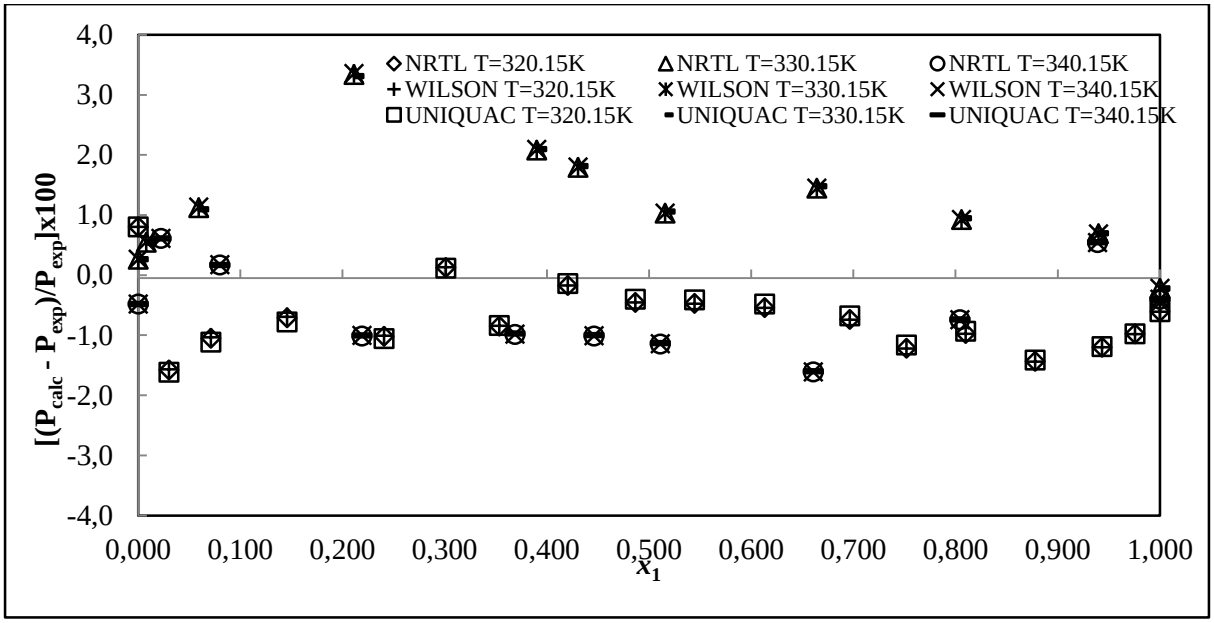

Figure 7-65: Point test for PR EOS (activity coefficient model variation) P-residual for the DIPE (1) + 2, 2, 4-trimethylpentane (2) system at: 320.15K, 330.15K and 340.15K

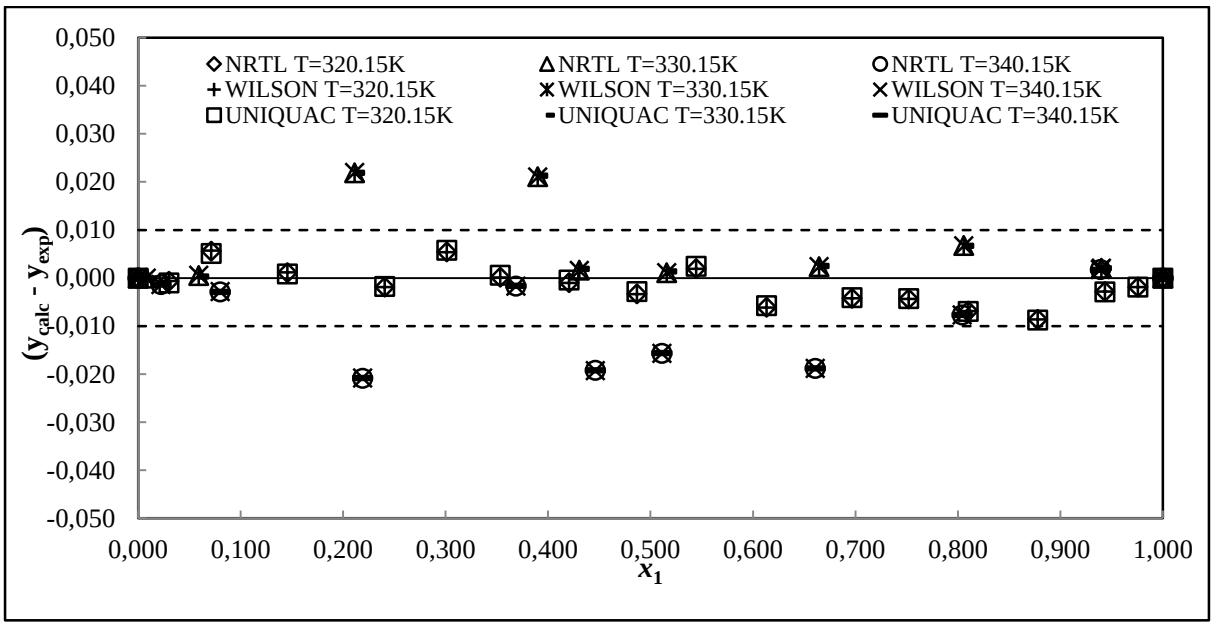

Figure 7-66: Point test for PR EOS (activity coefficient model variation) y-residual for the DIPE (1) + 2, 2, 4-trimethylpentane (2) system at: 320.15K, 330.15K and 340.15K

7.7.5. Consistency Test for the DIPE (1) + 1-propanol (2)

The models (for both the combined and direct method) generally provided decent data fit for the DIPE (1) + 1-propanol (2) system. The ΔP and Δ*y* values for this system are given in Tables 7-36 to 7-38; presenting also a summary of the point test analysis for the three data sets. The average vapour phase deviations were found to be less than the point test margin of 0.01 with all the models used for the

reduction of the 320.15, 330.15 and 340.15 K isotherm data sets. Higher average pressure deviations resulted upon variation of the activity coefficient model to Wilson for the PR EOS combination. The PR-MC-WS-Wilson thus gave the highest deviation at 340.15 K of 2.20. Figures 7-67 to 7-72 show the pressure-residuals and y_i-residuals of the point test for each model combination used excluding the plot for the RKS EOS model results which is shown in Appendix A. Changing the activity coefficient model (for the combined method regression; seen in Figures 7-67 to 7-70) resulted in an almost negligible variation in the results obtained. All the models fit the data without any anomalous behaviour, with reasonably good scatter about the *x*-axis for the P-residuals. Therefore it is possible to evaluate the data on the basis of the y_i-residuals. The *y*i-residuals also scattered reasonably well about the *x*-axis. This data set is therefore considered to be thermodynamically consistent with all the points included in the final reduction analyses.

Table 7-36: Results of the thermodynamic consistency testing for the DIPE (1) + 1-propanol (2) systems at 320.15, 330.15 and 340.15 K – Combined method; HOC EOS.

Model	**T±0.10/K**	**Total points measured**	**Consistent points**	**(ΔP) AAD**	**(Δy_i) AAD**
NRTL-HOC					
	320.15	16	16	0.43	0.004
	330.15	12	12	0.27	0.004
	340.15	12	12	1.15	0.005
Wilson-HOC					
	320.15	16	16	0.45	0.005
	330.15	12	12	0.17	0.004
	340.15	12	12	1.16	0.005
UNIQUAC-HOC					
	320.15	16	16	0.46	0.004
	330.15	12	12	0.32	0.005
	340.15	12	12	1.13	0.005

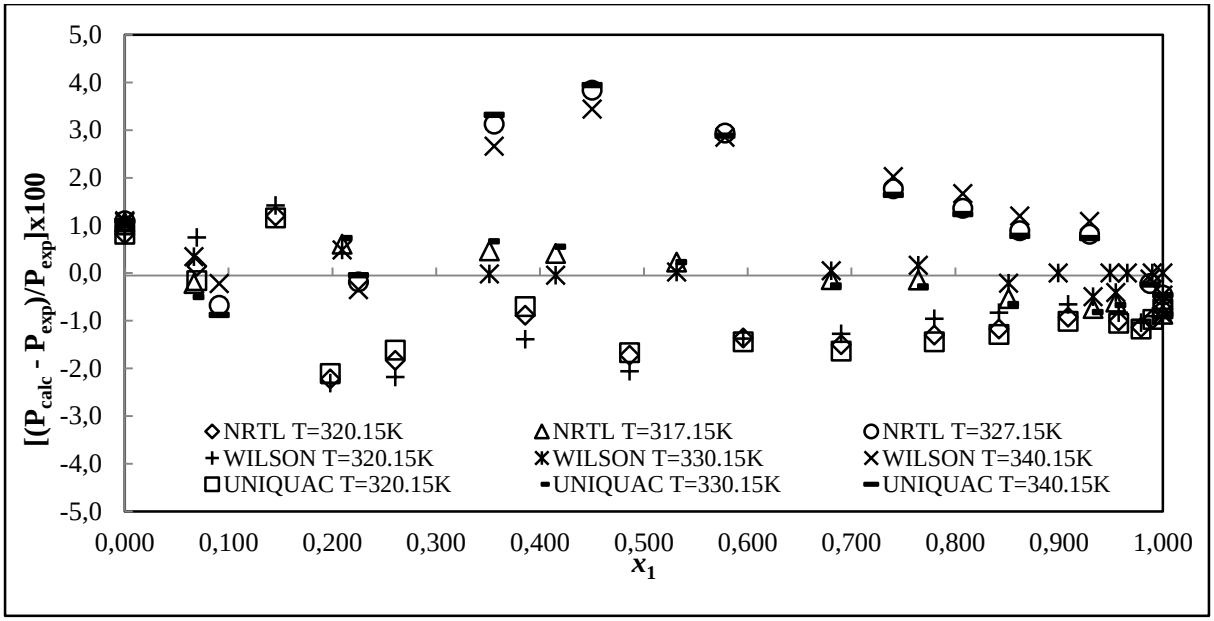

Figure 7-67: Point test for HOC EOS (activity coefficient model variation) P-residual for the DIPE (1) + 1-propanol (2) system at: 320.15K, 330.15K and 340.15K

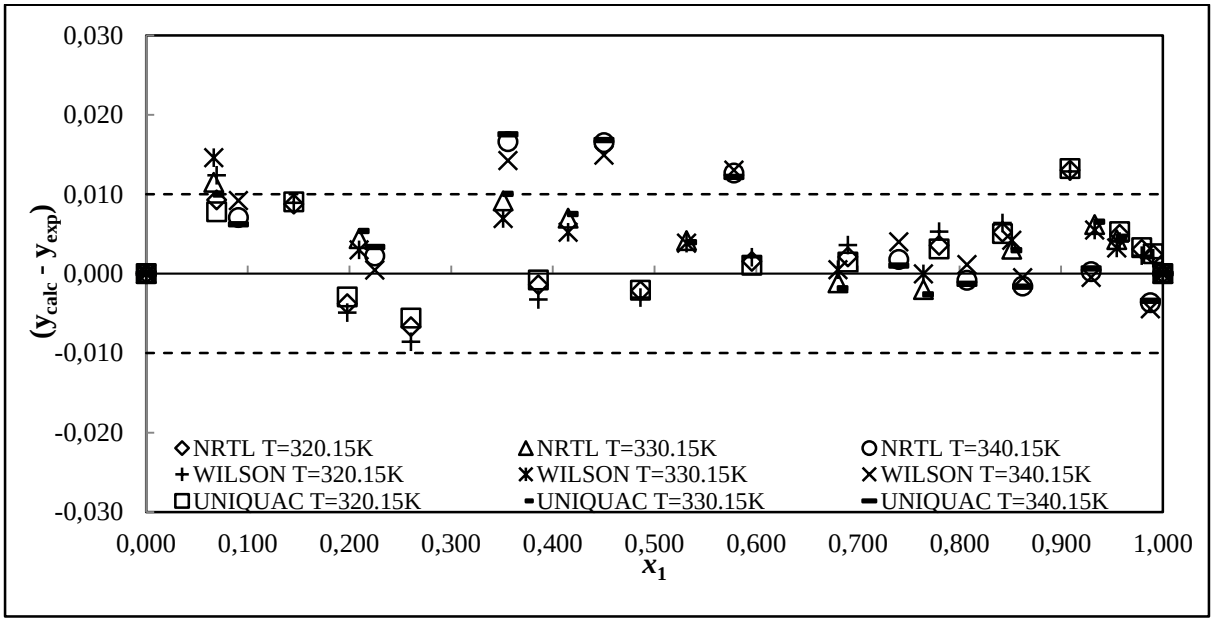

Figure 7-68: Point test for HOC EOS (activity coefficient model variation) y-residual for the DIPE (1) + 1-propanol (2) system at: 320.15K, 330.15K and 340.15K

Table 7-37: Results of the thermodynamic consistency testing for the DIPE (1) + 1-propanol (2) systems at 320.15, 330.15 and 340.15 K – Combined method; NTH EOS.

Model	T±0.10/K	Total points measured	Consistent points	(ΔP) AAD	(Δy_1) AAD
NRTL-NTH					
	320.15	16	16	0.30	0.004
	330.15	12	12	0.19	0.004
	340.15	12	12	0.96	0.004
Wilson-NTH					
	320.15	16	16	0.32	0.005
	330.15	12	12	0.17	0.004
	340.15	12	12	0.92	0.006
UNIQUAC-NTH					
	320.15	16	16	0.36	0.004
	330.15	12	12	0.32	0.005
	340.15	12	12	0.92	0.005

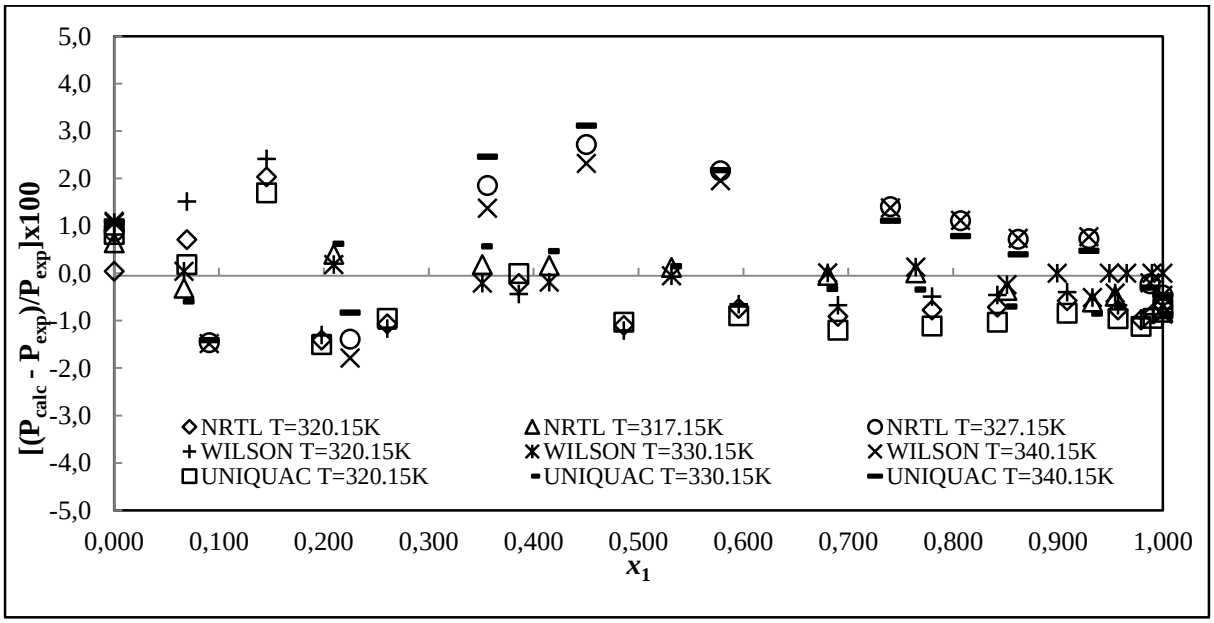

Figure 7-69: Point test for NTH EOS (activity coefficient model variation) P-residual for the DIPE (1) + 1-propanol (2) system at: 320.15K, 330.15K and 340.15K

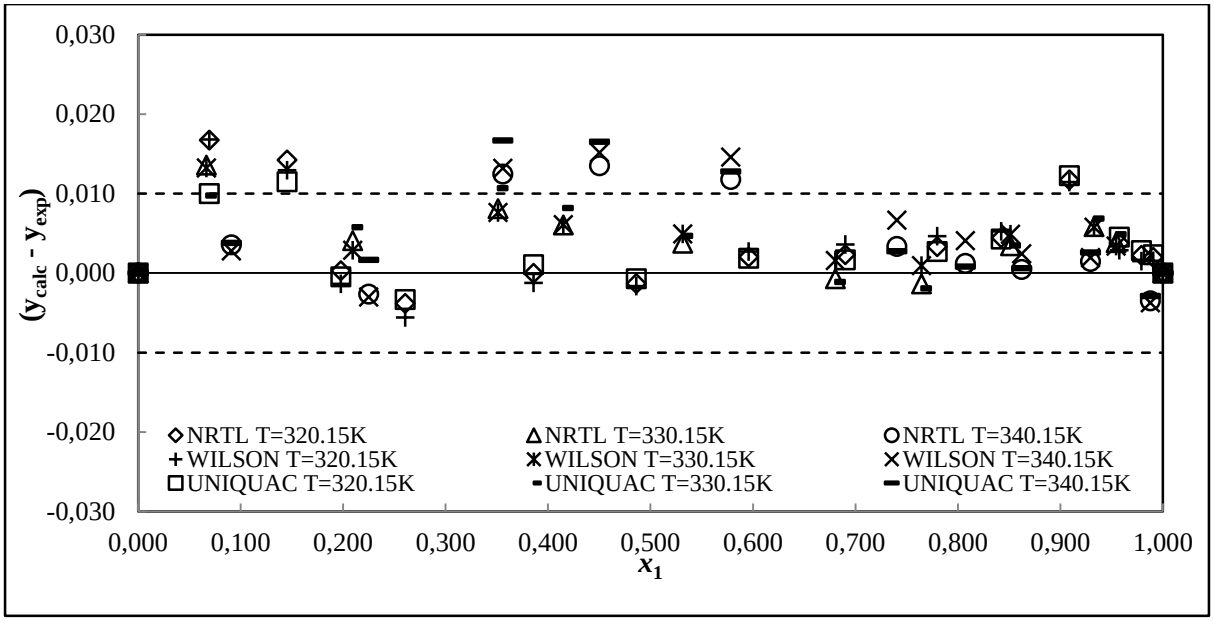

Figure 7-70: Point test for NTH EOS (activity coefficient model variation) y-residual for the DIPE (1) + 1-propanol (2) system at: 320.15K, 330.15K and 340.15K

Table 7-38: Results of the thermodynamic consistency testing for the DIPE (1) + 1-propanol (2) systems at 320.15, 330.15 and 340.15 K – Direct method.

Model	**T±0.10/K**	**Total points measured**	**Consistent points**	**(ΔP) AAD**	**(Δy_1) AAD**
PR-MC-WS-NRTL					
	320.15	16	16	0.37	0.005
	330.15	12	12	0.19	0.003
	340.15	12	12	0.67	0.004
PR-MC-WS-Wilson					
	320.15	16	16	0.89	0.012
	330.15	12	12	1.30	0.008
	340.15	12	12	2.20	0.011
PR-MC-WS-UNIQUAC					
	320.15	16	16	0.22	0.004
	330.15	12	12	0.28	0.005
	340.15	12	12	0.42	0.004

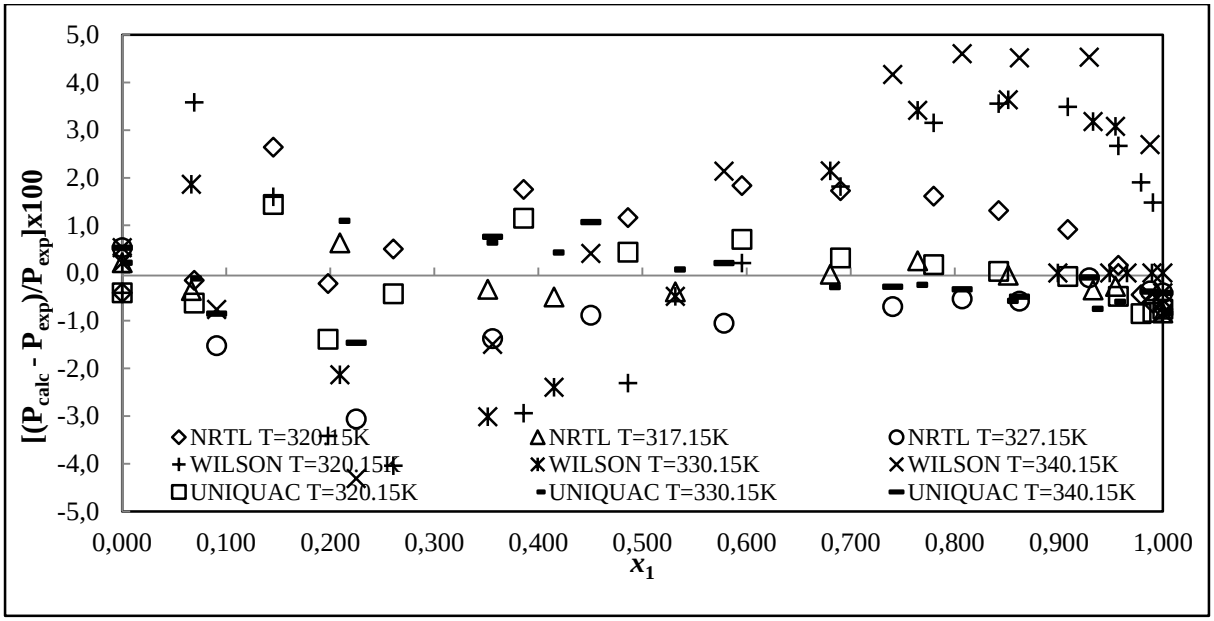

Figure 7-71: Point test for PR EOS (activity coefficient model variation) P-residual for the DIPE (1) + 1-propanol (2) system at: 320.15K, 330.15K and 340.15K

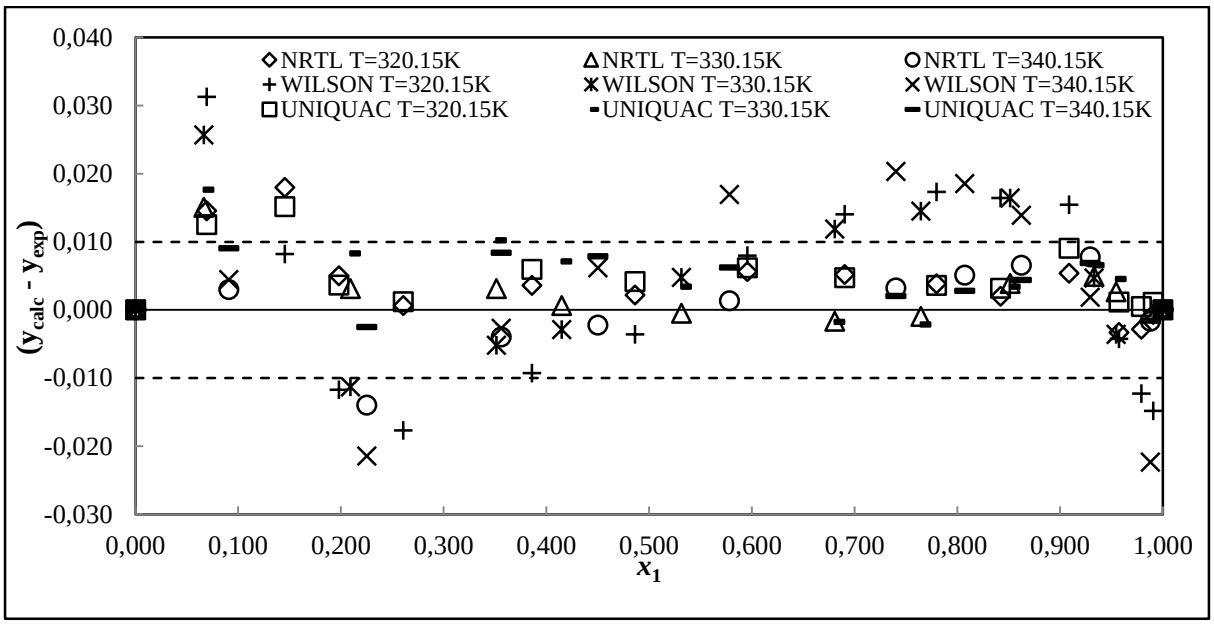

Figure 7-72: Point test for PR EOS (activity coefficient model variation) *y*-residual for the DIPE (1) + 1-propanol (2) system at: 320.15K, 330.15K and 340.15K

7.7.6. Consistency Test for the DIPE (1) + 2-butanol (2)

The ΔP and Δ*y* values for this system are presented in Tables 7-39 to 7-41. Pressure-residuals and y_i-residuals for these data sets are plotted in Figures 7-73 to 7-78. A summary of the point test consistency test analysis for the three temperature isotherms are also given in Tables 7-39 to 7-41.

Fairly satisfactory data correlation was provided by the models for the DIPE (1) + 2-butanol (2) system. The PR EOS and the RKS EOS model combinations (with varying local activity coefficient models) for the direct method gave the lowest vapour phase deviations. For the combined method the HOC EOS with varying activity coefficient models had a poor effect on the vapour phase deviation. The Wilson-HOC gave a vapour phase deviation of 0.012 at the 340.15 K data set, which is more than the point test margin of 0.01. However, varying the activity coefficient model for the NTH EOS had the opposite effect as the NRTL-NTH model had resulted in a vapour phase deviation of 0.013 while the Wilson and UNIQUAC models gave average vapour phase deviations less than the point test margin of 0.01. Since these deviations are quite marginal, this data set was considered to be thermodynamically consistent and all points were included in the final regression analyses. Additionally the models correlated the data without any anomalous behaviour exhibiting decent scatter about the *x*-axis for the pressure-residuals – the rationale behind the evaluation of the data using the $\underline{y}_i$-residuals. The y_i-residuals also scattered reasonably well about the *x*-axis. RKS EOS model results are is shown in Appendix A.

Table 7-39: Results of the thermodynamic consistency testing for the DIPE (1) + 2-butanol (2) systems at 320.15, 330.15 and 340.15 K – Combined method; HOC EOS.

Model	**T±0.10/K**	**Total points measured**	**Consistent points**	**(ΔP) AAD**	**(Δy_1) AAD**
NRTL-HOC					
	320.15	17	17	0.54	0.004
	330.15	16	16	0.32	0.003
	340.15	16	16	0.91	0.009
Wilson-HOC					
	320.15	17	17	0.58	0.004
	330.15	16	16	0.29	0.003
	340.15	16	16	0.89	0.012
UNIQUAC-HOC					
	320.15	17	17	0.61	0.004
	330.15	16	16	0.32	0.003
	340.15	16	16	0.91	0.009

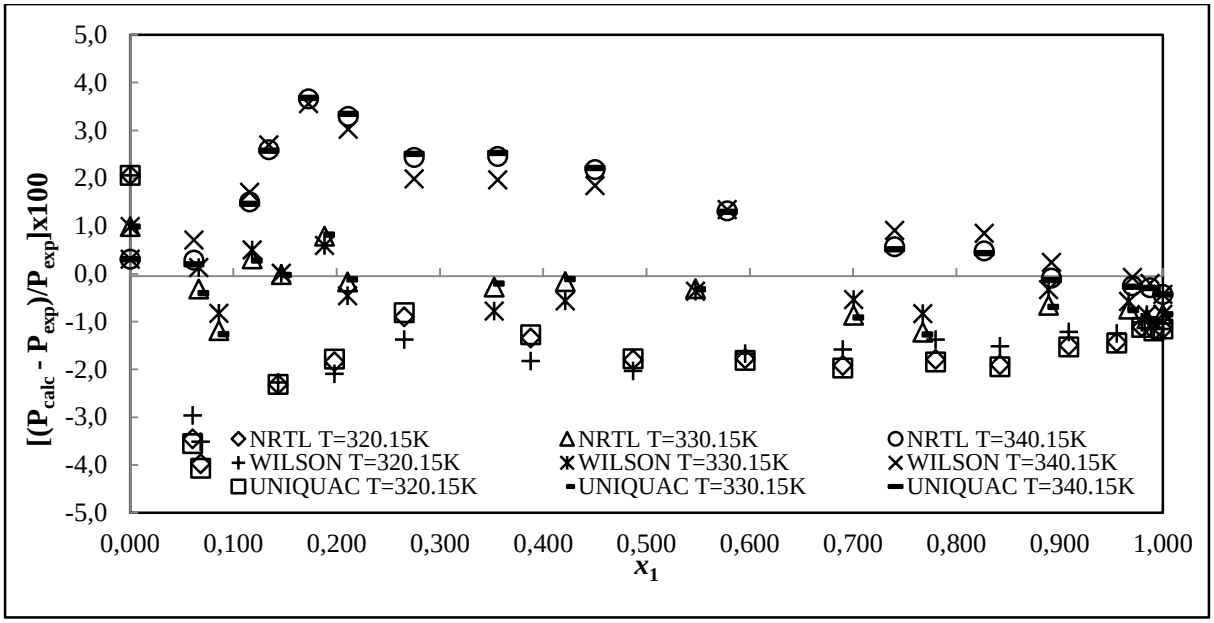

Figure 7-73: Point test for HOC EOS (activity coefficient model variation) P-residual for the DIPE (1) + 2-butanol (2) system at: 320.15K, 330.15K and 340.15K

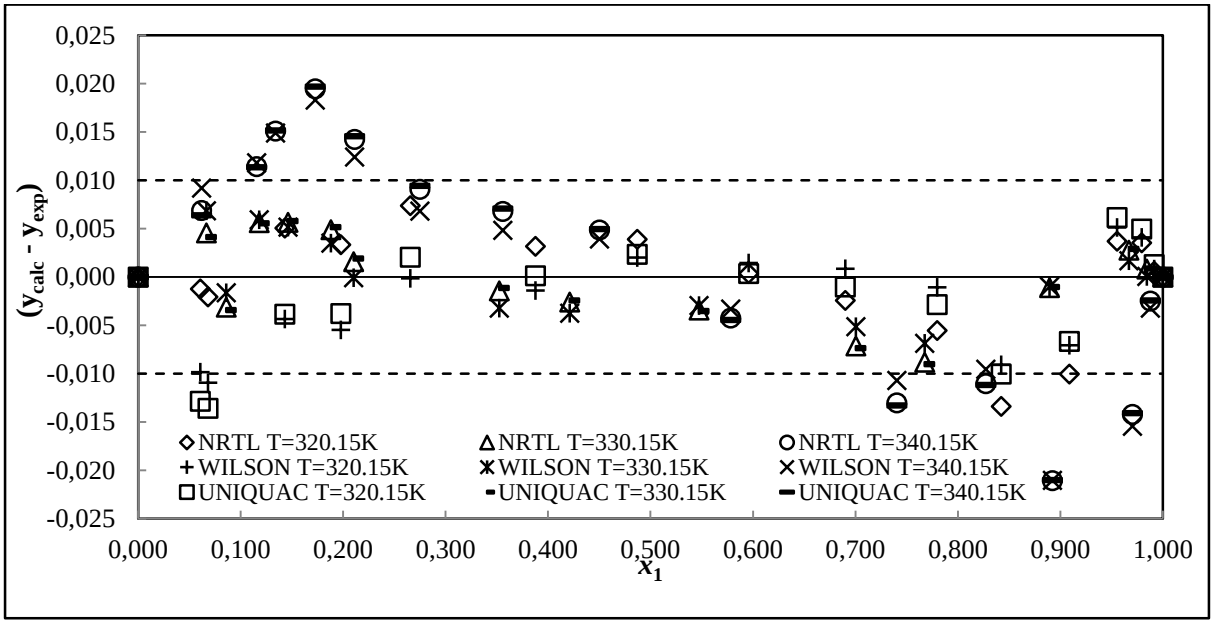

Figure 7-74: Point test for HOC EOS (activity coefficient model variation) y-residual for the DIPE (1) + 2-butanol (2) system at: 320.15K, 330.15K and 340.15K

Table 7-40: Results of the thermodynamic consistency testing for the DIPE (1) + 2-butanol (2) systems at 320.15, 330.15 and 340.15 K – Combined method; NTH EOS.

Model	T±0.10/K	Total points measured	Consistent points	(ΔP) AAD	(Δy_1) AAD
NRTL-NTH					
	320.15	17	17	0.74	0.005
	330.15	16	16	0.27	0.003
	340.15	16	16	1.46	0.013
Wilson-NTH					
	320.15	17	17	0.37	0.005
	330.15	16	16	0.26	0.003
	340.15	16	16	0.71	0.005
UNIQUAC-NTH					
	320.15	17	17	0.44	0.005
	330.15	16	16	0.30	0.003
	340.15	16	16	0.66	0.004

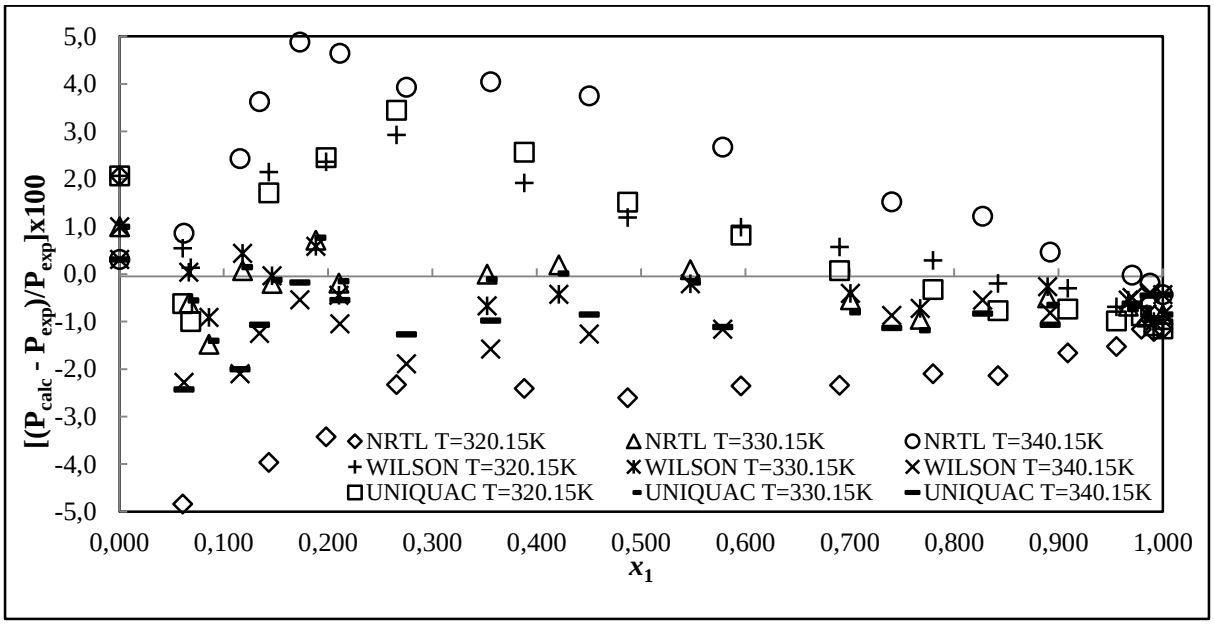

Figure 7-75: Point test for NTH EOS (activity coefficient model variation) P-residual for the DIPE (1) + 2-butanol (2) system at: 320.15K, 330.15K and 340.15K

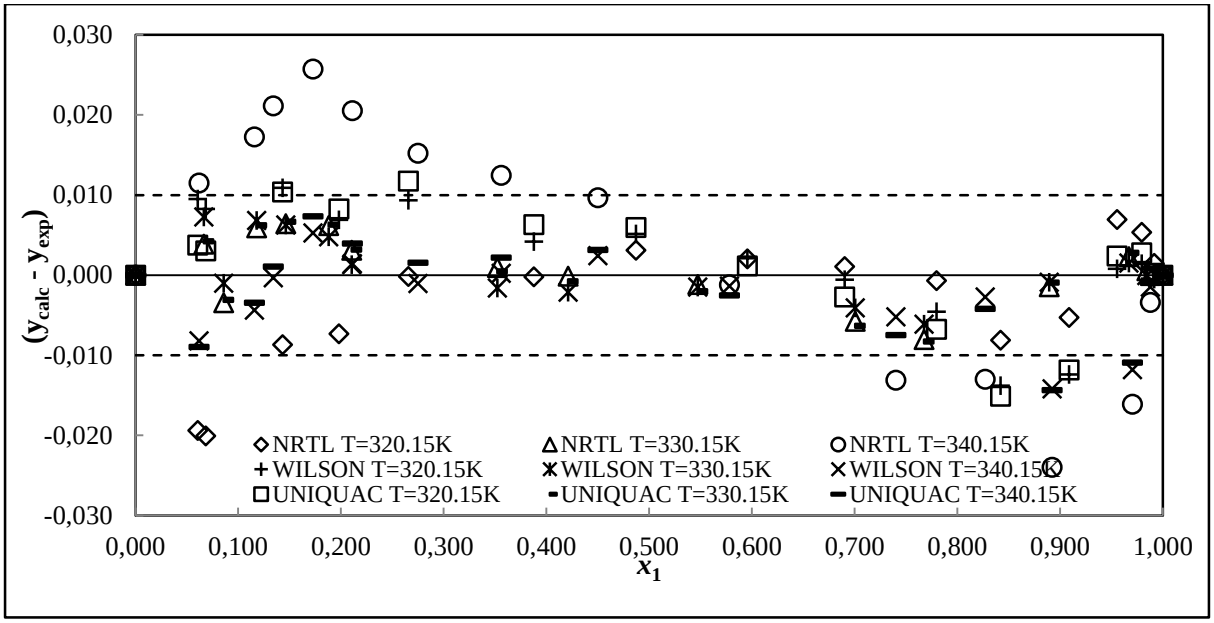

Figure 7-76: Point test for NTH EOS (activity coefficient model variation) y-residual for the DIPE (1) + 2-butanol (2) system at: 320.15K, 330.15K and 340.15K

Table 7-41: Results of the thermodynamic consistency testing for the DIPE (1) + 2-butanol (2) systems at 320.15, 330.15 and 340.15 K – Direct method.

Model	T±0.10/K	Total points measured	Consistent points	(ΔP) AAD	(Δy_1) AAD
PR-MC-WS-NRTL					
	320.15	17	17	0.19	0.007
	330.15	16	16	0.35	0.008
	340.15	16	16	0.44	0.008
PR-MC-WS-Wilson					
	320.15	17	17	0.40	0.007
	330.15	16	16	0.33	0.007
	340.15	16	16	0.52	0.008
PR-MC-WS-UNIQUAC					
	320.15	17	17	0.34	0.007
	330.15	16	16	0.32	0.008
	340.15	16	16	0.33	0.008

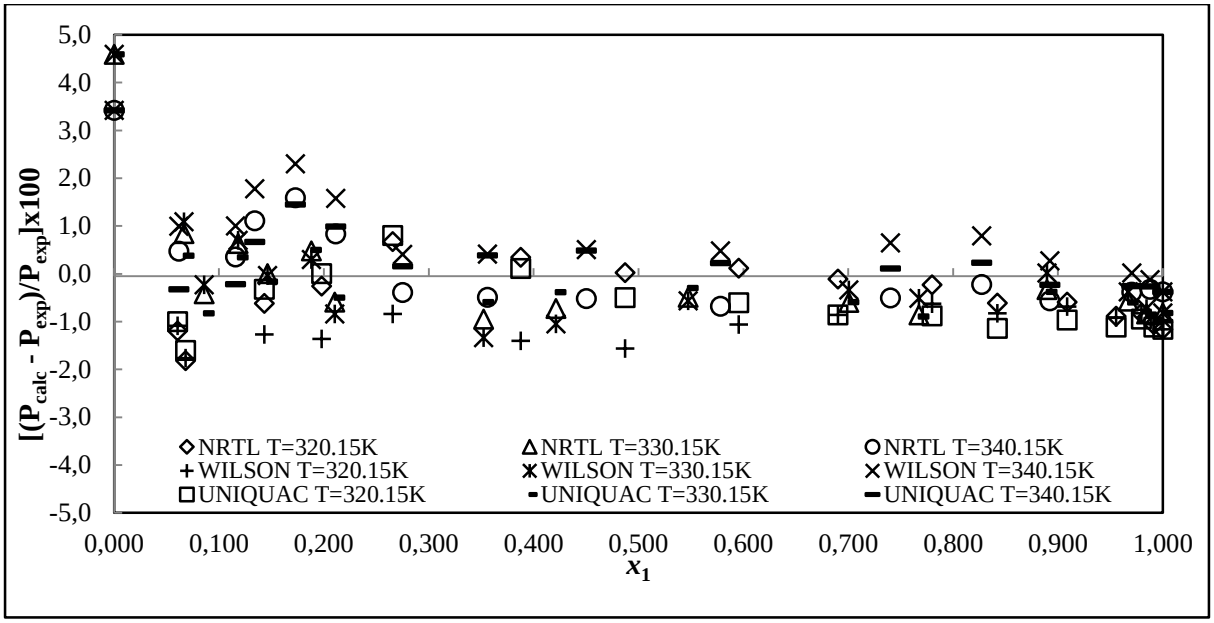

Figure 7-77: Point test for PR EOS (activity coefficient model variation) P-residual for the DIPE (1) + 2-butanol (2) system at: 320.15K, 330.15K and 340.15K

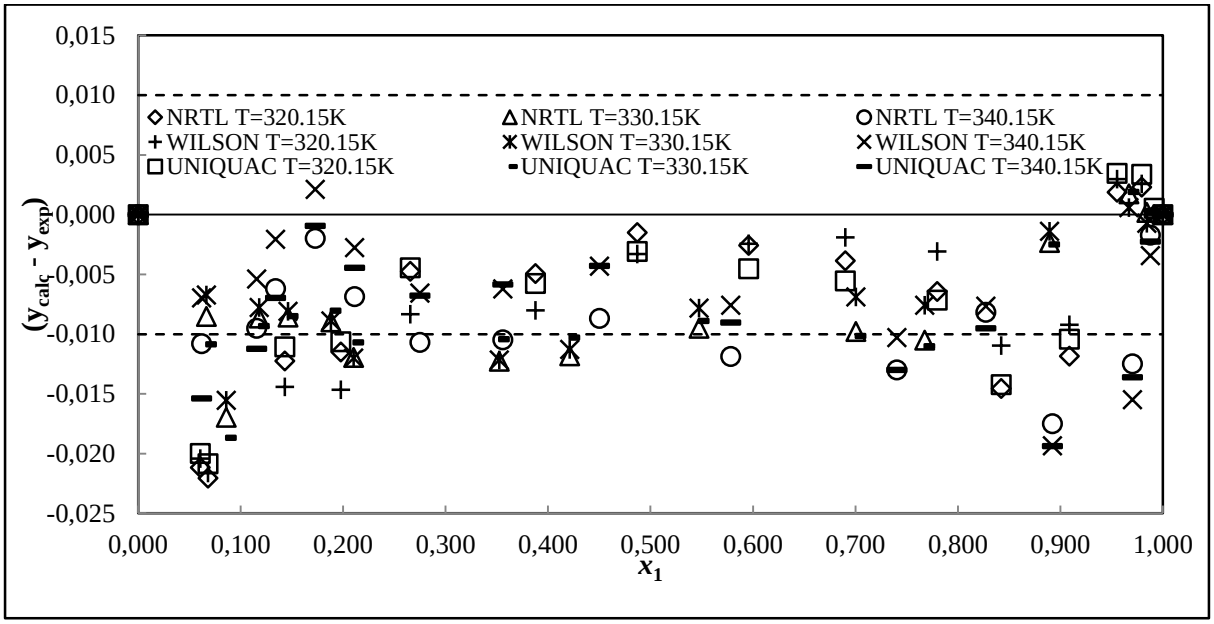

Figure 7-78: Point test for PR EOS (activity coefficient model variation) y-residual for the DIPE (1) + 2-butanol (2) system at: 320.15K, 330.15K and 340.15K

7.8. Relative Volatility

The mathematical expression for relative volatility in a binary VLE system with the species *i* and *j* is given as:

$$\alpha_{ij} = \frac{\frac{y_i}{x_i}}{\frac{y_j}{x_j}} = \frac{K_i}{K_j} \tag{7-3}$$

where, α is the relative volatility, x and y are both the liquid and vapour phase compositions respectively with the subscript *i* and *j* referring to the components *i* and *j*. K is the distribution ratio of vapour-liquid.

For chemical mixtures to be separated by distillation, relative volatility plays a significant role in the process. Chemical mixtures are only separated in a conventional distillation column by a measure of degree pertaining to relative volatility of the chemical species in the mixture. Chemical species having similar relative volatility, where it tends toward a unity, require large amounts of energy and an enumerable number of equilibrium stages in a conventional distillation column for separation. Moreover, a large difference in the relative volatility of chemical species indicates that is would be easier to distil the two compounds. When α_{ij} equals a unity, the two chemical species cannot be separated by conventional distillation. This is regardless of the number of equilibrium stages in the separation column and the energy input to the system. Such conditions indicate that the system has reached an azeotropic composition.

The 2, 2, 4-trimethylpentane (1) + 1-pentanol (2) and di-isopropyl ether (1) + 1-propanol (2) systems measured in this study both exhibit azeotropic behaviour at the respective isotherm temperatures. The relative volatility for all the measured isothermal VLE systems is presented in Appendix B.

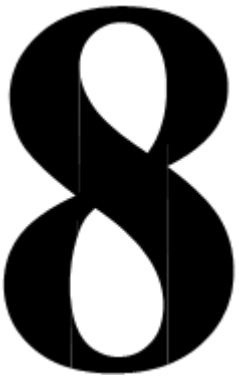

Chapter Eight

CONCLUSION

8.1. Experimental aspects

Experimental measurements and thermodynamic modeling of phase equilibrium data are essential for the optimum design, construction, commissioning and simulation of many industrial separation processes. The objective of this study was to investigate the phase equilibrium behaviour of systems involving oxygenated ether-alcohol and octane containing compounds for the ongoing research of biofuels. A survey of reliable literature sources was undertaken to determine the binary systems of industrial relevance for which data were unavailable. This assisted in determining that isothermal VLE measurements were required. Isothermal VLE data were then obtained for the following previously unmeasured binary systems (in addition to pure component vapour pressure measurements and the test system - cyclohexane + ethanol at 323.15K):

1) MTBE (1) + 1-pentanol (2) at 350.15, 360.15 and 370.15K
2) MTBE (1) + 2, 2, 4-trimethylpentane (2) at 307.15,317.15 and 327.15K
3) 2, 2, 4-Trimethylpentane (1) + 1-pentanol (2) at 307.15, 317.15 and 327.15 K
4) DIPE (1) + 2,2,4-trimethylpentane (2) at 320.15, 330.15 and 340.15K
5) DIPE (1) + 1-propanol (2) at 320.15, 330.15 and 340.15K
6) DIPE (1) + 2-butanol (2) at 320.15, 330.15 and 340.15K

The VLE data were measured with the modified apparatus of Raal (Raal and Mühlbauer, 1998). The modification, introduced by Ndlovu (2005), catered for the measurement of VLLE data by allowing a vapour sample to be sent directly to a gas chromatograph for composition analysis. However, for the purposes of this study, the modification by Ndlovu (2005) was removed as the systems measured in this project did not exhibit any VLLE behaviour. This became more evident from the PSRK and UNIFAC predictions that were performed to assess the system behaviour before undertaking measurements. The cyclohexane + ethanol test system at 323.15K (to confirm the proper functioning

of the apparatus and experimental procedures) was found to be in agreement with the data of Joseph et al. (2001). The uncertainty in pressure measurements with the glass VLE apparatus was estimated to be ±0.1 kPa (with a confidence factor of k=2) and was controlled within approximately 0.07 kPa during operation. The uncertainty in temperature measurements was estimated to be ±0.1 kPa with a confidence factor of k=2. The estimated uncertainty in the mole fractions are 0.007, 0.006 and 0.008 for the binary systems of 2, 2, 4-trimethylpentane + 1-pentanol, MTBE + 1-pentanol and MTBE + 2, 2, 4-trimethylpentane respectively. The uncertainty in molar composition measurements were ±0.012, ±0.001 and ±0.018 for the binary systems of DIPE + 2, 2, 4-trimethylpentane, DIPE + 1-propanol and DIPE + 2-butanol respectively.

8.2. Theoretical aspects

The measured vapour pressure data were regressed to obtain pure component parameters for the Antoine equation. These parameters were utilised in the binary VLE data regression. The experimental activity coefficients could not be obtained by using the conventional calculation procedure. This was attributed to the strong association that occurs with such systems under investigation, exhibited even at low pressures. Therefore; thermodynamic models that incorporate association characteristics were used to correlate the isotherms in this research. The binary VLE data were modelled and tested for consistency using the thermodynamic principals outlined in previous chapters.

The experimental VLE data were regressed using two different methods: the combined method and the direct method. The vapour phase fugacity coefficients were calculated using the methods capable of describing associating systems that were available in Aspen Plus®. For the combined method the method of Hayden and O'Connell (1974), Nothnagel et al. (1973) was employed. For the direct method, the Soave-Redlich-Kwong (Redlich-Kwong, 1949 and Soave, 1972) and Peng Robinson (1976) equations of state was combined using the temperature dependent function (α) of Mathias and Copeman (1983) with the Wong-Sandler (1992) mixing rule was used.
For the liquid phase (in both the combined and direct methods), three local-composition based activity coefficient models were utilised: namely the Wilson (Wilson, 1964), NRTL (Renon and Prausnitz, 1968) and UNIQUAC (Abrams and Prausnitz, 1975) models.

Optimization of each model parameter was performed with the ordinary least squares regression algorithm, which utilises the experimental pressure and vapour compositions in its objective function. The majority of the systems exhibited smooth data and were well-fitted by the models, which was determined by the deviations between the measured data and those predicted by the model. A summary of the models that gave the best-fit for the data in this study are shown in Table 8-1. The

binary interaction parameters obtained for the various models from the regression are given in Section 7.4.2.

For the thermodynamic consistency testing, the point test of Van Ness et al. (1973, 1975 & 1982) was used. It was established that several data points had to be excluded in order for the test criteria to be met. These data points were not used in the final reduction analysis. Wherever the test criterion was not satisfied, the data were inconsistent, the models employed in the test were deemed inapplicable to the systems under investigation.

Table 8-1: Best-fit models for systems investigated

Systems Measured	Isotherm Temperatures / K	Best-fitting Models
MTBE + 1-pentanol	317.15	HOC-NRTL/HOC-WILSON/ HOC-UNIQUAC;NTH-NRTL/NTH-WILSON/ NTH-UNIQUAC
	327.15	PR-WS-NRTL/PR-Wilson/PR-UNIQUAC
MTBE + 2, 2, 4-trimethylpentane	307.15	HOC-NRTL/HOC-WILSON/ HOC-UNIQUAC;NTH-NRTL/NTH-WILSON/ NTH-UNIQUAC
	317.15	HOC-NRTL/HOC-WILSON/ HOC-UNIQUAC;NTH-NRTL/NTH-WILSON/ NTH-UNIQUAC
	327.15	HOC-NRTL/HOC-WILSON/ HOC-UNIQUAC;NTH-NRTL/NTH-WILSON/ NTH-UNIQUAC
2, 2, 4-trimethylpentane + 1-pentanol	350.15	NTH-Wilson/PR-WS-Wilson
	360.15	PR-Wilson
	370.15	NTH-NRTL/NTH-WILSON/ NTH-UNIQUAC;PR-WS-

		NRTL/PR-Wilson/PR-UNIQUAC
DIPE + 2, 2, 4-trimethylpentane	320.15	NTH-NRTL/NTH-WILSON/ NTH-UNIQUAC;PR-WS-NRTL/PR-Wilson/PR-UNIQUAC
	330.15	PR-WS-NRTL/PR-Wilson/PR-UNIQUAC
	340.15	HOC-NRTL/HOC-WILSON
DIPE + 1-propanol	320.15	HOC-NRTL/HOC UNIQUAC;NTH-NRTL/ NTH-UNIQUAC
	330.15	PR-NRTL
	340.15	HOC-Wilson; NTH-NRTL; PR-NRTL
DIPE + 2-butanol	320.15	HOC-NRTL/HOC-WILSON/ HOC-UNIQUAC
	330.15	HOC-NRTL/HOC-WILSON/ HOC-UNIQUAC;NTH-NRTL/NTH-WILSON/ NTH-UNIQUAC
	340.15	NTH-UNIQUAC

9

Chapter Nine

RECOMMENDATIONS

Phase equilibrium data prediction is arguably the most efficient and economical way to obtain phase data. However, the measurement of resourceful and accurate data plays a pivotal role toward phase equilibrium data. Apart from this, another key factor is that the experimental data validates the model/s utilised in regression and prediction analyses.

Therefore, the operation of the experimental equipment used for measurements should be operating at optimum conditions. If under any circumstances this is not so, further improvements must be recommended in order to produce the most accurate and reliable experimental data. The operation of the equipment used in this study revealed areas where further modifications could be facilitated that could possibly improve both the operation of the equipment in measuring VLE but also VLLE substantially and in a versatile manner. Additionally, due to the difficulty related to the measurement and computation of data involving associating systems, improvement in both the experimental techniques, models and the methods of correlation and reduction of the experimental data is required.

With the aforementioned areas of concern overviewed, an expansive approach of the modification recommendations are the following:

1) A pre-mixing chamber with a magnetic stirrer, positioned before the reboiler, should be incorporated. This chamber contents should be mixed (by magnetic stirring perhaps), and heated in order to raise the temperature of the chamber mixture close to the reboiler mixture temperature. This arrangement will insure that the returning condensate pre-mixes with the liquid from the liquid receiver before it mixes with the bulk liquid in the boiling chamber and could prevent the “flashing” of systems with high relative volatility.
2) Investigating the effect of the packing in the equilibrium chamber pertaining to the type, the size and depth of dispersion could possibly curb the “flashing” dilemma of the more volatile component of the binary mixture.

3) Alternative models that could perhaps provide smoother data fit can be applied to the measured systems with both the direct and combined methods. Different or even newly developed models that are capable of accommodating the association of polar compounds should be investigated.
4) The optimization of the parameters for the regression should take into account the parameter uncertainty in the estimates. Therefore the regression algorithm could be substituted with the maximum likelihood method as opposed to using that of least squares as it takes into account errors in all the experimental variables such as pressure, temperature, and both liquid and vapour phase composition. The least squares method takes in account pressure and vapour phase composition only and assumes that the other experimental values are known.
5) The use of heat capacity/heat of mixing data instead of merely using VLE data can significantly improve the reliability of the results. This is merely the utilisation of multi-property regression for the binary interaction parameter optimisation.
6) The investigation of VLE systems involving lengthier carbon chain compounds (>C6) with the conditions of temperature and pressure being varied should be undertaken.
7) Jackson and Wilsak (1995) surmise that statistical procedures should be implemented for the effects of experimental uncertainty in all the measured variables and that these uncertainties should be promoted for binding the final results where thermodynamic consistency testing is involved. The reason for this is that the inappropriate choice of models can bias the test results leading to error as contrasting results are obtained with different model choice pertaining to the activity coefficient and/or equation of state.

REFERENCES

(NIST), N. I. O. S. A. T. 1994. Guidelines for Evaluating and Expressing the Uncertainty of NIST Measurement Results. *Combined Standard Uncertainty.* Washington: U.S. Government Printing Office.

ABBOTT, M. & VAN NESS, H. 1982. *Classical Thermodynamics of Non-electrolyte*

Solutions: With Applications to Phase Equilibria., New York, McGraw-Hill.

ABBOTT, M. M. 1979. Cubic equations of state: an interpretive review.

ABBOTT, M. M. 1986. Low-pressure phase equilibria: Measurement of VLE. *Fluid Phase Equilibria,* 29**,** 193-207.

ABRAMS, D. S. & PRAUSNITZ, J. M. 1975. Statistical thermodynamics of liquid mixtures: a new expression for the excess Gibbs energy of partly or completely miscible systems. *AIChE Journal,* 21**,** 116-128.

AMBROSE, D. & SPRAKE, C. 1970. Thermodynamic properties of organic oxygen compounds XXV. Vapour pressures and normal boiling temperatures of aliphatic alcohols. *The Journal of Chemical Thermodynamics,* 2**,** 631-645.

ANDERKO, A. 1990. Equation-of-state methods for the modelling of phase equilibria. *Fluid Phase Equilibria,* 61**,** 145-225.

ANDERSON, T. & PRAUSNITZ, J. 1978. Application of the UNIQUAC equation to calculation of multicomponent phase equilibria. 1. Vapor-liquid equilibria. *Industrial & Engineering Chemistry Process Design and Development,* 17**,** 552-561.

APELBLAT, A. 2007. Erratum to "The concept of associated solutions in historical development: Part 1. The 1884–1984 period" [J. Mol. Liq. 128 (2006) 1–31]. *Journal of molecular liquids,* 130**,** 133–162.

ASHOUR, I. & ALY, G. 1996. Effect of computation techniques for equation of state binary interaction parameters on the prediction of binary VLE data. *Computers & chemical engineering,* 20**,** 79-91.

BARNICKI, S. D. June 2002. How Good are Your Data? Some thoughts on the measurement and

interpretation of vapor-liquid equilibrium.

BELL, S. 1999. Measurement good practice guide no. 11. A beginner's guide to uncertainty of measurement. Tech. rep., National Physical Laboratory, 1999. 3.2.

BERNATOVÁ, S. & WICHTERLE, I. 2001. Isothermal vapour–liquid equilibria in the ternary system tert-butyl methyl ether+ tert-butanol+ 2, 2, 4-trimethylpentane and the three binary subsystems. *Fluid phase equilibria,* 180**,** 235-245.

BLACK, C. 1958. Phase Equilibria in Binary and Multicomponent Systems. Modified van Laar-Type Equation. *Industrial & Engineering Chemistry,* 50**,** 403-412.

BONILLA-PETRICIOLET, A., SEGOVIA-HERNANDEZ, J. G., BRIONES-RAMIREZ, A. & GUTIERREZ-ANTONIO, C. Effect of adjusted parameters of NRTL model in design, optimization, and control of homogeneous azeotropic distillation columns. Proceedings of the 24th European Symposium on Applied Thermodynamics, 2009. 154-160.

BOWNATH, R. 2008. *The Use of n-Dodecane as a Solvent in the Extraction of Light Alcohols from Water*. MSc, University of Kwa-Zulu Natal.

CHAMORRO, C. R., MARTíN, M. A. C., VILLAMAÑÁN, M. A. & SEGOVIA, J. J. 2004. Characterization and modelling of a gasoline containing 1, 1-dimethylethyl methyl ether (MTBE), diisopropyl ether (DIPE) or 1, 1-dimethylpropyl methyl ether (TAME) as fuel oxygenate based on new isothermal binary vapour–liquid data. *Fluid phase equilibria,* 220**,** 103-110.

CHOLIŃSKI, J., SZAFRAŃSKI, A. & WYRZYKOWSKA-STANKIEWICZ, D. 1986. *Computer-aided second virial coefficient data for organic individual compounds and binary systems,* Warsaw, PWN-Polish Scientific Publishers.

CIDLINSKÝ, J. & POLAK, J. 1969. Saturated vapour pressures of some ethers. *Collection of Czechoslovak Chemical Communications,* 34**,** 1317-1321.

CLIFFORD, S. 2004. *Low-Pressure Vapour-Liquid Equilibrium and Molecular Simulation of Carboxylic Acids* MSc, University of KwaZulu-Natal

COTTRELL, F. 1919. ON THE DETERMINATION OF BOILING POINTS OF SOLUTIONS. *Journal of the American Chemical Society,* 41**,** 721-729.

COULSON, E., HALES, J. & HERINGTON, E. 1948. Fractional distillation. II. The use of dilute solutions of thiophene in benzene as test mixtures and a comparison with mixtures of benzene and ethylene dichloride. *Transactions of the Faraday Society,* 44**,** 636-644.

DA SILVA, R., CATALUÑA, R., MENEZES, E. W. D., SAMIOS, D. & PIATNICKI, C. M. S. 2005. Effect of additives on the antiknock properties and Reid vapor pressure of gasoline. *Fuel,* 84**,** 951-959.

DANNER, R. P. & GESS, M. A. 1990. A data base standard for the evaluation of vapor-liquid-equilibrium models. *Fluid Phase Equilibria,* 56**,** 285-301.

DAUBERT, T., SIBUL, H., STEBBINS, C. & KENDALL, R. Policies and Procedures Documenting Compilation, Prediction, and Correlation for DIPPR Data Compilation Project. American Institute of Chemical Engineers Symposium, 1990. 62-92.

DE HAAN, A. B., HEINE, A., FISCHER, K. & GMEHLING, J. 1995. Vapor-Liquid Equilibria and Excess Enthalpies for Octane+ N-Methylacetamide, Cyclooctane+ N-Methylacetamide, and Octane+ Acetic Anhydride at 125. degree. C. *Journal of Chemical and Engineering Data,* 40**,** 1228-1232.

DEITERS, U. K. & DE REUCK, K. 1999. Guidelines for publication of equations of state: I. Pure fluids. *Fluid Phase Equilibria,* 161**,** 205-219.

DYMOND, J. H. & SMITH, E. B. 1980. *The Virial Coefficients of Pure Gases and Mixtures,* New York, Oxford University Press.

FISCHER, K. & GMEHLING, J. 1994. Px and. gamma.. infin. Data for the Different Binary Butanol-Water Systems at 50. degree. C. *Journal of Chemical and Engineering Data,* 39**,** 309-315.

FREDENSLUND, A., GMEHLING, J. & RASMUSSEN, P. 1977. Vapor-Liquid equilibrium using UNIFAC a group-contribution method. *Elsevier, Amsterdam*.

FREDENSLUND, J. G., P. RASMUSSEN 1977. *Vapor-liquid equilibria using UNIFAC: a group-contribution method,* Englewood Cliffs, New Jersey, Elsevier.

FU, Y.-H. & SANDLER, S. I. 1995. A simplified SAFT equation of state for associating compounds and mixtures. *Industrial & engineering chemistry research,* 34**,** 1897-1909.

GESS, M. A., DANNER, R. P. & NAGVEKAR, M. 1991. *Thermodynamic analysis of Vapor-liquid equilibria: Recommended models and a standard data base*, Design Institute for Physical Property Data. American Institute of Chemical Engineers.

GHOSH, P. 1999. Prediction of Vapor-Liquid Equilibria Using Peng-Robinson and Soave-Redlich-Kwong Equations of State. *Chemical engineering & technology,* 22**,** 379-399.

GIBBS, R. E. & VAN NESS, H. C. 1972. Vapor-liquid equilibria from total-pressure measurements. A new apparatus. *Industrial & Engineering Chemistry Fundamentals,* 11**,** 410-413.

GILLESPIE, D. 1946. Vapor-liquid equilibrium still for miscible liquids. *Industrial & Engineering Chemistry Analytical Edition,* 18**,** 575-577.

GMEHLING, J. 1999. The Basis for the Synthesis, Design and Optimization of Thermal Separation Processes. *In:* LETCHER, T. M. (ed.) *Chemical Thermodynamics: A Chemistry for the 21st Century.* Oxford: Blackwell Science.

GMEHLING, J. 2003. Potential of group contribution methods for the prediction of phase equilibria and excess properties of complex mixtures. *Pure and applied chemistry,* 75**,** 875-888.

GMEHLING, J. & ONKEN, U. 1977-1982. *Vapor-Liquid Equilibrium Data Collection,* Frankurt/Main.

HALA, E., PICK, J., FRIED, V. & VILIM, O. 1958. *Vapour-Liquid Equilibrium,* Oxford, London, Pergamon Press.

HALA, E., PICK, J., FRIED, V. & VILIM, O. 1967. *Vapour-Liquid Equilibrium,* Oxford, London, Pergamon Press.

HARLACHER, E. A. & BRAUN, W. G. 1970. A Four-Parameter Extension of the Theorem of Corresponding States. *Industrial & Engineering Chemistry Process Design and Development,* 9**,** 479-483.

HAYDEN, J. G. & O'CONNELL, J. P. 1975. A generalized method for predicting second virial coefficients. *Industrial & Engineering Chemistry Process Design and Development,* 14**,** 209-216.

HEERTJIES, P. M. 1960. Determination of Vapour-Liquid Equilibrium of Binary Mixtures. *Chemical and Process Engineering,* 41**,** 385-386.

HERNÁNDEZ-GARDUZA, O., GARCíA-SÁNCHEZ, F. & NEAU, E. 2001. Generalization of composition-dependent mixing rules for multicomponent systems: prediction of vapor–liquid and liquid–liquid equilibria. *Chemical Engineering Journal,* 84**,** 283-294.

HIRAWAN, R. 2007. *Development of a Thermodynamic Model for the Purification of 1-Hexene.* MSc, University of KwaZulu-Natal.

HORSTMANN, S., JABŁONIEC, A., KRAFCZYK, J., FISCHER, K. & GMEHLING, J. 2005. PSRK group contribution equation of state: comprehensive revision and extension IV, including critical constants and α-function parameters for 1000 components. *Fluid Phase Equilibria,* 227**,** 157-164.

HWANG, I.-C., PARK, S.-J. & CHOI, J.-S. 2008. Liquid–liquid equilibria for the binary system of di-isopropyl ether (DIPE)+ water in between 288.15 and 323.15 K and the ternary systems of DIPE+ water+ C< sub> 1</sub>–C< sub> 4</sub> alcohols at 298.15 K. *Fluid Phase Equilibria,* 269**,** 1-5.

INOUE, M., AZUMI, K. & SUZUKI, N. 1975. A new vapor pressure assembly for static vapor-liquid equilibrium. *Industrial & Engineering Chemistry Fundamentals,* 14**,** 312-314.

IWARERE, S. 2009. *Measurement of Phase Equilibria for Oxygenated Hydrocarbon Systems.* MSc, University of KwaZulu-Natal.

JACKSON, P. L. & WILSAK, R. A. 1995. Thermodynamic consistency tests based on the Gibbs-Duhem equation applied to isothermal, binary vapor-liquid equilibrium data: data evaluation and model testing. *Fluid Phase Equilibria,* 103**,** 155-197.

JAUBERT, J.-N. & MUTELET, F. 2004. VLE predictions with the Peng–Robinson equation of state and temperature dependent kij calculated through a group contribution method. *Fluid Phase Equilibria,* 224**,** 285-304.

JOSEPH, M., RAAL, J. & RAMJUGERNATH, D. 2001. Phase equilibrium properties of binary systems with diacetyl from a computer controlled vapour–liquid equilibrium still. *Fluid phase equilibria,* 182**,** 157-176.

JOSEPH, M. A., RAMJUGERNATH, D. & RAAL, J. 2002. Computer-aided Measurement of Vapour-Liquid Equilibria in a Dynamic Still at Sub-Atmospheric Pressures. *Developments in Chemical Engineering and Mineral Processing,* 10**,** 615-638.

KANG, J. W., LEE, J. H., YOO, K.-P. & LEE, C. S. 2002. Evaluation of equations of state applicable to polymers and complex systems. *Fluid phase equilibria,* 194**,** 77-86.

KEMME, H. R. & KREPS, S. I. 1969. Vapor pressure of primary n-alkyl chlorides and alcohols. *Journal of Chemical and Engineering Data,* 14**,** 98-102.

KNEISL, P., ZONDLO, J. W., WHITING, W. B. & BEDELL, M. 1989. The effect of fluid properties on ebulliometer operation. *Fluid phase equilibria,* 46**,** 85-94.

KOLBE, B. & GMEHLING, J. 1985. Thermodynamic properties of ethanol+ water. I. Vapour-liquid equilibria measurements from 90 to 150° C by the static method. *Fluid Phase Equilibria,* 23**,** 213-226.

LEE, S. C. 1931. Partial Pressure Isotherms II. *The Journal of Physical Chemistry,* 35**,** 3558-3582.

LEFFLER, W. L. 1985. *Petroleum refining for the nontechnical person,* United States, Pennwell Books,Tulsa, OK.

MAHER, P. J. & SMITH, B. D. 1979. Infinite dilution activity coefficient values from total pressure VLE data. Effect of equation of state used. *Industrial & Engineering Chemistry Fundamentals,* 18**,** 354-357.

MALANOWSKI, S. 1982. Experimental methods for vapour-liquid equilibria. Part I. Circulation methods. *Fluid Phase Equilibria,* 8**,** 197-219.

MARQUARDT, D. W. 1963. An algorithm for least-squares estimation of nonlinear parameters. *Journal of the Society for Industrial & Applied Mathematics,* 11**,** 431-441.

MARSH, K. N. 1989. New methods for vapor-liquid-equilibria measurements. *Fluid phase equilibria,* 52**,** 169-184.

MARTIENSSEN, M., FABRITIUS, H., KUKLA, S., BALCKE, G. U., HASSELWANDER, E. & SCHIRMER, M. 2006. Determination of naturally occurring MTBE biodegradation by analysing metabolites and biodegradation by-products. *Journal of contaminant hydrology,* 87**,** 37-53.

MARTIN, J. J. 1979. Cubic equations of state-which? *Industrial & Engineering Chemistry Fundamentals,* 18**,** 81-97.

MATHIAS, P. M. & COPEMAN, T. W. 1983. Extension of the Peng-Robinson equation of state to complex mixtures: evaluation of the various forms of the local composition concept. *Fluid Phase Equilibria,* 13**,** 91-108.

MCCLELLAN, A. L. 1963-1974. *Tables of experimental dipole moments,* San Francisco, WH Freeman.

MICHELSEN, M. L. & KISTENMACHER, H. 1990. On composition-dependent interaction coefficeints. *Fluid Phase Equilibria,* 58**,** 229-230.

MOODLEY, P. 2009. *Vapour-Liquid Equilibria Studies for Binary Systems Containing 1-Hexene and n-Hexane.* MSc, University of KwaZulu-Natal.

MQONDISI, N. 2012. *Measurements of Phase Equilibrium for Systems Containing*

Oxygenated Compounds. MSc, University of KwaZulu-Natal.

NADIM, F., ZACK, P., HOAG, G. E. & LIU, S. 2001. United States experience with gasoline additives. *Energy Policy,* 29**,** 1-5.

NAIDOO, P. 2004. *High Pressure Vapour-Liquid Equilibrium Studies.* PhD, University of KwaZulu-Natal.

NARASIGADU, C. 2006. *Phase Equilibrium Investigation of the Water and Acetonitrile Solvent with Heavy Hydrocarbons.* MSc, University of KwaZulu-Natal.

NARASIGADU, C. 2011. *Design of a Static Micro-Cell for Phase Equilibrium Measurements :*

Measurements and Modelling. PhD, Mines, ParisTech.

NDLOVO, M. 2005. *Development of a Dynamic Still for Measuring Low Pressure Vapour-Liquid-Liquid Equilibria (Systems of Partial Liquid Miscibility).* MSc, University of KwaZulu-Natal.

NOTHNAGEL, K.-H., ABRAMS, D. S. & PRAUSNITZ, J. M. 1973. Generalized correlation for fugacity coefficients in mixtures at moderate pressures. Application of chemical theory of vapor imperfections. *Industrial & Engineering Chemistry Process Design and Development,* 12**,** 25-35.

OH, J.-H., HWANG, I.-C. & PARK, S.-J. 2009. Isothermal vapor–liquid equilibrium at 333.15 K and excess molar volumes and refractive indices at 298.15 K for the mixtures of< i> di</i>-methyl carbonate, ethanol and 2, 2, 4-trimethylpentane. *Fluid Phase Equilibria,* 276**,** 142-149.

OTHMER, D. 1928. Composition of Vapors from Boiling Binary Solutions1. *Industrial & Engineering Chemistry,* 20**,** 743-766.

OTHMER, D. F. 1948. Composition of vapors from boiling binary solutions. *Industrial and Engineering Chemistry: Analytical Edition,* 20**,** 763.

OTHMER, D. F. & MORLEY, F. R. 1943. Composition of vapors from boiling binary solutions. *Industrial & Engineering Chemistry,* 35**,** 615-620.

PALMER, D. A. 1987. *Handbook of applied thermodynamics,* Boca Raton, CRC press.

PENG, D.-Y. & ROBINSON, D. B. 1976. A new two-constant equation of state. *Industrial & Engineering Chemistry Fundamentals,* 15**,** 59-64.

PERRY, R., GREEN, D. & MALONEY, J. 1998. Perry's Chemical Engineers' Handbook. *McGraw-Hill, 7th edition, ISBN.* New York.

PETRUCCI, R. H., HARWOOD, W. S., HERRING, G. F. & MADURA, J. D. 2006. *General chemistry: principles and modern applications,* Pearson Education International.

PILLAY, J. C. 2010. *Binary Vapour-Liquid Equilibria for Oxygen containing Compounds.* MSc, University of KwaZulu-Natal.

POLING, B. E., PRAUSNITZ, J. M. & O'CONNELL, J. P. 2001. *The properties of gases and liquids,* McGraw-Hill New York.

PRAUSNITZ, J., ANDERSON, T., GRENS, E., ECKERT, C., HSIEH, R. & O'CONNELL, J. 1980. Computer Calculations for Multicomponent VLE and LLE. *Prentice Hall,* 23.

PRAUSNITZ, J. M. 1969. *Molecular thermodynamics of fluid-phase equilibria,* Canada, Prentice Hall Inc.

PRAUSNITZ, J. M., LICHTENTHALER, R. N. & DE AZEVEDO, E. G. 1986. *Molecular thermodynamics of fluid-phase equilibria,* Englewood Cliffs, New Jersey, Prentice-Hall.

PRAUSNITZ, J. M., LICHTENTHALER, R. N. & DE AZEVEDO, E. G. 1999. *Molecular thermodynamics of fluid-phase equilibria,* Upper Saddle River, New Jersey., Prentice-Hall Inc.

RAAL, J. D. & MUHLBAUER, A. 1998. *Phase Equilibria: Measurement & Computation,* Bristol, PA, Taylor and Francis.

RAAL, J. D. A. M., A L 1998. *Phase Equilibria: Measurement & Computation,* Bristol, PA, Taylor and Francis.

REDDY, P. 2006. *The Developement of a Novel Apparatus for the Measurement of Vapour-Liquid Equilibria at Moderate Pressures.* PhD, University of KwaZulu-Natal.

REDDY, P., BENECKE, T. P. & RAMJUGERNATH, D. 2013. Isothermal (vapour+ liquid) equilibria for binary mixtures of diisopropyl ether with (methanol, or ethanol, or 1-butanol): Experimental data, correlations, and predictions. *The Journal of Chemical Thermodynamics,* 58**,** 330-339.

REDDY, P., BENECKE, T. P. AND RAMJUGERNATH 2012. Isothermal (vapour + liquid) equilibria for binary mixtures of diisopropyl ether with (methanol, or ethanol, or 1-butanol): Experimental data, correlations, and predictions. *Journal of Chemical Thermodynamics***,** 330–339.

REDLICH, O. & KWONG, J. 1949. On the thermodynamics of solutions. V. An equation of state. Fugacities of gaseous solutions. *Chemical Reviews,* 44**,** 233-244.

REID, R., PRAUSNITZ, J. & POLING, B. 1977. *The Properties of Gases and Liquids,* New York, McGraw-Hill.

REID, R. C., PRAUSNITZ, J. M. & POLING, B. E. 1988. *The properties of gases and liquids,* New York, McGraw-Hill.

RENON, H. & PRAUSNITZ, J. M. 1968. Local compositions in thermodynamic excess functions for liquid mixtures. *AIChE journal,* 14**,** 135-144.

REZANOVA, E. N., KAMMERER, K. & LICHTENTHALER, R. N. 1999. Excess properties of binary alkanol+ diisopropyl ether (DIPE) or+ dibutyl ether (DBE) mixtures and the application of the extended real associated solution model. *Journal of Chemical & Engineering Data,* 44**,** 1235-1239.

ROGER, H. 2004. *Robust Equipment for the Measurement of Vapour-Liquid Equilibrium at High Temperatures and High Pressures.* PhD, University of KwaZulu-Natal.

ROSE, A. & WILLIAMS, E. T. 1955. Vapor liquid equilibrium self-lagging stills. *Industrial & Engineering Chemistry,* 47**,** 1528-1533.

SAMESHIMA, J. 1918. ON THE SYSTEM ACETONE—ETHYL ETHER. *Journal of the American Chemical Society,* 40**,** 1482-1503.

SANDLER, S. I. 2003. Quantum mechanics: a new tool for engineering thermodynamics. *Fluid Phase Equilibria,* 210**,** 147-160.

SATYRO, M. A. & TREBBLE, M. A. 1998. A correction to Sandler–Wong mixing rules. *Fluid phase equilibria,* 143**,** 89-98.

SCATCHARD, G., RAYMOND, C. & GILMANN, H. 1938. Vapor—Liquid Equilibrium. I. Apparatus for the Study of Systems with Volatile Components1. *Journal of the American Chemical Society,* 60**,** 1275-1278.

SCOTT, R. L. 1956. Corresponding states treatment of nonelectrolyte solutions. *The Journal of Chemical Physics,* 25**,** 193-205.

SEKER, E. & SOMER, T. 1992. Vapour-liquid equilibrium still-a new design. *Measurement Science and Technology,* 4**,** 776.

SEWNARAIN, R., RAMJUGERNATH, D. & RAAL, J. D. 2002. Isobaric vapor-liquid equilibria for the systems propionic acid+ butyric acid, isobutyric acid+ butyric acid, butyric acid+ isovaleric acid, and butyric acid+ hexanoic acid at 14 kPa. *Journal of Chemical & Engineering Data,* 47**,** 603-607.

SEWPERSAD, R. 2012. *Phase Equilibrium Measurements at Low-To-Moderate Pressures for Systems Containing n-Hexane, 1-Hexane and n-Methyl-2-Pyrrolidone.* MSc, University of KwaZulu-Natal.

SMITH, J., ABBOTT, M. & VAN NESS, H. 2001. Introduction to chemical engineering thermodynamics. *McGraw-Hill, New York.*

SMITH, J., ABBOTT, M. & VAN NESS, H. 2005. *Introduction to chemical engineering thermodynamics,* New York, McGraw-Hill.

SMITH, J. & VANNESS, H. 1996. *Introduction to Chemical Engineering Thermodynamics,* MacGraw Hill, Singapore

SMYTH, C. P. 1955. Dipole Moment and Molecular Structure. *CCP5 Quarterly.*

SOAVE, G. 1972. Equilibrium constants from a modified Redlich-Kwong equation of state. *Chemical Engineering Science,* 27**,** 1197-1203.

SOAVE, G. 1993. Improving the Treatment of Heavy Hydrocarbons by the SRK EOS. *Fluid Phase Equilibria,* 84**,** 339-342.

SONI, M. 2003. *Vapour-Liquid Equilibria and Infinite Dilution Activity Coefficient Measurements of Systems Involving Diketones* MSc, University of KwaZulu-Natal.

SOO, C. B. 2011. *Experimental Thermodynamic Measurements of Biofuel-related Associating Compounds and Modeling using the PC-SAFT Equation of State.* PhD, Mines Paris Tech.

STREICHER, C., ASSELINEAU, L. & FORESTIERE, A. 1995. Separation of alcohol/ether/hydrocarbon mixtures in industrial etherification processes for gasoline production. *Pure and applied chemistry,* 67**,** 985-992.

STRYJEK, R. & VERA, J. 1986. PRSV—An improved peng-Robinson equation of state with new mixing rules for strongly nonideal mixtures. *The Canadian Journal of Chemical Engineering,* 64**,** 334-340.

TAYLOR, B. N. & KUYATT, C. E. 1994. NIST Technical Note 1297. *Guidelines for evaluating and expressing the uncertainty of NIST measurement results***,** 24.

TSUBOKA, T. & KATAYAMA, T. 1975. Modified Wilson equation for vapor-liquid and liquid-liquid equilibria. *Journal of Chemical Engineering of Japan,* 8**,** 181-187.

TURTON, R., BALLIE, R. C., WHITING, W. B. & SHAEIWITZ, J. A. 1998. Analysis, synthesis, and design of chemical process" 1998. published by Prentice Hall PTR.

TWU, C. H., BLUCK, D., CUNNINGHAM, J. R. & COON, J. E. 1991. A cubic equation of state with a new alpha function and a new mixing rule. *Fluid Phase Equilibria,* 69**,** 33-50.

TWU, C. H. & COON, J. E. 1996. CEOS/AE mixing rules constrained by vdW mixing rule and second virial coefficient. *AIChE journal,* 42**,** 3212-3222.

TWU, C. H., COON, J. E. & BLUCK, D. 1998. Comparison of the Peng-Robinson and Soave-Redlich-Kwong equations of state using a new zero-pressure-based mixing rule for the prediction of high-pressure and high-temperature phase equilibria. *Industrial & engineering chemistry research,* 37**,** 1580-1585.

UUSI-KYYNY, P., POKKI, J.-P., LAAKKONEN, M., AITTAMAA, J. & LIUKKONEN, S. 2002. Vapor liquid equilibrium for the binary systems 2-methylpentane+ 2-butanol at 329.2 K and n-hexane+ 2-butanol at 329.2 and 363.2 K with a static apparatus. *Fluid phase equilibria,* 201**,** 343-358.

VALDERRAMA, J. O. 2003. The state of the cubic equations of state. *Industrial & engineering chemistry research,* 42**,** 1603-1618.

VALTZ, A., COQUELET, C., BABA-AHMED, A. & RICHON, D. 2002. Vapor–liquid equilibrium data for the propane+ 1, 1, 1, 2, 3, 3, 3-heptafluoropropane (R227ea) system at temperatures from 293.16 to 353.18 K and pressures up to 3.4 MPa. *Fluid phase equilibria,* 202**,** 29-47.

VAN'T HOF, A., DE LEEUW, S., HALL, C. & PETERS, C. 2004. Molecular simulation of binary vapour–liquid equilibria with components differing largely in volatility. *Molecular Physics,* 102**,** 301-317.

VAN DER WAALS, J. D. & VAN DER WAALS, J. D. 1873. *Over de Continuiteit van den Gas-en Vloeistoftoestand,* AW Sijthoff.

VAN NESS, H. & ABBOTT, M. 1997. Perry's Chemical Engineers' Handbook, chapter 4 (Thermodynamics). McGraw-Hill.

VAN NESS, H., PEDERSEN, F. & RASMUSSEN, P. 1978. Vapor-liquid equilibrium: Part V. Data reduction by maximum likelihood. *AIChE Journal,* 24**,** 1055-1063.

VAN NESS, H., SMITH, J. M. & ABBOTT, M. M. 2001. *Introduction to chemical engineering thermodynamics*.

VAN NESS, H. C. & ABBOTT, M. M. 1978. A procedure for rapid degassing of liquids. *Industrial & Engineering Chemistry Fundamentals,* 17**,** 66-67.

VAN NESS, H. C., BYER, S. M. & GIBBS, R. E. 1973. Vapor-Liquid equilibrium: Part I. An appraisal of data reduction methods. *AIChE Journal,* 19**,** 238-244.

VETERE, A. 2000. A simple modification of the NRTL equation. *Fluid phase equilibria,* 173**,** 57-64.

VETERE, A. 2004. The NRTL equation as a predictive tool for vapor–liquid equilibria. *Fluid phase equilibria,* 218**,** 33-39.

VILLAMAÑÁN, R. M., MARTÍN, M. C., CHAMORRO, C. R. & SEGOVIA, J. J. 2006a. Vapor-liquid equilibrium of binary and ternary mixtures containing isopropyl ether, 2-butanol, and benzene at T= 313.15 K. *Journal of Chemical & Engineering Data,* 51**,** 148-152.

VILLAMAÑÁN, R. M., MARTÍN, M. C., CHAMORRO, C. R., VILLAMAÑÁN, M. A. & SEGOVIA, J. J. 2006b. Phase equilibrium properties of binary and ternary systems containing di-isopropyl ether+ 1-butanol+ benzene at 313.15 K. *The Journal of Chemical Thermodynamics,* 38**,** 547-553.

VORENBERG, D. G., RAAL, J. D. & RAMJUGERNATH, D. 2005. Vapor-liquid equilibrium measurements of MTBE and TAME with toluene. *Journal of Chemical & Engineering Data,* 50**,** 56-59.

WALAS, S. M. 1985. *Phase equilibria in chemical engineering,* Boston, Butterworth

WEIR, R. D. & DE LOOS, T. W. 2005. *Measurement of the thermodynamic properties of multiple phases,* Gulf Professional Publishing.

WILSON, G. M. 1964. Vapor-liquid equilibrium. XI. A new expression for the excess free energy of mixing. *Journal of the American Chemical Society,* 86**,** 127-130.

WONG, D. S. H. & SANDLER, S. I. 1992. A theoretically correct mixing rule for cubic equations of state. *AIChE Journal,* 38**,** 671-680.

YAWS, C. L. & GABBULA, C. 2003. *Yaws" Handbook of Thermodynamic and Physical Properties of Chemical Compounds,* Knovel.

YERAZUNIS, S., PLOWRIGHT, J. & SMOLA, F. 1964. Vapor-liquid equilibrium determination by a new apparatus. *AIChE Journal,* 10**,** 660-665.

ZAWADZKI, M., THOKOZANI NGEMA, P., DOMANSKA, U., NAIDOO, P. & RAMJUGERNATH, D. 2012. Vapor–Liquid Equilibrium Data for Binary Systems of 1 H-Pyrrole with Butan-1-ol, Propan-1-ol, or Pentan-1-ol. *Journal of Chemical & Engineering Data,* 57**,** 2520-2527.

APPENDICES

Appendix A: Thermodynamic Consistency Test

Table A-1: Results of the thermodynamic consistency testing for the 2, 2, 4-trimethylpentane (1) + 1-pentanol (2) systems at 350.15, 360.15 and 370.15 K – Direct method.

Model	T±0.10/K	Total points measured	Consistent points	(ΔP) AAD	(Δy_1) AAD
RKS-MC-WS-NRTL					
	350.15	14	9	0.29	0.004
	360.15	16	11	0.23	0.003
	370.15	15	10	0.20	0.003
RKS-MC-WS-WILSON					
	350.15	14	9	0.36	0.003
	360.15	16	11	0.25	0.002
	370.15	15	10	0.37	0.003
RKS-MC-WS-UNIQUAC					
	350.15	14	9	0.28	0.003
	360.15	16	11	0.25	0.003
	370.15	15	10	0.24	0.003

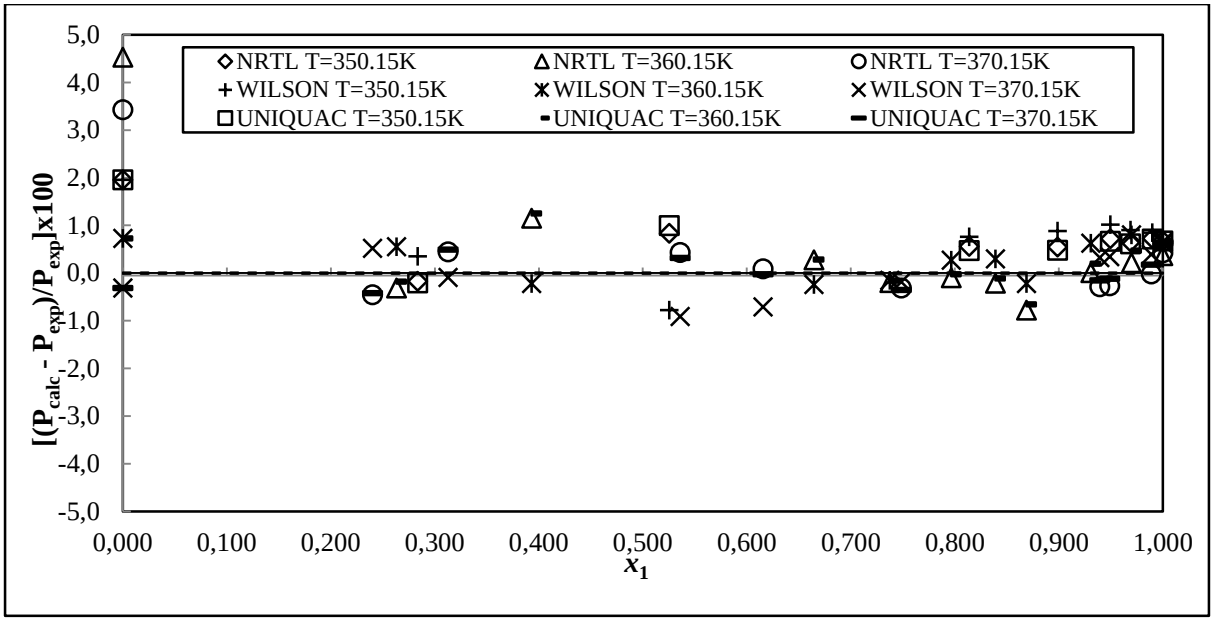

Figure A-1: Point test for SRK EOS (activity coefficient model variation) P-residual for the 2, 2, 4-trimethylpentane (1) + 1-pentanol (2) system at: 350.15 K, 360.15K and 370.15K

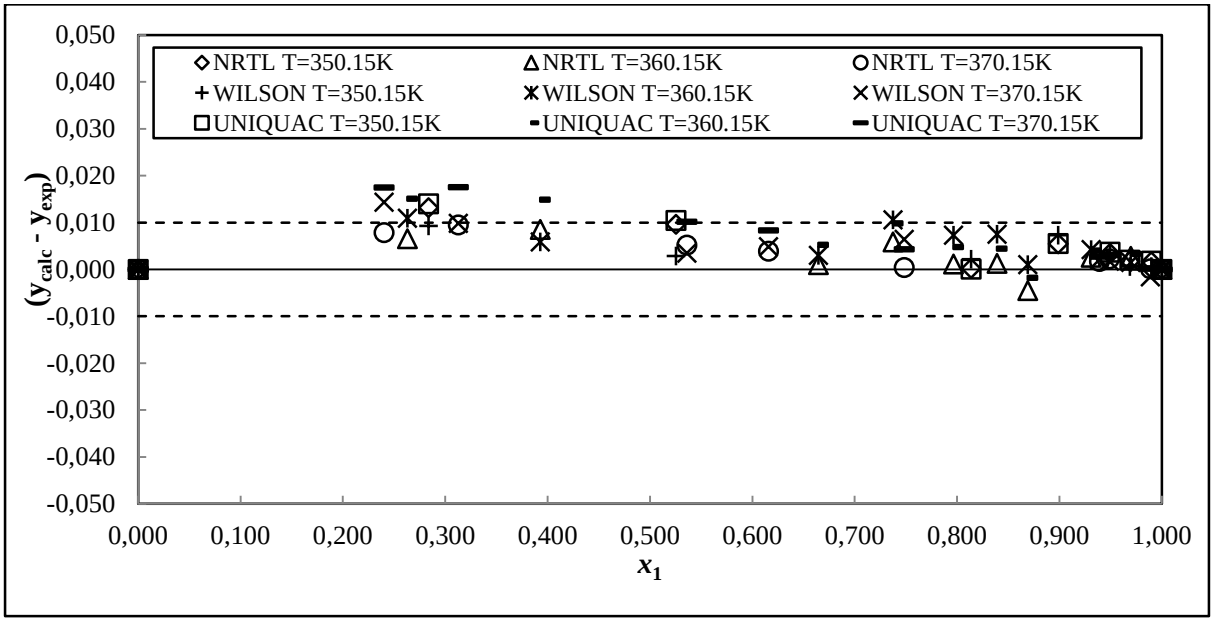

Figure A-2: Point test for SRK EOS (activity coefficient model variation) y-residual for the 2, 2, 4-trimethylpentane (1) + 1-pentanol (2) system at: 350.15 K, 360.15K and 370.15K

Table A-2: Results of the thermodynamic consistency testing for the MTBE (1) + 1-pentanol (2) systems at 317.15 and 327.15 K – Direct method.

Model	T±0.10/K	Total points measured	Consistent points	(ΔP) AAD	(Δy_1) AAD
RKS-MC-WS-NRTL					
	317.15	14	11	1.18	0.002
	327.15	17	13	1.63	0.004
RKS-MC-WS-WILSON					
	317.15	16	11	0.97	0.002
	327.15	15	13	1.41	0.004
RKS-MC-WS-UNIQUAC					
	317.15	16	11	1.12	0.002
	327.15	15	13	1.55	0.004

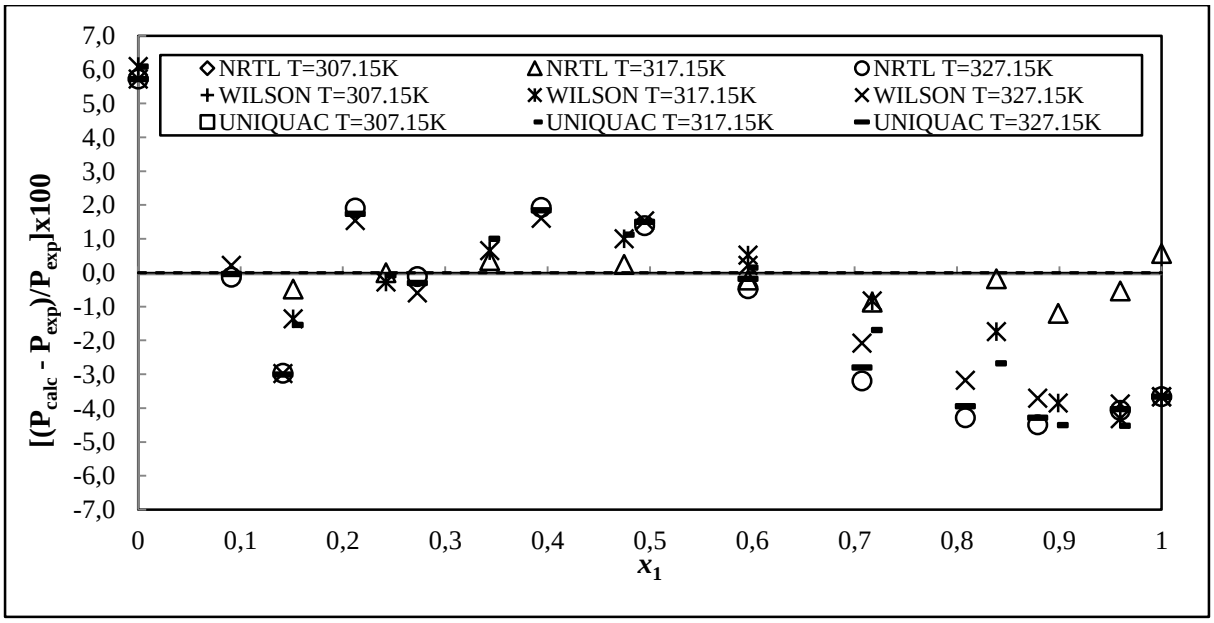

Figure A-3: Point test for SRK EOS (activity coefficient model variation) P-residual for the MTBE (1) + 1-pentanol (2) system at: 317.15 K and 327.15K

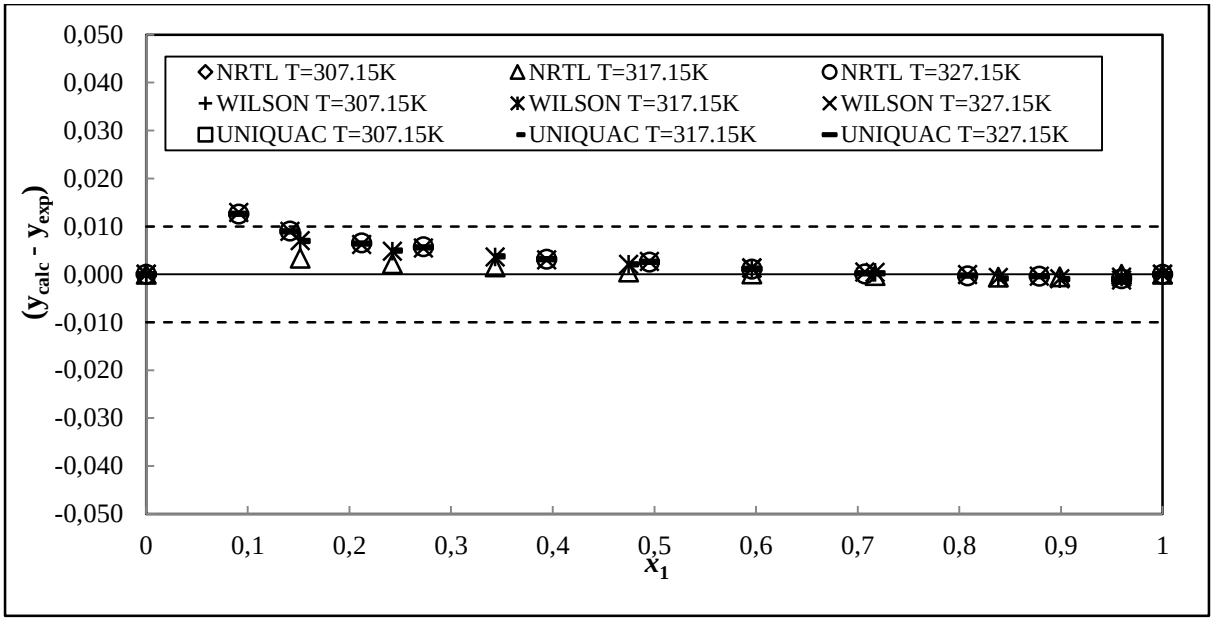

Figure A-4: Point test for SRK EOS (activity coefficient model variation) y-residual for the 2, 2, 4-trimethylpentane (1) + 1-pentanol (2) system at: 317.15 K and 327.15K

Table A-3: Results of the thermodynamic consistency testing for the MTBE (1) + 2, 2, 4-trimethylpentane (2) systems at 307.15, 317.15 and 327.15 K – Direct method.

Model	**T±0.10/K**	**Total points measured**	**Consistent points**	**(ΔP) AAD**	**(Δy_1) AAD**
RKS-MC-WS-NRTL					
	307.15	15	13	0.64	0.009
	317.15	17	17	1.22	0.010
	327.15	16	16	1.27	0.012
RKS-MC-WS-Wilson					
	307.15	15	13	0.59	0.009
	317.15	17	17	1.13	0.010
	327.15	16	16	1.13	0.011
RKS-MC-WS-UNIQUAC					
	307.15	15	13	0.62	0.009
	317.15	17	17	1.18	0.010
	327.15	16	16	1.19	0.012

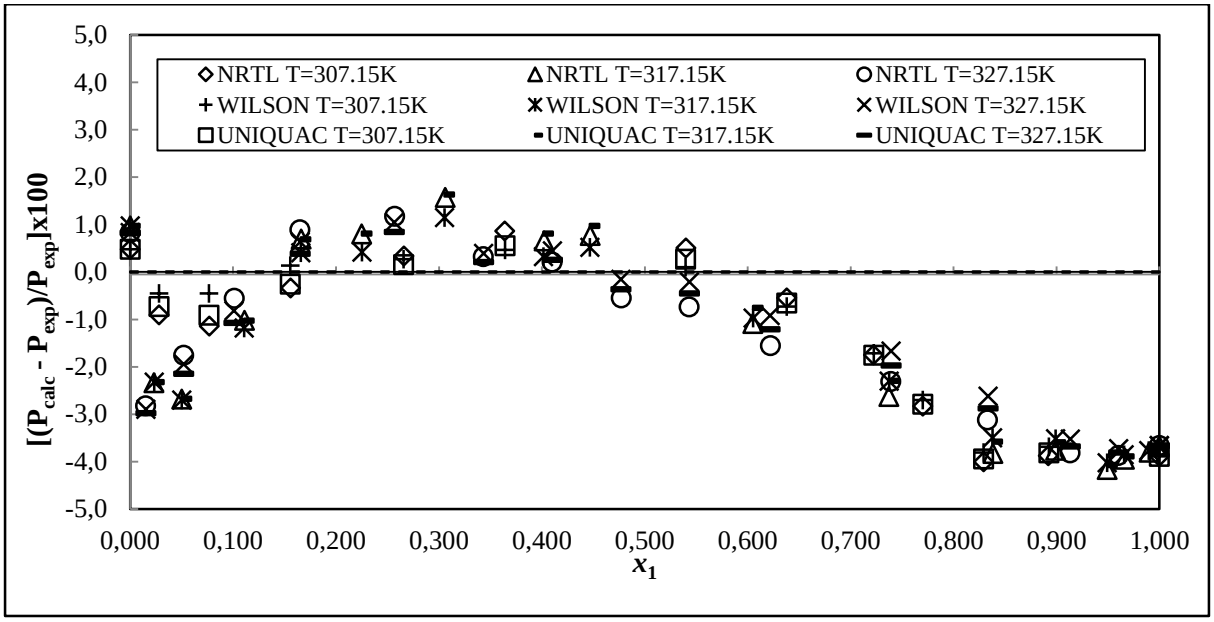

Figure A-5: Point test for SRK EOS (activity coefficient model variation) P-residual for the MTBE (1) + 2, 2, 4-trimethylpentane (1) system at: 307.15K, 317.15 K and 327.15K

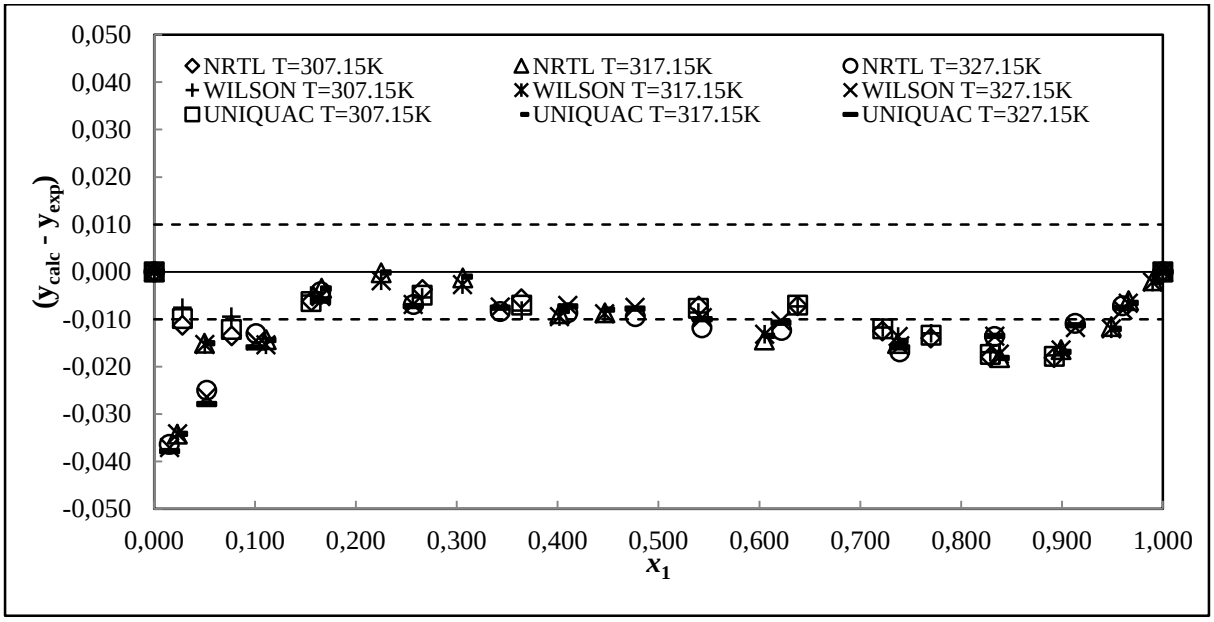

Figure A-6: Point test for SRK EOS (activity coefficient model variation) y-residual for the MTBE (1) + 2, 2, 4-trimethylpentane (2) system at: 307.15K, 317.15 K and 327.15K

Table A-4: Results of the thermodynamic consistency testing for the DIPE (1) + 2, 2, 4-trimethylpentane (2) systems at 320.15, 330.15 and 340.15 K – Direct method.

Model	T±0.10/K	Total points measured	Consistent points	(ΔP) AAD	(Δy_1) AAD
RKS-MC-WS-NRTL					
	320.15	18	18	0.21	0.003
	330.15	11	11	0.51	0.006
	340.15	11	11	0.53	0.008
RKS-MC-WS-Wilson					
	320.15	18	18	0.28	0.003
	330.15	11	11	0.51	0.006
	340.15	11	11	0.53	0.008
RKS-MC-WS-UNIQUAC					
	320.15	18	18	0.27	0.003
	330.15	11	11	0.51	0.006
	340.15	11	11	0.52	0.008

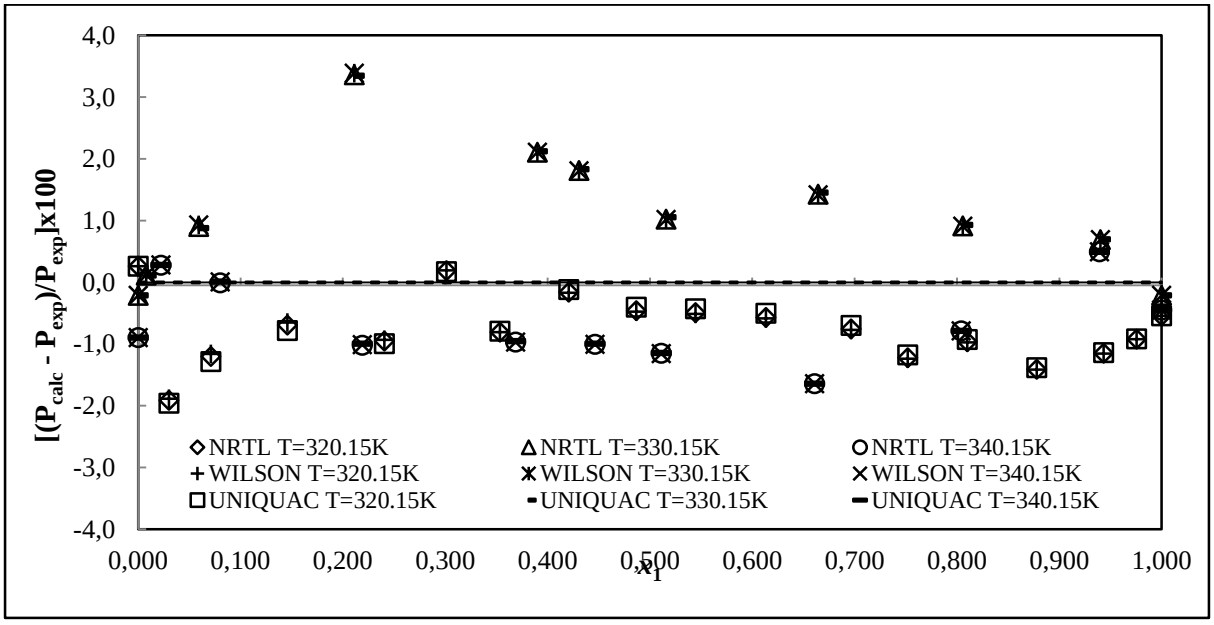

Figure A-7: Point test for SRK EOS (activity coefficient model variation) P-residual for the DIPE (1) + 2, 2, 4-trimethylpentane (1) system at: 320.15K, 330.15 K and 340.15K

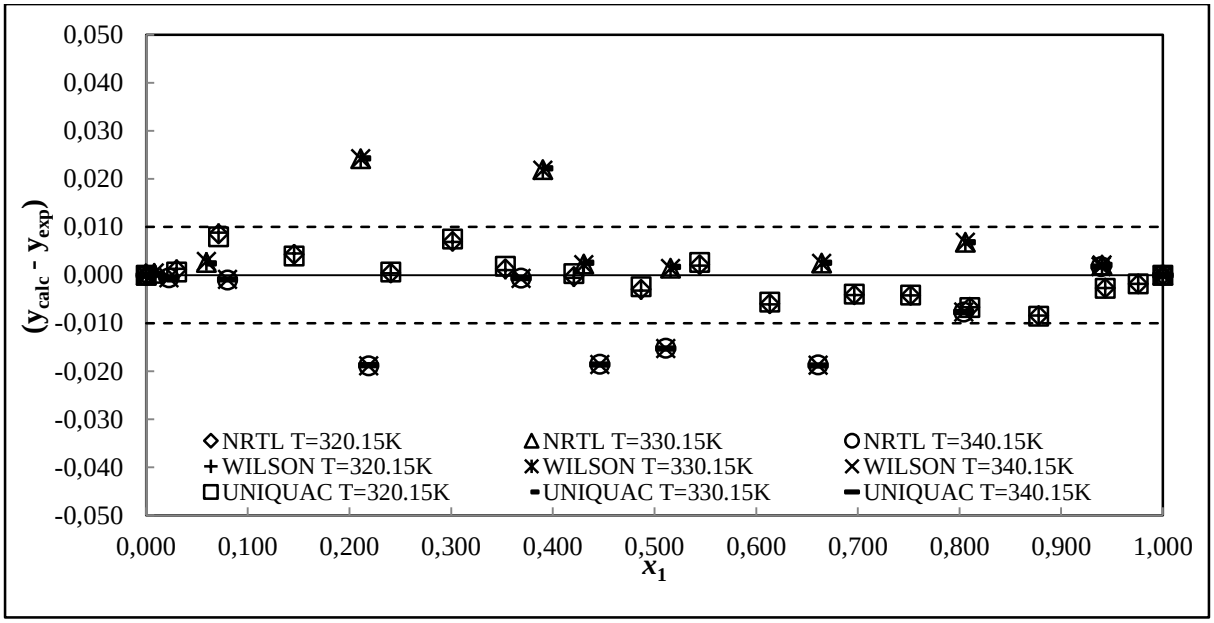

Figure A-8: Point test for SRK EOS (activity coefficient model variation) y-residual for the DIPE (1) + 2, 2, 4-trimethylpentane (1) system at: 320.15K, 330.15 K and 340.15K

Table A-5: Results of the thermodynamic consistency testing for the DIPE (1) + 1-propanol (2) systems at 320.15, 330.15 and 340.15 K – Direct method.

Model	T±0.10/K	Total points measured	Consistent points	(ΔP) AAD	(Δy_1) AAD
RKS-MC-WS-NRTL					
	320.15	16	16	0.27	0.004
	330.15	12	12	0.20	0.004
	340.15	12	12	0.86	0.004
RKS-MC-WS-Wilson					
	320.15	16	16	0.23	0.005
	330.15	12	12	0.19	0.005
	340.15	12	12	0.62	0.005
RKS-MC-WS-UNIQUAC					
	320.15	16	16	0.31	0.004
	330.15	12	12	0.26	0.005
	340.15	12	12	0.86	0.004

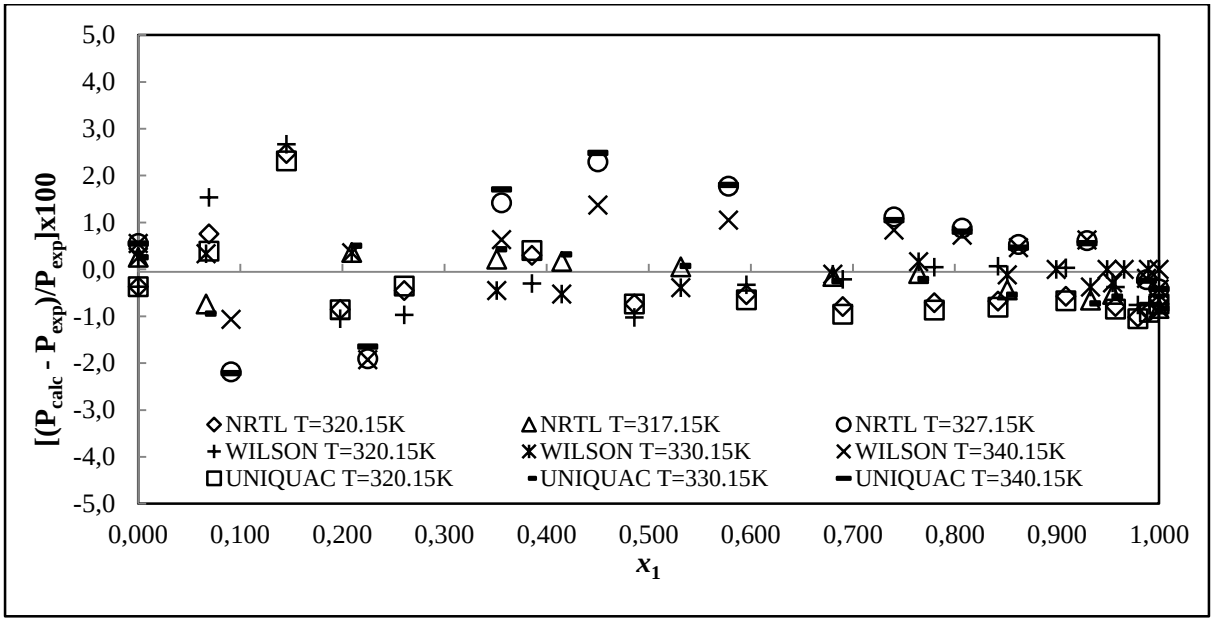

Figure A-9: Point test for SRK EOS (activity coefficient model variation) P-residual for the DIPE (1) + 1-propanol (1) system at: 320.15K, 330.15 K and 340.15K

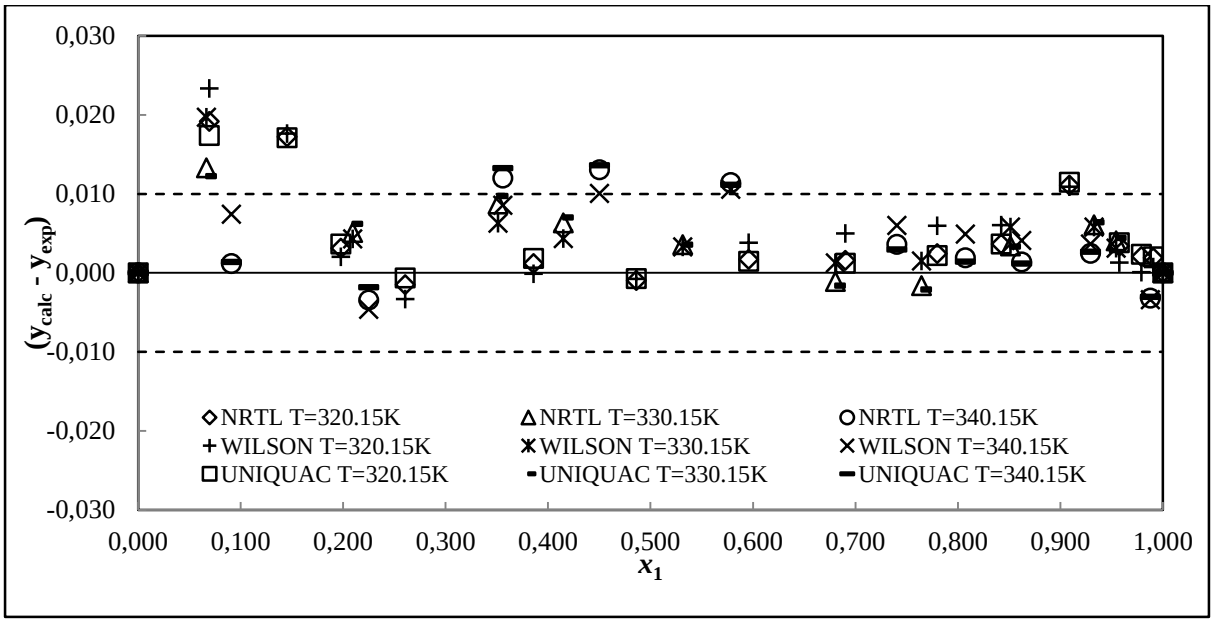

Figure A-10: Point test for SRK EOS (activity coefficient model variation) *y*-residual for the DIPE (1) + 1-propanol (1) system at: 320.15K, 330.15 K and 340.15K

Table A-6: Results of the thermodynamic consistency testing for the DIPE (1) + 2-butanol (2) systems at 320.15, 330.15 and 340.15 K – Direct method.

Model	T±0.10/K	Total points measured	Consistent points	(ΔP) AAD	(Δy_1) AAD
RKS-MC-WS-NRTL					
	320.15	17	17	0.24	0.007
	330.15	16	16	0.32	0.008
	340.15	16	16	0.27	0.008
RKS-MC-WS-Wilson					
	320.15	17	17	0.37	0.007
	330.15	16	16	0.33	0.007
	340.15	16	16	0.46	0.008
RKS-MC-WS-UNIQUAC					
	320.15	17	17	0.29	0.007
	330.15	16	16	0.36	0.008
	340.15	16	16	0.44	0.008

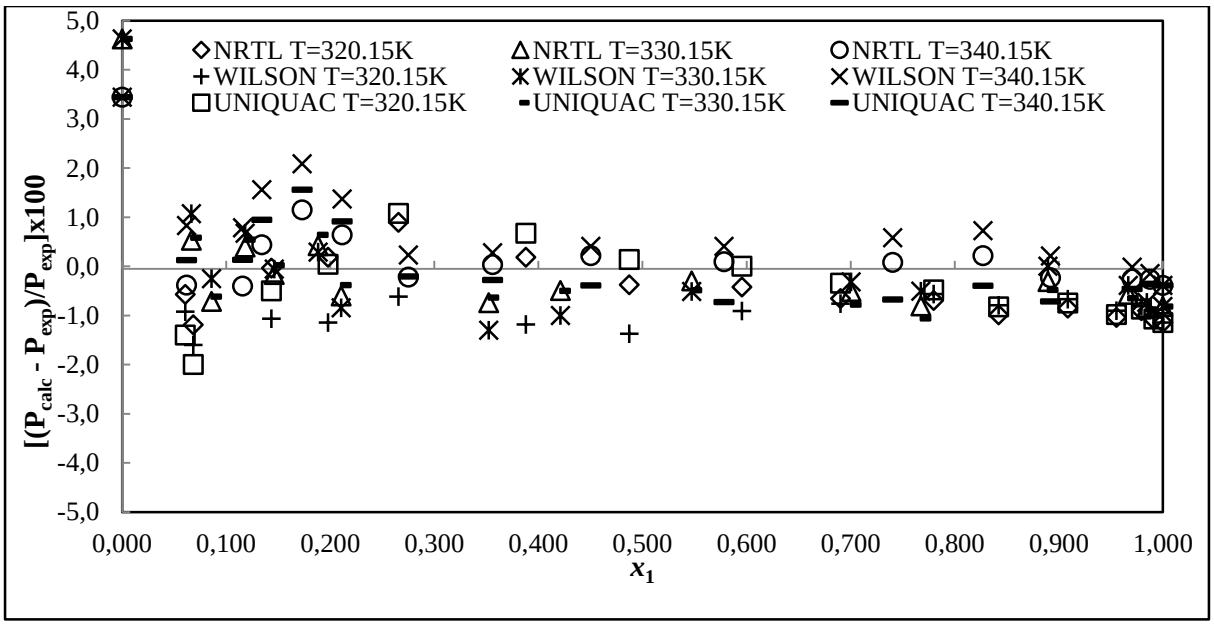

Figure A-11: Point test for SRK EOS (activity coefficient model variation) P-residual for the DIPE (1) + 2-butanol (1) system at: 320.15K, 330.15 K and 340.15K

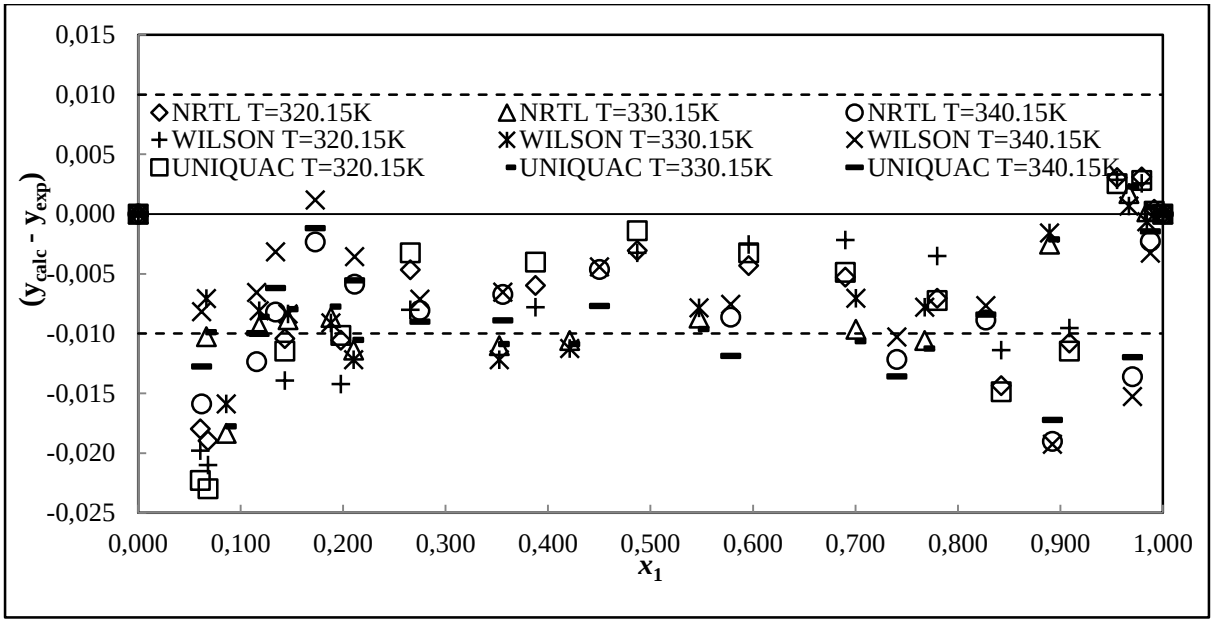

Figure A-12: Point test for SRK EOS (activity coefficient model variation) *y*-residual for the DIPE (1) + 2-butanol (1) system at: 320.15K, 330.15 K and 340.15K

Appendix B: Experimental and Modelled data

Table B-1: Direct Method Modeling results for 2, 2, 4-trimethylpentane (1) + 1-pentanol (2)

Model	**T±0.10/K**	α_{12}	k_{ij}	A_{12} **J/mol**	A_{21} **J/mol**	**(Δ*P*) AAD**	**AAD% (Δ*P*)**	**(Δy_1) AAD**	**AAD%(Δy_1)**
RKS-MC-WS-NRTL									
	350.15	0.30	-0.251	217.3	2170	0.29	0.76	0.004	0.45
	360.15	0.30	-0.238	217.3	2141	0.23	0.39	0.003	0.65
	370.15	0.30	-0.199	217.3	2038	0.20	0.23	0.003	0.75
RKS-MC-WS-Wilson									
	350.15	-	0.094	-406.8	-1755	0.36	0.91	0.003	0.33
	360.15	-	0.035	-602.7	-1794	0.25	0.43	0.002	0.55
	370.15	-	0.130	-301.5	-1698	0.37	0.44	0.003	0.56
RKS-MC-WS-UNIQUAC									
	350.15	-	-0.289	-240.1	-178.8	0.28	0.75	0.003	0.48
	360.15	-	-0.284	-242.3	-177.3	0.25	0.43	0.003	0.68
	370.15	-	-0.366	-260.1	-198.1	0.24	0.30	0.003	0.80

[a]Wilson: $A_{12} = a_{12} - a_{22}$ and $A_{21} = a_{21} - a_{11}$; NRTL: $A_{12} = g_{12} - g_{22}$ and $A_{21} = g_{21} - g_{11}$; UNIQUAC: $A_{12} = u_{12} - u_{22}$ and $A_{21} = u_{21} - u_{11}$; A_{12}: binary interaction parameters representation for the models in Aspen Plus®. k_{ij}: parameter for fitting with Wong and Sandler mixing rule.

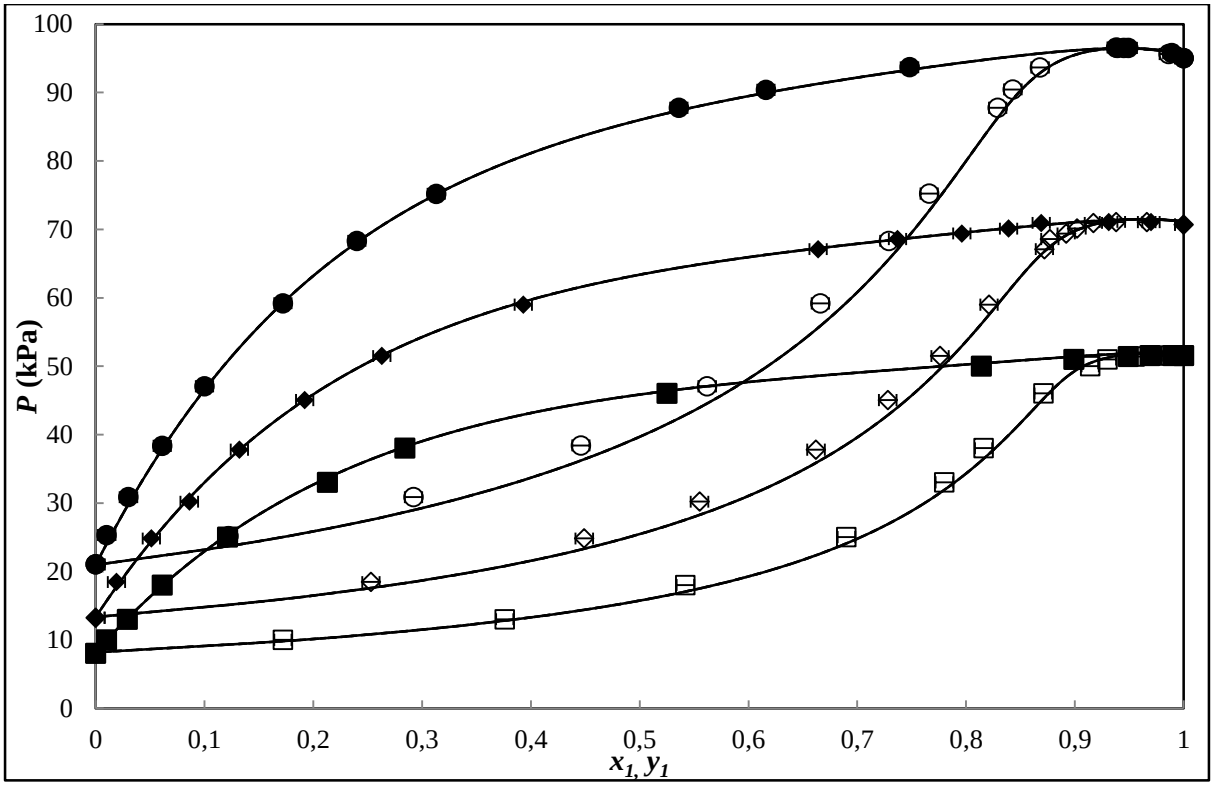

Figure B-1: Experimental VLE and modeling results: P-*x*-*y* data for the 2, 2, 4-trimethylpentane (1) + 1-pentanol (2) system at 350.15K (□); 360.15K (◊); 370.15K (●); — SRK-NRTL; - - - SRK-Wilson; ... SRK-UNIQUAC.

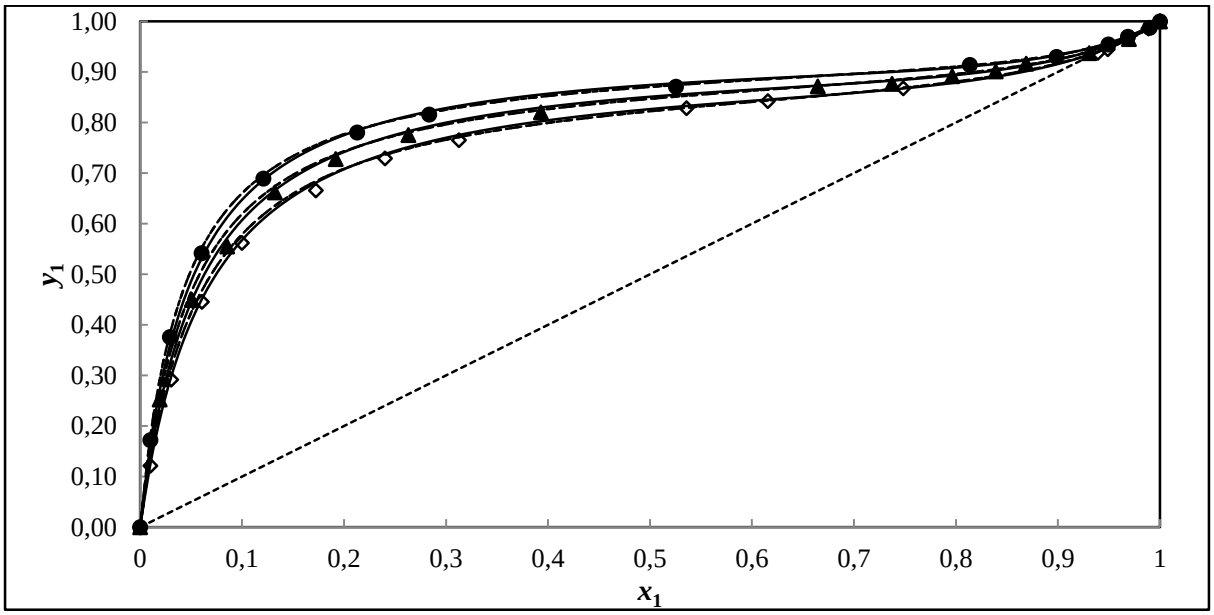

Figure B-2: Experimental VLE and modeling results: *x*-*y* data for the 2, 2, 4-trimethylpentane (1) + 1-pentanol (2) system at 350.15K (◊); 360.15K (▲); 370.15K (●); — SRK-NRTL; - - - SRK-Wilson; ... SRK-UNIQUAC.

Table B-2: Direct Method Modeling results for MTBE (1) + 1-pentanol (2)

Model	**T±0.10/K**	α_{12}	k_{ij}	A_{12} **J/mol**	A_{21} **J/mol**	**(Δ*P*) AAD**	**AAD% (Δ*P*)**	**(Δy_1) AAD**	**AAD%(Δy_1)**
RKS-MC-WS-NRTL									
	317.15	0.30	-0.071	-3872	1709	1.18	2.58	0.002	0.20
	327.15	0.30	-0.037	-3919	1656	1.63	2.20	0.004	0.35
RKS-MC-WS-Wilson									
	317.15	-	-0.423	-1852	-1810	0.97	2.21	0.002	0.20
	327.15	-	-0.431	-1821	-1975	1.41	1.94	0.004	0.36
RKS-MC-WS-UNIQUAC									
	317.15	-	-0.064	1927	-805.5	1.12	2.46	0.002	0.20
	327.15	-	-0.049	1928	-798.1	1.55	2.10	0.004	0.36

[a]Wilson: $A_{12} = a_{12} - a_{22}$ and $A_{21} = a_{21} - a_{11}$; NRTL: $A_{12} = g_{12} - g_{22}$ and $A_{21} = g_{21} - g_{11}$; UNIQUAC: $A_{12} = u_{12} - u_{22}$ and $A_{21} = u_{21} - u_{11}$; A_{12}: binary interaction parameters representation for the models in Aspen Plus®. k_{ij}: parameter for fitting with Wong and Sandler mixing rule.

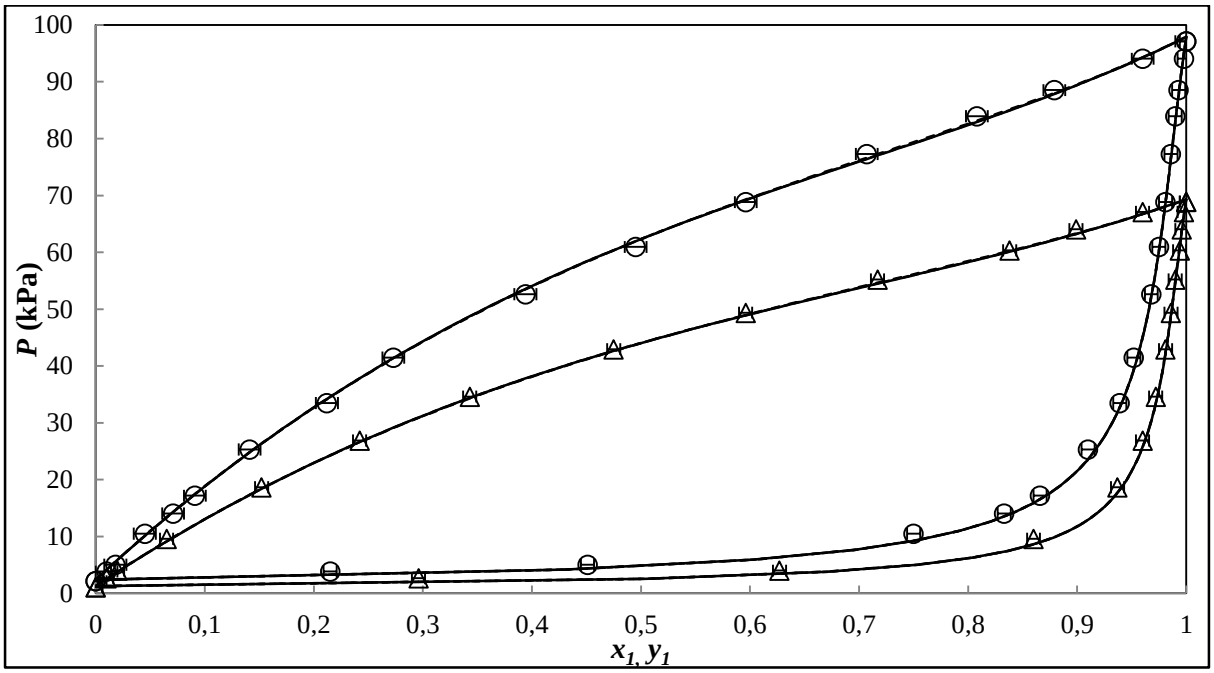

Figure B-3: Experimental VLE and modeling results: P-*x*-*y* data for the MTBE (1) + 1-pentanol (2) system at 317.15K (△); 327.15K (○); — SRK-NRTL; - - - SRK-Wilson; ... SRK-UNIQUAC.

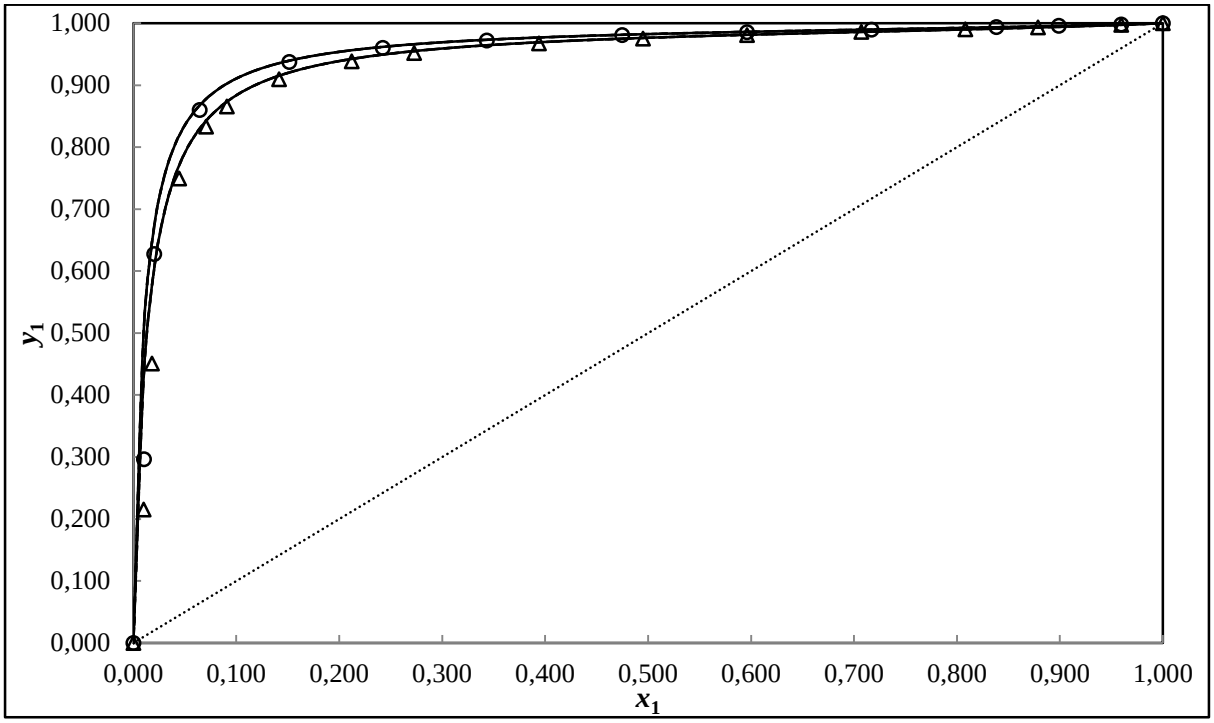

Figure B-4: Experimental VLE and modeling results: *x*-*y* data for the MTBE (1) + 1-pentanol (2) system at 317.15K (△); 327.15K (○); — SRK-NRTL; - - - SRK-Wilson; ... SRK-UNIQUAC.

Table B-3: Direct Method Modeling results for MTBE (1) + 2, 2, 4-trimethylpentane (2)

Model	**T±0.10/K**	α_{12}	k_{ij}	A_{12} **J/mol**	A_{21} **J/mol**	**(Δ*P*) AAD**	**AAD% (Δ*P*)**	**(Δy_1) AAD**	**AAD%(Δy_1)**
RKS-MC-WS-NRTL									
	307.15	0.30	-0.075	-8151	4482	0.64	1.65	0.009	1.61
	317.15	0.30	0.435	-1162	7663	1.22	2.49	0.010	2.76
	327.15	0.30	0.455	-1143	7818	1.27	1.76	0.012	3.48
RKS-MC-WS-Wilson									
	307.15	-	-0.499	-2547	-4820	0.59	1.45	0.009	1.37
	317.15	-	0.331	-3927	6730	1.13	2.31	0.010	2.82
	327.15	-	0.340	-4295	6650	1.13	1.59	0.011	3.51
RKS-MC-WS-UNIQUAC									
	307.15	-	0.010	3526	-2694	0.62	1.55	0.009	1.53
	317.15	-	0.511	5049	-4501	1.18	2.44	0.010	2.74
	327.15	-	0.027	3803	-2869	1.19	1.67	0.012	3.63

[a]Wilson: $A_{12} = a_{12} - a_{22}$ and $A_{21} = a_{21} - a_{11}$; NRTL: $A_{12} = g_{12} - g_{22}$ and $A_{21} = g_{21} - g_{11}$; UNIQUAC: $A_{12} = u_{12} - u_{22}$ and $A_{21} = u_{21} - u_{11}$; A_{12}: binary interaction parameters representation for the models in Aspen Plus®. k_{ij}: parameter for fitting with Wong and Sandler mixing rule.

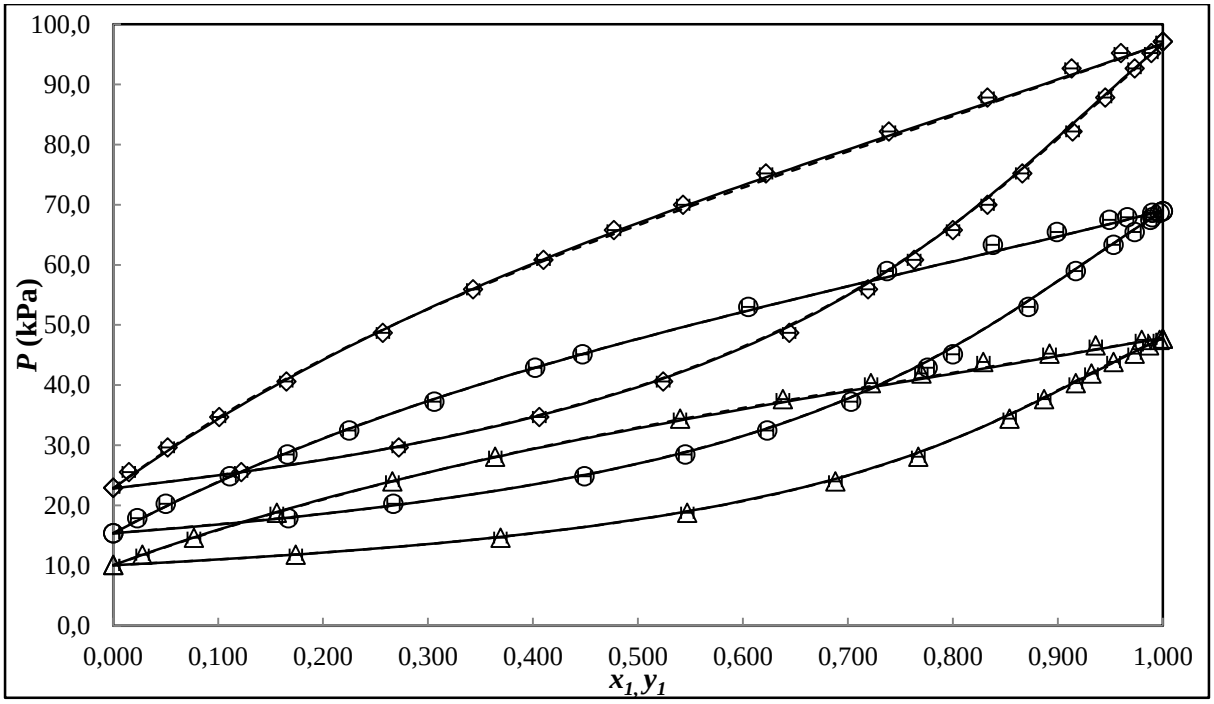

Figure B-5: Experimental VLE and modeling results: P-*x*-*y* data for the MTBE (1) + 2, 2, 4-trimethylpentane (2) system at 307.15K (△); 317.15K (◊); 327.15K (○); — SRK-NRTL; - - - SRK-Wilson; ... SRK-UNIQUAC.

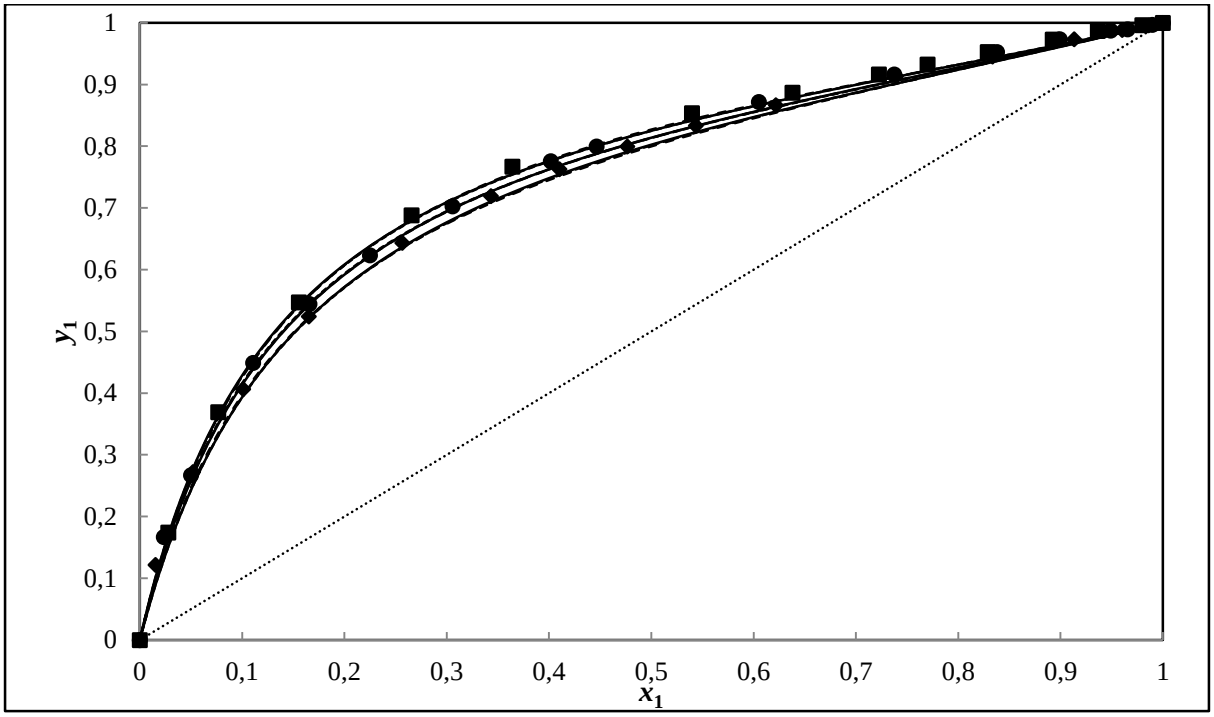

Figure B-6: Experimental VLE and modeling results: *x*-*y* data for the MTBE (1) + 2, 2, 4-trimethylpentane (2) system at 307.15K (♦); 317.15K (●); 327.15K (■); — SRK-NRTL; - - - SRK-Wilson; ... SRK-UNIQUAC.

Table B-4: Direct Method Modeling results for DIPE (1) + 2, 2, 4-trimethylpentane (2)

Model	**T±0.10/ K**	α_{12}	k_{ij}	A_{12} **J/mol**	A_{21} **J/mol**	(ΔP) **AAD**	**AAD%** (ΔP)	(Δy_1) **AAD**	**AAD%** (Δy_1)
RKS-MC-WS-NRTL									
	320.15	0.30	0.165	-607002	1357340	0.21	0.67	0.003	0.72
	330.15	0.30	-0.195	159883	602729	0.51	1.14	0.006	1.37
	340.15	0.30	0.169	373275	286291	0.53	0.79	0.008	1.27
RKS-MC-WS-Wilson									
	320.15	-	0.094	-825813	8708.05	0.28	0.67	0.003	0.77
	330.15	-	0.026	-450400	-191207	0.51	1.16	0.006	1.40
	340.15	-	0.146	-321275	-253367	0.53	0.79	0.008	1.26
RKS-MC-WS-UNIQUAC									
	320.15	-	0.206	20335.88	-133085	0.27	0.80	0.003	0.70
	330.15	-	-0.214	52315.40	-217957	0.51	1.17	0.006	1.34
	340.15	-	0.130	-99277.11	-75928.42	0.52	0.78	0.008	1.26

[a]Wilson: $A_{12} = a_{12} - a_{22}$ and $A_{21} = a_{21} - a_{11}$; NRTL: $A_{12} = g_{12} - g_{22}$ and $A_{21} = g_{21} - g_{11}$; UNIQUAC: $A_{12} = u_{12} - u_{22}$ and $A_{21} = u_{21} - u_{11}$; A_{12}: binary interaction parameters representation for the models in Aspen Plus®. k_{ij}: parameter for fitting with Wong and Sandler mixing rule.

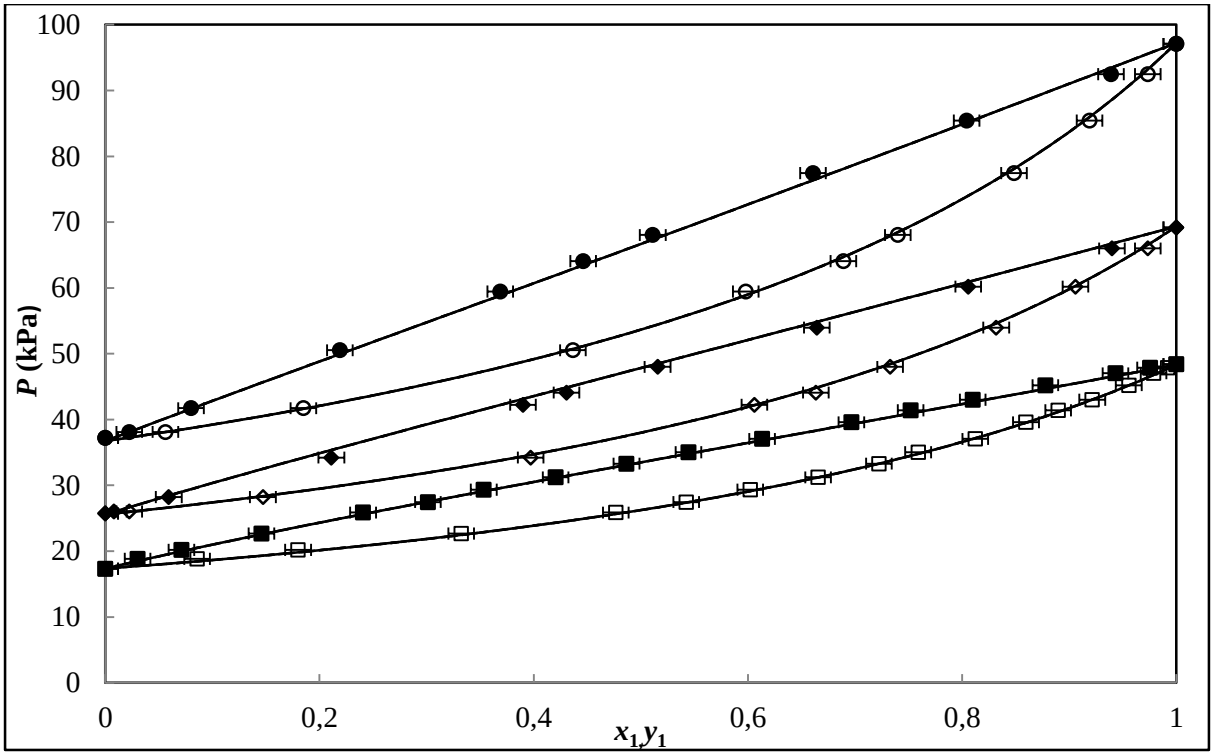

Figure B-7: Experimental VLE and modeling results: P-*x*-*y* data for the DIPE (1) + 2, 2, 4-trimethylpentane (2) system at 320.15K (□); 330.15K (◊); 340.15K (○); — SRK-NRTL; - - - SRK-Wilson; ... SRK-UNIQUAC.

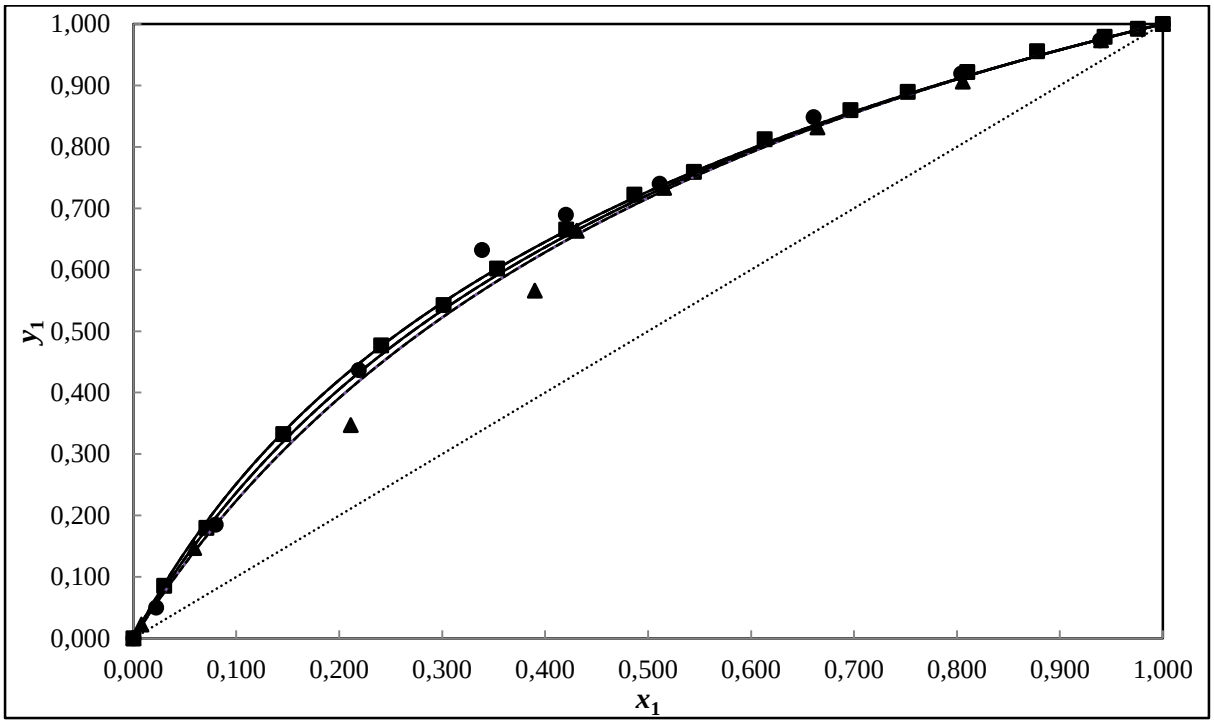

Figure B-8: Experimental VLE and modeling results: *x*-*y* data for the DIPE (1) + 2, 2, 4-trimethylpentane (2) system at 320.15K (▲); 330.15K (●); 340.15K (■); — SRK-NRTL; - - - SRK-Wilson; ... SRK-UNIQUAC.

Table B-5: Direct Method Modeling results for DIPE (1) + 1-propanol (2)

Model	**T±0.10/K**	α_{12}	k_{ij}	A_{12} **J/mol**	A_{21} **J/mol**	**(Δ*P*) AAD**	**AAD% (Δ*P*)**	**(Δy_1) AAD**	**AAD%(Δy_1)**
RKS-MC-WS-NRTL									
	320.15	0.30	-0.285	1517	488.1	0.27	0.75	0.004	0.70
	330.15	0.30	0.267	1775	-936.4	0.20	0.35	0.004	0.71
	340.15	0.30	-0.649	1552	1614	0.86	1.16	0.004	0.59
RKS-MC-WS-Wilson									
	320.15	-	0.058	-807.2	2496	0.23	0.66	0.005	0.81
	330.15	-	0.044	-862.5	2543	0.19	0.35	0.005	0.80
	340.15	-	0.138	-804.0	3007	0.62	0.82	0.005	0.73
RKS-MC-WS-UNIQUAC									
	320.15	-	-0.023	4561	-1523	0.31	0.81	0.004	0.68
	330.15	-	0.002	4490	-1482	0.26	0.47	0.005	0.73
	340.15	-	-0.252	4548	-1702	0.86	1.16	0.004	0.58

[a]Wilson: $A_{12} = a_{12} - a_{22}$ and $A_{21} = a_{21} - a_{11}$; NRTL: $A_{12} = g_{12} - g_{22}$ and $A_{21} = g_{21} - g_{11}$; UNIQUAC: $A_{12} = u_{12} - u_{22}$ and $A_{21} = u_{21} - u_{11}$; A_{12}: binary interaction parameters representation for the models in Aspen Plus®. k_{ij}: parameter for fitting with Wong and Sandler mixing rule.

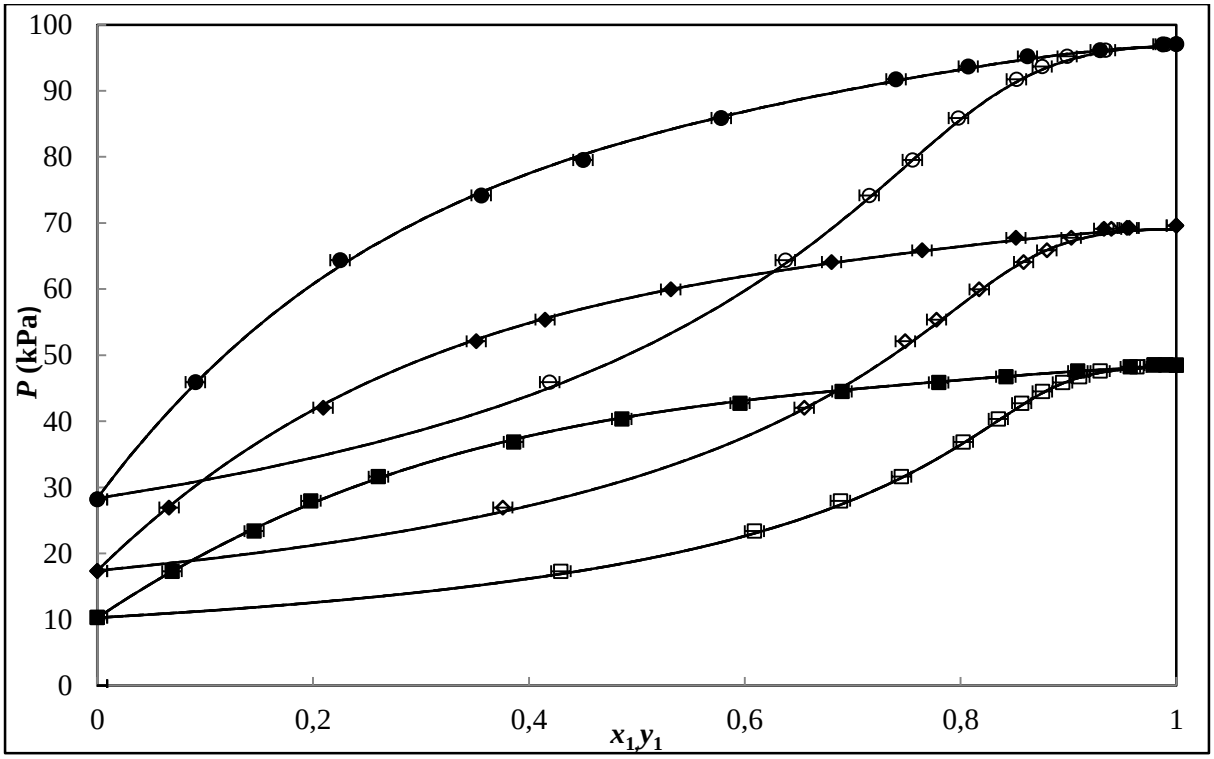

Figure B-9: Experimental VLE and modeling results: P-*x*-*y* data for the DIPE (1) + 1-propanol (2) system at 320.15K (□); 330.15K (◊); 340.15K (○); — SRK-NRTL; - - - SRK-Wilson; ... SRK-UNIQUAC.

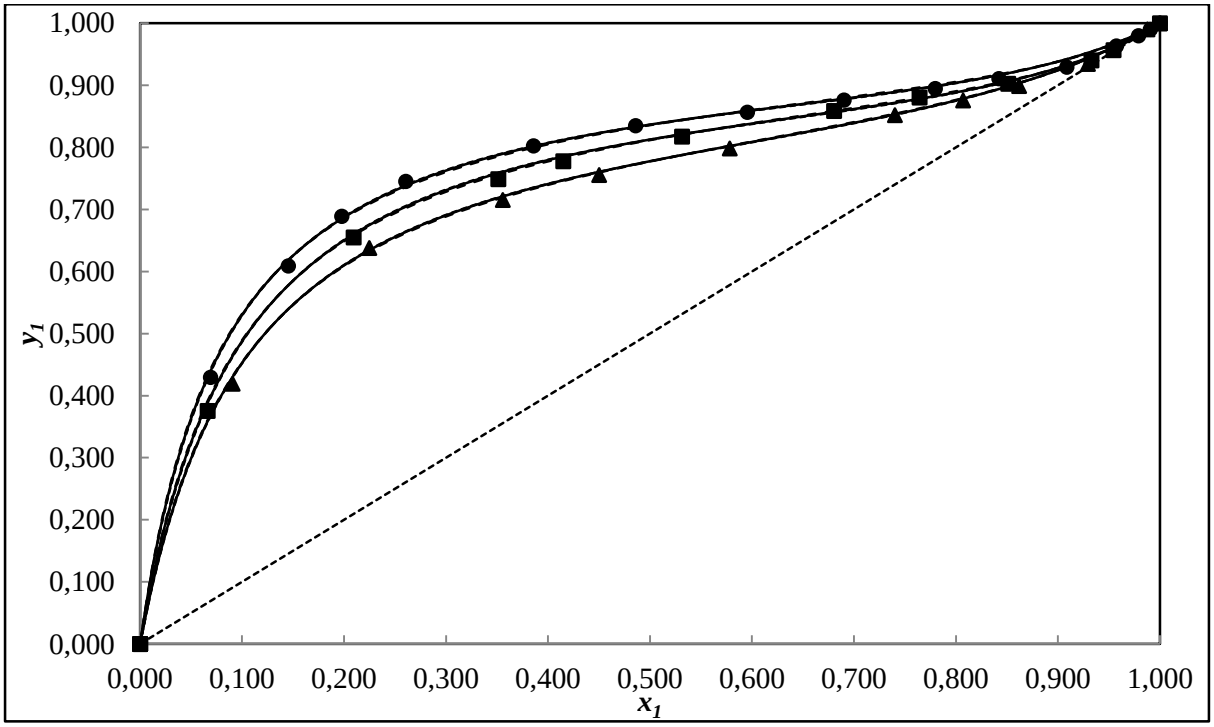

Figure B-10: Experimental VLE and modeling results: *x*-*y* data for the DIPE (1) + 1-propanol (2) system at 320.15K (▲); 330.15K (■); 340.15K (●); — SRK-NRTL; - - - SRK-Wilson; ... SRK-UNIQUAC.

Table B-6: Direct Method Modeling results for DIPE (1) + 2-butanol (2)

Model	**T±0.10/K**	α_{12}	k_{ij}	A_{12} **J/mol**	A_{21} **J/mol**	**(Δ*P*) AAD**	**AAD% (Δ*P*)**	**(Δy_1) AAD**	**AAD%(Δy_1)**
RKS-MC-WS-NRTL									
	320.15	0.30	-0.226	1328.81	-108.48	0.24	0.90	0.007	1.03
	330.15	0.30	0.0033	1192.07	-621.36	0.32	0.51	0.008	1.17
	340.15	0.30	0.284	1022.81	-1274.12	0.27	0.53	0.008	1.20
RKS-MC-WS-Wilson									
	320.15	-	-0.037	-326.97	-1387.90	0.37	1.15	0.007	1.09
	330.15	-	0.258	448.96	-1329.91	0.33	0.84	0.007	1.04
	340.15	-	0.292	468.50	-928.41	0.46	0.84	0.008	0.89
RKS-MC-WS-UNIQUAC									
	320.15	-	-0.023	1165.52	-478.54	0.29	1.09	0.007	1.10
	330.15	-	0.031	1079.54	-406.17	0.36	0.86	0.008	1.14
	340.15	-	0.288	1121.41	-254.97	0.44	0.73	0.008	1.14

[a]Wilson: $A_{12} = a_{12} - a_{22}$ and $A_{21} = a_{21} - a_{11}$; NRTL: $A_{12} = g_{12} - g_{22}$ and $A_{21} = g_{21} - g_{11}$; UNIQUAC: $A_{12} = u_{12} - u_{22}$ and $A_{21} = u_{21} - u_{11}$; A_{12}: binary interaction parameters representation for the models in Aspen Plus®. k_{ij}: parameter for fitting with Wong and Sandler mixing rule.

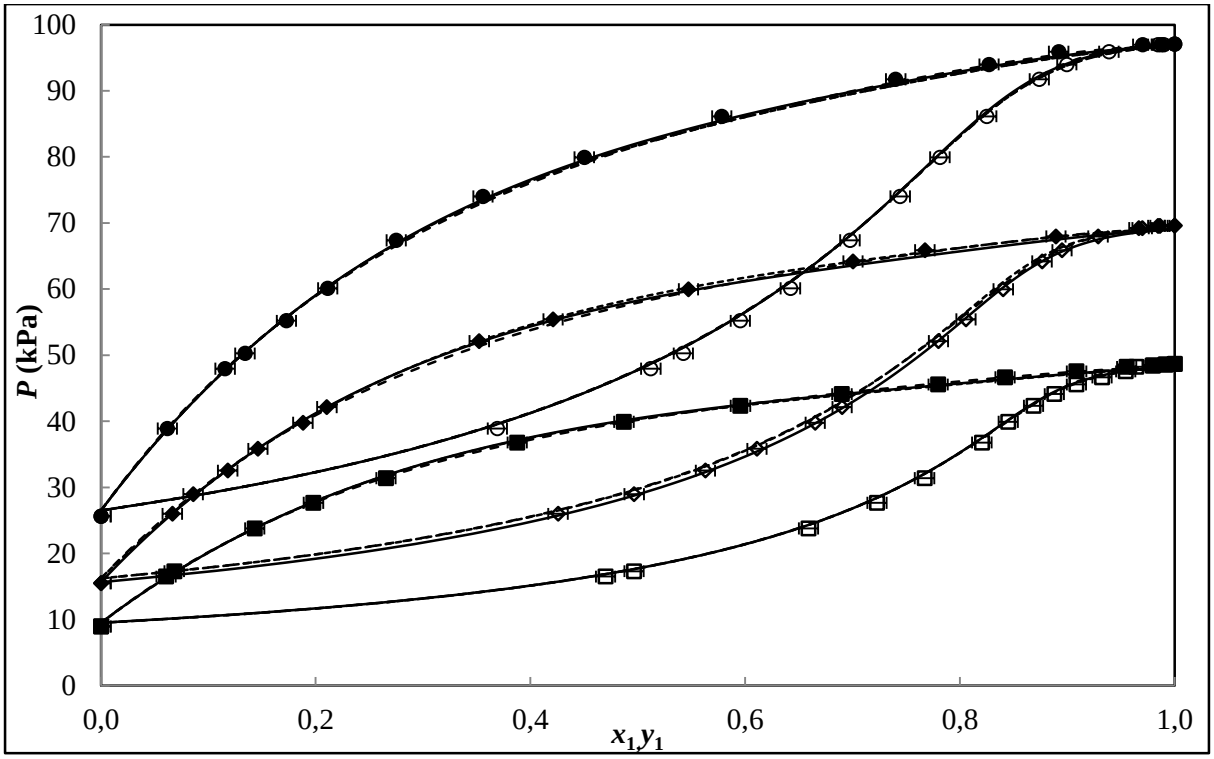

Figure B-11: Experimental VLE and modeling results: P-*x*-*y* data for the DIPE (1) + 2-butanol (2) system at 320.15K (□); 330.15K (◊); 340.15K (○); — SRK-NRTL; - - - SRK-Wilson; ... SRK-UNIQUAC.

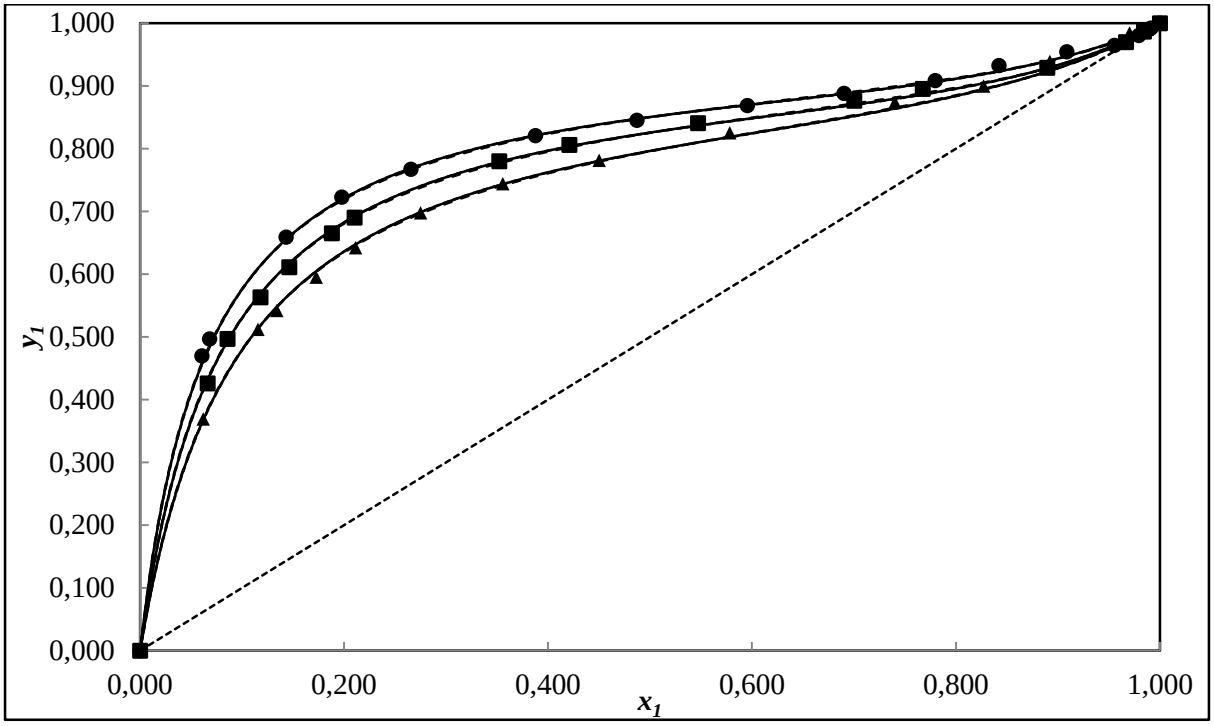

Figure B-12: Experimental VLE and modeling results: *x*-*y* data for the DIPE (1) + 2-butanol (2) system at 320.15K (▲); 330.15K (■); 340.15K (●); — SRK-NRTL; - - - SRK-Wilson; ... SRK-UNIQUAC.

Table B-7: Computed Azeotropic Conditions for the System 2, 2, 4-trimethylpentane (1) + 1-pentanol (2) using the HOC-Wilson Model.

Composition (x_1)	T/K	P/kPa
0.971	350.2	51.9
0.957	360.2	71.4
0.941	370.2	96.4

Appendix C: Experimental Activity Coefficients and Relative Volatilities

Table C-1: Experimental activity coefficient and relative volatility data for 2, 2, 4-trimethylpentane (1) + 1-pentanol (2) system at 350.15 K, 360.15 K and 370.15 K.

P/kPa	x_1	y_1	γ_1	γ_2	α_{12}
		T/K			
		350.15			
8.04	0.000	0.000	-	0,943	-
10.02	0.010	0.172	3,435	0,982	1,202
13.03	0.029	0.376	3,360	0,980	0,972
18.04	0.061	0.542	3,176	1,027	0,895
25.03	0.121	0.690	2,815	1,026	0,668
33.03	0.213	0.780	2,372	1,069	0,409
38.03	0.284	0.816	2,135	1,128	0,164
46.03	0.525	0.871	1,483	1,436	0,089
50.01	0.814	0.914	1,088	2,651	0,076
51.01	0.899	0.930	1,022	4,051	0,062
51.41	0.949	0.955	1,001	5,198	0,054
51.56	0.969	0.970	0,999	5,717	0,050
51.55	0.990	0.988	0,996	7,088	0,049
51.54	1.000	1.000	0,997	-	-
		T/K			
		360.15			
13.26	0.000	0.000	-	0,957	-
18.47	0.019	0.253	3,588	1,012	1,139
24.83	0.051	0.449	3,176	1,034	0,894
30.21	0.086	0.555	2,822	1,052	0,602
37.80	0.132	0.662	2,731	1,049	0,568
45.05	0.192	0.728	2,449	1,077	0,472
51.50	0.263	0.776	2,169	1,108	0,395
59.01	0.393	0.821	1,751	1,227	0,292
67.11	0.664	0.872	1,245	1,795	0,142
68.58	0.737	0.877	1,152	2,250	0,103
69.40	0.796	0.892	1,097	2,577	0,089
70.12	0.839	0.902	1,063	2,993	0,078

70.95	0.869	0.917	1,055	3,151	0,075
71.09	0.931	0.938	1,009	4,477	0,066
71.06	0.97	0.966	0,997	5,645	0,058
70.69	1.000	1.000	0,997	-	-
-	-	-	1.000	-	-
T/K					
370.15					
21.04	0.000	0.000	-	0,967	-
25.33	0.010	0.122	3,377	1,031	1,249
30.87	0.030	0.292	3,272	1,031	1,073
38.38	0.061	0.446	3,042	1,032	1,020
47.06	0.100	0.562	2,853	1,040	0,453
59.21	0.172	0.666	2,455	1,078	0,299
68.33	0.240	0.729	2,210	1,096	0,239
75.20	0.313	0.766	1,952	1,148	0,139
87.76	0.536	0.829	1,429	1,441	0,117
90.40	0.616	0.843	1,300	1,645	0,105
93.70	0.748	0.868	1,141	2,182	0,087
96.54	0.939	0.938	1,010	4,357	0,080
96.51	0.949	0.945	1,006	4,622	0,076
95.76	0.989	0.986	1,000	5,415	0,073
95.02	1.000	1.000	0,996	-	-

Table C-2: Experimental activity coefficient and relative volatility data for MTBE (1) + 1-pentanol (2) system at 317.15 K and 327.15 K.

P/kPa	x_1	y_1	γ_1	γ_2	α_{12}
		T/K			
		317.15			
1.12	0.000	0.000	-	0,986	-
2.66	0.010	0.296	1,183	1,662	0,025
4.01	0.020	0.627	1,888	1,340	0,012
9.59	0.065	0.860	1,899	1,255	0,011
18.66	0.152	0.937	1,714	1,203	0,012
26.89	0.242	0.960	1,582	1,223	0,013
34.62	0.343	0.972	1,449	1,264	0,015
42.96	0.475	0.981	1,304	1,323	0,018
49.38	0.596	0.986	1,197	1,448	0,021
55.23	0.717	0.990	1,114	1,644	0,026
60.34	0.838	0.994	1,042	1,875	0,033
64.06	0.899	0.996	1,032	2,122	0,038
67.11	0.960	0.998	1,012	2,800	0,043
68.93	1.000	1.000	0,999	-	-
		T/K			
		327.15			
2.14	0.000	0.000	-	0,984	-
3.83	0.010	0.215	0,890	1,395	0,037
5.03	0.018	0.451	1,362	1,290	0,022
10.49	0.045	0.750	1,884	1,255	0,016
14.06	0.071	0.833	1,774	1,152	0,015
17.18	0.091	0.866	1,756	1,152	0,016
25.31	0.141	0.910	1,747	1,199	0,016
33.47	0.212	0.939	1,580	1,165	0,018
41.47	0.273	0.952	1,535	1,224	0,019
52.63	0.394	0.968	1,365	1,233	0,022
60.95	0.495	0.975	1,262	1,330	0,025
68.83	0.596	0.981	1,186	1,419	0,029
77.30	0.707	0.986	1,124	1,610	0,035
83.95	0.808	0.990	1,069	1,897	0,041

88.54	0.879	0.993	1,037	2,214	0,048
94.06	0.960	0.998	1,011	2,025	0,057
97.13	1.000	1.000	1,003	-	-

Table C-3: Experimental activity coefficient and relative volatility data for MTBE (1) + 2, 2, 4-trimethylpentane (2) system at 307.15 K, 317.15 K and 327.15 K.

P/kPa	x_1	y_1	γ_1	γ_2	α_{12}
			T/K		
			307.15		
10.10	0.000	0.000	-	0,998	-
11.80	0.028	0.174	1,568	0,998	0,137
14.64	0.077	0.369	1,497	0,993	0,142
18.78	0.156	0.547	1,401	0,996	0,153
24.01	0.266	0.688	1,317	1,003	0,164
28.08	0.364	0.767	1,252	1,007	0,174
34.44	0.540	0.854	1,148	1,063	0,201
37.67	0.638	0.887	1,101	1,140	0,225
40.32	0.722	0.917	1,075	1,164	0,237
41.94	0.770	0.932	1,065	1,197	0,243
43.85	0.829	0.953	1,056	1,161	0,241
45.24	0.892	0.973	1,033	1,089	0,232
46.60	0.936	0.987	1,028	0,910	0,194
47.53	0.980	0.997	1,011	0,685	0,167
47.71	1.000	1.000	0,997	-	-
			T/K		
			317.15		
15.38	0.000	0.000	0,996	-	-
17.86	0.023	0.167	0,989	2,227	0,120
20.25	0.050	0.267	1,012	1,658	0,145
24.82	0.111	0.449	0,992	1,486	0,153
28.45	0.166	0.545	0,998	1,370	0,166
32.46	0.225	0.623	1,011	1,291	0,176
37.23	0.306	0.703	1,016	1,236	0,186

42.89	0.402	0.776	1,019	1,191	0,194
45.10	0.447	0.800	1,033	1,157	0,202
53.03	0.605	0.872	1,081	1,124	0,226
58.97	0.737	0.917	1,165	1,093	0,255
63.34	0.838	0.953	1,146	1,058	0,257
65.44	0.899	0.973	1,089	1,034	0,245
67.48	0.949	0.988	0,987	1,022	0,234
67.93	0.966	0.990	1,241	1,014	0,290
68.67	0.990	0.997	1,279	1,003	0,320
68.93	1.000	1.000	-	-	-
		T/K			
		327.15			
22.95	0.000	0.000	-	1,000	-
25.55	0.015	0.122	2,227	0,995	0,113
29.65	0.052	0.272	1,658	0,991	0,147
34.68	0.101	0.406	1,486	0,993	0,164
40.58	0.165	0.524	1,370	0,998	0,179
48.68	0.257	0.644	1,291	0,999	0,191
55.94	0.343	0.719	1,236	1,019	0,204
60.83	0.410	0.763	1,191	1,037	0,216
65.77	0.477	0.800	1,157	1,063	0,228
70.00	0.543	0.833	1,124	1,078	0,238
75.20	0.622	0.866	1,093	1,119	0,253
82.20	0.739	0.914	1,058	1,131	0,268
87.85	0.833	0.945	1,034	1,203	0,289
92.69	0.913	0.973	1,022	1,192	0,290
95.22	0.960	0.989	1,014	1,083	0,277
97.13	1.000	1.000	1,003	-	-

Table C-4: Experimental activity coefficient and relative volatility data for DIPE (1) + 2, 2, 4-trimethylpentane (2) system at 320.15 K, 330.15 K and 340.15 K.

P/kPa	x_1	y_1	γ_1	γ_2	α_{12}
			T/K		
			320.15		
17.32	0.000	0.000	-	0,992	-
18.83	0.030	0.086	1,141	1,015	0,329
20.18	0.071	0.180	1,080	1,018	0,386
22.67	0.146	0.332	1,087	1,012	0,395
25.87	0.241	0.477	1,077	1,014	0,470
27.46	0.301	0.542	1,039	1,022	0,526
29.35	0.353	0.602	1,051	1,024	0,571
31.22	0.421	0.666	1,036	1,020	0,643
33.29	0.487	0.722	1,034	1,021	0,738
35.02	0.545	0.759	1,021	1,048	0,803
37.05	0.613	0.812	1,026	1,015	0,913
39.59	0.697	0.860	1,020	1,030	1,049
41.40	0.752	0.890	1,022	1,032	1,179
43.01	0.810	0.922	1,020	0,991	1,365
45.22	0.878	0.956	1,025	0,914	1,783
47.03	0.943	0.979	1,015	0,970	2,234
47.89	0.976	0.992	1,012	0,893	2,692
48.43	1.000	1.000	1,006	-	-
			T/K		
			330.15		
25.72	0.000	0.000	-	0,997	-
26.32	0.008	0.022	1,060	0,995	0,458
29.21	0.059	0.147	1,040	0,990	0,544
35.22	0.211	0.347	0,950	1,008	0,627
43.25	0.390	0.566	0,964	1,046	0,784
47.50	0.431	0.663	0,995	1,000	0,911
51.00	0.516	0.733	0,999	1,011	1,003
56.87	0.664	0.832	0,987	1,026	1,438
62.40	0.806	0.906	0,985	1,104	2,252
67.07	0.940	0.973	0,991	1,120	2,788
69.17	1.000	1.000	1,002	-	-

			T/K		
			340.15		
37.22	0.000	0.000	-	1,005	-
39.52	0.022	0.050	1,032	0,993	0,453
43.73	0.080	0.185	1,025	0,995	0,472
54.73	0.219	0.437	1,066	0,975	0,574
62.45	0.339	0.632	1,014	1,008	0,770
67.06	0.420	0.689	1,040	0,954	0,867
72.04	0.511	0.740	1,033	0,957	1,033
79.94	0.661	0.849	1,038	0,907	1,438
87.42	0.804	0.919	1,015	0,924	2,047
93.69	0.939	0.973	0,993	1,066	2,428
97.08	1.000	1.000	1,004	-	-

Table C-5: Experimental activity coefficient and relative volatility data for DIPE (1) + 1-propanol (2) system at 320.15 K, 330.15 K and 340.15 K.

P/kPa	x_1	y_1	γ_1	γ_2	α_{12}
			T/K		
			320.15		
10.29	0.000	0.000	-	1,004	-
17.31	0.069	0.430	2,280	1,031	3,801
23.38	0.145	0.609	2,068	1,038	1,918
27.96	0.198	0.689	2,044	1,050	1,351
31.61	0.261	0.745	1,892	1,055	0,986
36.88	0.386	0.803	1,604	1,142	0,669
40.35	0.486	0.835	1,447	1,248	0,551
42.74	0.596	0.857	1,281	1,456	0,509
44.51	0.690	0.876	1,177	1,712	0,508
45.86	0.780	0.895	1,095	2,104	0,549
46.74	0.842	0.911	1,052	2,530	0,613
47.59	0.909	0.929	1,011	3,567	0,791
48.23	0.957	0.963	1,008	3,985	0,863
48.52	0.979	0.980	1,009	4,437	0,969
48.53	0.991	0.990	1,007	5,178	1,066

48.49	1.000	1.000	1,007	-	-
T/K					
330.15					
17.33	0.000	0.000	-	0,998	-
26.95	0.066	0.376	2,273	1,033	3,782
42.04	0.209	0.655	1,936	1,046	1,365
52.11	0.351	0.749	1,625	1,145	0,825
55.38	0.415	0.778	1,515	1,192	0,712
59.95	0.532	0.817	1,340	1,328	0,600
64.09	0.680	0.858	1,175	1,608	0,559
65.86	0.764	0.880	1,101	1,892	0,586
67.75	0.851	0.903	1,042	2,490	0,694
69.13	0.933	0.940	1,009	3,493	0,903
69.25	0.954	0.956	1,005	3,738	0,961
69.60	1.000	1.000	1,008	-	-
T/K					
340.15					
28.16	0.000	0.000	-	0,995	-
45.92	0.091	0.419	2,240	1,030	2,9479
64.37	0.225	0.638	1,917	1,048	1,3251
74.18	0.356	0.715	1,558	1,141	0,8882
79.54	0.450	0.755	1,392	1,229	0,7464
85.89	0.578	0.798	1,233	1,423	0,6606
91.74	0.740	0.852	1,095	1,803	0,6560
93.68	0.807	0.876	1,053	2,077	0,6994
95.21	0.862	0.899	1,028	2,403	0,7645
96.16	0.929	0.935	1,001	3,035	0,9325
97.05	0.988	0.990	1,006	2,787	0,8243
97.09	1.000	1.000	1,004	-	-

Table C-6: Experimental activity coefficient and relative volatility data for DIPE (1) + 2-butanol (2) system at 320.15 K, 330.15 K and 340.15 K.

P/kPa	x_1	y_1	γ_1	γ_2	α_{12}
		T/K			
		320.15			
8.94	0.000	0.000	-	0,980	-
16.49	0.061	0.470	2,705	1,015	4,375
17.31	0.068	0.497	2,691	1,018	3,931
23.78	0.143	0.659	2,318	1,029	1,831
27.66	0.198	0.723	2,130	1,038	1,262
31.39	0.266	0.767	1,904	1,081	0,916
36.78	0.388	0.821	1,631	1,166	0,620
39.92	0.487	0.845	1,448	1,307	0,524
42.34	0.596	0.869	1,288	1,488	0,474
44.11	0.690	0.888	1,183	1,728	0,465
45.56	0.780	0.909	1,105	2,044	0,483
46.64	0.842	0.933	1,075	2,148	0,473
47.55	0.909	0.954	1,037	2,613	0,524
48.23	0.955	0.964	1,012	4,196	0,805
48.41	0.979	0.980	1,007	5,020	0,959
48.60	0.991	0.992	1,011	4,708	0,946
48.69	1.000	1.000	1,011	-	-
		T/K			
		330.15			
15.49	0.000	0.000	-	0,990	-
25.99	0.066	0.426	2,506	1,015	3,942
28.97	0.086	0.497	2,495	1,012	3,186
32.53	0.118	0.563	2,306	1,021	2,364
35.82	0.146	0.611	2,222	1,033	1,904
39.76	0.188	0.665	2,079	1,037	1,458
42.15	0.210	0.690	2,044	1,045	1,287
52.12	0.352	0.780	1,693	1,116	0,752
55.40	0.421	0.806	1,551	1,171	0,642
59.97	0.547	0.840	1,343	1,335	0,541
64.18	0.700	0.877	1,169	1,660	0,516
65.87	0.767	0.895	1,116	1,874	0,526

67.95	0.889	0.929	1,030	2,748	0,673
69.23	0.967	0.970	1,006	3,990	0,912
69.55	0.985	0.986	1,009	4,120	0,882
69.59	1.000	1.000	1,008	-	-
T/K					
340.15					
25.61	0.000	0.000	-	0,997	-
38.89	0.062	0.369	2,487	1,011	4,014
47.96	0.116	0.512	2,259	1,020	2,444
50.25	0.134	0.542	2,166	1,023	2,137
55.21	0.173	0.595	2,017	1,040	1,685
60.12	0.211	0.642	1,937	1,048	1,379
67.37	0.275	0.698	1,802	1,076	1,058
74.01	0.356	0.744	1,623	1,127	0,830
79.94	0.450	0.781	1,451	1,219	0,690
86.14	0.578	0.825	1,281	1,368	0,592
91.74	0.740	0.874	1,125	1,704	0,573
94.00	0.827	0.900	1,060	2,085	0,631
95.91	0.892	0.939	1,045	2,084	0,596
96.97	0.970	0.985	1,019	1,872	0,531
97.00	0.988	0.990	1,006	3,123	0,824
97.06	1.000	1.000	1,004	-	-

Appendix D: Relative Volatility Plots

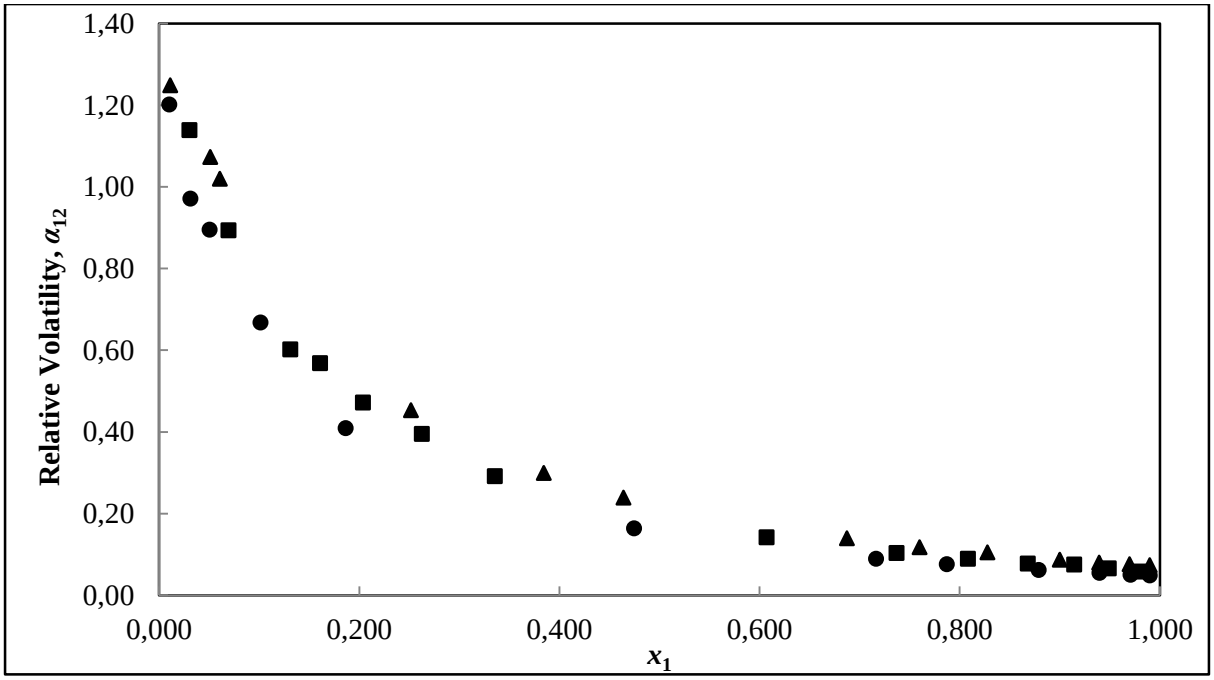

Figure D-1: Plot of relative volatility for the 2, 2, 4-trimethylpentane (1) + 1-pentanol (2) system at: ●, 350.15 K; ■, 360.15 K; ▲, 370.15 K

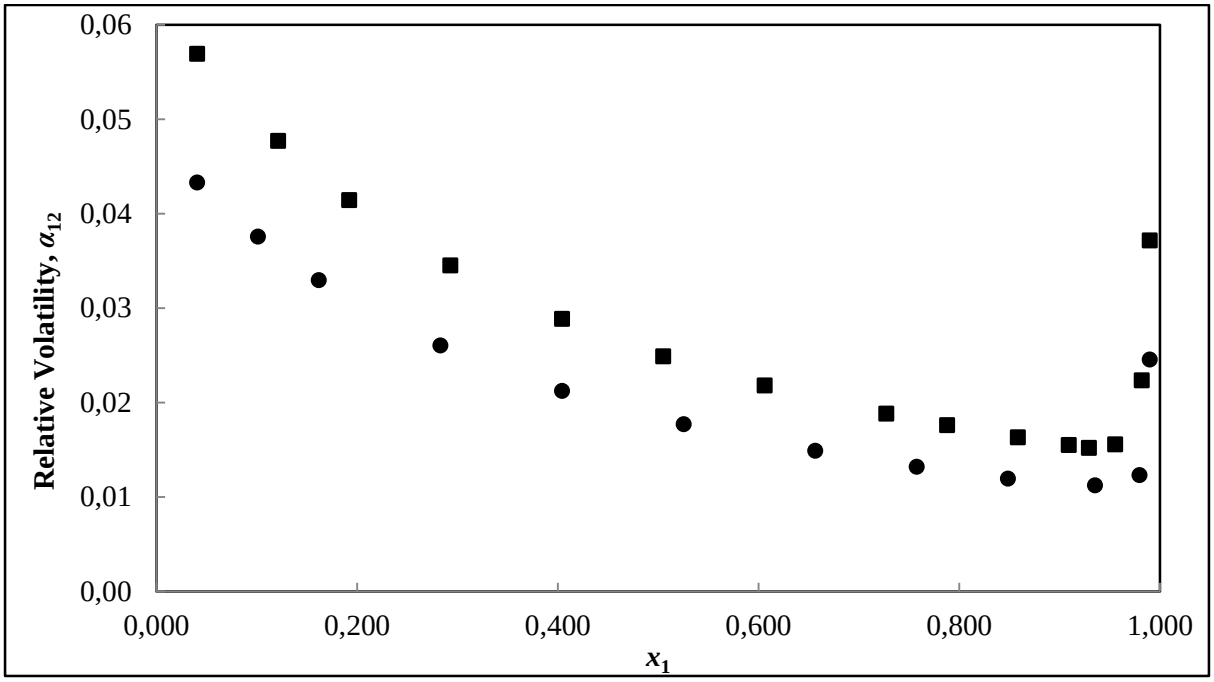

Figure D-2: Plot of relative volatility for the MTBE (1) + 1-pentanol (2) system at: ■, 317.15 K; ▲, 327.15 K

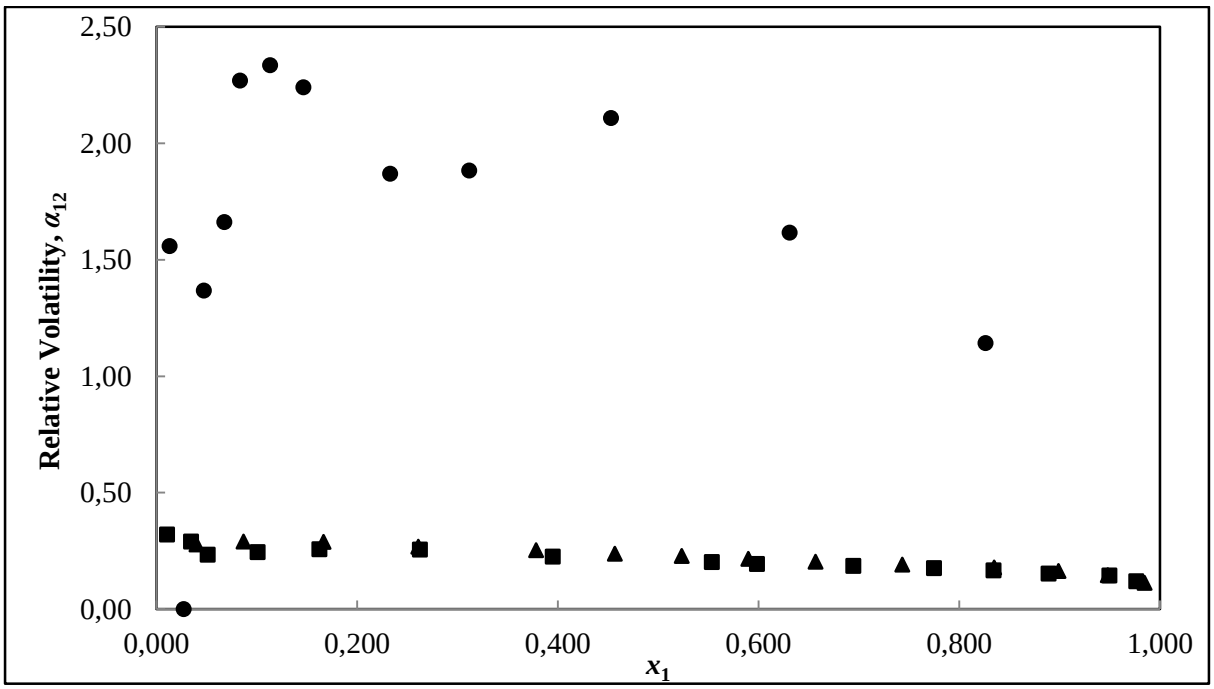

Figure D-3: Plot of relative volatility for the MTBE (1) + 2, 2, 4-trimethylpentane (2) system at: ●, 307.15 K; ■, 317.15 K; ▲, 327.15 K

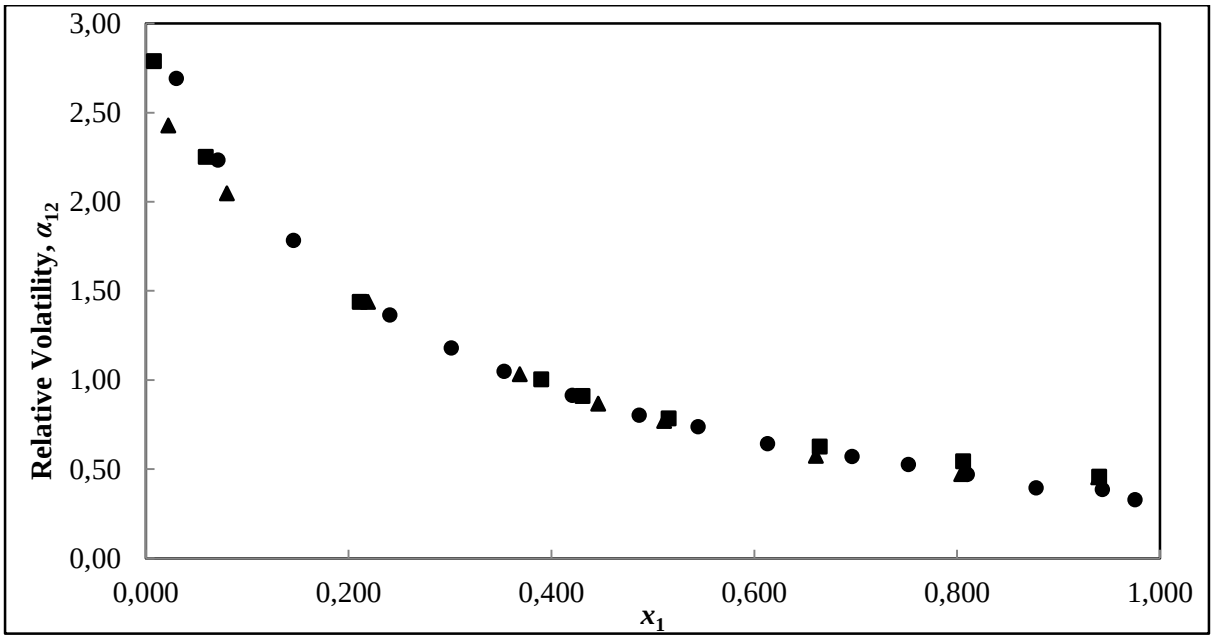

Figure D-4: Plot of relative volatility for the DIPE (1) + 2, 2, 4-trimethylpentane (2) system at: ●, 320.15 K; ■, 330.15 K; ▲, 340.15 K

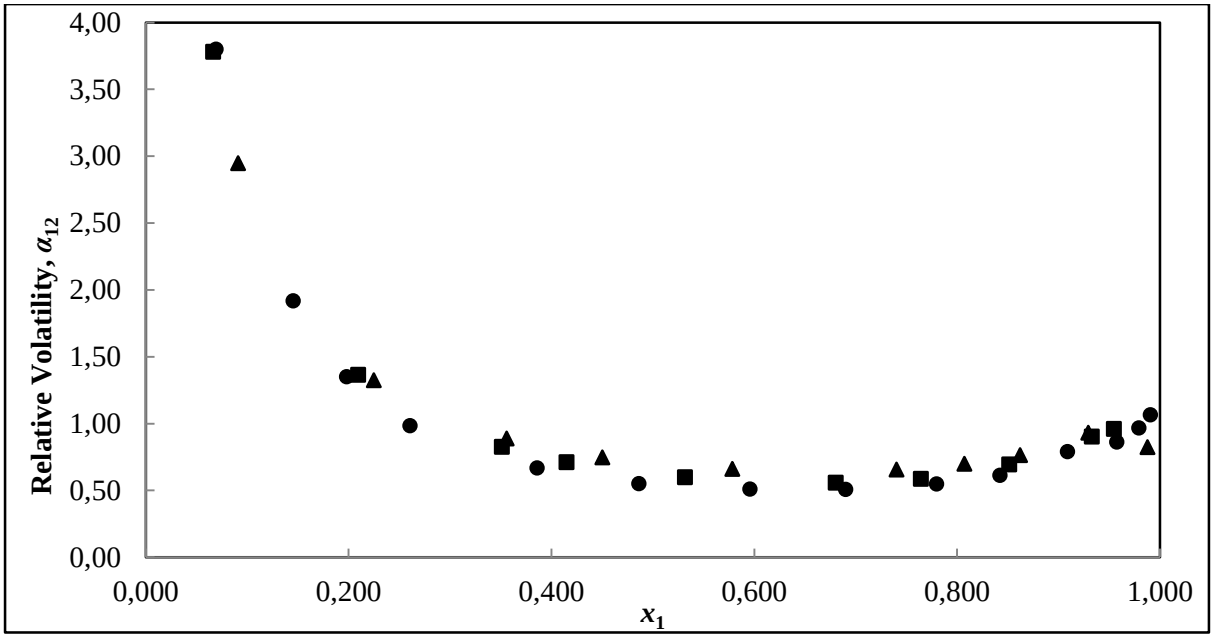

Figure D-5: Plot of relative volatility for the DIPE (1) + 1-propanol (2) system at: ●, 320.15 K; ■, 330.15 K; ▲, 340.15 K

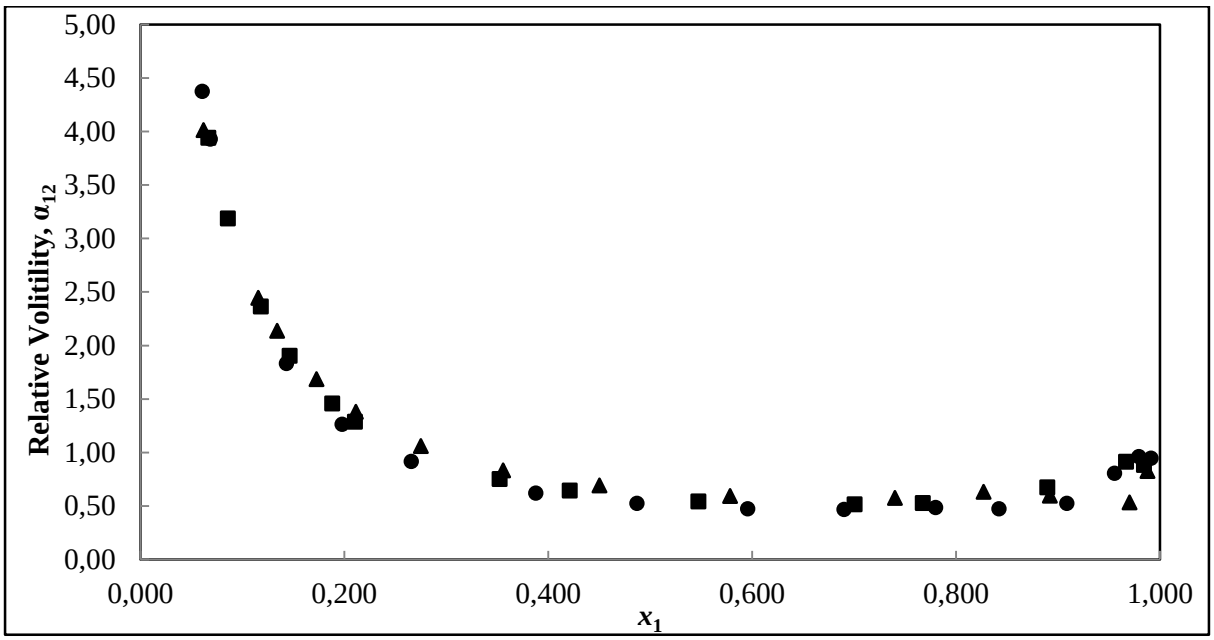

Figure D-6: Plot of relative volatility for the DIPE (1) + 2-butanol (2) system at: ●, 320.15 K; ■, 330.15 K; ▲, 340.15 K

Appendix E: Wong Sandler Mixing Rule

The partial derivative of a_m and b_m are:

$$\left(\frac{1}{n}\frac{\partial n^2 a_m}{\partial n_i}\right) = RT\left(D\frac{\partial n b_m}{\partial n_i} + b\frac{\partial nD}{\partial n_i}\right) \tag{E-01}$$

$$\left(\frac{\partial n b_m}{\partial n_i}\right) = \frac{1}{(1-D)}\left(\frac{1}{n}\frac{\partial n^2 Q}{\partial n_i}\right) - \frac{Q}{(1-D)^2}\left(1-\frac{\partial nD}{\partial n_i}\right) \tag{E-02}$$

The partial derivatives of 'Q' and 'D' are:

$$\left(\frac{1}{n}\frac{\partial n^2 Q}{\partial n_i}\right) = 2\sum_j x_j\left(b-\frac{a}{RT}\right)_{ij} \tag{E-03}$$

$$\left(\frac{\partial nD}{\partial n_i}\right) = \frac{a_i}{b_i RT} + \frac{\ln\gamma_i^{\infty}}{c} \tag{E-04}$$

The cross-parameter, required for the evaluation of activity is:

$$\left(b-\frac{a}{RT}\right)_{ij} = \frac{\left(b_i-\frac{a_i}{RT}\right)+\left(b_j-\frac{a_j}{RT}\right)}{2}\left(1-k_{ij}\right) \tag{E-05}$$

where: k_{ij} = an adjustable parameter (k_{ij} is obtained by the reduction of experimental VLE data).

Appendix F: Activity Coefficient

$$\overline{G}_i^E = RT \ln \gamma_i \tag{F-01}$$

Equation (2-82) is represented in terms of activity as follows:

$$\ln \gamma_i = \left[\frac{\partial \left(nG^E / RT \right)}{\partial n_i} \right]_{P,T,n_j} \tag{F-02}$$

ln γ_i is a partial property of **G^E/RT**, rendering the following summability relationship valid:

$$\frac{G^E}{RT} = \sum_i x_i \ln \gamma_i \tag{F-03}$$

Consequently, the Gibbs/Duhem equation is shown in terms of activity as follows:

$$d\left(\frac{nG^E}{RT} \right) = \frac{nV^E}{RT} dP - \frac{nH^E}{RT^2} dT + \sum_i \ln \gamma_i dn_i \tag{F-04}$$